PERGAMON

Progress in Materials Science 46 (2001) 1–184

Progress in Materials Science

www.elsevier.com/locate/pmatsci

Mechanical alloying and milling

C. Suryanarayana

Department of Metallurgical and Materials Engineering, Colorado School of Mines, Golden, CO 80401-1887, USA

Abstract

Mechanical alloying (MA) is a solid-state powder processng technique involving repeated welding, fracturing, and rewelding of powder particles in a high-energy ball mill. Originally developed to produce oxide-dispersion strengthened (ODS) nickel- and iron-base superalloys for applications in the aerospace industry, MA has now been shown to be capable of synthesizing a variety of equilibrium and non-equilibrium alloy phases starting from blended elemental or prealloyed powders. The non-equilibrium phases synthesized include supersaturated solid solutions, metastable crystalline and quasicrystalline phases, nanostructures, and amorphous alloys. Recent advances in these areas and also on disordering of ordered intermetallics and mechanochemical synthesis of materials have been critically reviewed after discussing the process and process variables involved in MA. The often vexing problem of powder contamination has been analyzed and methods have been suggested to avoid/minimize it. The present understanding of the modeling of the MA process has also been discussed. The present and potential applications of MA are described. Wherever possible, comparisons have been made on the product phases obtained by MA with those of rapid solidification processing, another non-equilibrium processing technique.

Contents

E-mail address: schallap@mines.edu (C. Suryanarayana).

0079-6425/01/$ - see front matter
PII: S0079-6425(99)00010-9

1. Introduction

Scientific investigations by materials scientists have been continuously directed towards improving the properties and performance of materials. Significant improvements in mechanical, chemical, and physical properties have been achieved through chemistry modifications and conventional thermal, mechanical, and thermomechanical processing methods. However, the ever-increasing demands for "hotter, stronger, stiffer, and lighter" than traditional materials have led to the

design and development of advanced materials. The high-technology industries have given an added stimulus to these efforts.

Advanced materials may be defined as those where first consideration is given to the systematic synthesis and control of the structure of the materials in order to provide a precisely tailored set of properties for demanding applications [1]. It is now well recognized that the structure and constitution of advanced materials can be better controlled by processing them under non-equilibrium (or far-from-equilibrium) conditions [2]. Amongst many such processes, which are in commercial use, rapid solidification from the liquid state [3,4], mechanical alloying [5–9], plasma processing [2,10], and vapor deposition [2,11] have been receiving serious attention from researchers. The central underlying theme in all these techniques is to synthesize materials in a non-equilibrium state by "energizing and quenching" (Fig. 1). The energization involves bringing the material into a highly non-equilibrium (metastable) state by some external dynamical forcing, e.g., through melting, evaporation, irradiation, application of pressure, or storing of mechanical energy by plastic deformation [12]. Such materials are referred to as "driven materials" by Martin and Bellon [13]. The energization may also usually involve a possible change of state from the solid to liquid or gas. The material is then "quenched" into a configurationally frozen state, which can then be used as a precursor to obtain the desired chemical constitution and/or microstructure by subsequent heat treatment/processing. It has been shown that materials processed this way possess improved physical and mechanical characteristics in comparison with conventional ingot (solidification) processed materials.

The ability of the different processing techniques to synthesize metastable structures can be conveniently evaluated by measuring or estimating the departure from equilibrium, i.e., the maximum energy that can be stored in excess of that of

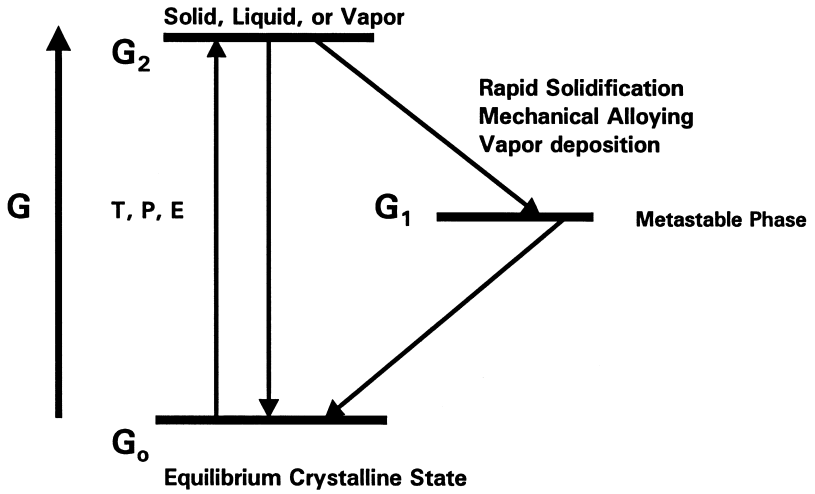

Fig. 1. The basic concept of "energize and quench" to synthesize non-equilibrium materials.

the equilibrium/stable structure. This has been done by different groups for different non-equilibrium processing techniques [12,14–16]. While the excess energy is expressed in kJ/mol in Refs. [14–16], Turnbull [12] expressed this as an "effective quenching rate". The way the departure is calculated is different in these different calculations and therefore the results do not correspond exactly in all the cases. However, it is clear that vapor deposition and ion implantation techniques have very large departures from equilibrium (or effective quench rates). It is also clear that mechanical alloying is a technique that allows the material to be processed much farther from equilibrium than, e.g., rapid solidification, which has been shown to have a tremendous potential in developing non-equilibrium materials [2–4]. Table 1 summarizes the departures calculated for the different processing techniques.

This present review article will discuss some of the recent advances that have occurred during the past few years in the synthesis of equilibrium and metastable alloy phases by a simple and inexpensive processing technique — mechanical alloying/milling of metal powders. The outline of the review will be as follows. In Section 2 of this review, we will briefly discuss the historical background that has led to the development of the technique. This will be followed by the nomenclature of the different mechanical alloying methods explored so far (Section 3) and then a description of the process, processing equipment, and process variables in Section 4. The mechanism of mechanical alloying will be discussed in Section 5 and Section 6 briefly describes the different methods of characterizing the mechanically alloyed powders. The temperature rise observed during milling of powders is discussed in Section 7. The synthesis of stable and metastable phases (supersaturated solid solutions and intermediate phases) are discussed in Sections 8 and 9, respectively. Disordering of ordered intermetallics is discussed in Section 10, while the synthesis of amorphous alloys by solid-state amorphization techniques is described in Section 11. Formation of nanostructured materials is considered in Section 12, while reduction of oxides, chlorides, etc. to pure metals and synthesis of nanocomposites by mechanochemical reactions is discussed in Section 13. The ubiquitous problem of powder contamination is

Table 1
Departure from equilibrium achieved in different non-equilibrium processing techniques

Technique	Effective quench rate (K/s)	Maximum departure from equilibrium (kJ/mol)	
	Ref. [12]	Ref. [14]	Refs. [15,16]
Solid state quench	10^3	–	16
Rapid solidification	10^5–10^8	2–3	24
Mechanical alloying	–	30	30
Mechanical cold work	–	–	1
Irradiation/ion implantation	10^{12}	–	30
Condensation from vapor	10^{12}	–	160

discussed in Section 14. Recent developments in understanding the process of mechanical alloying through modeling and milling maps is briefly described in Section 15. The applications of mechanically alloyed products are described in Section 16 and the problem of safety hazards in handling fine powders such as those produced by mechanical alloying are discussed in Section 17. The last Section will present the concluding remarks and possible future research directions in this area.

2. Historical perspective

Mechanical alloying (MA) is a powder processing technique that allows production of homogeneous materials starting from blended elemental powder mixtures. John Benjamin and his colleagues at the Paul D. Merica Research Laboratory of the International Nickel Company (INCO) developed the process around 1966. The technique was the result of a long search to produce a nickel-base superalloy, for gas turbine applications, that was expected to combine the high-temperature strength of oxide dispersion and the intermediate-temperature strength of gamma-prime precipitate. The required corrosion and oxidation resistance was also included in the alloy by suitable alloying additions. Benjamin [17–19] has summarized the historic origins of the process and the background work that led to the development of the present process.

In the early 1960s, INCO had developed a process for manufacturing graphitic aluminum alloys by injecting nickel-coated graphite particles into a molten aluminum bath by argon sparging. A modification of the same technique was tried to inoculate nickel-based alloys with a dispersion of nickel-coated, fine refractory oxide particles. The purpose of nickel coating was to render the normally unwetted oxide particles wettable by a nickel–chromium alloy. The early experiments used metal-coated zirconium oxide and this did not yield the desired result. A thorough analysis revealed that the reason for the failure of the experiment was because the vendor had supplied powder that was zirconia-coated nickel rather than nickel-coated zirconia. Since the reaction of aluminum with nickel produces a strong exothermic reaction, the heat generated cleansed the surface of the graphite and lowered the surface energy. On this basis, it was assumed that coating of the refractory oxide with aluminum would be ideal to produce the exothermic reaction. This also did not prove successful. When some other attempts also failed to yield the desired result, out of desperation, attention was turned to the ball milling process that had been used earlier to coat hard phases such as tungsten carbide with a soft phase such as cobalt or nickel. It was also known that metal powder particles could be fractured by subjecting them to heavy plastic deformation. Use of special chemicals could be employed to produce finer particles by preventing cold welding, suggesting that at some stage cold welding could be as rapid as fracturing. The reactivity of the element also had to be considered. Taking all these factors into consideration, Benjamin decided to produce composite powder particles by:

- using a high energy mill to favor plastic deformation required for cold welding and reduce the process times,
- using a mixture of elemental and master alloy powders (the latter to reduce the activity of the element, since it is known that the activity in an alloy or a compound could be orders of magnitude less than in a pure metal),
- eliminating the use of surface-active agents which would produce fine pyrophoric powder as well as contaminate the powder, and
- relying on a constant interplay between welding and fracturing to yield a powder with a refined internal structure, typical of very fine powders normally produced, but having an overall particle size which was relatively coarse, and therefore stable.

This method of making the composite powders reproduced the properties of TD (thoria dispersed) nickel synthesized by a completely different process. Encouraged by this success, experiments were conducted to produce a nickel–chromium–aluminum–titanium alloy containing a thoria dispersoid. This was also successfully produced, first in a small high-speed shaker mill and later in a one-gallon stirred ball mill, starting the birth of MA as a method to produce oxide dispersion strengthened (ODS) alloys on an industrial scale.

This process, as developed by Benjamin, was referred to as "milling/mixing", but Mr. Ewan C. MacQueen, a patent attorney for INCO coined the term *mechanical alloying* to describe the process in the first patent application, and this term has now come to stay in the literature.

Mechanical alloying is normally a dry, high-energy ball milling technique and has been employed to produce a variety of commercially useful and scientifically interesting materials. The formation of an amorphous phase by mechanical grinding of an Y–Co intermetallic compound in 1981 [20] and in the Ni–Nb system by ball milling of blended elemental powder mixtures in 1983 [21] brought about the recognition that MA is a potential non-equilibrium processing technique. Beginning from the mid-1980s, a number of investigations have been carried out to synthesize a variety of stable and metastable phases including supersaturated solid solutions, crystalline and quasicrystalline intermediate phases, and amorphous alloys [5–9]. Additionally, it has been recognized that powder mixtures can be mechanically activated to induce chemical reactions, i.e., mechanochemical reactions at room temperature or at least at much lower temperatures than normally required to produce pure metals, nanocomposites, and a variety of commercially useful materials [22,23]. Efforts were also under way since the early 1990s to understand the process fundamentals of MA through modeling studies [24]. Because of all these special attributes, this simple, but effective, processing technique has been applied to metals, ceramics, polymers, and composite materials. The attributes of mechanical alloying are listed in Table 2 and some important milestones in the development of the field are presented in Table 3.

The technique of MA to synthesize novel alloy phases and to produce oxide dispersion strengthened materials has attracted the attention of a large number of

Table 2
Attributes of mechanical alloying

Production of fine dispersion of second phase (usually oxide) particles
Extension of solid solubility limits
Refinement of grain sizes down to nanometer range
Synthesis of novel crystalline and quasicrystalline phases
Development of amorphous (glassy) phases
Disordering of ordered intermetallics
Possibility of alloying of difficult to alloy elements
Inducement of chemical (displacement) reactions at low temperatures
Scaleable process

researchers during the past 10 years or so. A number of stand-alone conferences have been organized on this topic [25–33]. Mechanical alloying has become an integral part of the triennial international conferences on Rapidly Quenched Metals (redesignated now as Rapidly Quenched and Metastable Materials) since RQ VI held in Montreal, Canada in 1987 [34–37]. Additionally, the proceedings of the International Symposia on Mechanically Alloyed, Metastable, and Nanocrystalline Materials (ISMANAM) contain many papers on mechanical alloying and these are regularly published in "Materials Science Forum" by Trans Tech Publications, Zürich, Switzerland [38–41]. A book on "Mechanical Alloying" has been recently published [8]. The literature on mechanical alloying and milling available between 1970 and 1994 has been collected together in an annotated bibliography published in 1995 [6]. A short-lived journal entitled "International Journal of Mechanochemistry and Mechanical Alloying" was started in 1994. Several reviews have also appeared over the past ten years with emphasis on a particular topic [42–50], but the present article is an attempt to review all aspects of MA in a comprehensive and critical manner at one place and present the potential and limitations of this technique as a non-equilibrium processing tool.

Table 3
Important milestones in the development of mechanical alloying

1966	Development of ODS nickel-base alloys
1981	Amorphization of intermetallics
1982	Disordering of ordered compounds
1983	Amorphization of blended elemental powder mixtures
1987/88	Synthesis of nanocrystalline phases
1989	Occurrence of displacement reactions
1989	Synthesis of quasicrystalline phases

3. Nomenclature

Two different terms are commonly used in the literature to denote the processing of powder particles in high-energy ball mills. *Mechanical Alloying* (MA) describes the process when mixtures of powders (of different metals or alloys/compounds) are milled together. Material transfer is involved in this process to obtain a homogeneous alloy. On the other hand, milling of uniform (often stoichiometric) composition powders, such as pure metals, intermetallics, or prealloyed powders, where material transfer is not required for homogenization, has been termed *Mechanical Milling* (MM). The destruction of long-range order in intermetallics to produce either a disordered intermetallic or an amorphous phase has been referred to as *Mechanical Disordering* (MD) [51]. The advantage of MM/MD over MA is that since the powders are already alloyed and only a reduction in particle size and/or other transformations need to be induced mechanically, the time required for processing is short. For example, MM requires half the time required for MA to achieve the same effect [52]. Additionally, MM of powders reduces oxidation of the constituent powders, related to the shortened time of processing [52]. Some investigators have referred to MM as *Mechanical Grinding* (MG). Since "grinding" is normally thought of as an abrasive machining process that involves mainly shear stresses and chip formation, the term "milling" is preferred to include the more complex triaxial, perhaps partly hydrostatic, stress states that can occur during ball milling of powders [5]. It should also be realized that MA is a generic term, and some investigators use this term to include both mechanical alloying and mechanical milling/disordering/grinding. However, we will distinguish between these two terms by using MA or MM depending on whether material transfer is involved or not during processing.

Some other terms are also used in the literature on Mechanical Alloying. These include reaction (or reactive ball) milling, cryomilling, rod milling, mechanically activated annealing (M2A), double mechanical alloying (dMA), and mechanically activated self-propagating high-temperature synthesis (MASHS).

Reaction Milling (RM) is the mechanical alloying process accompanied by a solid-state reaction and was pioneered by Jangg et al. [53]. In this process the powder is milled without the aid of any process control agent (see later for its function during milling) to produce fine dispersions of oxides and carbides in aluminum [54]. The dispersion of carbides is achieved by adding lamp-black or graphite during milling of aluminum. Adjusting the oxygen content via close control of the milling atmosphere (oxygen, argon, nitrogen, air, etc.) produces the oxides. Thus, the final product of milling contains a dispersion of Al_4C_3 and Al_2O_3 in an aluminum matrix and these alloys are given the trade name DISPAL. Milling of metal powders in the presence of reactive solids/liquids/gases (enabling a chemical reaction to take place) is now regularly employed to synthesize metal oxides, nitrides, and carbides [55,56]. Thus, milling of titanium in a nitrogen atmosphere has produced titanium nitride [57,58]. Several other compounds have also been produced in a similar way. Milling of tungsten with carbon (graphite) has produced tungsten carbide [59]. Milling of metal powders with boron has

produced borides, e.g., TiB_2 [60]. (Please see Section 9 for full details.) *Mechanochemical synthesis* of materials is the general name given to the process of milling of metal powders involving chemical reactions occurring during milling. These reactions can be used to reduce metal oxides and chlorides to pure metals, alloys, and compounds and now has become a large effort within the general field of mechanical alloying [23].

Another variation of milling that is being increasingly used now-a-days is *Cryomilling* [61] in which the milling operation is carried out at cryogenic (very low) temperatures and/or milling of materials is done in cryogenic media such as liquid nitrogen. Thus, when aluminum or aluminum alloys are cryomilled, this process produces 2–10 nm sized aluminum nitride or oxy-nitride particles that strengthen the aluminum matrix powder. It was noted that the powder quality was poor and the yield was low when cryomilling was conducted in a standard Szegvari-type attritor. Additionally, formation of dead zones in the tank, excessive powder loss due to liquid nitrogen evaporation and flow control, excessive seal wear, jamming of the stir arms, and freezing of the apparatus were some of the problems encountered. Aikin and Juhas [62] modified the attritor to minimize the above problems and reduce oxygen pick-up. These modifications improved the properties of the cryomilled product, including the homogeneity. They showed that by a proper choice of the process parameters it is possible to make materials with the desired AlN content in the powder.

Rod Milling is a technique that was developed in Japan [51] essentially to reduce the powder contamination during processing. In a conventional ball mill, impact forces scratch the surfaces of the milling media and the debris from the milling media contaminates the powder being milled. On the other hand, if shear forces predominate, they are more effective in kneading the powder mixtures and the resulting powder is much less contaminated. To achieve this, the balls were replaced by long rods in the rod mill [51] because long rods rotating in a cylindrical vial predominantly exert shear forces on the material. In fact, the level of impurity contamination for rod milling has been reported to be an order of magnitude less than for ball milling. (See Section 14 for details on the topic of powder contamination during milling).

Mechanically Activated Annealing (M2A) is a process that combines short mechanical alloying duration with a low-temperature isothermal annealing. The combination of these two steps has been found to be effective in producing different refractory materials such as silicides [63,64]. For example, MA of molybdenum and silicon powders for 1–2 h in a planetary ball mill followed by a 2- to 24-h annealing at 800°C produced the $MoSi_2$ phase [64]. A consequence of this method is that optimization of the M2A process could lead to a situation where the isothermal annealing can be carried out inside the milling container to avoid air contamination of the end-product.

Double Mechanical Alloying (dMA) involves two stages of milling. In the first stage, the constituent elemental powder sizes are refined and they are uniformly distributed as an intimate mixture. This mixture is then subjected to a heat treatment at high temperatures during which intermetallic phases are formed. The

size of the intermetallics ranges from <1 μm to a few μm. During the second stage, the heat treated powder is milled again to refine the intermetallics and reduce the grain size of the matrix. After degassing, the powders are consolidated to a bulk shape [65,66]. Fig. 2 shows the flow-sheet of the dMA process and the type of microstructures developed in an Al–5wt%Fe–4wt%Mn powder mixture [66]. This appears to be a useful process to produce fine intermetallics in alloy systems that cannot be directly produced by milling.

Yet another term recently coined is *Mechanically Activated Self-propagating High-temperature Synthesis* (MASHS), which is based on a combination of mechanical alloying (MA) and self-propagating high-temperature synthesis (SHS). In this process the powder mixture is mechanically alloyed to produce a nanocrystalline structure and then the SHS reaction is initiated by pressing the powder into a pellet and igniting it in a furnace. The prior MA step decreases the ignition temperature by as much as 100°C. Several iron aluminide and niobium aluminide intermetallics were synthesized by this method [67,68].

4. The process of mechanical alloying

The actual process of MA starts with mixing of the powders in the right proportion and loading the powder mix into the mill along with the grinding medium (generally steel balls). This mix is then milled for the desired length of time until a steady state is reached when the composition of every powder particle is the same as the proportion of the elements in the starting powder mix. The milled powder is then consolidated into a bulk shape and heat treated to obtain the desired microstructure and properties. Thus the important components of the MA process are the raw materials, the mill, and the process variables. We will now discuss the different parameters involved in the selection of raw materials, types of mills, and process variables.

4.1. Raw materials

The raw materials used for MA are widely available commercially pure powders that have particle sizes in the range of 1–200 μm. But, the powder particle size is not very critical, except that it should be smaller than the grinding ball size. This is because the powder particle size decreases exponentially with time and reaches a small value of a few microns only after a few minutes of milling. The raw powders fall into the broad categories of pure metals, master alloys, prealloyed powders, and refractory compounds. Dispersion strengthened materials usually contain additions of carbides, nitrides, and oxides. Oxides are the most common and these alloys are known as oxide-dispersion strengthened (ODS) materials. In the early days of MA, the powder charge consisted of at least 15 vol% of a ductile compressibly deformable metal powder to act as a host or a binder. However, in recent years, mixtures of fully brittle materials have been milled successfully resulting in alloy formation [5]. Thus, the requirement of having a ductile metal

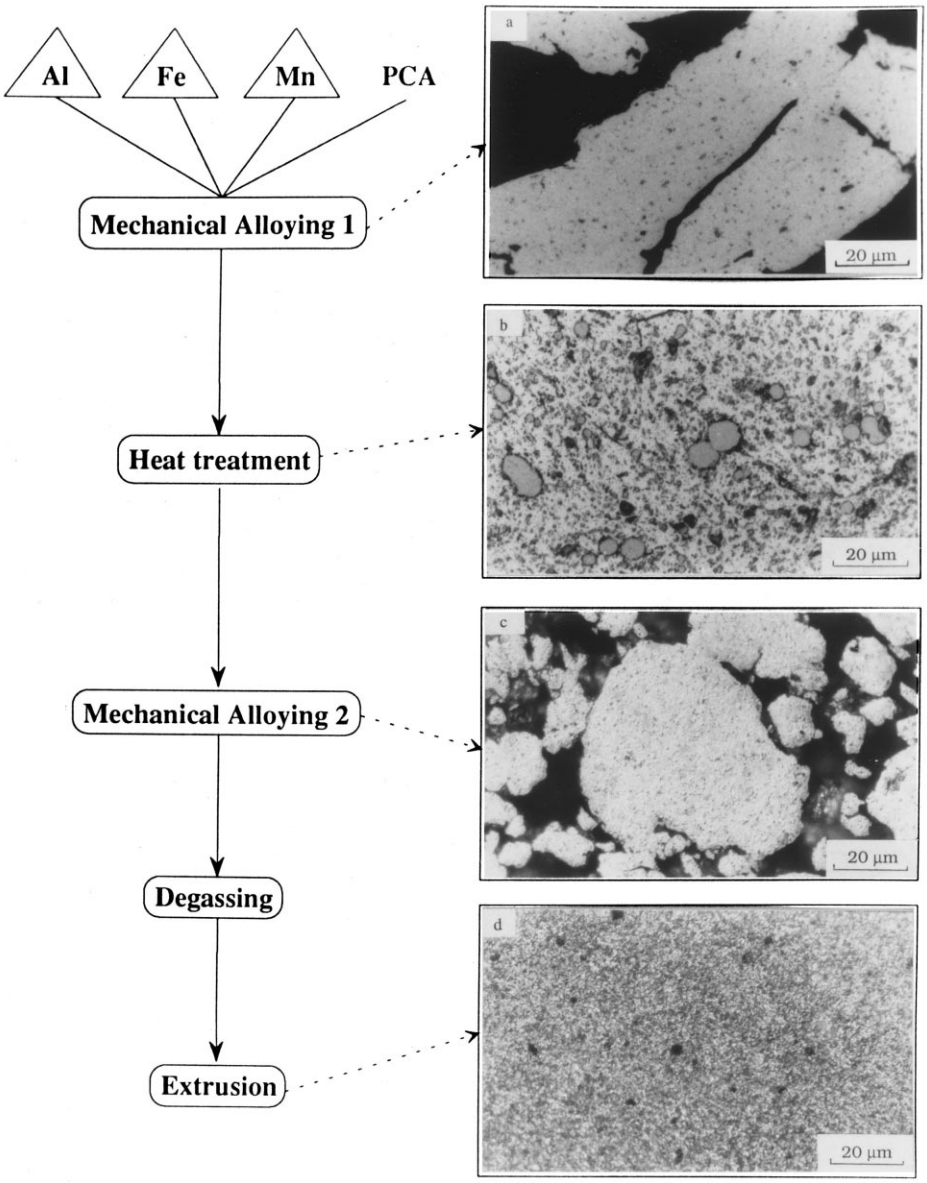

Fig. 2. Process flowsheet and the microstructures developed during double mechanical alloying (dMA) of an Al–5wt%Fe–4wt%Mn powder mixture.

powder during milling is no longer necessary. Accordingly, ductile–ductile, ductile–brittle, and brittle–brittle powder mixtures are milled to produce novel alloys. Mixtures of solid powder particles and liquids have also been milled in recent times [69,70].

Occasionally, metal powders are milled with a liquid medium and this is referred to as wet grinding [71–73]; if no liquid is involved then it is referred to as dry grinding. (Cryomilling also is wet grinding if the liquid used is at cryogenic temperatures). It has been reported that wet grinding is a more suitable method than dry grinding to obtain finer-ground products because the solvent molecules are adsorbed on the newly formed surfaces of the particles and lower their surface energy. The less-agglomerated condition of the powder particles in the wet condition is also a useful factor. It has been reported that the rate of amorphization is faster during wet grinding than during dry grinding [74]. A disadvantage of the wet grinding, however, is the increased contamination of the powder. Thus, most of the MA/MM operations have been carried out dry. Additionally, dry grinding has been found to be more efficient than wet grinding in the decomposition of $Cu(OH)_2$ to Cu [75].

4.2. Types of mills

Different types of high-energy milling equipment are used to produce mechanically alloyed powders. They differ in their capacity, efficiency of milling and additional arrangements for cooling, heating, etc. A detailed description of the different mills available for MA can be found in Ref. [76]; a brief description is provided below.

4.2.1. SPEX shaker mills

Shaker mills such as SPEX mills (Fig. 3a), which mill about 10–20 g of the powder at a time, are most commonly used for laboratory investigations and for alloy screening purposes. These mills are manufactured by SPEX CertPrep, Metuchen, NJ. The common variety of the mill has one vial, containing the sample and grinding balls, secured in the clamp and swung energetically back and forth several thousand times a minute. The back-and-forth shaking motion is combined with lateral movements of the ends of the vial, so that the vial appears to be describing a figure 8 or infinity sign as it moves. With each swing of the vial the balls impact against the sample and the end of the vial, both milling and mixing the sample. Because of the amplitude (about 5 cm) and speed (about 1200 rpm) of the clamp motion, the ball velocities are high (on the order of 5 m/s) and consequently the force of the ball's impact is unusually great. Therefore, these mills can be considered as high-energy variety.

The most recent design of the mills has provision for simultaneously milling the powder in two vials to increase the throughput. This machine incorporates forced cooling to permit extended milling times. A variety of vial materials is available for the SPEX mills and these include hardened steel, alumina, tungsten carbide, zirconia, stainless steel, silicon nitride, agate, plastic, and methacrylate. A typical

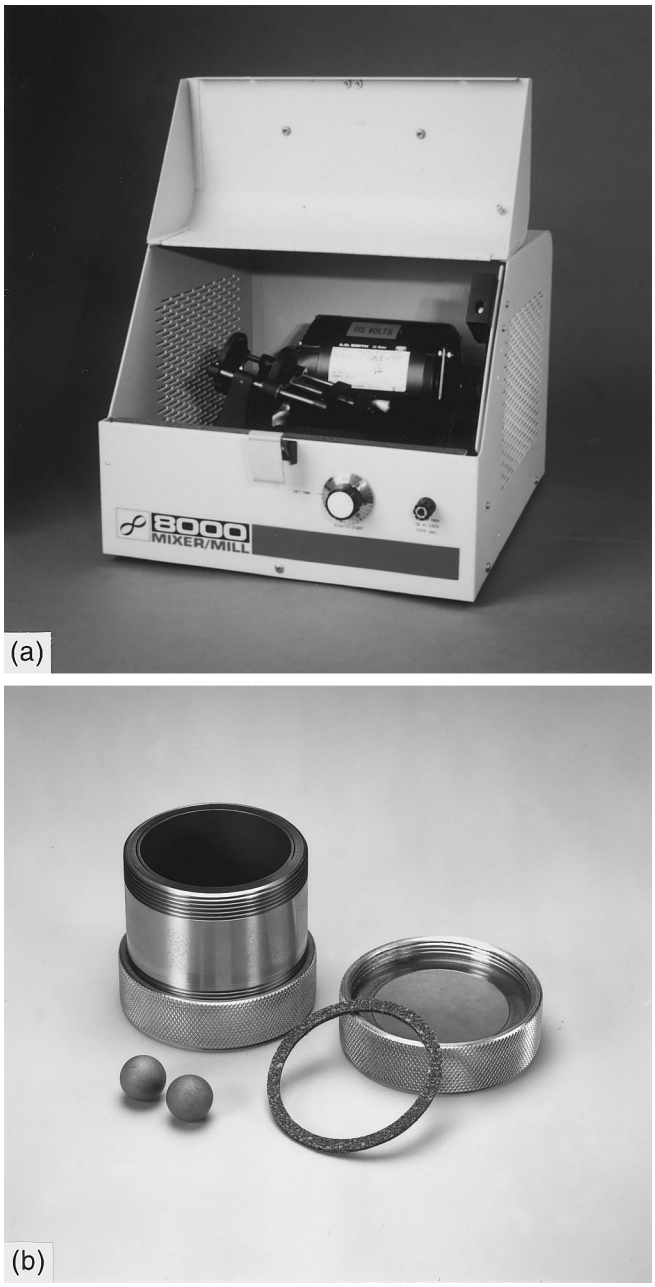

Fig. 3. (a) SPEX 8000 mixer/mill in the assembled condition. (b) Tungsten carbide vial set consisting of the vial, lid, gasket, and balls. Courtesy of SPEX CertiPrep, Metuchen, NJ.

example of a tungsten carbide vial, gasket and grinding balls for the SPEX mill is shown in Fig. 3b. Majority of the research on the fundamental aspects of MA has been carried out using some version of these SPEX mills.

4.2.2. Planetary ball mills

Another popular mill for conducting MA experiments is the planetary ball mill (referred to as Pulverisette) in which a few hundred grams of the powder can be milled at a time (Fig. 4a). These are manufactured by Fritsch GmbH in Germany and marketed by Gilson Co., in the US and Canada. The planetary ball mill owes its name to the planet-like movement of its vials. These are arranged on a rotating support disk and a special drive mechanism causes them to rotate around their own axes. The centrifugal force produced by the vials rotating around their own axes and that produced by the rotating support disk both act on the vial contents, consisting of material to be ground and the grinding balls. Since the vials and the supporting disk rotate in opposite directions, the centrifugal forces alternately act in like and opposite directions. This causes the grinding balls to run down the inside wall of the vial — the friction effect, followed by the material being ground and grinding balls lifting off and traveling freely through the inner chamber of the vial and colliding against the opposing inside wall — the impact effect (Fig. 4b).

Even though the disk and the vial rotation speeds could not be independently controlled in the earlier versions, it is possible to do so in the modern versions. In a single mill one can have either two (Pulverisette 5 or 7) or four (Pulverisette 5) milling stations. Recently, a single-station mill was also developed (Pulverisette 6). Grinding vials and balls are available in eight different materials — agate, silicon nitride, sintered corundum, zirconia, chrome steel, Cr–Ni steel, tungsten carbide, and plastic polyamide. Even though the linear velocity of the balls in this type of mill is higher than that in the SPEX mills, the frequency of impacts is much more in the SPEX mills. Hence, in comparison to SPEX mills, Fritsch Pulverisette can be considered lower energy mills.

4.2.3. Attritor mills

A conventional ball mill consists of a rotating horizontal drum half-filled with small steel balls. As the drum rotates the balls drop on the metal powder that is being ground; the rate of grinding increases with the speed of rotation. At high speeds, however, the centrifugal force acting on the steel balls exceeds the force of gravity, and the balls are pinned to the wall of the drum. At this point the grinding action stops. An attritor (a ball mill capable of generating higher energies) consists of a vertical drum with a series of impellers inside it. Set progressively at right angles to each other, the impellers energize the ball charge, causing powder size reduction because of impact between balls, between balls and container wall, and between balls, agitator shaft, and impellers. Some size reduction appears to take place by interparticle collisions and by ball sliding. A powerful motor rotates the impellers, which in turn agitate the steel balls in the drum.

Attritors are the mills in which large quantities of powder (from about 0.5 to 40

kg) can be milled at a time (Fig. 5a). Commercial attritors are available from Union Process, Akron, OH. The velocity of the grinding medium is much lower (about 0.5 m/s) than in Fritsch or SPEX mills and consequently the energy of the attritors is low. Attritors of different sizes and capacities are available. The

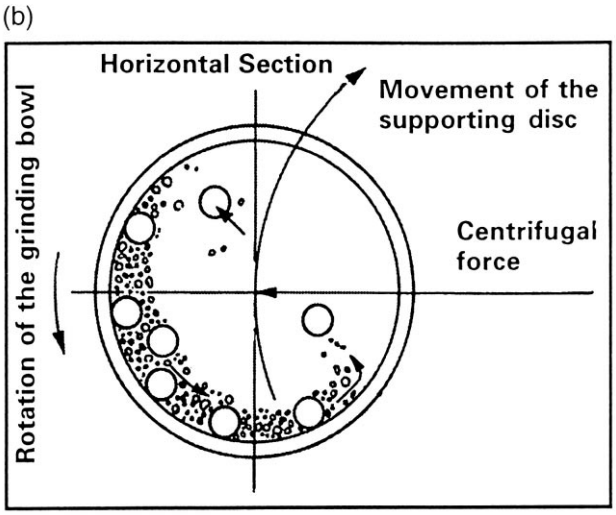

Fig. 4. (a) Fritsch Pulverisette P-5 four station ball mill. (b) Schematic depicting the ball motion inside the ball mill. Courtesy of Gilson Company, Inc., Worthington, OH.

grinding tanks or containers are available either in stainless steel or stainless steel coated inside with alumina, silicon carbide, silicon nitride, zirconia, rubber, and polyurethane. A variety of grinding media also is available — glass, flint stones, steatite ceramic, mullite, silicon carbide, silicon nitride, sialon, alumina, zirconium silicate, zirconia, stainless steel, carbon steel, chrome steel, and tungsten carbide.

The operation of an attritor is simple. The powder to be milled is placed in a stationary tank with the grinding media. This mixture is then agitated by a shaft with arms, rotating at a high speed of about 250 rpm (Fig. 5b). This causes the

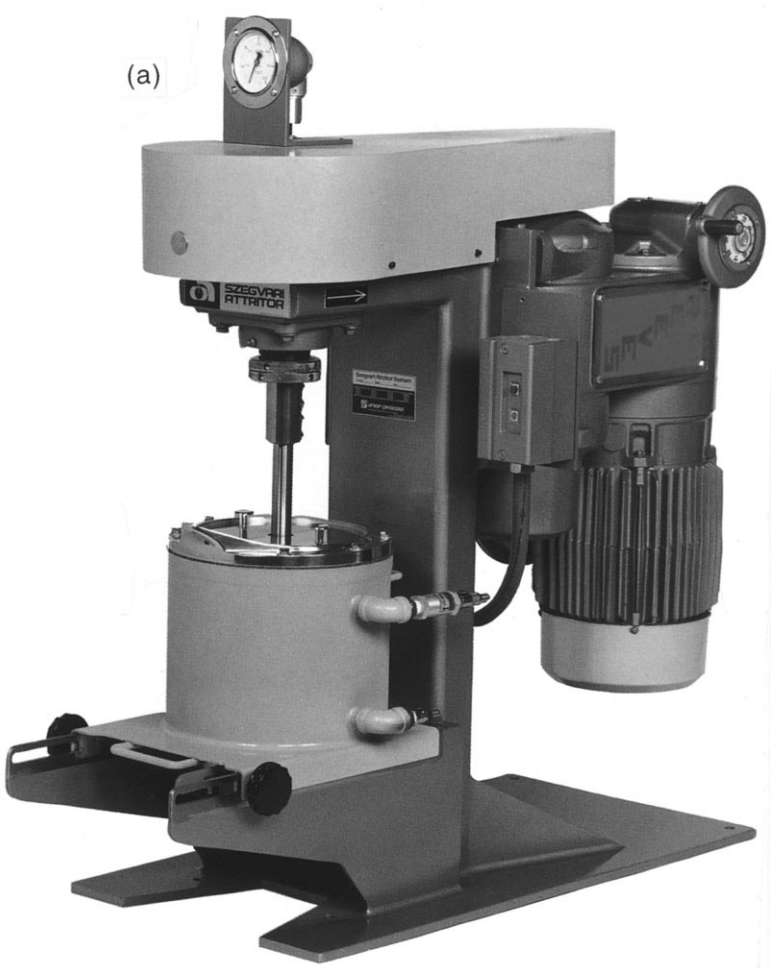

Fig. 5. (a) Model 1-S attritor. (b) Arrangement of rotating arms on a shaft in the attrition ball mill. Courtesy of Union Process, Akron, OH.

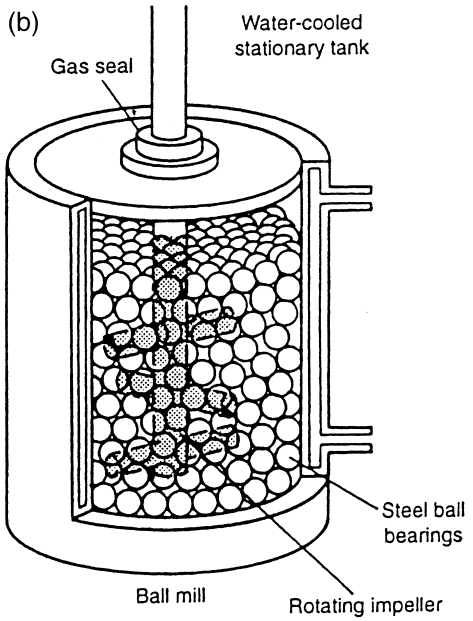

Fig. 5 (*continued*)

media to exert both shearing and impact forces on the material. The laboratory attritor works up to 10 times faster than conventional ball mills.

4.2.4. Commercial mills

Commercial mills for MA are much larger in size than the mills described above and can process several hundred pounds at a time. Mechanical alloying for commercial production is carried out in ball mills of up to about 3000 lb (1250 kg) capacity (Fig. 6).

The milling time decreases with an increase in the energy of the mill. It has been reported that 20 min of milling in a SPEX mill is equivalent to 20 h of milling in a low-energy mill of the type Invicta BX 920/2 [77]. As a rule of thumb, it can be estimated that a process that takes only a few minutes in the SPEX mill may take hours in an attritor and a few days in a commercial mill even though the details can be different depending on the efficiency of the different mills. Fig. 7 shows the times required to reach a specific particle size during milling in a planetary ball mill and an attritor. It may be noted that the times are an order of magnitude shorter in the attritor [78].

4.2.5. New designs

Several new designs of mills have been developed in recent years for specialized purposes. These include the rod mills, vibrating frame mills, and the equipment available from Dymatron, Cincinnati, OH; Super Misuni NEV-MA-8 from

Nisshin Giken, Tokyo, Japan (with the ability to control the temperature of milling from very low temperatures by spraying liquid nitrogen up to a high temperature of 300°C by electrical heating); Uni-Ball-Mill from Australian Scientific Instruments, Canberra, Australia (it is possible to control the nature and magnitude of impact of the balls in this machine by controlling the field strength with the help of adjustable magnets); HEMill from M.B.N. srl, Rome, Italy; and Zoz Maschinenbau GmbH, Kreuztal, Germany. Some special equipment is also designed for specific laboratory applications.

Bakker et al. [48] use a mill in which a large ball is placed together with the sample inside a vibrating spherical-like vessel. This mill has a low efficiency since the ball is moving from one side to another and the specimen gets milled only during the collisions with long repetition time. On the other hand, the shaker mills, e.g., SPEX mills, have a much higher efficiency. But, even in these mills, several non-head-on collisions occur, thus reducing the maximum possible

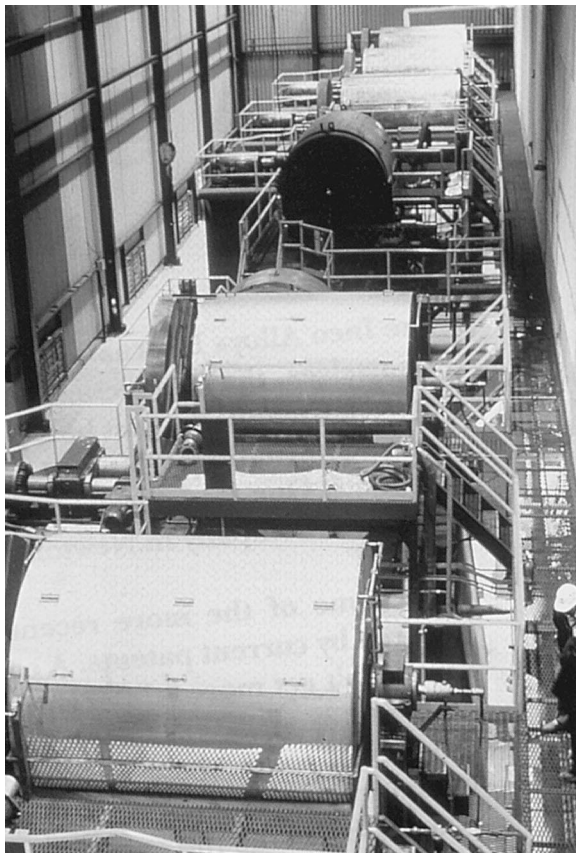

Fig. 6. Commercial production-size ball mills used for mechanical alloying. Courtesy of Inco Alloys International.

efficiency. Further, because of friction, the surface of the grinding medium gets eroded and contaminates the sample. To overcome this problem, Szymański et al. [79] designed a friction-free mechanical grinder. This grinder consists of seven steel rods (10 mm in diameter and 100 mm in height) arranged in a hexagonal motif with one rod in the center. These rods stand in a vertical position between a pair of parallel, horizontal steel anvils separated by a distance of 116 mm. The device moves up and down with an amplitude of 3.5 mm and a frequency of 25 Hz. This device is claimed to have a low contamination of the milled powder.

Taking into consideration that a high-energy ball mill should have high impact velocities and high impact frequencies of the grinding media, one can easily design a new mill for any specific purpose. For example, Basset et al. [80] and Kimura et al. [81] designed special high-energy ball mills to produce nanocrystalline materials and amorphous alloys, respectively. One could also design mills of higher capacity to produce large quantities of the mechanically alloyed powder at a time, or increase the productivity by increasing the MA speed (or reducing the MA times) [82].

The operating details and special features of the commercially available mills can be found in the respective brochures of the manufacturers.

Table 4 summarizes the capacities of the different mills for mechanical alloying/milling that are commercially available [83].

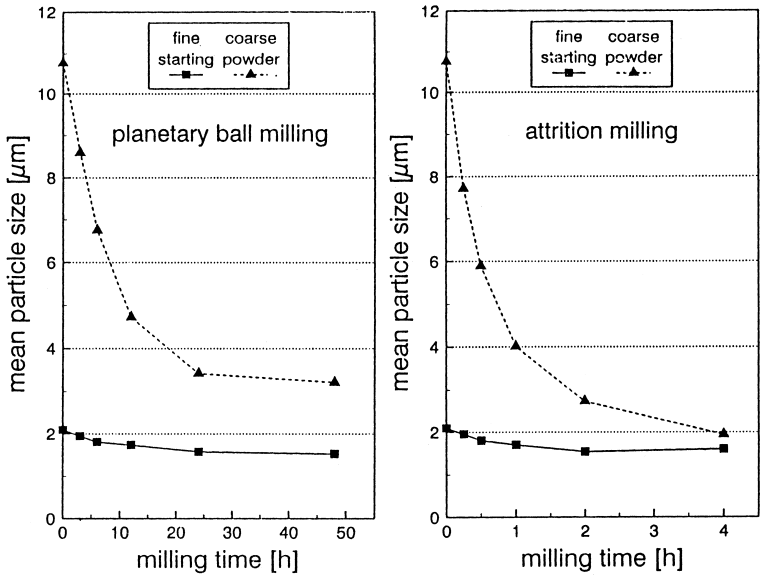

Fig. 7. Time to reach similar particle sizes during milling of TiB_2 powder in (a) planetary ball mill and (b) attritor.

4.3. Process variables

Mechanical alloying is a complex process and hence involves optimization of a number of variables to achieve the desired product phase and/or microstructure. Some of the important parameters that have an effect on the final constitution of the powder are:

- type of mill,
- milling container,
- milling speed,
- milling time,
- type, size, and size distribution of the grinding medium,
- ball-to-powder weight ratio,
- extent of filling the vial,
- milling atmosphere,
- process control agent, and
- temperature of milling.

All these process variables are not completely independent. For example, the optimum milling time depends on the type of mill, size of the grinding medium, temperature of milling, ball-to-powder ratio, etc. Even then, we will discuss, in the following paragraphs, the effect of these variables (Assuming mostly that other variables have no significant effect on the specific variable being discussed) on the final product obtained after MA.

4.3.1. Type of mill

As described above (Section 4.2) there are a number of different types of mills for conducting MA. These mills differ in their capacity, speed of operation, and their ability to control the operation by varying the temperature of milling and the extent of minimizing the contamination of the powders. Depending on the type of powder, the quantity of the powder, and the final constitution required, a suitable mill can be chosen. Most commonly, however, the SPEX shaker mills are used for alloy screening purposes. The Fritsch Pulverisette planetary ball mills or the attritors are used to produce large quantities of the milled powder. Specially designed mills are used for specific applications.

Table 4
Typical capacities of the different types of mills [83]

Mill type	Sample weight
Mixer mills	Up to 2×20 g
Planetary mills	Up to 4×250 g
Attritors	0.5–100 kg
Uni-ball mill	Up to 4×2000 g

4.3.2. Milling container

The material used for the milling container (grinding vessel, vial, jar, or bowl are some of the other terms used) is important since due to impact of the grinding medium on the inner walls of the container, some material will be dislodged and get incorporated into the powder. This can contaminate the powder or alter the chemistry of the powder. If the material of the grinding vessel is different from that of the powder, then the powder may be contaminated with the grinding vessel material. On the other hand, if the two materials are the same, then the chemistry may be altered unless proper precautions are taken to compensate for the additional amount of the element incorporated into the powder. Hardened steel, tool steel, hardened chromium steel, tempered steel, stainless steel, WC–Co, WC-lined steel [84], and bearing steel are the most common types of materials used for the grinding vessels. Some specific materials are used for specialized purposes; these include copper [85], titanium [86], sintered corundum, yttria-stabilized zirconia (YSZ) [87], partially stabilized zirconia + yttria [88,89], sapphire [90,91], agate [92–94], hard porcelain, Si_3N_4 [95], and Cu–Be [96–100]. The shape of the container also seems to be important, especially the internal design of the container. Both flat-ended and round-ended SPEX mill containers have been used. Alloying was found to occur at significantly higher rates in the flat-ended vial than in the round-ended container [101]. The time required to reach a constant intensity and shape of the (111) peak in the X-ray diffraction pattern of the Si–Ge mixture was 9 h for the flat-ended vial and 15 h in the round-ended vial.

4.3.3. Milling speed

It is easy to realize that the faster the mill rotates the higher would be the energy input into the powder. But, depending on the design of the mill there are certain limitations to the maximum speed that could be employed. For example, in a conventional ball mill increasing the speed of rotation will increase the speed with which the balls move. Above a critical speed, the balls will be pinned to the inner walls of the vial and do not fall down to exert any impact force. Therefore, the maximum speed should be just below this critical value so that the balls fall down from the maximum height to produce the maximum collision energy.

Another limitation to the maximum speed is that at high speeds (or intensity of milling), the temperature of the vial may reach a high value. This may be advantageous in some cases where diffusion is required to promote homogenization and/or alloying in the powders. But, in some cases, this increase in temperature may be a disadvantage because the increased temperature accelerates the transformation process and results in the decomposition of supersaturated solid solutions or other metastable phases formed during milling [102]. Additionally, the high temperatures generated may also contaminate the powders. It has been reported that during nanocrystal formation, the average crystal size increases and the internal strain decreases at higher milling intensities due to the enhanced dynamical recrystallization [103]. The maximum temperature reached is different in different types of mills and the values vary widely. (This aspect will be discussed in detail in Section 7.)

Calka et al. [104] reported that when vanadium and carbon powders were milled together at different energy levels (by adjusting the positions of the magnets in the Uni-Ball mill), the final constitution of the powder was different. For example, at very low milling energy (or speed), the powder consisted of nanometer-sized grains of vanadium and amorphous carbon, which on annealing formed either V_2C or a mixture of V + VC. At intermediate energy level, the as-milled powder contained a nanostructure, which on annealing transformed to VC. At the highest energy level, the VC formed directly on milling. Similarly, a fully amorphous phase formed in a Ni–Zr powder mixture at high energy of milling whereas a mixture of crystalline and amorphous phases formed at low and intermediate milling energies [105].

4.3.4. Milling time

The time of milling is the most important parameter. Normally the time is so chosen as to achieve a steady state between the fracturing and cold welding of the powder particles. The times required vary depending on the type of mill used, the intensity of milling, the ball-to-powder ratio, and the temperature of milling. These times have to be decided for each combination of the above parameters and for the particular powder system. But, it should be realized that the level of contamination increases and some undesirable phases form if the powder is milled for times longer than required [58]. Therefore, it is desirable that the powder is milled just for the required duration and not any longer.

4.3.5. Grinding medium

Hardened steel, tool steel, hardened chromium steel, tempered steel, stainless steel, WC–Co, and bearing steel are the most common types of materials used for the grinding medium. The density of the grinding medium should be high enough so that the balls create enough impact force on the powder. However, as in the case of the grinding vessel, some special materials are used for the grinding medium and these include copper [85], titanium [86], niobium [106], zirconia (ZrO_2) [107,108], agate [93,94], yttria stabilized zirconia (YSZ) [87], partially stabilized zirconia + yttria [88,89], sapphire [91], silicon nitride (Si_3N_4) [95], and Cu–Be [100]. It is always desirable, whenever possible, to have the grinding vessel and the grinding medium made of the same material as the powder being milled to avoid cross contamination.

The size of the grinding medium also has an influence on the milling efficiency. Generally speaking, a large size (and high density) of the grinding medium is useful since the larger weight of the balls will transfer more impact energy to the powder particles. It has also been reported that the final constitution of the powder is dependent upon the size of the grinding medium used. For example, when balls of 15 mm diameter were used to mill the blended elemental Ti–Al powder mixture, a solid solution of aluminum in titanium was formed. On the other hand, use of 20 and 25 mm diameter balls resulted in a mixture of only the titanium and aluminum phases, even after a long milling duration [8]. In another set of investigations [109,110] it has been reported that an amorphous phase could

be produced faster in Ti–Al alloys by using steel balls of 3/16″ diameter than by using balls of 3/4″ diameter. In fact, in some cases, an amorphous phase was not produced and only the stable crystalline compound formed when milling was done with large steel balls [109]. In yet another investigation it was reported that an amorphous phase formed only when the Ti–Al powder mixture was milled using either 5 or 8 mm diameter balls; an amorphous phase did not form when 12 mm diameter balls were used for milling [110,111]. A similar situation was also reported in the Pd–Si system where it was reported that a smaller ball size favored amorphous phase formation [112]. It was suggested that the smaller balls produced intense frictional action, which promoted the amorphous phase formation. In fact, it appears that "soft" milling conditions (small ball sizes, lower energies, and lower ball-to-powder ratios) seem to favor amorphization or metastable phase formation [85,111,113,114].

Even though most of the investigators generally use only one size of the grinding medium, there have been instances when different sized balls have been used in the same investigation [115]. It has been predicted that the highest collision energy can be obtained if balls with different diameters are used [116]. In the initial stages of milling, the powder being milled gets coated onto the surface of the grinding medium and also gets cold welded. This is advantageous since it prevents excessive wear of the grinding medium and also avoids contamination of the powder due to the wear of the grinding medium. However, the thickness of this layer must be kept to a minimum to avoid formation of a heterogeneous final product [42]. But, the disadvantage of this powder coating is that it is difficult to detach this powder and so the powder yield is low. It has been reported that a combination of large and small size balls during milling minimizes the amount of cold welding and the amount of powder coated onto the surface of the balls [117]. Although no specific explanation has been given for the improved yield under these conditions, it is possible that the different sized balls produce shearing forces that may help in detaching the powder from the surface of the balls.

Use of grinding balls of the same size in either a round or a flat bottom vial has been shown to produce tracks. Consequently, the balls roll along a well-defined trajectory instead of hitting the end surfaces randomly. Therefore it is necessary to use several balls, generally a combination of smaller and larger balls to "randomize" the motion of the balls [118].

4.3.6. Ball-to-powder weight ratio

The ratio of the weight of the balls to the powder (BPR), sometimes referred to as charge ratio (CR), is an important variable in the milling process. This has been varied by different investigators from a value as low as 1:1 [119] to as high as 220:1 [120]. Generally speaking, a ratio of 10:1 is most commonly used while milling the powder in a small capacity mill such as a SPEX mill. But, when milling is conducted in a large capacity mill, like an attritor, a higher BPR of up to 50:1 or even 100:1 is used.

The BPR has a significant effect on the time required to achieve a particular phase in the powder being milled. The higher the BPR, the shorter is the time

required. For example, formation of an amorphous phase was achieved in a Ti–33at%Al powder mixture milled in a SPEX mill in 7 h at a BPR of 10:1, in 2 h at a BPR of 50:1 and in 1 h at a BPR of 100:1 [121]. At a high BPR, because of an increase in the weight proportion of the balls, the number of collisions per unit time increases and consequently more energy is transferred to the powder particles and so alloying takes place faster. Several other investigators also have reported similar results. It is also possible that due to the higher energy, more heat is generated and this could also change the constitution of the powder. The amorphous phase formed may even crystallize if the temperature rise is substantial.

As mentioned earlier, "soft" conditions (e.g., low BPR values, low speeds of rotation, etc.) of MA produce metastable phases whereas "hard" conditions produce the equilibrium phases. This was first very clearly demonstrated in the Zr–Co system when an amorphous phase was obtained under "soft" milling conditions, while a mixture of the equilibrium crystalline phases was obtained under "hard" milling conditions [113]. Similar results were also reported for other alloy systems [85,111,114]. For example, a metastable cubic phase was formed at low BPR, while the stable equilibrium tetragonal phase was formed at higher BPR in the mechanically alloyed Cu–In–Ga–Se powder system [85].

4.3.7. Extent of filling the vial

Since alloying among the powder particles occurs due to the impact forces exerted on them, it is necessary that there is enough space for the balls and the powder particles to move around freely in the milling container. Therefore, the extent of filling the vial with the powder and the balls is important. If the quantity of the balls and the powder is very small, then the production rate is very small. On the other hand, if the quantity is large, then there is not enough space for the balls to move around and so the energy of the impact is less. Thus, care has to be taken not to overfill the vial; generally about 50% of the vial space is left empty.

4.3.8. Milling atmosphere

The major effect of the milling atmosphere is on the contamination of the powder. Therefore, the powders are milled in containers that have been either evacuated or filled with an inert gas such as argon or helium. (Nitrogen has been found to react with metal powders and consequently it cannot be used to prevent contamination during milling, unless one is interested in producing nitrides.) High-purity argon is the most common ambient to prevent oxidation and/or contamination of the powder. It has also been noted that oxidation can be generally prevented or minimized in the presence of a nitrogen ambient. But, this does not appear to be true when reactive powders such as titanium or its alloy powders are milled. It has been reported that a Ti–48Al–2W (at%) powder milled in an oxygen atmosphere picked up 1.5 wt% oxygen after 20 h of milling. The same powder milled for the same length of time, but in a nitrogen atmosphere, picked up 4.7 wt% oxygen [122]; a difficult to explain observation.

Normally, the loading and unloading of the powders into the vial is carried out

inside atmosphere-controlled glove boxes. These glove boxes are usually repeatedly evacuated and refilled with the argon gas. Some investigators have even conducted the milling operation in mills that have been placed inside the evacuated glove boxes.

Different atmospheres have been used during milling for specific purposes. Nitrogen or ammonia atmospheres have been used to produce nitrides [123,124]. Hydrogen atmosphere was used to produce hydrides [125]. The presence of air in the vial has been shown to produce oxides and nitrides in the powder, especially if the powders are reactive in nature. Thus, care has to be taken to use an inert atmosphere during milling.

The type of atmosphere also seems to affect the nature of the final phase. For example, it has been shown that when Cr–Fe powder mixtures were milled in different types of atmosphere, the constitution of the final powder was different [126]. When the powder was milled in an argon atmosphere, no amorphous phase formed and Cr peaks remained in the X-ray diffraction pattern. On the other hand, when the powder was milled in either air containing argon or a nitrogen atmosphere, the powder became completely amorphous. Similarly, oxygen was shown to enhance the kinetics of amorphization in the Ni–Nb system [127].

4.3.9. Process control agents

The powder particles get cold-welded to each other, especially if they are ductile, due to the heavy plastic deformation experienced by them during milling. But, true alloying among powder particles can occur only when a balance is maintained between cold welding and fracturing of particles. A process control agent (PCA) (also referred to as lubricant or surfactant) is added to the powder mixture during milling to reduce the effect of cold welding. The PCAs can be solids, liquids, or gases. They are mostly, but not necessarily, organic compounds, which act as surface-active agents. The PCA adsorbs on the surface of the powder particles and minimizes cold welding between powder particles and thereby inhibits agglomeration. The surface-active agents adsorbed on particle surfaces interfere with cold welding and lower the surface tension of the solid material. Since the energy required for the physical process of size reduction, E is given by

$$E = \gamma \cdot \Delta S \tag{1}$$

where γ is the specific surface energy and ΔS is the increase of surface area, a reduction in surface energy results in the use of shorter milling times and/or generation of finer powders.

A wide range of PCAs has been used in practice at a level of about 1–5 wt% of the total powder charge. The most important of the PCAs include stearic acid, hexane, methanol, and ethanol. A partial listing of the PCAs used in different investigations and their quantities is presented in Table 5. Additionally, other exotic PCAs such as sodium-1,2-bis-(dodecyl carbonyl)ethane-1-sulfonate, lithium-1,2-bis-dodecyloxy carbonyl sulfasuccinate, diodecyl dimethyl ammonium acetate (DDAA), didocyldimethyl ammonium bromide (DDAB), trichlorotrifluoroethane,

Table 5
Process control agents (PCAs) and the quantities used in different investigations

PCA	Chemical formula	Quantity	Selected reference
Benzene	C_6H_6	–	[128,129]
C wax	$H_{35}C_{17}CONHC_2H_4NHCOC_{17}H_{35}$	1.5 wt%	[130]
Didodecyl dimethyl ammonium acetate (DDAA)	$C_{28}H_{59}NO_2$	–	[131]
Dihexadecyl dimethyl ammonium acetate (DHDAA)	$C_{36}H_{75}NO_2$	–	[131]
Dodecane	$CH_3(CH_2)_{10}CH_3$	–	[132]
Ethanol	C_2H_5OH	4 wt%	[133]
Ethyl acetate	$CH_3CO_2C_2H_5$	–	[65]
Ethylenebisdistearamide Nopcowax-22 DSP	$C_2H_2–2(C_{18}H_{36}ON)$	2 wt%	[134]
Graphite	C	0.5 wt%	[65,135]
Heptane	$CH_3(CH_2)_5CH_3$	0.5 wt%	[136,137]
Hexane	$CH_3(CH_2)_4CH_3$	–	[128,131,138–140]
		5 wt%	[141]
Lithium-1,2-bis-dodecyloxy carbonyl sulfasuccinate	–	–	[131]
Methanol	CH_3OH	–	[142–146]
		1 wt%	[147]
		3 wt%	[148]
		4 wt%	[149]
Octane	$CH_3(CH_2)_6CH_3$	1 wt%	[150]
Paraffin	–	–	[82]
Polyethylene glycol	$H(OCH_2CH_2)_nOH$	–	[151]
Silicon grease	–	–	[82]
Sodium chloride	NaCl	2 wt%	[152]
Sodium-1,2-bis(dodecyl carbonyl)ethane-1-sulfonate	–	–	[131]
Stearic acid	$CH_3(CH_2)_{16}COOH$	1 wt%	[153–156]
Tetrahydrofuran	–	–	[128]
Toluene	$C_6H_5CH_3$	5 ml	[23,157,158]

and others such as polyethylene glycol, dodecane, ethyl acetate, oxalic acid, boric acid, borax, alumina, and aluminum nitrate have also been used. Majority of these compounds decompose during milling, interact with the powder and form compounds, and these get incorporated in the form of inclusions and/or dispersoids into the powder particles during milling. Thus hydrocarbons containing hydrogen and carbon, and carbohydrates containing hydrogen, carbon, and oxygen are likely to introduce carbon and/or oxygen into the powder particles, resulting in the formation of carbides and oxides which are uniformly dispersed in the matrix. These are not necessarily harmful to the alloy system since they can contribute to dispersion strengthening of the material resulting in increased strength and higher hardness [159]. The hydrogen subsequently escapes as a gas or is absorbed into the metal lattice on heating or sintering. Even though hydrogen gas primarily serves as a surfactant and does not usually participate in the alloying process [160], some reports indicate that hydrogen acts as a catalyst for amorphous phase formation in titanium-rich alloys [161,162]. It has also been reported that PCAs affect the final phase formation, changing the solid solubility levels [163], modifying the glass-forming range [146,163,164], and altering the contamination levels.

The presence of air in the milling container or milling of the powders at very low temperatures (cryomilling) also has been shown to minimize welding, most probably due to the increased brittleness of the powder particles at such low temperatures [165,166]. Metal powders (with an fcc structure) milled in a hydrogen atmosphere have been found to become brittle and not stick to themselves or the container; probably due to the formation of a hydride phase [167].

The nature and quantity of the PCA used and the type of powder milled would determine the final size, shape, and purity of the powder particles. Use of a larger quantity of the PCA normally reduces the particle size by 2–3 orders of magnitude. For example, Lu and Lai [8] have reported that milling of aluminum for 5 h produced a particle size of about 500 μm when 1 wt% stearic acid was used as a PCA. But, when 3 wt% of stearic acid was used, the particle size was only about 10 μm. Similar results were reported for other PCAs as well. It was also reported that an increase of the PCA content leads to an exponential decrease of the powder size for a given milling duration. For example, the powder particle size reached a value of 1000 μm without the use of a PCA; with 2.3 wt% of PCA, the mean powder particle size reduced to 18 μm [168]. Results similar to the above may not be observed when brittle materials are milled; no large particles were observed even if a small quantity of the PCA was used. In fact, use of a PCA is not required for milling of brittle materials. Niu [169] noted that a homogeneous distribution of particle size could be easily achieved when the PCA is in the liquid state (e.g., ethyl acetate) than when it is in the solid state (e.g., stearic acid). A very detailed discussion on the effect of PCAs during milling of metal powders is available in Ref. [8].

Lee and Kwun [129] conducted a detailed investigation on the effects of the nature and quantity of PCA on the constitution of mechanically alloyed Ti–

48at%Al powders. They observed that an amorphous phase formed after milling for 300 h without a PCA, and a metastable fcc phase formed after milling for 500 h. But, when 0.3 wt% methanol was used as a PCA, a metastable disordered Ti_3Al phase formed after 300 h of milling and an amorphous phase after 1000 h. On the other hand, when 3 ml of benzene was used as a PCA, a metastable fcc phase formed after milling for 1000 h. From these observations they concluded that the formation of the metastable fcc phase is caused by atomic penetration into the interstitial sites of the lattice. They had also noted that the activation energy for crystallization of the amorphous phase increases (from 281 kJ/mol without a PCA to 411 kJ/mol when 3 wt% methanol was used) as the number of impurity atoms, especially oxygen, in the PCA increases.

The choice of a PCA for milling depends on the nature of the powder being milled and the purity of the final product desired. The nature and amount of PCA used during milling determine the final powder particle size and powder yield. In fact, one way of determining the effectiveness of the PCA is to determine the powder yield after MA. If the powder yield is high, the PCA is effective. If the powder yield is not high, then either the amount of PCA used is not sufficient, or probably it is not the right PCA. It has been reported [8] that after milling for 15 h, only 50% of the powder was recovered if 2 wt% of polyethylene glycol was used, while almost 100% of the powder was recovered if stearic acid was used.

It should be realized that there is no universal PCA. The amount of the PCA is dependent upon the (a) cold welding characteristics of the powder particles, (b) chemical and thermal stability of the PCA, and (c) amount of the powder and grinding medium used. The powder particle size tends to increase if the weight proportion of the PCA to the powder is below a critical value, while above this value the particle size tends to decrease. One has to decide on a PCA by looking at the possible interactions between the metal and the components in the PCA. A critical discussion of the role of PCAs in the milling of Al–Cu powder mixtures is presented in Ref. [170].

4.3.10. Temperature of milling

The temperature of milling is another important parameter in deciding the constitution of the milled powder. Since diffusion processes are involved in the formation of alloy phases irrespective of whether the final product phase is a solid solution, intermetallic, nanostructure, or an amorphous phase, it is expected that the temperature of milling will have a significant effect in any alloy system.

There have been only a few investigations reported where the temperature of milling has been intentionally varied. This was done by either dripping liquid nitrogen on the milling container to lower the temperature or electrically heating the milling vial to increase the temperature of milling. These investigations were undertaken to study the effect of milling temperature on the variation in solid solubility levels, or to determine whether an amorphous phase or a nanocrystalline structure forms at different

temperatures. During the formation of nanocrystals, it was reported that the root mean square (rms) strain in the material was lower and the grain size larger for materials milled at higher temperatures [171]. The extent of solid solubility was reported to decrease at higher milling temperatures. For example, during planetary ball milling of a Cu–37at%Ag powder mixture, it was noted that a mixture of an amorphous and crystalline (supersaturated solid solution) phases was obtained on milling at room temperature; instead, only a Cu–8at%Ag solid solution was obtained on milling the powder at 200°C [172]. Similar results were also reported by others in the Cu–Ag [173], Zr–Al [174], and Ni–Ag [175] alloy systems and were explained on the basis of the increased diffusivity and equilibration effects at higher temperatures of milling.

There have been conflicting reports on the formation of an amorphous phase as a function of the temperature of milling. As explained later, amorphization during MA involves formation of micro-diffusion couples of the constituent powders followed by a solid-state amorphization reaction. Thus, higher milling temperatures should enhance the amorphization kinetics. This has been observed in the Ni–Ti [176] and Ni–Zr [177] systems. During milling of a Ni–50at%Zr powder mixture in a vibrating mill, amorphous phase formation was not observed when the powder was milled at liquid nitrogen temperature for 15 h. On the other hand, milling for the same period of time produced a fully amorphous phase at 200°C; a partially amorphous phase was produced on milling at room temperature.

Formation of an amorphous phase by MM occurs by a different mechanism than during MA. The increase in free energy of the crystalline phase by the introduction of defects such as anti-site chemical disorder or increased grain boundary area through formation of a nanocrystalline structure is considered responsible for amorphization during MM. Thus, lower milling temperatures are expected to favor amorphization. However, both increased and decreased kinetics have been reported. Shortened milling times for amorphization were reported for milling of NiTi at 170°C than at 60°C [176]. Enhanced amorphization kinetics were also observed for $NiZr_2$ intermetallic [98,177]. In contrast to these observations, others have reported reduced amorphization kinetics for the $Ni_{10}Zr_7$, $Ni_{11}Zr_9$ intermetallics [178,179]. Koch et al. [77,180] also reported reduced amorphization kinetics with temperature during milling of the NiTi intermetallic. They reported that while it took 2 h for amorphization at liquid nitrogen temperature, it required 18 h of milling at 220°C. Similar results were also reported for the CoZr and $NiZr_2$ intermetallics. These results were rationalized on the basis that amorphization occurred in this system due to the increased grain boundary energy through formation of a nanocrystalline structure; and that the nanocrystalline structure formed more rapidly at lower milling temperatures. Fig. 8(a) shows the variation of grain size with milling time for CoZr milled for different times in the SPEX mill [180]. It can be easily seen that reduction in grain size is much more rapid at liquid nitrogen temperature than at higher temperatures. The band representing the critical grain size, below which

amorphization occurs, is also included. Fig. 8(b) shows a plot of the milling time for amorphization against the normalized milling temperature ($T_{milling}/T_{melting}$). It may be noted that the milling time for amorphization increases with increased normalized milling temperature for the NiTi, $NiZr_2$, and CoZr intermetallics [181].

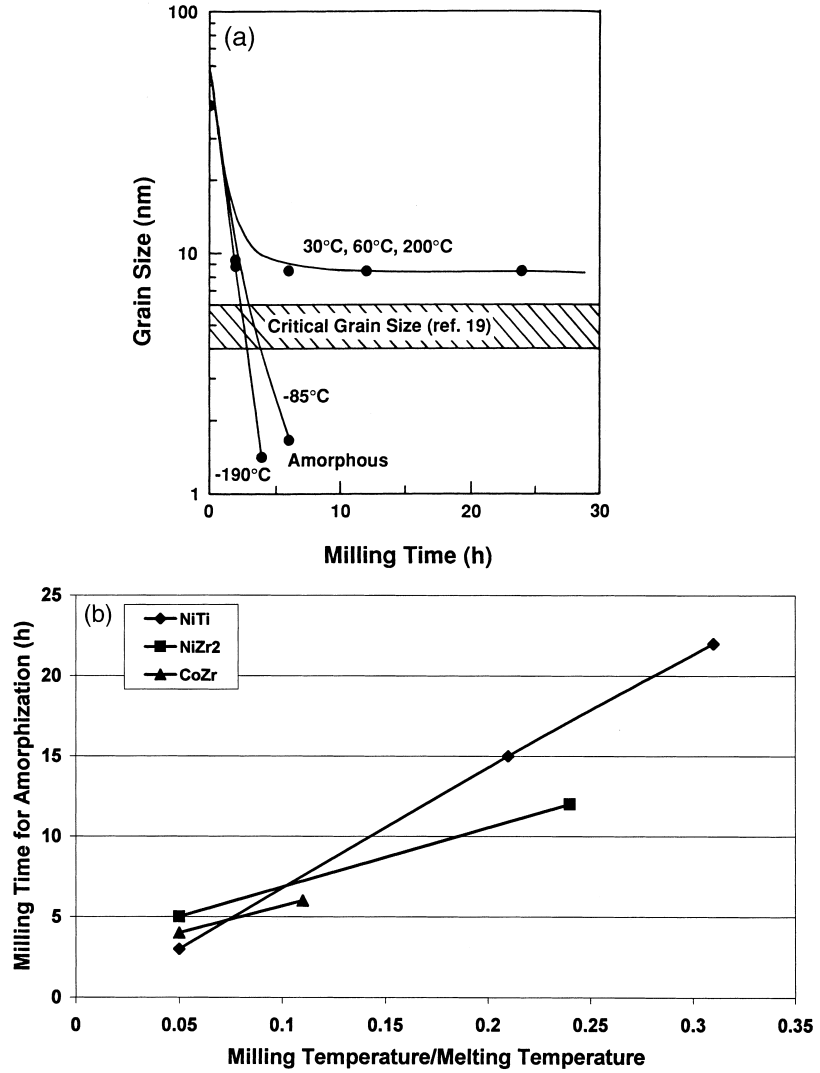

Fig. 8. (a) Grain size vs. milling time for CoZr milled at different temperatures in a SPEX mill. The shaded area represents the grain size below which the alloy becomes amorphous. (b) Milling time for amorphization vs. normalized milling temperature for CoZr, NiTi, and $NiZr_2$. A direct relationship exists between these two parameters.

5. Mechanism of alloying

During high-energy milling the powder particles are repeatedly flattened, cold welded, fractured and rewelded. Whenever two steel balls collide, some amount of powder is trapped in between them. Typically, around 1000 particles with an aggregate weight of about 0.2 mg are trapped during each collision (Fig. 9). The force of the impact plastically deforms the powder particles leading to work hardening and fracture. The new surfaces created enable the particles to weld together and this leads to an increase in particle size. Since in the early stages of milling, the particles are soft (if we are using either ductile-ductile or ductile-brittle material combination), their tendency to weld together and form large particles is high. A broad range of particle sizes develops, with some as large as three times bigger than the starting particles. The composite particles at this stage have a characteristic layered structure consisting of various combinations of the starting constituents. With continued deformation, the particles get work hardened and fracture by a fatigue failure mechanism and/or by the fragmentation of fragile flakes. Fragments generated by this mechanism may continue to reduce in size in the absence of strong agglomerating forces. At this stage, the tendency to fracture predominates over cold welding. Due to the continued impact of grinding balls, the structure of the particles is steadily refined, but the particle size continues to be the same. Consequently, the inter-layer spacing decreases and the number of layers in a particle increase.

However, it should be remembered that the efficiency of particle size reduction is very low, about 0.1% in a conventional ball mill. The efficiency may be

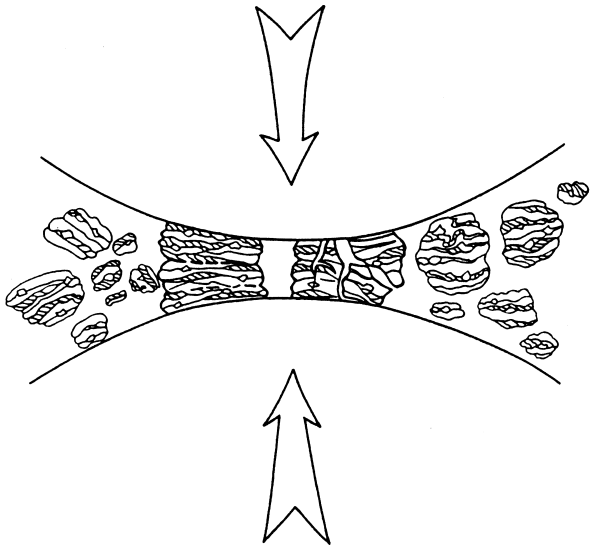

Fig. 9. Ball–powder–ball collision of powder mixture during mechanical alloying.

somewhat higher in high-energy ball milling processes, but is still less than 1%. The remaining energy is lost mostly in the form of heat, but a small amount is also utilized in the elastic and plastic deformation of the powder particles.

After milling for a certain length of time, steady-state equilibrium is attained when a balance is achieved between the rate of welding, which tends to increase the average particle size, and the rate of fracturing, which tends to decrease the average composite particle size. Smaller particles are able to withstand deformation without fracturing and tend to be welded into larger pieces, with an overall tendency to drive both very fine and very large particles towards an intermediate size [17]. At this stage each particle contains substantially all of the starting ingredients, in the proportion they were mixed together and the particles reach saturation hardness due to the accumulation of strain energy. The particle size distribution at this stage is narrow, because particles larger than average are reduced in size at the same rate that fragments smaller than average grow through agglomeration of smaller particles (Fig. 10) [182].

From the foregoing it is clear that during MA, heavy deformation is introduced into the particles. This is manifested by the presence of a variety of crystal defects such as dislocations, vacancies, stacking faults, and increased number of grain boundaries. The presence of this defect structure enhances the diffusivity of solute

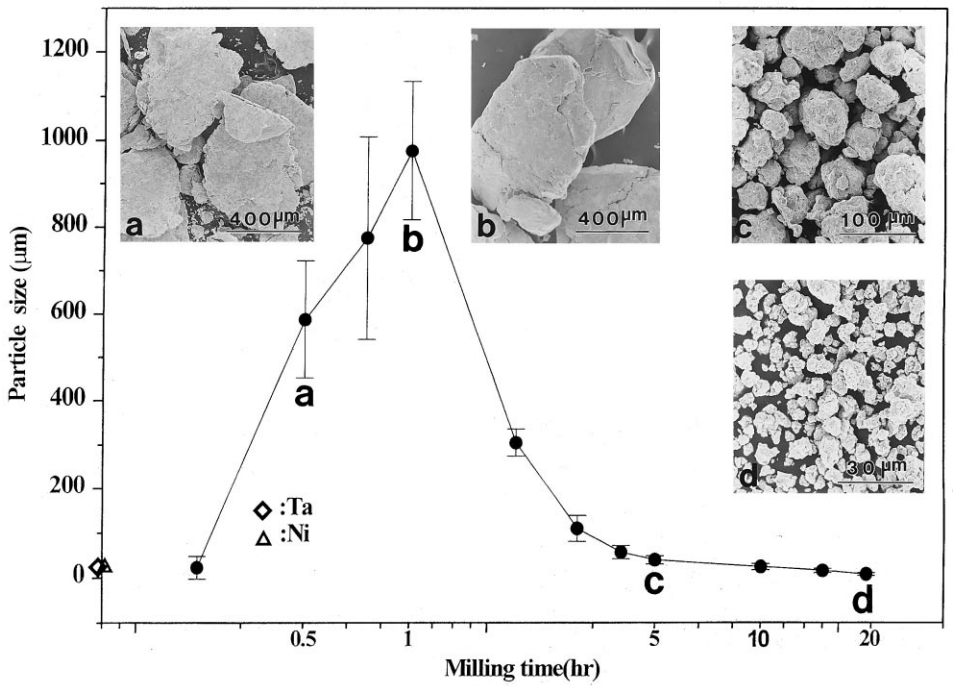

Fig. 10. Narrow particle size distribution caused by tendency of small particles to weld together and large particles to fracture under steady-state conditions.

elements into the matrix. Further, the refined microstructural features decrease the diffusion distances. Additionally, the slight rise in temperature during milling further aids the diffusion behavior, and consequently, true alloying takes place amongst the constituent elements. While this alloying generally takes place nominally at room temperature, sometimes it may be necessary to anneal the mechanically alloyed powder at an elevated temperature for alloying to be achieved. This is particularly true when formation of intermetallics is desired.

The specific times required to develop a given structure in any system would be a function of the initial particle size and characteristics of the ingredients as well as the specific equipment used for conducting the MA operation and the operating parameters of the equipment. But, in most of the cases, the rate of refinement of the internal structure (particle size, crystallite size, lamellar spacing, etc.) is roughly logarithmic with processing time and therefore the size of the starting particles is relatively unimportant. In a few minutes to an hour, the lamellar spacing usually becomes small and the crystallite (or grain) size is refined to nanometer (1 nm = 10^{-9} m or 10 Å) dimensions (Fig. 11). The ease with which nanostructured materials can be synthesized is one reason why MA has been extensively employed to produce nanocrysatlline materials [183,184].

As mentioned above, it is possible to conduct MA of three different combinations of metals and alloys: (i) ductile–ductile, (ii) ductile–brittle, and (iii) brittle–brittle systems. Therefore, it is convenient to discuss the mechanism of MA also under these categories.

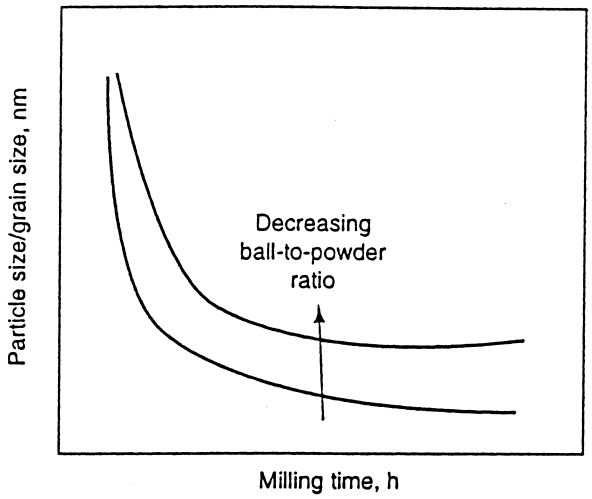

Fig. 11. Refinement of particle and grain sizes with milling time. Rate of refinement increases with higher milling energy, ball-to-powder weight ratio, lower temperature, etc.

5.1. Ductile–ductile components

This is the ideal combination of materials for MA. Benjamin [17] suggested that it was necessary to have at least 15% of a ductile component for achieving alloying. This was because true alloying occurs due to the repeated action of cold welding and fracturing of powder particles; cold welding cannot occur if the particles are not ductile.

Benjamin and Volin [185] first described the mechanism of alloying in a system involving two different ductile components. It was suggested that in the early stages of MA, the ductile components get flattened to platelet/pancake shapes by a micro-forging process. A small quantity of the powder, usually one or two particle thickness, also gets welded onto the ball surfaces. This coating of the powder on the grinding medium is advantageous since it prevents excessive wear of the grinding medium; additionally the wear of the grinding medium does not contaminate the powder. But, the thickness of the powder layer on the grinding medium must be kept to a minimum to avoid forming a heterogeneous product [42]. In the next stage, these flattened particles get cold welded together and form a composite lamellar structure of the constituent metals. An increase in particle size is also observed at this stage. With increasing MA time, the composite powder particles get work hardened, the hardness and consequently the brittleness increases, and the particles get fragmented resulting in particles with more

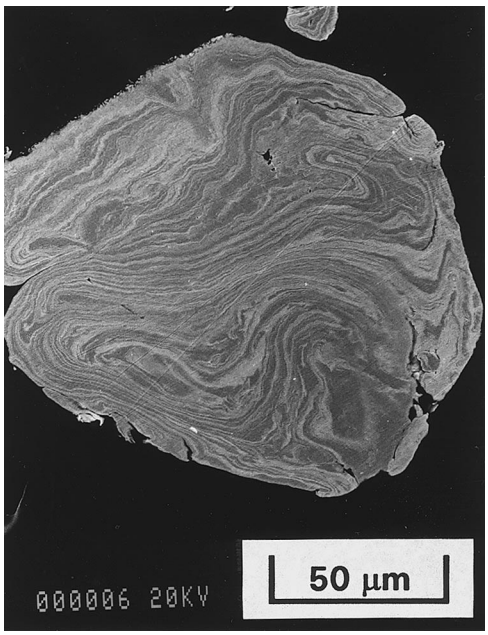

Fig. 12. Scanning electron micrograph depicting the convoluted lamellar structure obtained during milling of a ductile–ductile component system (Ag–Cu).

equiaxed dimensions. With further milling, the elemental lamellae of the welded layer and both the coarse and fine powders become convoluted rather than being linear (Fig. 12). This is due to the random welding together of equiaxed powder particles without any particular preference to the orientation with which they weld. Alloying begins to occur at this stage due to the combination of decreased diffusion distances (interlamellar spacing), increased lattice defect density, and any heating that may have occurred during the milling operation. The hardness and particle size tend to reach a saturation value at this stage, called the steady-state processing stage. With further milling, true alloying occurs at the atomic level resulting in the formation of solid solutions, intermetallics, or even amorphous phases. The layer spacing becomes so fine or disappears at this stage that it is no longer visible under an optical microscope.

An indication of the completion of the MA process and of the attainment of a homogeneous structure in the powder is the ease with which the powder could be removed from the grinding medium. Benjamin [17] has shown that it was possible to produce a true Ni-Cr alloy starting from elemental powders by demonstrating that the magnetic behavior of the mechanically alloyed powder was identical to that of a homogeneous Ni–Cr alloy produced by melting and working.

Even though the structural refinement is a statistical process since a wide variety of structures exist, especially in the initial stages of MA, the rate of structural refinement was found to depend on the rate of mechanical energy input into the process and the work hardening rate of the material being processed [185].

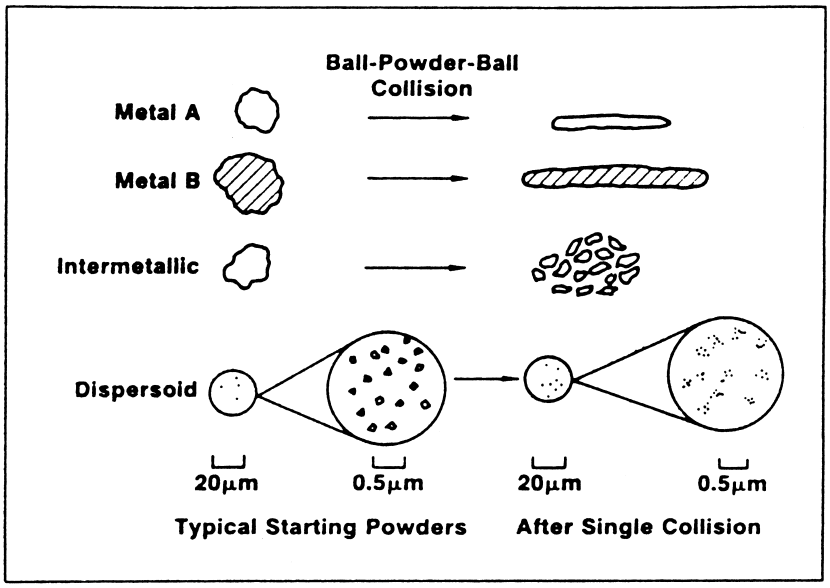

Fig. 13. Deformation characteristics of representative constituents of starting powders used in mechanical alloying.

5.2. Ductile–brittle components

The traditional ODS alloys fall in this category because the brittle oxide particles are dispersed in a ductile matrix. The microstructural evolution in this type of system was also described by Benjamin and others [19,42]. In the initial stages of milling, the ductile metal powder particles get flattened by the ball–powder–ball collisions, while the brittle oxide or intermetallic particles get fragmented/comminuted (Fig. 13). These fragmented brittle particles tend to become occluded by the ductile constituents and trapped in the ductile particles. The brittle constituent is closely spaced along the interlamellar spacings (Fig. 14a). With further milling, the ductile powder particles get work hardened, the lamellae get convoluted, and refined (Fig. 14b) (as described in Section 5.1). The composition of the individual particles converges toward the overall composition of the starting powder blend. With continued milling, the lamellae get further refined, the interlamellar spacing decreases, and the brittle particles get uniformly dispersed, if they are insoluble, in the ductile matrix, e.g., as in an ODS alloy (Fig. 14c). A typical transmission electron micrograph showing the dispersion of Er_2O_3 in a mechanically milled α_2-titanium aluminide matrix is shown in Fig. 15. On the other hand, if the brittle phase is soluble, alloying occurs between the ductile and brittle components also and chemical homogeneity is achieved. Formation of an amorphous phase on milling a mixture of pure Zr (ductile) and $NiZr_2$ intermetallic (brittle) powder particles is a typical example of this type of system [186]. Whether alloying occurs or not in a ductile–brittle system also depends on the solid solubility of the brittle component in the ductile matrix. If a component has a negligible solid solubility then alloying is unlikely to occur, e.g., boron in iron. Thus, alloying of ductile–brittle components during MA requires

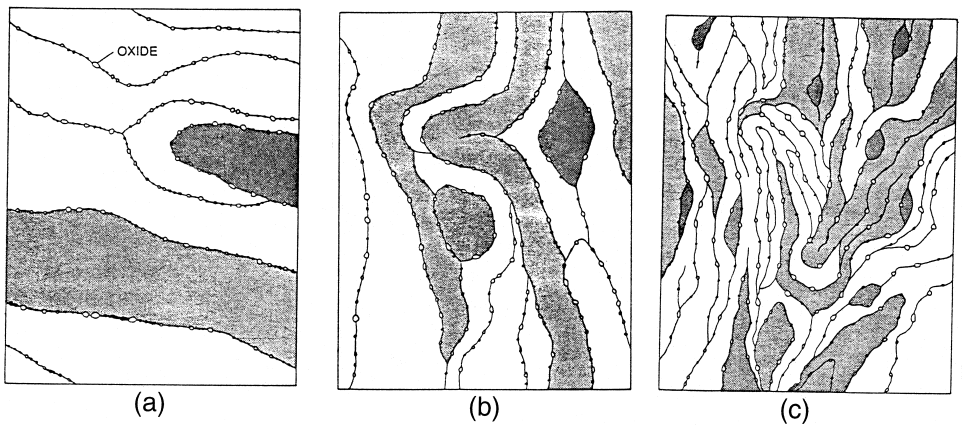

Fig. 14. Schematics of microstructural evolution during milling of a ductile–brittle combination of powders. This is typical of an oxide dispersion strengthened case.

not only fragmentation of brittle particles to facilitate short-range diffusion, but also reasonable solid solubility in the ductile matrix component.

5.3. Brittle–brittle components

From an intuitive stand point it would appear that it is unlikely that alloying occurs in a system consisting of two or more brittle components. This is because the absence of a ductile component prevents any welding from occurring, and in its absence, alloying is not expected to occur. However, alloying has been reported to occur in brittle–brittle component systems such as Si–Ge and Mn–Bi [187,188]. Milling of mixtures of brittle intermetallics [189] also produced amorphous phases.

As mentioned above, the brittle components get fragmented during milling and their particle size gets reduced continuously. However, at very small particle sizes the powder particles behave in a ductile fashion, and further reduction in size is not possible; this is termed the limit of comminution [190].

During milling of brittle–brittle component systems, it has been observed that the harder (more brittle) component gets fragmented and gets embedded in the softer (less brittle) component. Thus, the harder Si particles are embedded in the softer Ge matrix. (Fig. 16). Further, even though diffusion appears to be essential for alloying to occur in all types of systems, it appears that alloying did not occur

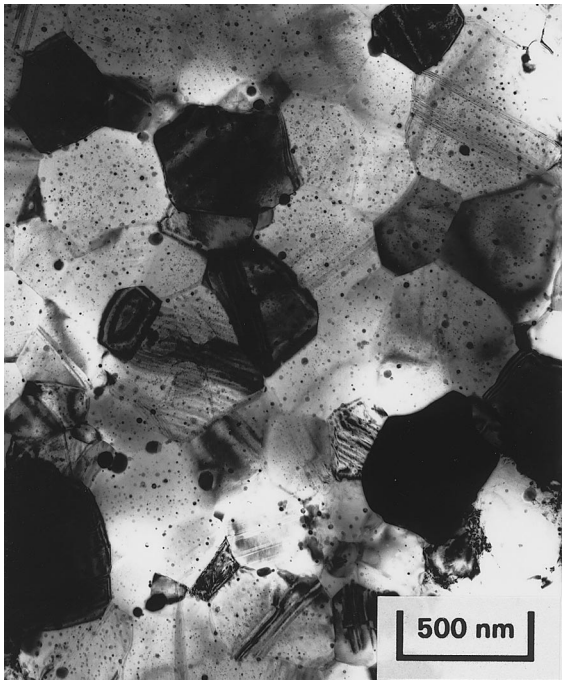

Fig. 15. Transmission electron micrograph showing a uniform dispersion of Er_2O_3 particles in a mechanically milled α_2-titanium aluminide alloy matrix.

in the brittle–brittle systems (Si–Ge) at very low temperatures, e.g., liquid nitrogen temperatures, while alloying was found to occur at sub-ambient temperatures in the ductile–ductile and ductile–brittle systems. This may be due to the longer diffusion distances required in the brittle–brittle granular vs. ductile–ductile lamellar geometry, and/or the enhanced diffusion paths provided by severe plastic deformation in ductile–ductile systems.

Possible mechanisms that may contribute to material transfer during milling of brittle components may include plastic deformation, which is made possible by (a) local temperature rise, (b) microdeformation in defect-free volumes, (c) surface deformation, and/or (d) hydrostatic stress state in the powders during milling [188].

6. Characterization of powders

The powders obtained after MA or MM need to be characterized for their size, shape, surface area, phase constitution, and microstructural features. Additionally, one could also characterize the transformation behavior of the mechanically alloyed powders on annealing or other treatments. The measurement of crystallite size and lattice strain in the mechanically alloyed powders is very important since

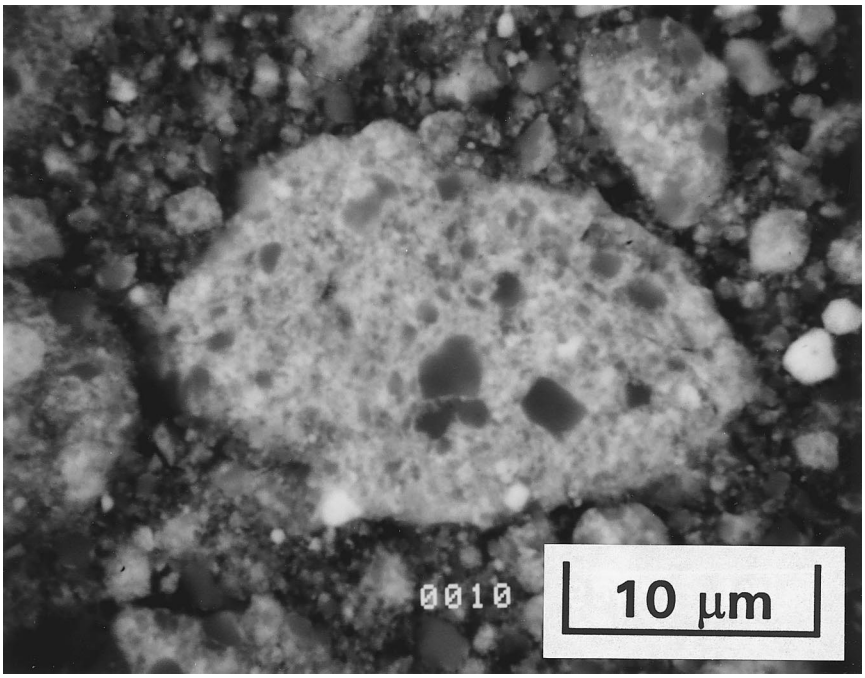

Fig. 16. Scanning electron micrograph showing that the harder Si particles are incorporated in a softer Ge matrix after mechanically alloying the Si–Ge powder mix for 12 h.

the phase constitution and transformation characteristics appear to be critically dependent on them.

In principle, the general techniques used to characterize conventional powders can also be used to characterize the mechanically alloyed powders. These techniques have been described in detail in standard textbooks on Powder Metallurgy (e.g., see Ref. [191]) and so will not be described in detail here.

The size and shape of the powder particles may be determined accurately using direct methods of either scanning electron microscopy (SEM) for relatively coarse powders or transmission electron microscopy (TEM) for fine powders. Special methods have also been developed to prepare thin film specimens from the mechanically alloyed powders to observe the microstructural features in the TEM [192]. If the powders are spherical in shape, their size is defined by the particle diameter. But, very rarely, the mechanically alloyed powder particles have a perfect spherical shape. In the early stages of milling (and also at late stages in some cases) the powder may have a flaky shape. In such cases, the equivalent spherical diameter can be determined from the volume, surface area, or projected area or settling rate measurements. For example, if the measured volume is V, then the equivalent spherical diameter D_v is given as:

$$D_v = (6V/\pi)^{1/3} \tag{2}$$

Alternatively, for a measured surface area S, the equivalent spherical surface diameter D_s is simply

$$D_s = (S/\pi)^{1/2} \tag{3}$$

The particles may not be spherical in shape in many cases. In such a case, the equivalent spherical projected diameter D_A is calculated by setting the projected area equal to the equivalent area of a circle, A and thus

$$D_A = (4A/\pi)^{1/2} \tag{4}$$

The particle size distribution can be conveniently obtained by the technique of sieving (or screening). The powder mix is sieved through successively finer (or coarser) sieves, which have a square cross section. The sieve is often referred to by its mesh size; determined by the number of wires per unit length. The opening size varies inversely with mesh size; large mesh sizes imply small opening sizes and vice versa. For example, if the powders pass through a 325 mesh, then they are referred to as having a -325 mesh size, or the particle size is <45 μm. Thus, by measuring the particle size and calculating the weight percentage of each particle size a histogram relating the weight percentage and particle size can be constructed. It is of interest to note that the particle size distribution in mechanically alloyed powders is generally Gaussian (log-normal), i.e., a bell curve is obtained when the frequency is plotted on a linear scale against the logarithm of the particle size.

It is important to remember that the powder particles are usually agglomerated

and therefore care has to be exercised in determining the accurate particle size. A powder particle may consist of several individual particles. Further, an individual powder particle may contain a number of crystallites defined as coherently diffracting domains. Microscopic examination normally gives the particle size (or even grain size if sufficient resolution is available), whereas diffraction techniques (e.g., X-ray) give the crystallite size.

The crystallite size and lattice strain in the powder particles can be determined using the X-ray peak broadening techniques. X-ray diffraction peaks are broadened due to (a) instrumental effects, (b) small particle size, and (c) lattice strain in the material. The individual contributions of these effects to the total broadening can be separated using standard techniques and these may be found in some of the textbooks [193] and/or research papers [194–196]. These can be consulted for the details and limitations of the techniques. Most commonly the crystallite size is determined by measuring the Bragg peak width at half the maximum intensity and using the Scherrer formula:

$$d = \frac{0.9\lambda}{B\cos\theta} \tag{5}$$

where d is the crystallite size, λ is the wavelength of the X-radiation used, B is the peak width at half the maximum intensity, and θ is the Bragg angle. This method can give correct values only if proper corrections for instrumental and strain broadening have been made. However, if one is interested only in following the trend of change of crystallite size with milling conditions, this simple technique may be acceptable.

While the X-ray peak broadening due to small crystallite size is inversely proportional to $\cos\theta$, that due to lattice strain is proportional to $\tan\theta$. Thus, by combining these two equations one gets an equation for the total broadening (after subtracting the instrumental broadening) as:

$$B = \frac{0.9\lambda}{d\cos\theta} + \eta\tan\theta \tag{6}$$

where η is the strain. And on rearrangement, the above equation can be written as:

$$B\cos\theta = \frac{0.9\lambda}{d} + \eta\sin\theta \tag{7}$$

Thus, when $B\cos\theta$ is plotted against $\sin\theta$, a straight line is obtained with the slope as η and the intercept as $0.9\lambda/d$. From these, one can calculate the crystallite size, d and the lattice strain η.

The crystallite sizes obtained by the indirect X-ray peak broadening studies and the direct electron microscopic techniques may not always match exactly. Whereas the electron microscopic techniques can be used to determine almost any crystallite size, X-ray peak broadening methods are most appropriate for crystallite sizes in the range of 10–100 nm.

It will be shown later that MA and MM have produced amorphous phases in several alloy systems. Differentiation between a "truly" amorphous (i.e., without translational symmetry as in a liquid) and microcrystalline structure (i.e., an assembly of randomly oriented fragments of a bulk crystalline phase) has not been easy on the basis of diffraction studies; considerable confusion exists in the literature. In a diffraction experiment of an "amorphous" structure, the intensity but not the phase of the scattered radiation is measured. Fourier inversion of these data can yield only the radial distribution function of the structure that cannot uniquely specify the atomic positions. To determine the structure, the experimentally determined radial distribution function must be compared with the radial distribution functions calculated from the structural models being considered [197].

The occurrence of an amorphous phase is generally inferred by observing the presence of broad peaks in the X-ray diffraction patterns. It should be noted, however, that X-ray diffraction patterns present only an average picture. Thus, by observing the broad X-ray peaks alone, it is not possible to distinguish amongst materials which are (a) truly amorphous, (b) extremely fine grained, or (c) a material in which very small crystals are embedded in an amorphous matrix. Hence, in recent years, it has been the practice to recognize such observations as "X-ray amorphous", suggesting that the identification was done only by X-ray diffraction methods. There have been several examples of observation of a phase produced as "amorphous" on the basis of X-ray diffraction studies alone; but, based on supplementary investigations by neutron diffraction and transmission electron microscopy, it could be unambiguously confirmed that the phase produced was not truly amorphous [198,199]. Neutron diffraction techniques have the advantage that one can detect light atoms in the presence of heavy atoms. Additionally, the technique of neutron diffraction has the ability to distinguish between neighboring elements in the periodic table [200]. X-ray diffraction techniques will be unsuitable for this because neighboring elements will have the atomic scattering factors very close to each other and so their difference will be very small to detect any reasonable amount of scattering. Thus, it is desirable that the X-ray diffraction observations are confirmed by other techniques as well. For example, transmission electron microscopic studies can confirm the lack of contrast in the micrographs for a truly amorphous phase. The appearance of a glass transition temperature during differential thermal analysis (DTA) studies is a clear and unambiguous indication of the presence of an amorphous phase. But, a glass transition may be obscured by the onset of crystallization (since the glass transition and crystallization temperatures are very close to each other in many metallic systems) and hence may not be observed in all cases. However, DTA studies can show the presence of an exothermic peak on heating the sample indicating that crystallization of the amorphous phase has occurred. If the material is extremely fine grained (nanocrystalline, and not amorphous), then only grain growth, driven by the decrease in grain boundary free energy, can occur in these alloys on heating them to high temperatures. In this case, a monotonically decreasing isothermal signal will be observed in the DTA studies. Other

indications of grain growth are scanning peaks that are low and wide with a long high-temperature tail; further, these peaks shift to higher temperatures after preannealing [201,202]. Thus one should be able to differentiate between amorphous and microcrystalline (fine grained) samples processed by MA techniques by using a combination of techniques such as microscopy, diffraction, and thermal analysis.

7. Temperature rise during milling

The intense mechanical deformation experienced by the powders leads to generation of crystal defects and this plus the balance between cold welding and fracturing operations among the powder particles is expected to affect the structural changes in the powder. Another important parameter, the temperature experienced by the powder during milling, dependent on the kinetic energy of the balls, can also determine the nature of the final powder product. If the temperature generated is high, the associated higher diffusivity (higher atomic mobility) leads to processes resulting in recovery (and recrystallization). In such a case, a stable phase, e.g., an intermetallic, would form. On the other hand, if the temperature is low, then defect recovery would be less and an amorphous (or a nanocrystalline) phase would form.

The temperature of the powders during milling can be high due to two different reasons. Firstly, as mentioned above it is due to the kinetic energy of the grinding medium. Secondly, it is possible that exothermic processes occurring during the milling process generate heat. But, in practice, when the temperature of the powder or the milling container is measured, it is probably due to a combination of these two factors. Additionally, one can intentionally raise the temperature of the container, but this would not be considered here.

Let us now consider the temperature rise during MA, due to the kinetic energy of the grinding medium, either observed experimentally or calculated using some appropriate theoretical models. The intentional raising of powder temperature to study the structural changes in the mechanically alloyed powder has been partially discussed in Section 4.3.10 and will be further discussed in the individual sections on Solid Solubility Extensions, Intermetallic Phase Formation, Amorphous Phases, and Nanostructures. A comprehensive review on the temperature effects during mechanical attrition has been prepared by Koch [203], which also contains details of the different models used for these calculations.

The macroscopic temperature of the vial (or powder) has been measured with thermocouples in some cases. A maximum temperature of 40–42°C was recorded [203] when the experiments were conducted with no balls in the container; even with 13 balls in the SPEX mill, the temperature rise was noted to be only about 50°C. Hence, it was concluded that most of the temperature rise comes from the motor and bearings. Some investigators have, however, reported very large temperature rises. The data available on the measured temperatures is summarized

in Table 6. It may be noted from the table that the maximum measured temperature is about 215°C, and more commonly it is about 100–120°C. It should be realized that this is the macroscopic temperature rise, even though it is recognized that local (microscopic) temperatures can be very high, often exceeding the melting points of some of the component metals.

It is very difficult to measure the local microscopic temperature during milling because of the dynamic nature of the milling process. But, these temperatures can be estimated using the appropriate models proposed by Schwarz and Koch [211], Davis et al. [188], Maurice and Courtney [24], Bhattacharya and Arzt [212], or Magini et al. [213].

The temperature rise in some cases was also estimated by observing the microstructural and/or crystal structure changes during milling, i.e., these are indirect inferences. For example, the tempering response of a quenched Fe–1.2wt%C steel during MA was studied by determining the relative amounts of martensite and cementite at different stages. It was estimated that the maximum temperature rise during milling was about 300°C [188]. By milling Sb or Ga–Sb alloys, and observing that the antimony metal got oxidized and formed the high-temperature orthorhombic Sb_2O_3 phase, it was estimated that the local rise in temperature was at least 570°C [92,214]. Similarly, by observing the transformation of boehmite or gibbsite into α-alumina during milling, the temperature rise was estimated to be at least 1000°C [215,216]. Other estimated temperatures varied between 180°C [210] in a Ni–Zr powder and 590°C [217] in

Table 6
Temperature rise during mechanical alloying

Alloy system	Type of mill	Temperature rise (°C)	Reference
Measured			
–	SPEX 8000	50	[203]
Al–Cr	Conventional ball mill	90	[204]
Al–Mg	SPEX 8000	120	[205]
Al–Mg	Attritor	125	[206]
Co–Fe–Si–B	Vibrational ball mill	100	[207]
Cr–Cu	Vibrational ball mill	100	[208]
Fe–Al	Fritsch Pulverisette 5	80	[103]
Ni-base superalloy	Attritor	< 100–215	[209]
Ni–Ti	High-speed ball mill	172	[172]
Ni–Zr	SPEX 8000	180	[204]
Estimated			
Al–Cu–Mn	Fritsch Pulverisette 5	590	[217]
Fe–1.2wt%C	SPEX 8000	300	[188]
Ni–Al	Planetary ball mill	220	[218]
Ni–Zr	SPEX 8000	180	[210]
Sb or Sb–Ge	Centrifugal ball mill	> 570	[92,214]
γ-AlOOH or $Al(OH)_3$	Fritsch Pulverisette 7	> 1000	[215,216]

an Al–Cu–Mn powder milled in Fritsch Pulverisette 5 at an intensity of 9. These values also are summarized in Table 6.

8. Solid solubility extensions

Solid solubility extensions have been achieved in many alloy systems by non-equilibrium processing methods such as RSP [219] and vapor deposition [2]. Similarly, mechanically alloyed powders also exhibit extension of equilibrium solid solubility limits. In addition to synthesizing stable (equilibrium) solid solutions, it has also been possible to synthesize metastable (non-equilibrium) supersaturated solid solutions by MA starting from blended elemental powders in several binary and higher order systems. In the early years of MA research, observation of solid solubility extensions was not the primary objective; instead, formation of solid solutions was noted as a secondary result during amorphization of metal powder mixtures. Consequently, systematic studies were not conducted on the variation of solid solubility limits with the different process parameters. On mechanically alloying blended elemental powder mixtures, interdiffusion between the components occurs and, if conditions permit, solid solutions form. This solid solubility limit is expected to increase with milling time as diffusion progresses and reach a (super)saturation level, beyond which no further extension of solid solubility occurs (Fig. 17). This saturation value has been listed as the solid solubility level achieved by MA. On the other hand, when the two component metals form an isomorphous system, the lattice parameter of one of the metals decreases and that of the other increases with milling time. Once steady-state conditions are established, the two lattice parameters merge and a homogeneous solid solution with the expected lattice parameter is formed (Fig. 18). Table 7 lists the solid solubility values obtained by mechanical alloying in several powder mixtures.

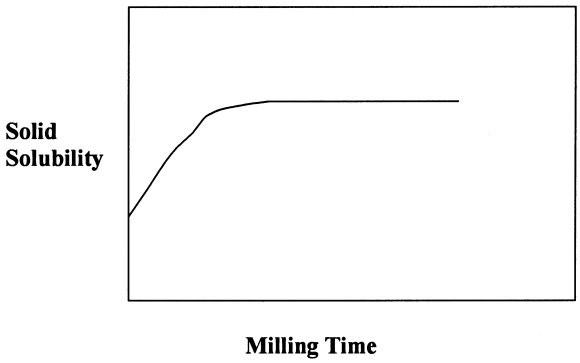

Fig. 17. Schematic diagram showing the variation of solid solubility with time during mechanical alloying of metal powder mixtures.

8.1. Difficulties in solid solubility determination

Solid solubility levels have been generally determined from changes in the lattice parameter values calculated from shifts in peak positions in the X-ray diffraction patterns. Very frequently, the absence of second phase reflections in the X-ray diffraction patterns has been inferred as the absence of a second phase, and hence the formation of a homogeneous solid solution. Both these conclusions are fraught with problems and so the values reported may not always be accurate. Therefore, caution must be exercised in attaching too much importance to the values reported. The difficulties associated with the determination of solid solubility limits determined this way in mechanically alloyed powders are discussed below.

(1) The absence of solute peaks in the X-ray diffraction patterns is usually taken as a proof of complete dissolution, and this has been interpreted as evidence for enhanced solid solubility limits. It has been recently shown that the solid solubility limits cannot be accurately determined only by noting the absence of solute peaks in the X-ray diffraction patterns. Kim et al. [396] mechanically alloyed Al–20wt%Ti powder mixtures and observed that the Ti reflections were absent in the X-ray diffraction pattern recorded from the powder mechanically alloyed for 15 h. But, TEM investigations of the same powder clearly showed the presence of nanometer-sized Ti particles in an aluminum matrix, suggesting that the absence of X-ray diffraction peaks from the solute phase may not be sufficient evidence for complete solid solubility. Thus, it is desirable to use more than one technique to unambiguously determine the true solid solubility limits.

Huang et al. [303] have recently analyzed the data on ten alloy systems of equiatomic composition processed by MA where solid solubility extensions have been reported by noting the absence of second-phase reflections. The authors have noted that the X-ray diffraction peaks associated with one of the elements

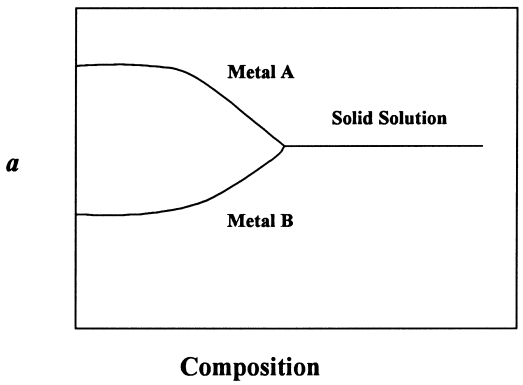

Fig. 18. Schematic variation of the lattice parameter (solid solubility) of the individual component phases with milling time in a binary alloy system.

Table 7
Solid solubility limits (at%) achieved by MA of blended elemental powders

Solvent	Solute	Equilibrium value		By MA	Reference
		At RT	Maximum		
Ag	Al	9.6	20.4	20	[220]
	Cu	0.0	14.0	100	[221–223]
	Gd	0.0	0.95	5	[224]
	Pd	100	100	85[a]	[196]
Al	Cr	0.0	0.37	5	[204]
	Cu	0.0	2.48	2.7	[148]
				0.2 (in Al–10Cu)	[225]
				5.6 (in Al–15Cu)	[225,226]
	Fe	0.0	0.025	1.0	[133]
				2.0	[227]
				4.5	[228]
				4–5	[229]
	Ge	0.0	2.0	14.1	[226]
	Mg	1.2	18.6	3.7 (in Al–10Mg)	[225]
				10.0 (in Al–20Mg)	[225]
				14.1 (in Al–30Mg)	[225,226]
				13 (in Al–30Mg)	[230]
				24 (in Al–50Mg)	[230]
				18	[231]
				23	[205]
				40	[231]
	Mn	0.4	0.62	18.5	[232]
	Mo	0.0	0.06	0.4 (in Al–3Mo)	[233]
				1.3 (in Al–10Mo)	[233]
				2.4 (in Al–17Mo)	[233]
	Nb	0.0	0.065	Unspecified	[234]
				15	[235]
				25	[236]
	Ni	0.0	0.11	10	[237]
	Ni–Co	–	–	8Ni, 4Co	[238]
	Ru	0.0	0.008	14	[239]
	Si	0.0	1.5	0.7 (in Al–5Si)	[225]
				1.3 (in Al–10Si)	[225]
				4.5	[225,226]
AlSb	InSb	–	–	100	[240]
Al	Ti	0.0	0.75	3.0	[241]
				4 (in Al–25Ti)	[242]
				10.4	[243]
				12	[244]
				15–36	[140]
				20	[245]
				25	[246–248]
				35	[249]
				36	[250]
	Ti–Cr	–	–	12Ti and 5–8Cr	[251]

(continued on next page)

Table 7 (*continued*)

Solvent	Solute	Equilibrium value		By MA	Reference
		At RT	Maximum		
	Ti–Fe	–	–	Unspecified	[252]
				12Ti and 3–5Fe	[251]
	Ti–Mn–Nb	–	–	23Ti, 8Mn, 2Nb	[253]
Al_2O_3	Fe_2O_3			25 mol%	[254]
Au_2Nb (PA)		9.0	57	33	[255]
Bi	Sb	100	100	10[a]	[256]
Cd	Zn	3.1	4.35	50	[257]
Co	C	0.0	4.1	6	[258]
	Cr	4.0	43.0	40	[259]
	Cu	0.0	19.7	100	[260–263]
	Fe	100	100	10[a]	[264]
	Li_2O_3	–	–	Unspecified	[265]
	Mn	43.5	59.0	40	[259]
	Ni	100	100	70[a]	[266]
	V	1.6	35.0	33	[259]
	Zr	0.0	< 1.0	5	[259]
Cr	Co	4.9	53.0	30	[259]
				40	[259]
Cu	Ag	0.0	5.0	100	[222]
	Ag–Fe	–	–	10Ag, 20Fe	[267]
	Al	18.6	19.7	18	[148]
	Co	0.0	8.0	100	[260,268,269]
	Cr	0.0	0.0	50	[270]
	Fe	0.3	11.0	20	[271]
				30	[221,272,273]
				40	[274]
				50	[275]
				55	[276,277]
				60	[278–280]
				65 (w/o ethanol)	[163]
				68 (w/ethanol)	[163]
				65	[281,282]
	Hg	0.0	5.0	17	[69]
	Mn	100	100	35[a]	[268]
	Nb	0.1	0.1	3	[283]
	Ni	100	100	13[a]	[284]
				100	[285]
	Sb	1.1	5.8	3.7	[120]
	Sn	0.0	9.1	Unspecified	[286,287]
				9.8	[288,289]
	Ti	0.9	8.0	0.6 (in Cu–10Ti)	[290]
				2.8 (in Cu–20Ti)	[290]
				3.7 (in Cu–30Ti)	[290]
				9.4 (in Cu–40Ti)	[290]
	V	0.0	0.1	Unspecified	[268]
	W	0.0	0.97	Unspecified	[291]
Fe	Ag	0.0	0.0	10	[292]

Table 7 (*continued*)

Solvent	Solute	Equilibrium value		By MA	Reference
		At RT	Maximum		
	Ag–Cu	–	–	10Ag, 10Cu	[267]
	Al	20.8	45.0	4	[293]
				20	[294]
				25	[295–297]
				40	[155,298]
				50	[103,133,299,300]
	B	0.0	0.0	4.0	[301]
	B–Cu	–	–	13B, 1Cu	[302]
	B–Si	–	–	5Si, 4B	[303]
	Co	100	100	20[a]	[264]
	Cr	100	100	46.5[a]	[304]
				50	[305]
				70	[306]
	Cu	7.2	15.0	15	[276,277,281,282]
				20	[274,280]
				25	[279]
				30	[278]
				40	[273]
				18 (w/ethanol)	[163]
				24.5 (w/o ethanol)	[163]
	Ge	10.0	17.5	25	[297,307,308]
	Hf	0.0	0.51	10	[309]
	Mg	0.0	0.0	20	[310]
	Ni	2.0	4.7/100	36	[311]
				40	[312]
	Si	3.0	19.5	Unspecified	[313]
				5	[301]
				12	[314]
				26	[315]
				25	[171,297,316,317]
	Si–Nb	–	–	23.75Si, 5Nb	[[316]]
	Sn	0.0	9.2	25	[171,294,318]
				30	[319]
	Ta	0.3	2.5	40	[320]
	W	0.0	14.3	Unspecified	[321,322]
	W			20	[323]
				30	[324]
	Zn	0.0	42.0	25	[171,297]
	Zr	0.0	6.5	5	[325–328]
				10	[309]
				14	[302]
	Zr–B	–	–	7Zr, 7B	[302]
	Zr–B–Cu	–	–	7Zr, 6B, 1Cu	[302]
	Zr–Cu	–	–	7Zr, 7Cu	[302]
				13Zr, 1Cu	[302]
				11Zr, 3Cu	[302]
FeS	Al	–	–	7Al in Fe	[329]

(*continued on next page*)

Table 7 (*continued*)

Solvent	Solute	Equilibrium value		By MA	Reference
		At RT	Maximum		
	Mn	–	–	Unspecified Mn	[329]
Ge	Si	100	100	89[a]	[330]
	Sn	0.48	1.1	24	[331]
Mg	Al	0.9	11.0	2.2 (in Mg–10Al)	[225]
				3.7 (in Mg–15Al)	[225,226]
	Fe			5	[310]
	Ti	0.0	0.0	6	[152,332]
Mn	Co	4.0	38.0	50	[259]
Mo	Al	0.0	20.5	Unspecified	[233]
Nb	Al	5.9	21.5	15.4	[139]
				25	[333–335]
				33.3	[336]
				60	[235,236]
Nb_3Al (PA)	–	–	–	25	[337]
Nb_3Au (PA)	–	19.0	54.0	25	[255,338]
Nb	Be	9.1	16.0	Unspecified	[339]
	Ge	2.8	9.2	8.6	[340]
	Ni	1.2	5.0	10	[127]
	Si	0.0	3.5	Unspecified	[341]
Ni	Al	7.5	21.2	0.5	[303]
				25	[229,307,342–344]
				27	[345]
Ni_3Al (PA)	–	–	–	25	[346]
NiAl (PA)			39–55Al	33–62Al	[347]
				40–65Al	[345]
Ni	C	0.0	7.4	9.0 (in Ni–10C)	[258]
				12.0 (in Ni–15C)	[258]
	Co	100	100	60[a]	[285]
	Co	100	100	70[a]	[266]
	Cr	22.6	50.0	50	[229]
	Fe	3.8	100	40	[321]
	Ga	10.8	24.3	50	[348]
	Ge	9.6	12.0	25	[307]
	In	0.0	14.5	13	[348]
	Mg	0.0	0.0	10	[349]
	Mo			23	[350]
	Nb	3.2	14.0	10	[127]
				15	[351]
	Ru	4.6	34.5	31	[352]
	Si	10.0	15.8	24	[353]
				25	[307]
Ni_3Si (PA)	–	–	–	25	[354]
Ni	Sn	0.0	10.6	17.5	[348]
	Ta	3.0	17.2	30	[355]
	Ti	6.0	13.9	6	[356]
				28	[357]
				8.9 (in Ni–10Ti)	[290]

Table 7 (*continued*)

Solvent	Solute	Equilibrium value		By MA	Reference
		At RT	Maximum		
				13.8 (in Ni–20Ti)	[290]
				18.3 (in Ni–25Ti)	[290]
Ni_3V (PA)	–	15.0	43.0	25	[358]
Ni_2V (PA)	–			33	[358]
Ni	W	12.5	17.5	14	[229]
				23	[359]
				28	[360]
Pd	Ag	100	100	95[a]	[196]
	Y	7.6	13.0	12	[361]
PTFE	PE	–	–	Unspecified	[362]
Ru	Al	0.6	4.0	14	[239]
	Ni	6.4	50.0	53	[352]
Si	Ge	100	100	28[a]	[188]
				50[a]	[187]
	Sn	0.0	0.0	Unspecified	[363]
Ta	Al	0.0	4.0	33	[364]
				50	[90]
	Cu	0.0	0.0	30	[365]
Ti	Al	11.0	47.5	10	[366]
				16	[367,368]
				25	[246,249,337,369,370]
				28	[252]
				≥ 30	[367]
				33	[121]
				50	[249,371]
				60	[246,247]
Ti–49Al (PA)	–	–	–	49	[246,247]
Ti	Al-Nb	–	–	Unspecified	[372,373]
				24Al, 11Nb(hcp)	[335]
	Al-Ni	–	–	6Al, 6Ni	[374]
	Cu	0.0	1.6(α), 13.5 (β)	10	[375]
	Mg	0.0	0.0	3.6	[376]
				6	[154,377,378]
				30	[152,332]
				38	[379]
				50	[152]
				100	[380]
	Ni	0.0	10.0	2	[381]
	Si	0.0	3.5	8	[382]
				37.5	[336]
V	Co	7.3	22.0	Unspecified	[268]
				40	[259]
V_3Ga (PA)	–	9.2	41.0	25	[84]
V_3Ni (PA)	–	2.0	24.0	25	[358]
W	Fe	2.0	2.6	3.4	[383]
				20	[323]
				40	[384]

(continued on next page)

Table 7 (*continued*)

Solvent	Solute	Equilibrium value		By MA	Reference
		At RT	Maximum		
	Ni–Fe	–	–	Unspecified	[385]
	Re	–	–	25	[386]
Yb	Ce	0.0	1.0	Unspecified	[387]
Zr	Al	1.0	26.0	Unspecified	[107,388]
				12.5 (at RT)	[174]
				8.0 (at 300°C)	[174]
				15	[389–391]
				17.5	[392]
				50	[388]
	Co	1.0	5.0	4	[259]
	Ni	0.0	3.0	7	[328,393]
ZrO_2	ZrN	–	–	Unspecified	[394]
Zr_2O_3	Al_2O_3	–	–	Unspecified	[395]
	CoO	–	–	16.7 mol%	[395]
	Fe_2O_3	–	–	16.7 mol%	[395]
	Y_2O_3	–	–	16.7 mol%	[395]

[a] In these cases, the composition of the alloy investigated is mentioned.

disappear during milling while those of the other persist. They have concluded that the element with the higher atomic number persisted in the X-ray diffraction pattern, while the one with the lower atomic number did not. Since the atomic scattering factor is directly proportional to the atomic number of the element, the element with the lower atomic number, and hence lower atomic scattering factor, has a lower intensity and hence with continued milling it tends to disappear. This argument assumes that atomic scattering factor is the major factor contributing to the intensity of a reflection, and this is not far from true. Accordingly, in the Al–Mo system, Mo ($Z = 42$) peaks persist while Al ($Z = 13$) peaks disappear. Similarly, in the Ni–Ru system, Ru ($Z = 44$) peaks persist while those of Ni ($Z = 28$) disappear.

(2) Due to the mechanical deformation introduced into the powder, particle and crystallite refinement occurs and the lattice strain increases. These two effects lead to broadening of the X-ray diffraction peaks and a consequent decrease in the peak heights. In fact, formation of nanocrystalline solid solutions can significantly broaden the X-ray diffraction peaks. Further, if the weight fraction of the second component is small, the corresponding peaks may even be ''absent''. Thus, the disappearance of Al reflections in the X-ray diffraction pattern of a mechanically alloyed Ni–Al powder mixture has been attributed to crystallite refinement to the level of about 5 nm, even though a solid solution has not actually formed.

Even if a reflection is present in the diffraction pattern, its broadening makes the location of the peak position difficult and consequently, the lattice parameters calculated are inaccurate.

(3) Another difficulty associated with small particle sizes is their detectability by

the technique of X-ray diffraction. It has been shown that while 2 wt% of Ti can be easily detected if the particle size is in the range of 26–38 μm, one requires about 25 wt% Ti if the particle size is in the range of 0.05–1.0 μm. Thus, a much larger amount of material is required when the particle size is in the sub-micron range [396]. Mechanically alloyed materials often have particle sizes in the latter range of <1 μm, and consequently the presence of small amounts of second phases with small particle sizes cannot be easily detected by X-ray diffraction techniques.

(4) Very often the solid solubility levels are determined by extrapolating the data of lattice parameter vs. solute content obtained either for equilibrium solid solutions or for metastable supersaturated solid solutions obtained by other non-equilibrium processing techniques. In the absence of such data, the Vegard's law (linear variation of lattice parameter (or atomic diameter or atomic volume) with solute content) is assumed to be valid. Extrapolations can be erroneous, especially if the solid solubility is small under equilibrium or metastable conditions. Further, the assumption of applicability of Vegard's law may not be valid. The extent of deviation from linearity of lattice parameter(s) with solute content (positive deviation due to the positive sign of heat of mixing and negative deviation due to the negative sign of heat of mixing) may be significant when one is dealing with pairs of metals which have different crystal structures. This problem is more serious when the components involved have non-cubic structures.

(5) Heavy deformation (cold working) introduces stacking faults on (111) planes in fcc metals and alloys. Stacking faults can also be introduced in the basal (0001) or prismatic $\{10\bar{1}0\}$ planes of the hexagonal close-packed alloys. These faults can cause anomalous *hkl*-dependent peak broadening in the X-ray diffraction patterns [371,397]. The effective crystallite size (D_{eff}) measured from a reflection results from the true average crystallite size (D_{true}) and the "effective stacking fault diameter" (D_{SF}) according to the relation:

$$\frac{1}{D_{\text{eff}}} = \frac{1}{D_{\text{true}}} + \frac{1}{D_{\text{SF}}} \tag{8}$$

The presence of stacking faults leads to a refined "effective" crystallite size, as determined by both the true crystallite size and the density of stacking faults. In other words, the calculated crystallite size, assuming that the peak broadening is only due to the small crystallite size, grossly underestimates the true crystallite size. It has been shown [397] that the true crystallite size was 3 to 10 times the apparent crystallite size in mechanically alloyed Cu–Co alloys. The contribution of stacking faults to broadening/shift of peak positions is very important in alloys with low to moderate stacking fault energy, where a high density of stacking faults can be expected.

The peak shift caused by the presence of stacking faults can further complicate the situation in that the effects of solid solubility and stacking faults can cause the peak shifts to occur in opposite ways.

(6) The technique of MA often introduces impurities (substitutional impurities

like iron, chromium, and nickel from the milling container and the grinding medium and interstitial impurities like nitrogen, oxygen, and carbon from either the atmosphere and/or the process control agent) and their amounts increase with milling time. (See the Section on "Contamination" for further details on the levels of contamination in mechanically alloyed powders.) The interstitial impurities dilate the lattice and the substitutional impurities can either dilate or contract the lattice depending on the relative atomic sizes of these elements with respect to the solvent atom. These effects must be taken into account while determining the real solid solubility values. An accurate chemical analysis for the impurity content and the effect of these impurities on the magnitude of peak shift should be evaluated before the solid solubility extensions can be accurately reported.

(7) It has also been noted in several instances that the solid solubility level increases with increasing initial solute content in the powder mix (see Table 7). This was a true observation since the milling was carried out to the steady-state condition for each alloy composition and has been repeatedly reported by several investigators. The temperature of milling also appears to alter the solid solubility levels. Thus, it is difficult to list one specific solid solubility value for a given alloy system, in at least some cases. These observations can be further complicated by variations in the nature of the mill, intensity of milling, milling atmosphere, etc.

Even though all the above-listed factors have not been taken into account in all of the cases, solid solubility extensions, beyond the equilibrium values, have been reported in a number of alloy systems (Table 7).

In some cases equilibrium solid solutions were synthesized starting from blended elemental powders. In those alloy systems, which exhibit complete solid solubility under equilibrium conditions (isomorphous systems), the lower values indicted in Table 7, represent the composition of the alloy investigated and not the true maximum solid solubility level achievable by MA. One of the interesting observations made is that supersaturated solid solutions could be synthesized by MA even in those immiscible systems which show a positive heat of mixing, and hence do not have any solid solubility under equilibrium conditions.

The formation of solid solutions (both equilibrium and metastable) during MA maybe attributed to the effects of severe plastic deformation. As mentioned earlier, plastic deformation refines the particle and grain sizes and increases the grain boundary area. The decreased particle size reduces the diffusion distances between particles and facilitates pipe diffusion. Diffusion is further aided by the increased defect density and a local rise in temperature. The combination of these effects would permit sufficient diffusion to occur in the interfacial regions of the nanocrystalline grains to form solid solutions.

The effect of different process variables on the formation of solid solutions has also been recently investigated. Amongst these, the temperature of milling seems to play an important role. During milling, the continuous shearing across interfaces of the two component metals A and B results in an increase of the A/B interface area and this results in intermixing of the two components. On the other hand, thermally activated jumps of vacancies favor decomposition. A dynamic equilibrium is maintained between these two competing processes and the final

steady state is determined by the ratio γ between the forced jump frequency (that helps thorough intermixing of the components) and the thermally activated frequency (that aids in the equilibration of the system). For zero or low values of γ, thermally activated diffusion will drive the system to its equilibrium state. On the other hand, for infinitely large values of γ, the microstructure is continuously refined until a random solid solution is obtained. Usually the value of γ is neither of these two extremes, but has an intermediate value. Klassen et al. [173,398] ball milled an Ag–50at%Cu powder mixture to various steady states at different temperatures ranging from 85 to 473 K and noted that a homogeneous fcc alloy was obtained after milling at subambient temperatures. On the other hand, a fully decomposed two-phase mixture was obtained after milling at 473 K. Co-existence of an equiatomic alloy phase and decomposed terminal solid solutions was reported at intermediate temperatures of milling. A similar situation was also reported in the Zr–Al system. The maximum solid solubility achieved was 12.5 at% Al in Zr when milling was conducted at room temperature, while it was only 8.0 at% Al at 300°C [174]. Considering the mechanical alloying behavior of two immiscible systems Ag–Fe and Cu–Fe, it was observed that Cu–Fe undergoes atomic level mixing and alloying forming solid solutions, while Ag–Fe remains unalloyed. Ma et al. [399] explained this difference in the alloying behavior using the concept of the intensity of external forcing, viz., the γ factor, referred to above.

The use of a process control agent (PCA) also appears to affect the maximum achieved solid solubility limit, although the results reported are not consistent. For example, Gaffet et al. [163] reported that the solid solubility of Fe in copper was increased to 68 at% Fe when ethanol was used as a PCA, while it was only 65 at% Fe without the use of ethanol. Contrary to this, they reported that the solubility decreased with the use of ethanol as a PCA on the Fe-rich side of the Cu–Fe phase diagram. Accordingly, the solid solubility was 18 at% Cu in Fe when ethanol was used and it was 25 at% Cu in Fe without ethanol [163]. These two effects appear to be contradictory, but no explanation has been offered for this. Kaloshkin et al. [102] noted that formation of supersaturated solid solutions was promoted if the Fe–Cu alloys were milled in an atmosphere containing oxygen. Yavari and Desré [400] suspected that the solid solubilities are higher in oxygen-containing alloys because the presence of oxygen results in a negative heat of mixing of the multi-component mixture. Another possible reason for this could be that oxygen will act like a PCA and promotes fracturing of the particles and helps in the formation of very fine-grained (nanostructured) material. The oxygen present in the PCAs may also have a similar effect; but, it is surprising that decreased solubilities were reported in some cases when the powders were milled with a PCA.

Another interesting observation that has been made in mechanically alloyed materials is that the solid solubility limit achieved increases with increasing solute content in the starting blended elemental powder mixture. This has been observed in several aluminum-, copper-, and nickel-base alloys, amongst others (see Table 7). Such a situation may possibly arise during rapid solidification of metallic

melts when the solute concentration at the dendrite tip can be quite high and is determined by the operative solute partition ratio. But, since there is no melting and consequently no dendrite formation involved in the MA process, such a mechanism may not be occurring here. The increased solid solubility level with increasing initial solute content has been tentatively explained on the basis that the concentration gradients are steeper at higher solute contents and that these are expected to result in increased diffusion and consequently in higher solid solubility levels. This variation may arise possibly due to kinetic considerations only since thermodynamically the maximum solubility that can be achieved is fixed for a given alloy system.

8.2. Mechanisms of solid solubility extension

Neither the actual mechanism(s) for the formation nor the limits for the solid solubility extensions in alloy systems obtained by MA have been well investigated. For example, it was suggested [357] that the increased solid solubility of Ti in Ni in mechanically alloyed Ni–Ti powder mixtures was due to the metastable equilibrium between the α-Ni solid solution and the Ni–Ti amorphous phase as opposed to the stable equilibrium between the α-Ni and Ni_3Ti phases. That is, the extent of supersaturation is limited to the composition where the amorphous phase starts forming. A similar conclusion was also arrived at by others [290]. However, it has been noted in recent years that significant solid solubility extensions can be achieved in alloy systems (e.g., Ti–Mg) even when an amorphous phase did not form in those alloy systems [376]. Thus, alternative explanations need to be sought to explain the formation of solid solutions and their limits of solid solubility.

It has also been suggested that the solid solubility can be extended up to the position of the intermetallic compound in the phase diagram if the base metal and the intermetallic have similar crystal structures [348].

It was suggested that the formation of supersaturated solid solutions is closely related to the formation of nanocrystalline phases [154]. The large volume fraction of atoms in the grain boundaries in these materials is expected to enhance diffusion and consequently the solid solubility levels in these types of systems. In support of this argument it was shown that the solid solubility of Mg in Ti is zero when the grain size of the titanium phase is on the order of micrometers, while significant solubility (about 3 at%) was detected when the titanium grain size was on the order of nanometers. Similar results have also been reported by a number of other investigators [261,401]. For example, Huang et al. [261] reported that the solute content was higher the smaller the particle/crystallite size in their mechanically alloyed Co–Cu powders; this was confirmed by transmission electron microscopy and energy dispersive X-ray analysis of the powders.

In a nanocrystalline structure, there is an increase in the grain boundary volume. Further, the diffusivity of the component atoms is increased due to the large amount of structural defects and the local stresses in such a material. Under these conditions, the solute atoms substitute the solvent atoms in the grain

boundaries and vice versa. The rapid diffusion of atoms from one grain into the other leads to quick homogenization and results in the formation of solid solutions. Veltl et al. [402] suggested that the energy stored in the grain boundaries of nanocrystalline materials serves as a driving force for the formation of a solid solution. It has been shown earlier [403] that a substantial amount of enthalpy can be stored in nanocrystalline materials due to the large grain boundary area. It was also suggested that the enhanced solid solubility might be due to the high dislocation density produced during milling [276,404].

Yavari et al. [405–407] proposed another mechanism based on the assumption that upon deformation, elemental fragments with small tip radii are formed and a small fraction of the material is expected to be as crystallites ≤ 2 nm in diameter. In these cases the capillary pressure forces the atoms at the tips of the fragments to dissolve. This process will continue to full dissolution with increased milling time, due to generation of such small particles by necking at tips of larger ones. A similar mechanism was also suggested by Gente et al. [260]. They suggested that the chemical enthalpy associated with the interface between the elemental components can enhance the free energy of a composite above that of the related solid solution thus providing a driving force for alloying in systems with a positive free energy of mixing. The main difference between the models proposed by Yavari et al. and Gente et al. is that the former assumes incoherent interfaces between the elemental components, whereas the latter suggests the formation of composites with coherent elemental domains before alloying occurs. The experimental information presently available is not sufficient to decide between these two models.

Formation of (supersaturated) solid solutions by MA is more noteworthy in liquid- and solid-immiscible systems than in solid-miscible systems. Gente et al. [260], Huang et al. [261,269], and Jiang et al. [408] reported formation of extensive solid solutions in the Cu–Co and Fe–Cu systems. These authors suggested that the increased diffusivity due to the presence of structural defects and local stresses in nanocrystals is responsible for the formation of supersaturated solid solutions in these systems. Formation of homogeneous solid solutions was favored when the crystallite size of the constituents was reduced to below about 1–2 nm.

Hume-Rothery rules [409] suggest that the metallic radii of the solvent and solute should differ by less than 15% to achieve good solid solubility of one element in the other (5 at% at moderate temperatures). This was observed to be true in mechanically alloyed Co-transition metal alloys [259]. To further confirm whether a similar situation could be obtained in other alloy systems processed by MA, Bansal et al.[297] studied the alloying behavior of powder blends of Fe with 25 at% Al, As, Ge, In, Sb, Si, Sn, and Zn. They concluded that good solubility (5 at%) could be achieved by MA even when the difference in the atomic radii was about 30%. Stated differently, if the atomic radius difference was $<15\%$, solubilities of up to 25 at% could be achieved.

Fig. 19 compares the equilibrium solid solubilities of several solute elements in copper as the solvent with the extended solubilities obtained by MA. It may be noted that MA achieves a significant increase in solid solubility limits. Hume-

Rothery rules [409] suggest that complete solid solubility of one component in the other can result if the two components have (a) an atomic size difference of less than ±15%, (b) the same crystal structure, (c) the same valency, and (d) very close electronegativity values. If any one of these conditions is not satisfied, then the extent of solid solubility will be limited. To rationalize the solid solubility increase in mechanically alloyed powders in terms of the Hume-Rothery rules, the solid solubility values of these solute elements are plotted against atomic radius in Fig. 20. The ±15% limits of the atomic radius of copper are also indicated in Fig. 20. It is interesting to note that in all those cases where the solid solubility limit has been considerably increased by MA, the atomic radius of the solute is well within the 15% limit suggested by Hume-Rothery. In some cases significant increases in solid solubility limits have been observed even when the atomic size difference is quite large (e.g., Cu–Hg). The plot also makes it very clear that the solid solubility increase is very little when the difference in the atomic sizes between the solvent and the solute is very large (e.g., Cu–Sb). This analysis confirms that the rules applicable for solid solution formation under equilibrium conditions are valid under non-equilibrium conditions also. Further, the maximum limits not observed under equilibrium conditions when the Hume-Rothery rules are satisfied are realized under non-equilibrium conditions. The best example for this is the Cu–Ag system, where the Hume–Rothery rules predict complete mutual solid solubility of Cu and Ag whereas only a limited solid solubility is observed under equilibrium conditions. Complete solid solubility of one element in the

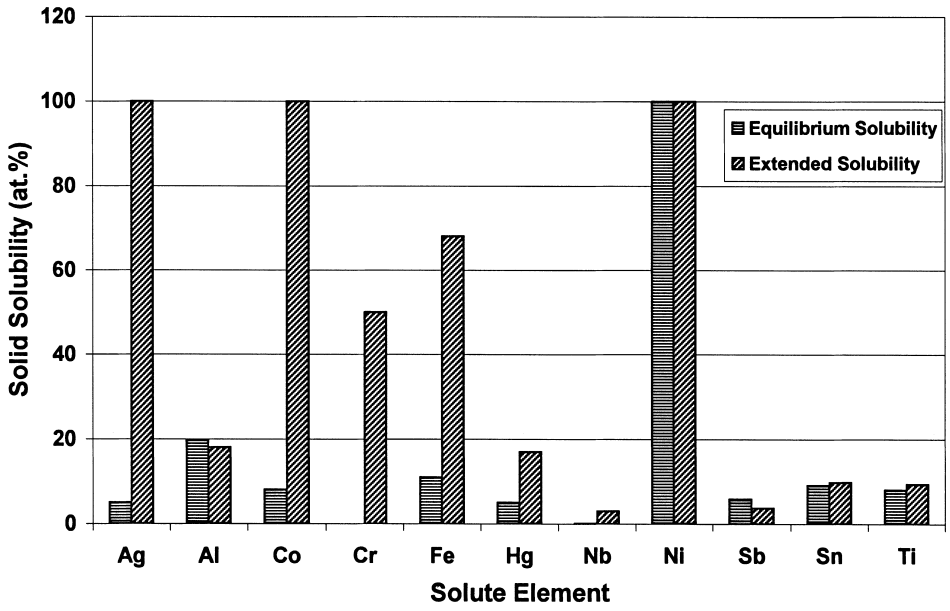

Fig. 19. Comparison of the equilibrium and extended solid solubility limits of several solute elements in copper achieved by MA.

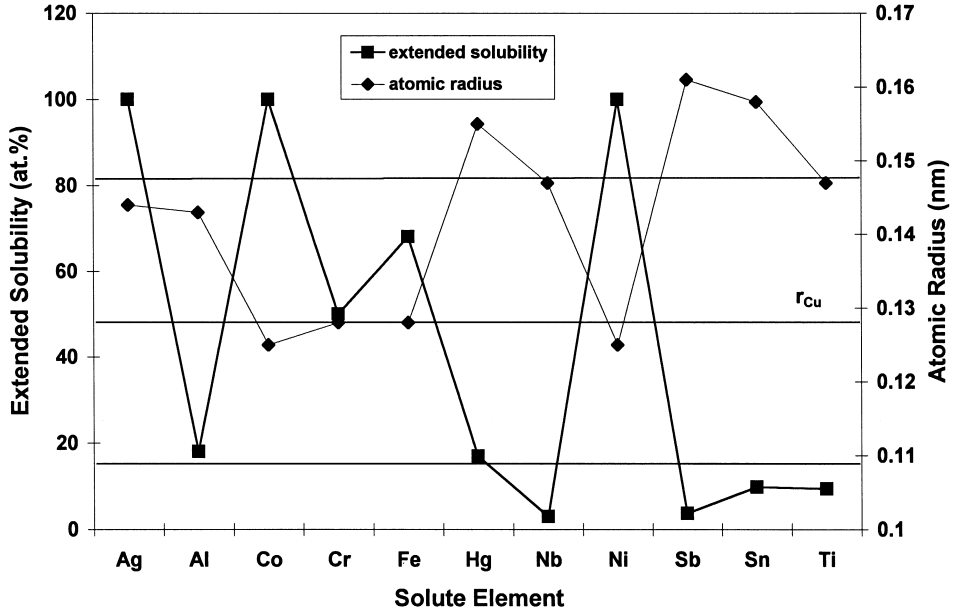

Fig. 20. The extended solid solubility limits of different solute elements in copper achieved by mechanical alloying of blended elemental powder mixtures plotted against the atomic radius of the solute element.

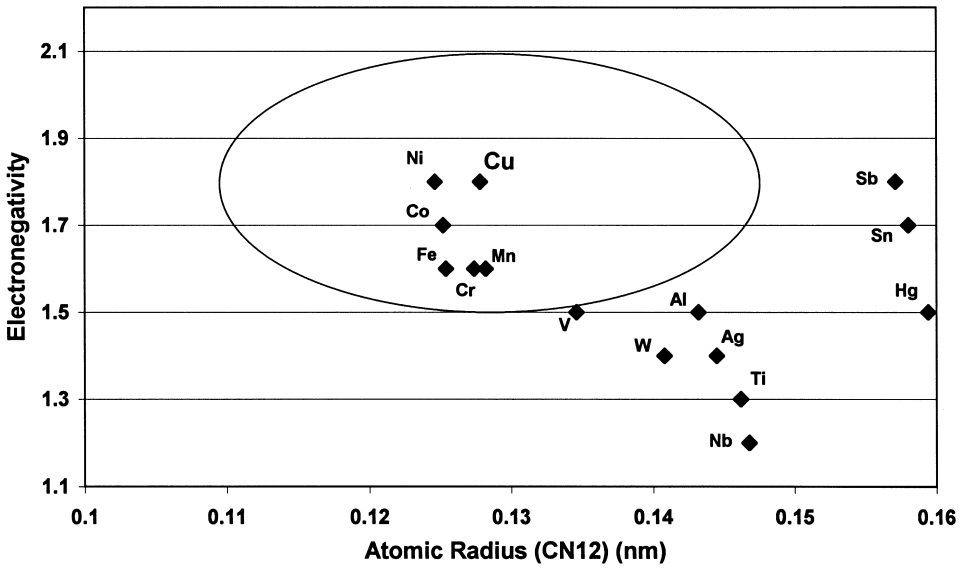

Fig. 21. Darken–Gurry (electronegativity vs. atomic size) plot for mechanically alloyed Cu-based powder mixtures.

other is obtained under non-equilibrium conditions achieved during rapid solidification or MA.

Similarly good predictions of solubility were obtained with a modified Darken–Gurry plot [410] of electronegativity versus metallic radius. Fig. 21 shows the Darken–Gurry plot for mechanically alloyed Cu-base powder mixtures. Here also it may be noted that solid solubility extensions have been observed with solute elements that have greater than 15% atomic mismatch and with electronegativites that differ by more than 0.3 units.

8.3. Comparison between mechanical alloying and rapid solidification

The absolute limits of solid solubility extension in alloys processed by rapid solidification processing (RSP) have been determined from thermodynamic considerations using the concept of T_0 temperature at which, for a given composition, the solid and liquid phases have the same free energy. Supersaturated solid solutions can be obtained only when the liquid could be undercooled to a temperature below T_0 [411]. Even though MA also is a non-equilibrium processing technique, there have not been any attempts so far to rationalize the available experimental data of solid solubility extensions; further, the possible limits have not been defined theoretically. However, since no liquid phase is involved during MA, it is doubtful if the same criterion as in RSP can be used to rationalize the solid solubility extensions achieved during MA.

The mechanisms by which supersaturated solid solutions form by MA and RSP techniques are different; even then comparisons have been frequently made, with no specific conclusions. Table 8 compares the available data. For example, solid solutions have been formed in the whole composition range in the Cu–Ag system by both the techniques. Rapid solidification processing produced continuous series of solid solutions in many other alloy systems [219], but MA did not obtain similar results. Solid solutions have been obtained in the full composition range in the Cu–Fe, AlSb–InSb, and Cu–Co systems by MA but not by RSP. The levels of solid solubility achieved are also different in different systems by these two techniques.

It was reported that the extent of supersaturation in rapidly solidified alloys increases with the quenching rate [2–4]. Thus, the solubility extension is higher in an alloy system when the liquid was melt spun at about 10^5–10^6 K/s than when the melt was atomized at 10^2–10^3 K/s. But, a similar situation has not been reported in mechanically alloyed powders. For example, one could investigate the solubility extensions as a function of milling intensity, energy input, or other parameters. In fact, taking all these variables into consideration one can define an effective "quench" rate or milling efficiency. It will be then worthwhile to investigate if the solid solubility extensions are higher at higher milling efficiencies in the MA case also.

The limits of solid solubility extensions achieved by MA have also been compared with the values obtained by other methods. Fig. 22 shows schematically the room temperature solid solubility of Fe in Cu obtained by different non-

equilibrium processing methods. It may be noted that the mechanically alloyed powders show the maximum solid solubility extension.

It was shown in Table 1 that the maximum departure from equilibrium obtainable by MA is higher than that by RSP. Therefore, one expects larger solid solubility extensions during MA than during RSP. But, the available results do not always confirm this (Table 8). On looking through the data in Table 8, one can make a general observation that the maximum solid solubility extension

Table 8
Comparison of solid solubility limits (at%) achieved by rapid solidification processing (RSP) and mechanical alloying (MA)

Solvent	Solute	Equilibrium value		By MA	By RSP
		At RT	Maximum		
Ag	Cu	0.0	14.0	100	100
	Gd	0.0	0.95	5.0	5.0–6.0
Al	Cr	0.0	0.37	5	6
	Cu	0.0	2.48	5.6	18
	Fe	0.0	0.025	4.5	6.0
	Ge	0.0	2.0	14.1	40
	Mg	1.2	18.6	40	40
	Mn	0.4	0.62	18.5	9
	Mo	0.0	0.06	2.4	2.4
	Nb	0.0	0.065	25	2.4
	Ni	0.0	0.11	10	7.7
	Ru	0.0	0.008	14	4.5
	Si	0.0	1.5	4.5	16
	Ti	0.0	0.75	36	2.0
Cd	Zn	3.1	4.35	50	35
Co	Zr	0.0	< 1.0	5	1.5
Cu	Ag	0.0	5.0	100	100
	Cr	0.0	0.0	50	4.5
	Fe	0.3	11.0	68	20
	V	0.0	0.1	Unspecified	1.0
Fe	B	0.0	0.0	4.0	4.3
	Ge	10.0	17.5	25	25
	Sn	0.0	9.2	25	20.0
	W	0.0	14.3	Unspecified	20.8
Mg	Al	0.9	11.0	3.7	21.6
Nb	Al	5.9	21.5	60	25
Ni	C	0.0	7.4	12	8.2
	Ge	9.6	12.0	25	22
	Nb	3.2	14.0	15	15.1
	Si	10.0	15.8	24	20
	Sn	0.0	10.6	17.5	17.0
	Ta	3.0	17.2	30	16.6
	V	15.0	43.0	25	51.0
Ti	Si	0.0	3.5	37.5	6.0

achieved by MA is higher than that by RSP when the room temperature solid solubility is very small or almost zero. This is understandable because MA is a near-room temperature process and therefore the room temperature solid solubility is more important than the maximum solid solubility at the higher temperatures; the latter is important in RSP studies.

9. Synthesis of intermetallics

The ordered nature of intermetallics leads to attractive elevated temperature properties such as high strength, increased stiffness, and excellent corrosion/oxidation resistance. These attributes are a result of the reduced dislocation motion (since pairs of dislocations — superdislocations — need to move together to retain the ordered nature of the lattice) and low diffusivities. Also associated with the reduced dislocation activity is the low ambient temperature ductility and fracture toughness, which preclude large-scale industrial applications of intermetallics. Hence, several attempts have been made in recent years to alleviate this problem. The common routes adopted to improve the room-temperature ductility of intermetallics are:

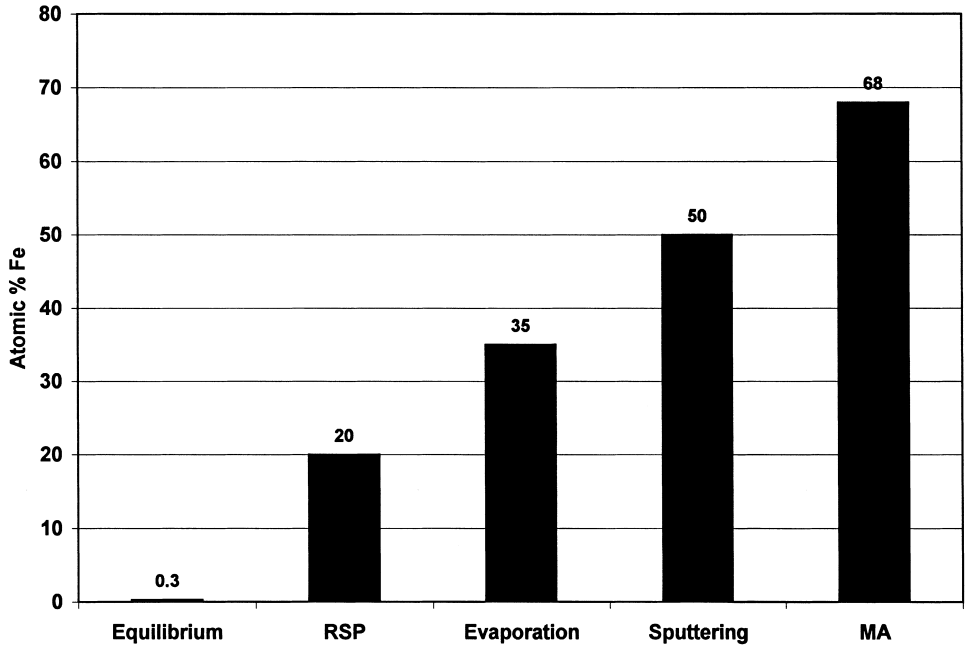

Fig. 22. Solid solubility of Fe in Cu obtained by different non-equilibrium processing techniques.

1. reduction in grain size,
2. disordering of the lattice, to improve the dislocation motion (superdislocations do not exist in disordered lattices and therefore only single dislocations need to move for deformation to occur), and
3. modifying the crystal structure of the phase into a more symmetric, e.g., cubic one.

Mechanical alloying can achieve all the above effects simultaneously and therefore, this processing technique has been extensively employed to synthesize intermetallics and study their mechanical behavior. In this section, however, we will only discuss the synthesis of intermetallics by MA and not discuss the aspects of improved ductility. For the latest situation on this topic, the reader is advised to consult Refs. [412,413].

The types of intermetallics synthesized by MA include both quasicrystalline and crystalline intermetallic phases. Both equilibrium and metastable phases have been synthesized in the latter category and these also include the disordered and ordered phases.

Table 9
Quasicrystalline phases formed by MA of blended elemental powders

Alloy/composition	Mill	BPR	Intensity of milling	Time (h)	Reference
$Al_{65}Cu_{20}Co_{15}$	Fritsch P5	15:1	–	55[a]	[418]
Al–Cu–Cr	Fritsch P5	15:1	9	–	[418]
$Al_{65}Cu_{20}Fe_{15}$	Fritsch P7	15:1	7	15	[419,420]
$Al_{65}Cu_{20}Mn_{15}$	Fritsch P5	15:1	5	–	[217]
	Fritsch P5	15:1	7	90	[217,416,418]
	Fritsch P5	15:1	9	60	[217]
$Al_{40}Cu_{10}Mn_{25}Ge_{25}$	Fritsch	20:1	450–650 rpm	66	[421]
$Al_{65}Cu_{20}Ru_{15}$	–	–	–	–	[422]
$Al_{70}Cu_{12}Ru_{18}$	–	–	–	–	[422]
$Al_{75}Cu_{15}V_{10}$	Fritsch P5/P7	15:1	9	[b]	[418,423]
$Al_{50}Mn_{20}Ge_{30}$	Fritsch	20:1	45–650 rpm	47	[424]
$Al_{50}Mn_{20}Si_{20}Ge_{10}$	Fritsch	20:1	45–650 rpm	80	[424]
$Al_{75}Ni_{10}Fe_{15}$	–	–	–	[c]	[425]
$Al_{70}Pd_{20}Mn_{10}$	Fritsch P7	15:1	7	30	[426]
$Mg_{32}Cu_8A_{l4}$	Planetary	–	900 rpm	–	[416,417,427,428]
Mg–Al–Pd	Planetary	40:1	150G[e]	4 h	[429]
$Mg_{32}(Al,Zn)_{49}$	Planetary	–	–	3 min	[417,427,428,430,431]
	Fritsch	–	600 m/s^2	10 min	[432]
$Mg_3Zn_{5-x}Al_x$ (x = 2–4)	Planetary	–	900 rpm	–	[416,428]
$Ti_{56}Ni_{18}Fe_{10}Si_{16}$	SPEX 8000	6:1	–	[d]	[433]

[a] MA for 55 h to a nanocrystalline phase followed by annealing for 1 h at 600°C.
[b] MA for 20 h to an amorphous phase followed by annealing at 450°C.
[c] MA for 400 h followed by annealing for 20 h at 800°C.
[d] MA for 30 h to an amorphous state followed by annealing for 30 min at 750°C.
[e] G represents the gravitational force.

9.1. Quasicrystalline phases

Quasicrystalline phases are metallic phases, which exhibit the traditionally forbidden translational symmetries. Instead, these phases have non-crystallographic rotational symmetries, e.g., 5-fold, 7-fold, 10-fold, etc. and quasi-periodic translational order. The structure and properties of quasicrystalline phases have been discussed in some earlier reviews (see, for example, Refs. [414,415]).

The first report of synthesis of quasicrystalline phases by MA appeared only in 1989 [416,417] and even today only a few reports exist on the synthesis and transformation behavior of these quasicrystalline phases. The quasicrystalline phases synthesized to-date have been summarized in Table 9 along with the milling conditions employed to synthesize them. It should be noted that all the quasicrystalline phases synthesized so far are of the icosahedral type (having the 5-fold symmetry) and that there are no reports of synthesis of phases with other symmetries; a number of the latter category have been synthesized by other methods such as rapid solidification from the melt [414,415]. The broadening of the X-ray diffraction peaks during MA may hinder a clear identification of the phases produced and also a proper distinction amongst the different types of quasicrystalline phases. This could be one reason why phases other than those with the icosahedral symmetry have not been obtained/reported by MA. Confirmatory transmission electron microscopy studies are necessary and useful for an unambiguous identification of these phases. The icosahedral phases synthesized by MA have been found to be similar to those produced by RSP.

Eckert et al. [217] reported that the nature of the phase synthesized in the Al–Cu–Mn system was different depending up on the intensity of milling in the Fritsch Pulverisette. They noted that an amorphous phase formed when the blended elemental powder was milled at an intensity of 5, and an equilibrium intermetallic phase formed at an intensity of 9. At an intermediate intensity of 7, a quasicrystalline phase was formed. This was explained on the basis of the temperature rise during milling. The estimated temperatures were 247°C at an intensity of 5, 407°C at an intensity of 7, and 590°C at an intensity of 9. The temperature rise at the milling intensity of 9 is above the crystallization temperature of the quasicrystalline phase produced and therefore an equilibrium intermetallic phase formed under this condition of milling. This observation again confirms that "soft" milling conditions favor the formation of metastable phases - both amorphous and quasicrystalline [85,113,114]. Yet another conclusion that can be drawn from the above observation is that an amorphous phase is farthest from equilibrium while the quasicrystalline phase is intermediate in departure from equilibrium between an amorphous phase and an equilibrium crystalline phase.

Like in the case of amorphization of intermetallics on milling (to be discussed later), amorphization has also been reported to occur on milling the quasicrystalline phases. Accordingly, it has been reported that the $Al_{65}Cu_{20}Fe_{15}$ quasicrystalline phase becomes amorphous (as detected by XRD methods) after

milling for 300 h in a QM-1SP planetary ball mill at a BPR of 10:1 [434]. TEM investigations have, however, shown the presence of a few quasicrystalline phase particles with a size of 10–15 nm. Further, there are also reports of formation of a quasicrystalline phase on annealing an amorphous phase [423,433]. This is somewhat similar to the mechanical crystallization behavior observed when an amorphous alloy crystallizes on milling. This aspect also will be discussed in a later section.

Apart from an early curiosity to synthesize quasicrystalline phases by a route other than RSP and the possibility of producing large amounts of powders for subsequent consolidation to form bulk alloys, interest in this aspect has now come down. The discovery of stable (equilibrium) quasicrystals in recent years [415] has further lessened the interest in the synthesis and characterization of quasicrystals by MA.

9.2. Crystalline intermetallic phases

The equilibrium Hume–Rothery electron compounds — β-brass, γ-brass, and ε-brass phases — were synthesized by MA starting from blended elemental pure Cu and Zn powders mixed in proper proportions [435,436]. Similarly, a number of other intermetallic phases have been synthesized. In some cases, formation of intermetallics seems to have taken place by a combustion reaction. Amongst these cases, there are also examples where the combustion took place only after ''interrupted milling'', i.e., milling of the powders for a given length of time, aging the powder at room temperature after stopping the milling, and then resuming the milling operation. An NiAl compound was synthesized this way [115]. Similar results were also reported in other systems and in fact these results compare very favorably with those obtained in the self-propagating high-temperature synthesis or combustion synthesis process [437].

9.2.1. Metastable crystalline phases

The synthesis of only a few metastable crystalline intermetallic phases has been reported by MA. This is in stark contrast to the large number of metastable intermediate phases reported in rapidly solidified alloys in the early years of the development of the technique [219]. A metastable deformation-induced martensite phase has been reported to form in mechanically alloyed Cu–Zn alloy powders [157,435]. It is surprising that not many such deformation-induced metastable phases have been reported in mechanically alloyed powder mixtures in view of the fact that there are several instances where metastable phases are formed by cold working; a good example being the formation of deformation-induced metastable ε (hcp) martensite in austenitic stainless steels. The synthesis of a bct-Fe phase by prolonged processing of iron powder in a nitrogen atmosphere has also been reported [438]. Recently, a metastable crystalline phase with rhombohedral crystal structure was reported to form in mechanically alloyed Al–Ge powders [439,440]. Two metastable phases designated β′ (Ni_3Sn) and β″ (Ni_3Sn_2) have been detected in mechanically alloyed Ni–Sn alloys at 25 and 40 at% Sn compositions,

respectively [441]. The nature of the phases and the conditions under which these metastable phases were formed in mechanically alloyed powder mixtures are summarized in Table 10. It is of interest to note that a number of metastable ordered phases are also formed directly on MA.

If a phase, which is stable at high temperatures and/or high pressures is retained by MA at room temperature and atmospheric pressure, then also it is considered metastable. However, such phases are listed separately in Table 11.

As mentioned earlier (Section 7), the room temperature formation of phases stable at high temperatures during milling has been used to estimate the maximum temperature reached during milling. Accordingly, formation of the high-temperature orthorhombic Sb_2O_3 phase during milling of Sb and Sb–Ga alloys at room temperature was inferred to indicate that the maximum temperature reached was at least 570°C, the temperature above which this phase is stable [92,214]. The

Table 10
Metastable phases formed in mechanically alloyed powder mixtures

Alloy	Mill	BPR	Time	Phase	Reference
Al–Cu	Ball mill	90:1	400 h	m-bcc	[148]
Al–Ge	SPEX 8000	–	120 h	Rhombohedral γ_1	[439]
Al–Ge	Fritsch P5	10:1	100 h	Rhombohedral	[440]
Al–Hf	SPEX 8000	–	20 h	Ll_2Al_3Hf	[138,442]
Al–Hf–Fe	SPEX 8000	10:1	8 h	$Ll_2(Al,Fe)_3Hf$	[443]
Al–Hf–Ni	SPEX 8000	10:1	10 h	$Ll_2(Al,Ni)_3Hf$	[443]
Al–Mn	SPEX 8000	10:1	[a]	Fcc	[232]
Al–Ti	Fritsch P5	10:1	100 h	Ll_2Al_3Ti	[138,444]
Al–Zr	Fritsch P5	10:1	20 h	Ll_2Al_3Zr	[138,442]
Al–Zr–Fe	SPEX 8000	10:1	20 h	$Ll_2(Al,Fe)_3Zr$	[445]
Al–Zr–Ni	SPEX 8000	10:1	20 h	$Ll_2(Al,Ni)_3Zr$	[438]
Co–C	Ball mill	100:1	500 h	m-Co_3C	[258]
Cu–In–Ga–Se	Fritsch P5	10:1	2 h	Cubic $CuIn_{0.7}Ga_{0.3}Se_2$	[85]
Cu–Zn	SPEX 8000	5:1	0.5 h	Deformation martensite	[435]
Cu–Zn	Fritsch P5	10:1	–	Martensite	[157]
Fe–B	Fritsch	50:1	3 h	m-Fe_2B	[446]
Mg–Sn	SPEX 8000	10:1	12 h	Orthorhombic	[447]
Nb–Ge	SPEX 8000	–	5 h	Fcc	[340]
Ni–Al	SPEX 8000	6:1	20 h	m-Ni_3Al	[115]
Ni–C	Ball mill	100:1	500 h	m-Ni_3C	[258]
Ni–Sn	SPEX 8000	–	1 h	β' and β''	[441]
Te–Ag	SPEX 8000	8:1	50 h	π phase	[158]
Ti	Super Misuni NEV MA-8	6:1	100 h	m-Ti_2N	[448]
Ti–Al	Fritsch P5	10:1	10 h	Fcc γ-TiAl	[367,368]
Ti–Al	Fritsch P5	10:1	25 h	Fcc γ-TiAl	[111]
Ti–Si	Fritsch P5	10:1	–	m-$TiSi_2$ (C49)	[246,382]
Ti–Si	Ball mill	–	180 h	Bcc	[59]
Zr–Al	Attritor	10:1	25 h	m-Zr_3Al (DO_{19})	[107]

[a] MA/12 h plus aged for 30 days at room temperature.

Table 11
Polymorphic phase transformations in metals and alloys by MA

Starting phase	MA time	Final phase	Comments	Reference
γ-AlOOH (boehmite)	Fritsch P7/2.5 h	α-Al_2O_3 (corundum)		[215]
$Al(OH)_3$ (gibbsite)	Fritsch P7/7 h	α-Al_2O_3 (corundum)		[215]
γ-Al_2O_3	56 h	α-Al_2O_3		[254]
γ-Al_2O_3	Fritsch P9/2 h	δ-Al_2O_3		[449]
δ-Al_2O_3	Fritsch P9/2 h	θ-Al_2O_3		[449]
Co (fcc + hcp)	20 h	Co (hcp)	BPR 10:1	[450]
Co (fcc + hcp)	20 h	Co (hcp + fcc)	BPR 20:1	[450]
Co (fcc + hcp)	20 h	Co (fcc)	BPR 30:1	[450]
Co (fcc)		Co (hcp)		[269]
Co (fcc)	5 h	Co (hcp)		[401]
Co (hcp)	2 h	Co (fcc)	HT phase[a]	[401]
	15 h	Co (fcc)	HT phase	[451]
	20 h	Co (fcc)	HT phase	[261]
Co_3Sn_2 (ordered orthorhombic)	48 h	Co_3Sn_2 (disordered hexagonal)	HT phase	[452]
Cr_2O_3 (hexagonal)	18 h	Cr_2O_3 (cubic)		[453]
Dy_2O_3 C-type (Bixbyte)	–	Monoclinic Dy_2O_3 B-type		[454]
γ-Dy_2S_3	–			[455]
Er_2O_3 C-type (Bixbyte)	–	Monoclinic Er_2O_3 B-type		[454]
β-FeB (HT form)	Fritsch P7/62 h	α-FeB (LT form)	LT phase[b]	[456,457]
Fe_2B (bct)	Fritsch	Fe_2B (orthorhombic)		[458]
γ′ Fe_4N (fcc)	–	ε-Fe_4N (hexagonal)	HT phase	[459]
α-Fe_2O_3	SPEX 8000/70 h	Fe_3O_4		[460]
γ-Fe_2O_3	Oscillating mill/40 min	α-Fe_2O_3		[461]
Fe_3O_4	SPEX 8000/70 h	α-Fe_2O_3		[462]
GeO_2	–		Rutile type	[454]
Iron anhydrous ammonia	–		HT phase	[463]
α-$MgCl_2$	96 h	δ-$MgCl_2$		[464]
α-$MoSi_2$	–	β-$MoSi_2$	Due to reduction in particle size	[465]
Ni_3Sn_2 (orthorhombic)	40 h	Ni_3Sn_2 (B8-type hexagonal)	HT phase	[466]

(continued on next page)

Table 11 (*continued*)

Starting phase	MA time	Final phase	Comments	Reference
PbO	–			[467]
TaN (CoSn-type)	Fritsch P7/1 h	TaN (WC-type)		[468]
TiO_2	–		HP phase[c]	[469]
TiO_2 (anatase)	Uni-Ball mill/140 h	TiO_2 (rutile)	HT phase	[470]
TiO_2 (anatase)	–	TiO_2 (rutile)		[454]
TiO_2 (anatase)	SPEX 8000	Orthorhombic TiO_2(II)	HP phase	[471]
TiO_2 (anatase)	SPEX 8000	Monoclinic TiO_2(B)		[471]
Y_2O_3 (C-type)	–	Y_2O_3 (B-type)		[454]
γ-Y_2S_3	–			[455]
Yb (divalent)	–	Yb (trivalent)		[472,473]
Yb_2O_3 (C-type)	–	Yb_2O_3 (B-type)		[454]
$Zn_{10}Fe_3$ (τ)	–	Zn_7Fe (δ)		[474]
$Zn_{21}Fe_5$ (τ_1)	–	$Zn_{13}Fe$ (ξ)		[474]
ZrO_2 monoclinic	–	CaF_2-type ZrO_2		[475]
ZrO_2 monoclinic (baddeleyite)	Uni-Ball mill/70 h	Tetragonal or cubic ZrO_2		[395,470]
ZrO_2 monoclinic (baddeleyite)	–	cubic ZrO_2 (CaF_2 type)		[454]
ZrO_2 (tetragonal)	–	ZrO_2 (cubic)	HT phase; due to reduction in particle size	[476]

[a] HT phase: high-temperature polymorph.
[b] LT phase: low-temperature polymorph.
[c] HP phase: high-pressure polymorph.

occurrence of the high-temperature orthorhombic Sb_2O_3 phase at room temperature is metastable in nature.

The pure metal cobalt is well known to undergo a martensitic transformation on cold working; the room temperature hcp form transforms to the elevated temperature fcc form. Both the pure metal Co and Co-base alloys have been subjected to MA and the hcp $\leftrightarrow$ fcc martensitic transformation has been observed. However, the end product of mechanical milling has been the fcc form in some cases [261,401,450] and the hcp form in some others [269]. In some instances, the fcc phase has been shown to transform to the hcp form after milling for a short time and then again to the fcc form after longer hours of milling. Since the fcc $\rightarrow$ hcp transformation and the reverse transformation are known to occur via formation of stacking faults, the nature and density of stacking faults present in the sample might have been responsible for the specific phase present in the sample. Several other high-temperature polymorphs have also been reported to form at room temperature by MA. Some of the available results on these polymorphic transformations are summarized in Table 11.

9.2.2. High-pressure phases

The pressures generated during MA have been estimated to be of the order of 6 GPa [24,188], and these should be sufficient to stabilize the high-pressure polymorphs of phases at atmospheric pressure. The high-pressure polymorphs of Dy_2S_3 and Y_2S_3 have been reported to be retained on MA at atmospheric pressure [455]. Similarly, high-pressure phases of other chalcogenides, such as $Cu_{2-x}S$ and $CuSe_2$ were also synthesized by MA at atmospheric pressure [477]. Sen et al. [471] synthesized the high-pressure orthorhombic form of TiO_2 (II) at atmospheric pressure by MA at room temperature. Alonso et al. [478] reported that they could synthesize the high-pressure fcc polymorphs of lanthanide metals Dy, Gd, Nd, and Sm by mechanically alloying the powders for about 24 h in a SPEX mill using a hardened steel vial and alloy steel balls. It was, however, later recognized by them [479] that these are the NaCl-type phases formed by reaction of these reactive metals with oxygen, nitrogen, and hydrogen during milling in a poorly sealed vial. For example, the milled Nd powder contained 16.2 at% oxygen, 22.3 at% nitrogen, and 10.3 at% hydrogen. Thus, it is not clear whether the high-pressure phases of pure metals, especially the reactive ones, can be synthesized by MA. But, it looks that high-pressure compound phases of oxides, chalcogenides, etc. can certainly be synthesized by MA, since contamination is not likely to play any role in the formation of these compounds.

The above observation reminds us that extreme caution should be exercised in identifying metastable crystalline phases produced by MA. During the MA processing, the powder picks up appreciable quantities of interstitial elements like oxygen, nitrogen, hydrogen, and carbon (from the ambient atmosphere and/or the process control agents) and also iron and chromium (from the grinding media and/or the mill walls). These metallic and non-metallic impurities can have a very significant effect on the stability of the phases. Additionally, these interstitials can combine with the metallic elements and can form interstitial compounds. Thus, it

Table 12
Formation of Intermetallics by MA

System	Phase	Structure	Comments	Ref.
Ag–Al	ζ	Hcp, A3 (hP2)		[220]
Ag–Al	μ	Complex cubic, A13 (cP20)		[220]
Ag–33.3Cu–33.3Se	AgCuSe			[93]
Ag–33.3S	Ag_2S			[93]
Ag–33.3Se	Ag_2Se			[93]
Ag–34.5Te	$Ag_{1.9}Te$			[93]
Ag–40Te	Ag_3Te_2			[93]
Al–40Co	AlCo	B2		[480]
Al–18.2 to 50Co	β′-AlCo			[401]
Al–Fe	Al_6Fe		MA + 300°C	[229]
Al–12.5Fe	Al_3Fe		MA/12 h + 500°C	[481,482]
Al–20, 25Fe	Al_3Fe			[482]
Al–25, 29Fe	Al_5Fe_2			[483,484]
Al–25Ge–10Fe	Al_4Ge_2Fe	Tetragonal, $a = 0.6417$, $c = 0.9521$ nm		[485]
Al–Mg	Al_3Mg_2	γ		[205]
	$Al_{12}Mg_{17}$	A12		[205]
Al–4Mn	Al_6Mn	Orthorhombic	MA + extrusion	[232,486]
Al–3Mo	$Al_{12}Mo$		MA + HT	[142,487]
	Al_5Mo			[142,487]
	Al_4Mo			[142,487]
	Al_8Mo_3			[142,487]
Al–Nb	Al_3Nb			[236,333,488–490]
Al–Nb–Ti	Nb_2Al			[490]
Al–25Ni	Al_3Ni			[115]
Al–35 to 50Ni	B2-NiAl			[115,491,492]
Al–8Ni–4Co	$Al_9(Co,Ni)_2$			[238]
Al–40 to 49Ni–2 to 20Cr	B2	Cubic		[493]
Al–Ni–Fe	B2			[494]
Al–40 to 49Ni–2 to 20Fe	B2			[493]
Al–39Ni–22Ti	Disordered NiAl	Cubic		[374]
Al–40Ru	RuAl	B2		[239]
Al–Sb	AlSb			[240]
Al–Ti	Al_3Ti		50 h	[495,496]
Al–25$TiH_{1.924}$	Al_3Ti		MA/10 h + 620°C / 7 days	[497]
Al–Zr	AlZr	Orthorhombic		[388,498]
Al–Zr	Al_3Zr_2	Orthorhombic		[388,498]
Be–Nb	$NbBe_{12}$		MA/72 h + 1000°C/4 h	[339]

Be–Nb	Nb_2Be_{17}		MA/72 h + 1000°C/4 h	[339]
Co–30 to 60Sn	Co_3Sn_2, CoSn, $CoSn_2$			[499]
Co–25Ti	Co_3Ti	Bcc	Cyclic Am → Cryst → Am	[500]
Co–50Ti	CoTi	Bcc	Cyclic Am → Cryst → Am	[501]
Cr–40C	Cr_3C_2		MA + 800°C/2 h	[286,502]
Cr–33Nb	Cr_2Nb			[503]
Cr–Si	Cr_3Si		MA/35 h (Cr-Si) + 900°C/4 h	[504]
Cr–67Si	$CrSi_2$			[505]
Cu–25In–50S	$CuInS_2$			[93]
Cu–25In–50Se	$CuInSe_2$			[93]
Cu–25In–50Te	$CuInTe_2$			[93]
Cu–30 to 70Al	Cu_9Al_4			[506]
Cu–11Ni–18P	Cu_3P, Ni_3P			[507]
Cu–20P	Cu_3P			[284]
Cu–33S	$Cu_{2-x}S$			[477]
Cu–25 to 75Sb	η-Cu_2Sb			[120]
Cu–66.7Se	$CuSe_2$			[477]
Cu–Sn	Cu_6Sn_5, Cu_3Sn			[289]
Cu–46.8, 49.3Zn	β-CuZn			[435]
CuY–33.3 mol% CuBa	$YBa_2Cu_3O_{7-\delta}$		MA + anneal in oxygen atm.	[508]
Cu–Zn	β	Bcc		[157]
	γ	Cubic		
	ϵ	Hexagonal		
Fe	ϵ-Iron nitride		In NH_3 atm., HT phase	[509]
Fe–10 to 30Al	FeAl	B2	MA/48h + 1150°C/4 h	[510]
Fe–25Al	Fe_3Al		MA/4h (SS) + 550 K	[295]
Fe–25Al	FeAl			[150]
Fe–40Al	FeAl (disordered)			[155]
Fe–Al	FeAl		MA (Fe(Al)) + 700°C	[299]
Fe–50Co	FeCo			[511]
Fe–S	FeS			[512]
Fe–Si	α-$FeSi_2$		MA + 300°C	[63,513]
Fe–Si	β-$FeSi_2$		500 h	[514]
Fe–Si	β-$FeSi_2$		MA/500 h + 973 K/200 h	[515]
Fe–Si	α-$FeSi_2$, FeSi			[513]
Fe–25 to 50Si	FeSi			[313]
Fe–40 Si	FeSi			[516]
Fe–Sn	Fe_3Sn_2			[517]
	FeSn			[517]
	$FeSn_2$			[517]
Fe–Ti	FeTi			[518]
Fe–33W	Fe_2W			[519]
Fe–33Zr	Fe_2Zr			[520]

(continued on next page)

Table 12 (*continued*)

System	Phase	Structure	Comments	Ref.
Fe_3O_4–Nd_2O_3	$NdFeO_3$			[521]
Fe_2O_3–33.3ZnO	$ZnFe_2O_4$		MA/18 min + 1100 K/400 min	[522]
Hf–50Ru	HfRu	Cubic, B2		[523]
In–Sb	InSb			[240]
Mg–Ge	Mg_2Ge	Cubic, a = 0.6445 nm		[447]
Mg	MgH_2		H_2 atm./47.5 h	[125]
Mg–33.3Ni	Mg_2Ni	Hexagonal,	> 10 h	[524]
Mg–Si	Mg_2Si	Cubic, a = 0.6359 nm		[447,525]
Mg–Sn	Mg_2Sn	Cubic, a = 0.6761 nm		[447]
Mn–47Al	β-MnAl	B2		[526]
Mn–50Bi	MnBi			[188]
Mo–25Si	Mo_5Si_3			[89]
Mo–37Si	Mo_5Si_3			[527]
Mo–37.5Si	Mo_5Si_3			[467]
	β-$MoSi_2$		MA + 500°C	
Mo–38Si	Mo_5Si_3			[88,89]
Mo–67Si	α-$MoSi_2$		SHS reaction occurred	[88,89]
Mo–66.7Si	α-$MoSi_2$		MA/6 min	[465]
	β-$MoSi_2$		MA/40 min	
Mo–66.7Si	$MoSi_2$		MA/210 h	[528]
Mo–66.7Si	t-$MoSi_2$		SHS at ≥ 3 h	[529,530]
Mo–66.7Si	$MoSi_2$		MA + 760°C/24 h	[64]
Mo–67Si	$MoSi_2$(α and β)			[527]
Mo–80Si	$MoSi_2$(α and β)			[88,89]
Mo–Si	α-$MoSi_2$		SHS; 14 h 15 min	[88]
	Mo_5Si_3		100 h	
Nb–Al	Nb_3Al		MA + 800-950°C	[106]
Nb–15.4Al	Nb_3Al		MA + 1150K	[139]
Nb–74Al	Nb_2Al		200 h	[489]
	$NbAl_3$		300 h	
Nb–25Al	Nb_3Al		MA + 1500 K/30MPa/3-4 min.	[334]
Nb–33.3 to 70Al	σ-Nb_2Al + $NbAl_3$		MA + 825°C/2 h	[236]
Nb–25Al	Nb_3Al		MA + 825°C/2 h	[236]
Nb–25Ge	Nb_3Ge,Nb_5Ge_3, δ-$NbGe_2$			[340]
Nb–S	$Nb_{1-x}S$			[512]
Nb–16Si	Nb_3Si			[531]
Nb–35Si	α-Nb_5Si_3			[532]
Nb–45 to 59Si	$NbSi_2$ + β-Nb_5Si_3			[523]
Nb–37.5Si	Nb_5Si_3 (α, β, and γ-types)			[532,533]

Nb–66.7Si	$NbSi_2$		SHS partly; reaction takes place abruptly after 65 min	[341,503,505,533]
Nb–Sn	Nb_3Sn		MA + 750–850°C	[106]
Ni–60 to 65Al	NiAl			[491]
Ni–Al	B2 NiAl			[299]
Ni–Al	Al_3Ni (ordered), NiAl (ordered), Ni_3Al (disordered)			[157]
Ni–24Al	$L1_2Ni_3Al$			[534,535]
Ni–25Al	Disordered Ni_3Al			[344]
Ni–25Al	Ni_3Al			[536]
Ni–49Al	NiAl			[535]
Ni–50Al	B2NiAl			[103,299,300,303,342]
Ni–63Al	NiAl (disordered)			[345]
Ni–65Al	Ni_2Al_3		17 min	[218,345]
	NiAl		125 min	
Ni–70Al	Ni_2Al_3			[345]
Ni–75Al	$NiAl_3$, Ni_2Al_3			[218]
Ni–7.5Al–17.5Nb	$Ni_3Al + Ni_3Nb$			[535]
Ni–38.7Al–19.3Nb	NiAl + NiAlNb			[535]
Ni–50Al–25Fe	β′-(Fe,Ni)Al			[537]
Ni–25 to 30Al–20 to 25Ti	β′-Ni(Al,Ti)			[538,539]
Ni–40S	Ni_3S_2			[512,540]
Ni–Si	Ni_5Si_2 and Ni_2Si		200 h	[541]
Ni–25Si	Ni_3Si_2			[527]
Ni–33Si	Ni_2Si			[527]
Ni–50Si	NiSi			[527]
Ni–50Si	NiSi		MA + 700°C/1 h	[59]
Ni–67Si	$NiSi_2$	Fcc		[527]
Ni–40Ti	Ni_3Ti			[542,543]
Pb–Te	PbTe	Cubic, NaCl-type	2 min	[544]
PbO–TiO_2	$PbTiO_3$			[545]
PbO_2–TiO	$PbTiO_3$			[545]
Pd–50Al	PdAl			[546]
Pd–19 Si	Pd_9Si_2 and Pd_3Si			[547]
Pd–20Si	Pd_3Si			[547]
Sm–Fe	$SmFe_2$		MA/7 h + 500°C/2 h	[548]
Sm–Fe	Sm_2Fe_{17}		MA/7 h + 800°C/2 h	[548,549]
Sm–57.2Se	Sm_3Se_4			[93]
Sm–60Se	Sm_2Se_3			[93]
Sm–50Te	SmTe			[93]
Sn–66.7S	SnS_2			[512]
Ta–66.7Si	$TaSi_2$			[533]
Te–25 to 67 Ag	π-Phase	SC, $a = 0.306$ nm		[158]
Ti–45Al	α_2-DO_{19}		MA/200 h + VHP 1173 K/1 h	[550]
Ti–48Al	TiAl		MA + 1000°C/1 h hot press + 1200°C/4 h	[551]

(continued on next page)

Table 12 (*continued*)

System	Phase	Structure	Comments	Ref.
Ti–50Al	Ti_3Al			[336]
Ti–50Al	Disordered TiAl			[368]
Ti–60Al	Fcc γ-TiAl			[111,367]
Ti–50Al	TiAl		MA/650 h + 800°C/2 h	[552]
Ti–24Al–11Nb	B2	Cubic		[372]
Ti–25Al–25Nb	B2	Cubic		[373]
Ti–28.5Al–23.9Nb	B2	Cubic		[373]
Ti–37.5Al–12.5Nb	B2	Cubic		[373]
Ti–Ni	Ti_2Ni		1 min	[553]
	TiNi	B2	5 min	[553]
Ti–25Ru–25Fe	Ti_2RuFe			[554]
Ti–37.5Si	Ti_5Si_3			[336,555]
Ti–37Si	Ti_5Si_3		MA/180 h (Am) + 800°C/10 min	[59]
Ti–67Si	$TiSi_2$		m-bcc + 800°C/30 min	[59]
Ti–Si	Ti_5Si_3, Ti_5Si_4			[556]
Ti–50V	TiV	Bcc		[557]
	$TiVH_{4.7}$	Fcc		[557]
$TiH_{1.924}$–50Al	TiAl	Fct	MA/16.5 h + 620°C /7 days	[497]
TiO_2–$Ba(OH)_2.8H_2O$	$BaTiO_3$			[558]
V–25Si	V_3Si + V_5Si_3			[114]
V–37.5Si	V_5Si_3			[533]
V–66.7Si	VSi_2			[533]
W–Si	WSi_2		MA(W + Si) + HIP 1200°C/100 MPa/ 3 h	[286,559]
W–66.7Si	WSi_2		MA/210 h	[528]
W–66.7Si	WSi_2 + W			[560]
Y_2O_3–$BaCO_3$–CuO	$Y_2Cu_2O_5$			[561]
Y_2O_3–CuO	$Y_2Cu_2O_5$			[561]
Y_2O_3–BaO_2–CuO	Y_2BaCuO_5			[561]
Zn–15Cu	ϵ-Phase		Milling for 1 h	[562]
	γ-Phase		After long milling	[562]
Zn–Fe				[171]
Zn–50S	ZnS			[512,540]
Zr	$ZrH_{1.66}$			[125]

is possible to misinterpret these interstitial phases (e.g., carbides, nitrides, hydrides, oxides, oxynitrides) as new intermetallic phases. An accurate chemical analysis of the final resultant powder can, in many cases, clear up this confusion [58].

9.2.3. Equilibrium crystalline phases

Both disordered and ordered intermetallics have been synthesized by MA. In some cases, the intermetallics were synthesized directly by MA; but, in others, an additional heat treatment was required after MA to form the intermetallic. The intermetallics synthesized include aluminides (mostly based on titanium, nickel, and iron), silicides, composites, and some exotic varieties. Table 12 presents a listing of the intermetallics synthesized by MA. As a typical example we will now describe the phase evolution in mechanically alloyed blended elemental Ti–Al powder mixtures.

The Ti–Al binary phase diagram features three intermetallics, viz., Ti_3Al (α_2),

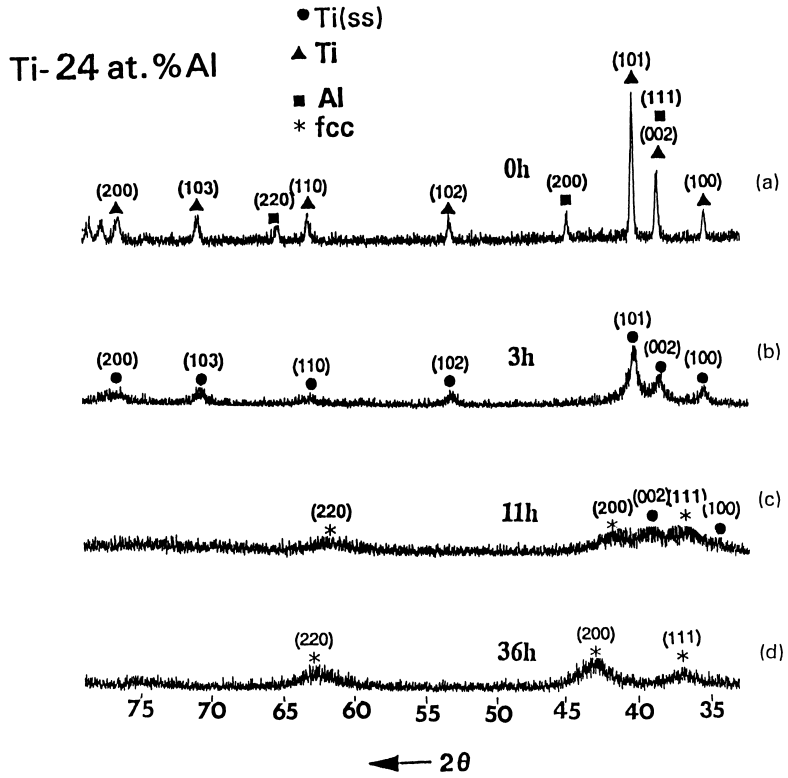

Fig. 23. X-ray diffraction patterns of blended elemental Ti–24at%Al powder mixture mechanically alloyed for different times. (a) as-mixed powder, (b) milled for 3 h showing the formation of Ti(Al) solid solution, (c) milled for 11 h showing the co-existence of Ti(Al) solid solution, amorphous, and, fcc phases, and (d) milled for 36 h showing the fcc phase.

TiAl (γ), and $TiAl_3$. All these intermetallics are lightweight, have high specific strengths, high elastic moduli, good corrosion resistance, and retain sufficient strength at elevated temperatures. The two titanium-rich aluminides — α_2 and γ — are attractive candidate materials for potential applications in advanced aerospace engine and airframe components [563]. There has been lot of activity in utilizing the technique of MA to synthesize these intermetallics to produce them in a nanocrystalline and disordered state to improve their ductility. Even though actual improvement in ductility is yet to be realized in mechanically alloyed nanostructured titanium aluminides, a vast amount of information is generated on the phase evolution in these alloys.

Fig. 23 shows a series of X-ray diffraction (XRD) patterns indicating the phase evolution as a function of milling time in a Ti–24at%Al powder mixture [366]. The as-mixed elemental blend (Fig. 23a) shows the presence of both elemental titanium and aluminum phases. On milling for 3 h, one could detect the formation of a solid solution of Al in Ti, as evidenced by the absence of the Al peaks in the XRD pattern (Fig. 23b). On continued milling for 11 h, the powder started losing crystallinity, as shown by a broad peak in the XRD pattern, indicative of formation of an amorphous phase (Fig. 23c). Some crystalline peaks are also superimposed on this peak suggesting the co-existence of the Ti(Al) solid solution and another crystalline phase. Further milling to 36 h produced an fcc phase, which has been identified as (Ti,Al)N, a contaminant phase (Fig. 23d). Thus, the phase formation sequence in this powder mixture can be represented as:

$$\text{BE Ti} + \text{Al} \rightarrow \text{Ti(Al) solid solution} \rightarrow \text{amorphous phase} \rightarrow \text{fcc (contaminant) phase} \tag{9}$$

If the milling were to be stopped at the correct time, the powder would not get seriously contaminated, and one can end up with either a solid solution or an amorphous phase. Even in these cases, if proper precautions are not taken, the powder would be somewhat contaminated, especially when reactive powders like titanium are being milled. See Section 14 for a discussion of powder contamination during MA.

Most of the investigators reported a similar sequence of events in the phase evolution on MA of Ti–Al powder blends, with the difference that the time required for the formation of different phases is different depending on the process variables (type of mill, BPR, use or absence of PCA, etc.). Further, depending on the purity of the milling atmosphere, the contaminant phase is minimized or completely avoided and also the extent of supersaturation has been reported to be different. (See Table 7 for the extent of supersaturation achieved by different investigators.) A concise summary of structural evolution in mechanically alloyed Ti–Al alloys, including the presence of a contaminant phase, is presented in Ref. [58].

In all the investigations on the Ti–Al system it has been reported that either a supersaturated solid solution or an amorphous phase formed on MA, and that the α_2 and γ phases could not be synthesized directly by milling. The desired

intermetallic could be obtained in the appropriate composition range, only after a suitable heat treatment. For example, annealing of the mechanically alloyed Ti–24at%Al powder for 4 weeks at 903 K produced the α_2-Ti_3Al phase [366]. Similarly, the γ-TiAl phase could be produced only after annealing the as-milled amorphous powder of appropriate composition for 168 h at 888 K [564]. These temperature and time combinations required for producing the intermetallics could vary considerably depending on the powder particle/grain size. The $TiAl_3$ phase, however, could be synthesized in a metastable $L1_2$ structure directly by MA [138].

Unlike in rapidly solidified alloys, systematic studies on the transformation behavior of metastable phases to the equilibrium phases have not been undertaken in mechanically alloyed powders. Only a few reports are available. For example, the transformation behavior of the $L1_2$-type Al_3Ti phase produced in Al–25Ti alloys was studied by annealing the powder at different temperatures. The as-milled powder contained the $L1_2$ and Al(Ti) solid solution phases. Annealing of this two-phase mixture at 673 K for 1 h produced another metastable DO_{23} phase. The equilibrium DO_{22} phase was obtained only after annealing the as-milled powder for 1 h at temperatures >1073 K [138] or 1273 K [552]. The $Al_{24}Ti_8$ phase was produced on annealing the as-milled powder at 1073 K [552]. Thus, it has not been easy to synthesize the equilibrium intermetallic phases in the Ti–Al system directly by MA.

The Ti–Al binary phase diagram suggests that the γ-TiAl phase is ordered up to the melting point, i.e., it is a permanently ordered intermetallic (or irreversibly ordered) phase. Formation of an fcc phase is theoretically expected to occur if the γ-TiAl phase (fct) were to be disordered, and this hypothetical fcc phase is expected to have a lattice parameter of $a = 0.402$ nm. There have been some reports on the possible synthesis of the disordered γ-TiAl (fcc) phase by MA of blended elemental powders [111,367,368,565,566]. But, a detailed analysis of the XRD patterns and a calculation of the expected intensities for the fcc phase reflections clearly show that the fcc phase interpreted as the disordered form of the γ-TiAl phase was indeed the contaminant nitride phase referred to above [58]. Further, it should be noted that disordered forms of the ordered phases have been synthesized by MA only when that phase exists in the phase diagram at high temperatures, i.e., the phase is reversibly ordered (see Section 10 for full details on this aspect). Since this is not the situation in the Ti–Al system, the disordered form of the γ-phase is not expected to be produced by MA.

As indicated above, a contaminant fcc phase is produced by MA in the Ti–Al system; this has been identified to be a nitride phase formed due to reaction of titanium with nitrogen in the milling atmosphere. The use of a PCA can also introduce contamination in the powder and therefore contamination of the powder can be minimized by avoiding the use of a PCA. Since a PCA is used mainly to minimize excessive cold welding and obtain a balance between fracturing and cold welding of powder particles, non-usage of the PCA may result in excessive cold welding and formation of large particles; true alloying also may not occur. This problem can be overcome by using brittle intermetallics or other

compounds. Accordingly, Suryanarayana et al. [567] synthesized the γ-TiAl phase by mixing titanium hydride (instead of pure titanium) and the Al_3Ti intermetallic (instead of pure aluminum) powders in the proper proportion, according to the relation:

$$Al_3Ti + 2TiH_2 \rightarrow 3TiAl + 2H_2 \uparrow \quad (10)$$

On mechanically alloying the above powder mixture for 52 h in a SPEX mill, they were able to obtain 55 vol% of the γ-TiAl phase; this value was increased to 95% on hot isostatically pressing the mechanically alloyed powder at 1023 K and 275 MPa for 5 h. This technique has been subsequently employed to synthesize the Ti_3Al, TiAl, and Al_3Ti phases by milling the titanium hydride and aluminum powders in the ratio of 3:1, 1:1, and 1:3, respectively [497,568]. But, in these cases, the intermetallics could not be synthesized directly by MA. A subsequent annealing treatment at 893 K for 7 days was necessary to produce the TiAl and Al_3Ti phases. The Ti_3Al phase could not be synthesized even after the heat treatment, probably due to the very high amount of hydrogen in the powder. But, the Ti_3Al phase could be produced after dehydrogenation of the mechanically alloyed powder at 873 K for 22 h, and then annealing this powder at 893 K for 7 days. One of the important advantages of using the titanium hydride instead of titanium is that PCA's need not be used during milling thus avoiding/minimizing contamination of the powder.

Considerable amount of literature also exists on the synthesis of nickel- and iron-aluminides by MA. Several intermetallic phases such as Ni_3Al, NiAl and Al_3Ni have been synthesized by MA in the appropriate composition ranges. An interesting observation is that the equiatomic NiAl phase is produced via a combustion synthesis (also known as the self-propagating high-temperature synthesis reaction) [115]. In this and similar cases, the combustion reaction took place only after "interrupted milling", i.e., milling of the powders for a given length of time, aging the powder at room temperature after stopping the milling, and then resuming the milling operation. For example, in the Al–Ni system, an intimate mixture of Al and Ni phases was detected after milling the blended elemental Al–Ni mixture for 2 h in a SPEX mill. If the milling is stopped and the powder is stored at room temperature for 30 min, and then milling is resumed, it is noted that the NiAl phase forms just after 1 minute of milling due to the occurrence of an explosive reaction [115]. Similar reactions were also observed in the synthesis of $MoSi_2$ [88], $NbSi_2$ [341], TiB_2 [569], $PbTiO_3$ [545], and a few other compounds. In all these cases, the MA operation produces a fine intimate mixture of the two or more phases involved; then an explosive reaction occurs and the compound suddenly forms. It has been recently reported that the time for the initiation of the explosive reaction can be delayed by 20–30 min by the addition of ternary elements (diluents) such as Ti and Fe to an Al–Ni mixture [494].

Explosive reactions were also reported to occur when the grinding container was opened soon after milling was stopped [570]. This can be attributed to the energy released due to the oxidation of the component metal powders. On the

other hand, the absence of an explosive reaction when the Ni–Al powders were milled in air [345] suggests that the elements were getting continuously oxidized. Thus the slow diffusion between the oxide-coated components would have resulted in reduced kinetics and prevented the explosive reaction from occurring. Reactions similar to the explosive reaction, termed "discontinuous additive mixing" were also reported [157]. In these cases, it has been reported that the reactions occurred only when the component powder particles were refined to a minimum size. This minimum critical crystallite size below which only the explosive-type reaction occurs was found to increase with a decrease in the enthalpy of formation of the ordered intermetallic.

It has also been reported in some cases that intermixing amongst the powder particles takes place continuously and metastable phases form prior to the formation of the equilibrium phases. In other cases, a series of other equilibrium phases form before the actual expected phase forms. For example, the α-$MoSi_2$ phase formed when the Mo-Si powder mixture was milled in a planetary ball mill for 6 min, while the β-$MoSi_2$ phase formed after milling for 40 min [465]. Similarly, the Ni_2Al_3 phase formed after milling for 17 min in an Ni–65Al powder; but the NiAl formed after 125 min; both these phases forming by an exothermic reaction [218].

The times required to form a particular phase depend on the initial concentration of the solute in the powder mixture. If the solute content is much less than the exact stoichiometry, the expected phase (although the proportion of the phase in the mixture of phases is less), would form at much longer milling times. For example, while investigating the formation of the β'-AlCo phase in Al–Co alloys, Sui et al. [401] noted that it required 10 h to form the β'-AlCo phase in an Al–50Co powder mixture. On the other hand, it required 30 h in Al–28.6Co, 70 h in Al–23.5Co, and 200 h in Al–18.2Co mixtures to form the β'-AlCo phase under identical milling conditions. This is easy to understand since formation of a particular phase requires diffusion and equilibration, both requiring time at a given temperature. The times can be probably reduced if the temperature at which milling is conducted is increased. But, there have not been any investigations reported to confirm this hypothesis. The time required to form a phase can also be substantially reduced if the BPR is increased. This has been shown to be true in many cases.

Another interesting observation made is that an amorphous phase can be crystallized to produce a crystalline intermetallic phase and this is referred to as mechanical crystallization. On the other hand, an intermetallic can be amorphized by MM and this is sometimes referred to as mechanical disordering or amorphization. There have been only a few reports of combining these two phenomena in the same alloy. It has been reported that the cyclic crystalline $\rightarrow$ amorphous $\rightarrow$ crystalline transformation occurs in the Co–25Ti and Co–50Ti powder mixtures [500,501]. Fig. 24 shows the formation of the amorphous phase forming after milling the Co–25Ti powder mixture for 3 h and the bcc Co_3Ti phase forming after continuing to mill for 24 h. These transformations are repeated at subsequent times [500]. Since the amorphous Co–Ti phase is

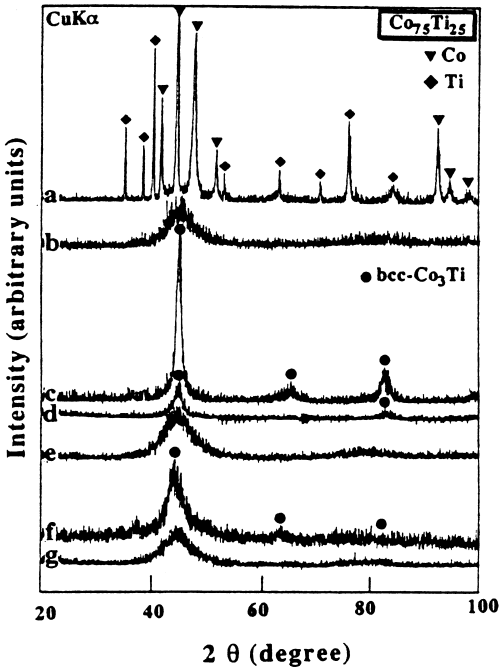

Fig. 24. X-ray diffraction patterns of Co–25at%Ti powder milled for (a) 0, (b) 3, (c) 24, (d) 48, (e) 100, (f) 150, and (g) 200 h. Note the cyclic transformation of amorphous and crystalline compounds.

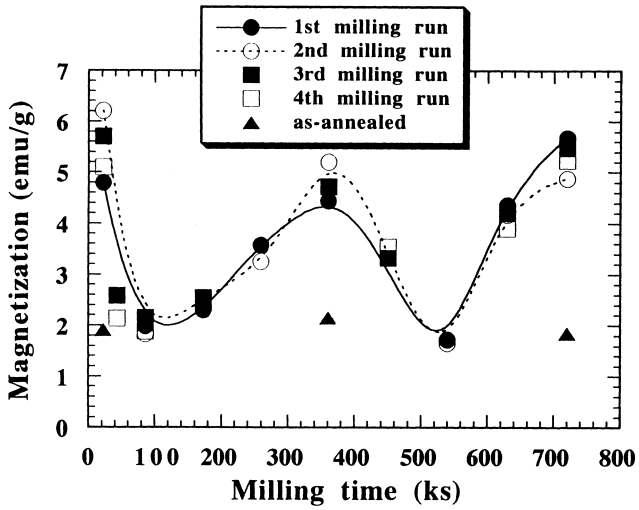

Fig. 25. Dependence of the magnetization behavior of mechanically milled Co–50at%Ti alloy powder with milling time. While the amorphous phase is ferromagnetic the bcc-CoTi phase is not.

ferromagnetic in nature and the crystalline bcc-CoTi phase is not, one could follow the amorphization and crystallization of the phases formed by measuring the magnetization behavior of the mechanically milled powder. This shows a cyclic behavior with time as represented in Fig. 25. It has also been shown earlier that formation of some crystalline phases on continued milling after the formation of the amorphous phase is due to severe contamination of the milled powder. But, these authors have shown that both the metallic and interstitial contamination of the powder is much less than 1 at% for each of these. However, such cyclic transformations are yet to be demonstrated in other alloy systems.

Schaffer [571] has shown that mixtures of intermetallic phases can be produced via MA by choosing the appropriate compositions. If the two phases are in equal proportion, then it has been observed that grain growth can be considerably hindered. Thus, by having approximately equal proportions of the NiAl and Ni_3Al phases in a nanocrystalline state, it was shown that grain growth could be slowed down up to at least 500°C.

Even though the intermetallics synthesized by MA include both the ordered and disordered types, it is not surprising that MA produces disordered phases. This is because MA involves heavy deformation and it is known to destroy long-range ordering in the lattice [572]. A large number of disordered intermetallic phases have been synthesized by MA and these are listed in Table 12.

In some instances, ordered intermetallics have been found to form directly on MA. This has been shown to be particularly true in Al-rich Al-transition metal systems. Some of the examples include Al_5Fe_2 [484], Al_3Hf [443] and (Al, X)$_3$Hf where X = Fe or Ni [443], Al_3Nb [573], Al_3Zr [138,442,443,445] and (Al, X)$_3$Zr where X = Fe or Ni [445,574].

Reasons for the formation of ordered intermetallics have not been investigated in detail. It may be assumed that a phase will exist either in the ordered or disordered condition depending upon the balance between atomic disordering introduced by MA and the thermally activated reordering. The reordering is caused by the difference in energy between the ordered and disordered states. Thus, if this difference in energy is small, the alloy will exist in the disordered state whereas if it is large the alloy will be in the ordered state. It has been shown that the NiAl phase can be produced in the ordered state by MA of the blended elemental powder, and upon milling the ordered NiAl compound it continues to be in the ordered state without getting disordered. However, the FeAl phase was found to be in the disordered state both in the as-produced condition by MA and also on milling the ordered compound [300]. The ordering energy is related and scales up with the enthalpy of formation (ΔH_f) and ΔH_f values for NiAl and FeAl are 72 and 25 kJ/mol, respectively [300]; confirming the above argument.

Superconducting compounds such as Nb_3Sn [106] and $YBa_2Cu_3O_{7-\delta}$ [508,561] have also been prepared by MA. Thus, the capabilities of MA in synthesizing a variety of intermetallic phases appear unlimited.

9.3. Refractory compounds

Refractory compounds based on metals and metalloids have desirable properties such as extremely high hardness, high-temperature stability, high thermal conductivity, and good corrosion resistance. They are usually synthesized on a commercial scale by direct reaction of the metal with the appropriate ambient at high temperatures and pressures. This process is carried out under isothermal conditions and the end product is often heterogeneous with some unreacted metal being present. Thus, the conventional methods of preparing refractory compounds are time-consuming, expensive, and involved. Mechanical alloying has been a one-step successful route in synthesizing these compounds in powder form in an inexpensive and faster way. Tables 13–15, respectively, list the borides, carbides, and nitrides synthesized by MA.

It is clear from the data presented in these Tables that the boride phases are synthesized by milling the metal powder along with boron. The TiB_2 powder produced by MA can be successfully used in the development of dispersion-strengthened materials, since these powder particles have nanometer dimensions. It is also possible to produce TiB_2 dispersions in situ by milling blended elemental mixtures of Ti, Al, and B [608].

The boride phases are not always directly produced by MA. In some cases, e.g., Fe–B system, MA of iron and boron powder mixture produces either an amorphous phase or a solid solution [577] depending on the milling conditions. Heat treatment of these powders then precipitates the boride phases such as Fe_2B and FeB. Direct synthesis of FeB by MA was reported by Ruuskanen and Heczko [516].

Detailed investigations were also conducted on the synthesis of carbide phases by MA. Whereas some carbides were synthesized directly by MA, e.g., Al_4C_3,

Table 13
Synthesis of boride phases by mechanical alloying

System	Phase	Comments	Reference
Co–33B	Co_2B	MA (Am) + 500°C	[575]
Co–33 to 50B	t-Co_2B		[576]
Co–20 to 50B	t-Co_2B	MA (Am) + HT	[451]
Fe–20B	Fe_2B	MA/400 h (α-Fe) + 800°C/2 h	[577]
Fe–20 to 30B	Fe_2B		[516]
Fe–50B	FeB		[516]
Fe–50B	FeB, Fe_3B		[446]
Nb–50B	NbB		[503,505]
Nb–67B	NbB_2		[505]
Ni–B	Ni_3B		[578]
Ti–B	TiB_2		[569]
Ti–66B	TiB_2		[60,569]
TiO_2 − B	TiB_2	MA/25 h + 1050°C	[579]
ZrO_2 + B	ZrB_2	MA/20 h + 100°C	[579]

Table 14
Synthesis of carbide phases by mechanical alloying

System	Phase	Comments	Reference
Al–C	Al_4C_3		[580]
Co–C	Co_3C		[87,580]
Cr–C	Cr_3C_2		[286,502,580,581]
	Cr_7C_3		[502,581]
Cr–21.5C	$Cr_{23}C_6$	MA + 800°C/2 h	[286,502]
Fe–17 to 25C	Fe_3C		[582]
Fe– 29 to 70C	Fe_7C_3		[582]
Fe–C	Fe_3C		[87]
Fe–C	Fe_3C		[580]
	Fe_5C_2		
	Fe_2C		
	Fe_7C_3		
Fe–25C	Fe_3C	5 h	[80]
Fe–25C	ε-Fe_2C and χ $Fe_{2.5}C$	10 h	[80]
Fe–50C	Fe_7C_3	210 h	[583]
	Fe_3C	MA/210 h + 500°C/15 min	[583]
Fe–60 to 70C	Fe_7C_3		[584]
Mn–Al–C			[526]
Mn–C	Mn_3C		[580]
Mo–C	MoC and MoC_x ($x < 0.5$)		[580]
Nb–C	$NbC_{0.75}$ and NbC_x ($x < 0.5$)		[580]
Nb + graphite or hexane	NbC		[585]
Ni–C	Ni_3C		[87,580]
Re–C	ReC		[580]
Si–C	β-SiC	MA/300 h	[580,586–588]
Ti–45Al	Ti_2AlC	MA/200 h + VHP 1173 K/1 h	[550]
Ti–Al–V–C	(Ti,Al,V)C		[580]
Ti–C	TiC		[94,580,588–590]
V–C	VC and VC_x ($x < 0.5$)		[580]

(continued on next page)

Table 14 (*continued*)

System	Phase	Comments	Reference
V–30C	V_2C	Only at high energy milling	[591]
V–30C	V_2C	Low energy milling for 700 h + anneal	[592]
V–50C	VC	Only at high energy milling	[591]
V–50C	VC	Low energy milling for 700 h + anneal	[592]
V–50C	VC	High-energy	[104]
	VC	Medium energy + anneal	[104]
	V_2C	Low energy MA (nano V+ am.C) + anneal	[104]
	V + VC	Low energy MA (nano V+ am.C) + anneal	[104]
W–50C	WC		[593]
W–C–Co	WC	> 100 h	[594]
W–C	FeW_3C and $(Fe,W)_6C$		[580]
W–activated C	WC	MA/310 h + 1000°C/1 h	[595]
WO_3–Mg–C	WC		[596]
Y–Ni–B–C	YNi_2B_2C		[597]
Zr–C	ZrC		[580]

Fe_3C, Fe_7C_3, etc., an appropriate heat treatment was necessary in other cases. Some phase transformations were also observed on continued milling and/or heat treatment. For example, during milling of Fe–25C powders it was noted that the Fe_3C phase was produced after 5 h, whereas a mixture of ε-Fe_2C and χ-$Fe_{2.5}C$ phases was produced after 10 h [80]. Similarly, Wang et al. [583] reported that the Fe_7C_3 phase was produced on milling an Fe–50C powder mixture for 210 h in a

Table 15
Synthesis of nitride phases by mechanical alloying

System	Phase	Comments	Reference
Al	AlN	In a nitrogen atmosphere	[124]
B	BN	MA/140 h in a nitrogen atm + 800°C/1 h	[124]
B	BN	In a nitrogen or ammonia atmosphere	[104]
Cr	CrN, Cr_2N	MA/300 h + 800°C/1 h	[124]
Cu	Cu_3N	MA/60 h in N_2 atm.	[124]
Fe	ξ-Fe_2N		[598]
Fe	Fe_4N		[598]
Fe	ε-Fe_3N		[56]
Ga	GaN	In ammonia atm./300 h	[599]
Mg	Mg_3N_2	N_2 atm./60 h	[124]
Mo	Mo_2N	MA/300 h + 800°C/1 h; N_2 atm.	[124]
	Mo_2N	Nanostr.+ 520°C/72 h; N_2 atm.	[104]
	MoN	Nanostr.+ 800°C/1 h; N_2 atm.	[104]
Mo	Mo_2N	NH_3 atm./280 h	[104]
Nb	NbN		[91]
Si	α-Si_3N_4		[104,124,600]
Ta	TaN	In a nitrogen atm; MA + 580°C/72 h	[104]
Ta	TaN	In an ammonia atm., MA + 900°C/24 h	[104]
Ta	Ta_2N	In an ammonia atm., MA + 450°C/72 h	[104]
Ta–Al	(Ta,Al)N and TaN	In a nitrogen atm.	[90]
Ti	TiN	High or medium energy milling	[104]
	Ti_2N	Low energy milling	
Ti	TiN	In N_2 atm.	[121,125,244,601–605]
Ti	Ti_2N	N_2 atm.	[598]
Ti	Ti(O,N)		[606]
Ti–5Al	Ti(O,N)		[606]
Ti–25Al	(Ti,Al)N		[245,604,605]
Ti–50Al	(Ti,Al)N	In N_2 atm.	[604]
Ti–50V	$TiVN_{0.16}$		[557]
Ti–50Zr	$(Ti,Zr)N_{0.9}$		[607]
V	VN		[124]
V–30Cu	$(V_{0.7}Cu_{0.3})N$	In N_2 atm.	[100]
W	WN and W_2N	In a N_2 atm., MA/300 h + 800°C/1 h	[124]
W	WN and W_2N	In NH_3 atm., MA (nano) + 1000°C/1 h	[104]
Zr	ZrN	N_2 atm.	[57,124]
Zr	ZrN	N_2 atm.	[57,104]
Zr	ZrN	NH_3 atm.	[103]

Uni-Ball-mill. On annealing the above milled powder for 15 min at 500°C, it transformed into the Fe_3C phase.

As mentioned in Section 4.2.5, it is possible to change the intensity of milling in a Uni-Ball-mill by changing the position of the magnets. Thus, one can have high energy (HE), medium energy (ME), or low energy (LE). Calka et al. [104] milled a V–50C mixture under these three different conditions and observed differences in the nature of the final product. At the highest energy of milling, the equiatomic VC was directly produced. At intermediate milling energy, a nanostructured phase was produced, which on annealing transformed to the VC phase. At the lowest energy of milling a mixture of amorphous carbon and nanostructured vanadium phases was produced, which on heat treatment transformed to the V_2C phase. At slightly higher energies than the lowest energy, the mixture of amorphous carbon and nanostructured vanadium transformed to a mixture of vanadium and VC on annealing. Similarly, direct formation of TiN was observed only when milling was conducted at high energies and not at lower energies; low-energy milling led to the formation of the Ti_2N phase [104].

Several nitride phases have been synthesized by milling pure metals either in a nitrogen or ammonia atmosphere. These have been listed in Table 15. Whereas majority of the nitride phases have formed directly by MA, in some cases an additional heat treatment was necessary. For example, nitrides of Al, B, Cu, Fe, Ga, Mg, Nb, Ta, Ti, V, and Zr could be produced directly by MA. In the case of molybdenum, it was noted that milling in a nitrogen atmosphere produced a nanocrystalline phase, which on annealing for 72 h at 520°C produced a mixture of the Mo and Mo_2N phases. The same as-milled nanocrystalline phase transformed to a mixture of Mo, MoN, and Mo_2N on annealing at 800°C for 1 h [104]. A similar situation was reported in the synthesis of tungsten nitrides by MA [104].

Milling of reactive metals like titanium and zirconium in improperly sealed containers always produced the nitride phases. Since a minimum amount of nitrogen is required for the formation of the nitride phase, the nitride phase does not form in the initial stages. Very often, the nitride contamination phase forms after the formation of an amorphous phase in the titanium and zirconium base alloy systems. See Ref. [58] for a critical discussion of the nitride phase formation by MA in titanium alloys.

10. Disordering of intermetallics

It has been long known that partially ordered phases are stronger than those wholly disordered or fully ordered (because at a certain value of the long-range order parameter, S, superdislocations separate into unlinked singles). Thus, it is of interest to study the mechanical behavior of materials in various states of partial order. Disordering phenomena of ordered alloys have also been studied to understand the mechanism of disordering and also to produce the disordered material that has a higher ductility/formability than the ordered alloy. Alloys can

be disordered by irradiation [609,610], rapid solidification [611], or heavy plastic deformation [572]. The present section will deal with the phenomenon of disordering of ordered intermetallics by mechanical milling. Large amounts of plastic deformation result in the generation of a variety of defect structures (dislocations, vacancies, stacking faults, grain boundaries, etc.) and these destabilize the ordered nature of the lattice leading to the formation of a disordered (crystalline or amorphous) phase. The first observation of disordering of an ordered compound $ZnFe_2O_4$ by MM was reported by Ermakov et al. in 1982 [612]. Disordering of Fe_3Si by mechanical grinding was reported later in 1983 [613]. An exhaustive review on this aspect of disordering of intermetallics was published a few years ago [48].

A variety of ordered compounds with the B2, $L1_2$, A15, and B8 structures have been disordered by MM. The progress of disordering has been monitored by several techniques including X-ray diffraction techniques to measure the lattice parameter and long-range order parameter, measurement of superconducting transition temperature and magnetic susceptibility (if the compound is superconducting in the initial state), Mössbauer techniques, differential scanning calorimetry, etc.

Mechanical milling introduces high energy into the material being processed. This energy can be stored in the material as atomic disorder and/or grain boundaries, i.e.,

$$\Delta G(\text{milling}) = \Delta G(\text{disorder}) + \Delta G(\text{grain boundaries}) \tag{11}$$

The atomic disorder in an intermetallic can be manifested in three different ways [48]. Firstly, the two atomic species involved can occupy the "wrong" sublattices and this is referred to as *anti-site disorder*. This introduces strain into the lattice. This type of disorder was observed in a number of mechanically milled compounds with the A15 structure, e.g., Ni_3Al, Ni_3Si, Fe_3Ge and those with the B2 structure, e.g., CoGa and AlRu. Secondly, *triple-defects* can be generated. In an equiatomic compound such as CoGa, for example, the transition metal Co atoms can substitute on the Ga lattice, and this is anti-site disorder. But, the Ga atoms stay on their own lattices. This leads to the presence of vacancies in the Co lattice to maintain the stoichiometry. Thus, vacancies on the Co-sublattice in combination with Co anti-site atoms in a ratio of 2:1 constitute the triple defects. Third, there could also be *redistribution of interstitials* wherein the interstitial atoms in the octahedral sites are transferred to the tetrahedral sites, e.g., Mn_3Sn_2, Fe_3Ge_2. Additionally, grain refinement increases the grain boundary area and this also raises the free energy of the system. The sum of the energy of these two effects (disordering and creation of grain boundaries) will be the total energy introduced into the material during milling.

Mechanical milling of ordered intermetallics has been shown to result in one of the three following transformations [48,614]:

1. Formation of a solid solution of one component in the other, i.e., the terminal solid solution based on the major component; this has been observed in

compounds such as Nb_3Al, V_3Ga, Ni_3Al, Fe_3Ge, Ni_2V, and $NbAu_2$,
2. Formation of an amorphous phase, observed, for example, in Nb_3Sn, NiZr, NiV_2, and CoZr, or
3. Formation of a different phase with a complex crystal structure, noted in Ni_3Sn_2 and $TiSi_2$.

It has been noted that upon milling, the long-range order parameter (S) in the intermetallic is gradually reduced and, in many cases, the material may become totally disordered ($S = 0$), e.g., Ni_3Al [615]. In other cases, S is reduced with milling time but does not reach $S = 0$, i.e., partial order and partial disorder co-exist, e.g., CuTi [616] and AlRu [617]. In other cases, the S value does not decrease at all and is maintained at $S = 1$; but, with continued milling the material becomes amorphous, e.g., CoZr [354]. These three situations are schematically represented in Fig. 26. Thus, upon milling, an ordered intermetallic can transform, with or without complete loss of long-range order, either into a disordered crystalline phase (solid solution) or an amorphous phase. If the product is a crystalline phase, the material has an extremely fine grain size, usually in the nanometer range. Fig. 27 summarizes the types of changes that can occur on milling an intermetallic compound [618].

Disordering of intermetallics has been studied primarily by X-ray diffraction techniques [193]. By measuring the intensity of the superlattice reflections relative to that of the fundamental reflections, the long-range order parameter S is evaluated using the relationship:

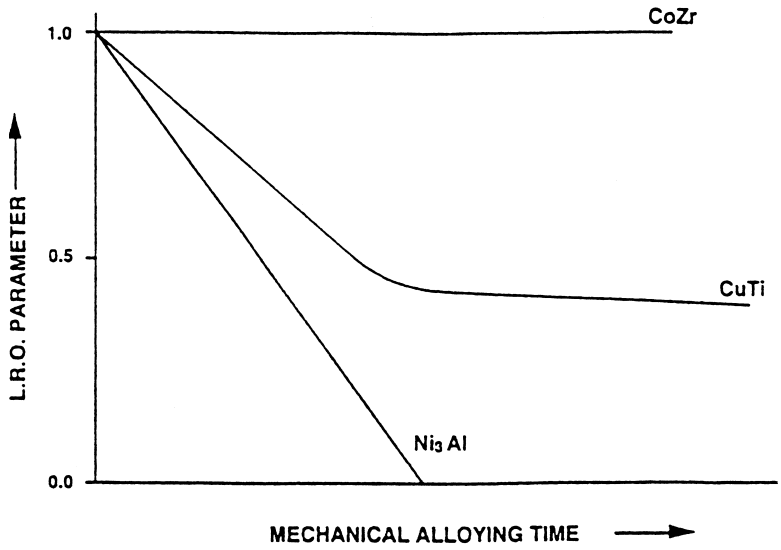

Fig. 26. Variation of the long-range order parameter S with milling time. Three different situations, viz., complete loss of order, partial loss of order, and no loss of order on milling have been represented.

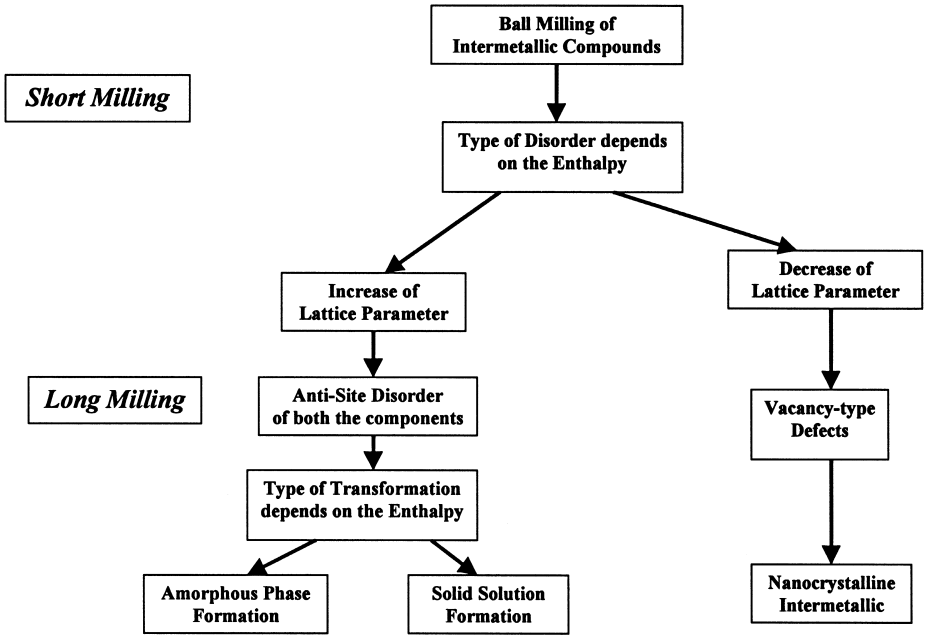

Fig. 27. Schematic showing the expected situation on mechanically alloying an intermetallic compound.

$$S^2 = \frac{I_{S(dis)}/I_{F(dis)}}{I_{S(ord)}/I_{F(ord)}} \tag{12}$$

where I_s and I_f represent the integrated intensities of the superlattice and fundamental reflections, respectively and the subscripts (dis) and (ord) refer to the disordered and ordered states, respectively [193]. Additionally, it has been noted that the lattice parameter increases slightly (0.3–0.8%) in the disordered state, if the disordering occurs by anti-site disorder [619] (Fig. 28), whereas the lattice

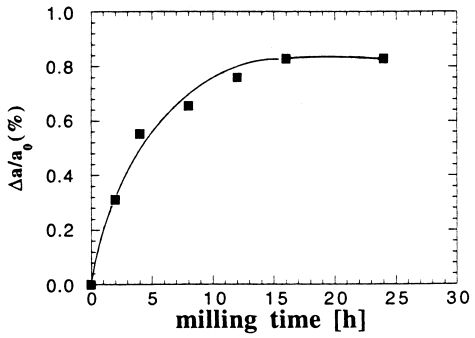

Fig. 28. Lattice expansion with milling time for FeAl powder.

parameter decreases if disordering occurs by the triple defect disorder [48]. The change in lattice parameter continues after the compound has completely disordered and formed a solid solution (Fig. 29). This measurement of change in lattice parameter, of course, is not possible if there is a change in the crystal structure due to disordering. Mössbauer spectroscopy techniques and measurement of superconducting transition temperature and/or magnetic susceptibility have also been employed to study the disordering phenomenon. Recently, Zhou and Bakker [620] have demonstrated that magnetic measurements are very powerful in determining the nature of disordering if one of the atoms involved has magnetic moments.

During disordering of CoZr, Cho and Koch [354] did not observe any decrease in the intensity of superlattice reflections (relative to fundamental lines) with milling time before amorphization occurred. It was thus concluded that the grain boundary energy in this system is high enough to drive the crystal-to-amorphous transition, and not the destruction of long-range order. Zhou and Bakker [620] observed that magnetization in the mechanically milled Co–Zr alloys increased continuously with milling time up to about 40 h (no reduction in the relative intensity of superlattice reflections was observed) and also that the lattice parameter of the disordered nanocrystalline phase increased with milling time. From these two observations, they concluded that disordering of CoZr occurs by atomic disorder and grain refinement (i.e., creation of additional grain boundaries). Thus, a combination of techniques can shed additional evidence and provide an accurate account of the mechanism of disordering.

Whether an intermetallic transforms to a solid solution or an amorphous phase on milling is determined by the relative free energy values of the amorphous and crystalline phases with respect to the energy stored in the intermetallic by mechanical milling. For example, the intermetallic will transform to the solid solution if the enthalpy of the amorphous state as estimated by the Miedema

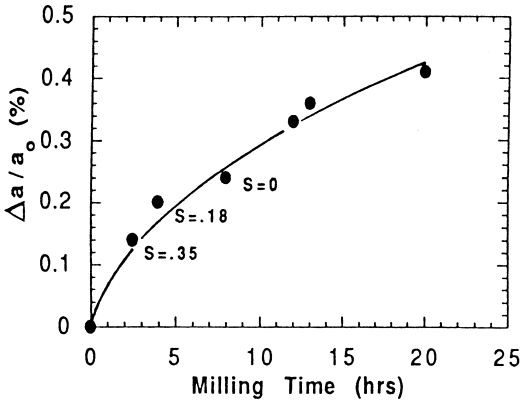

Fig. 29. Lattice expansion in mechanically alloyed $Ni_3Al + B$ powder as a function of milling time. The long-range order parameter S is also shown in the figure.

analysis [621] is higher than that of the solid solution. Thus, if $\Delta G(\text{milling}) > \Delta G^{a-c}$, where ΔG^{a-c} represents the difference in free energy between the ordered crystalline and amorphous phases, complete amorphization occurs. On the other hand, if $\Delta G(\text{milling}) < \Delta G^{a-c}$, no amorphization occurs; instead, a solid solution forms. Similar conclusions can also be reached by observing the nature of the phase diagrams. If the phase diagram shows that the intermetallic transforms to a (disordered) solid solution before it melts, i.e., it is a reversibly ordered intermetallic, then milling of the intermetallic will result in the formation of a (disordered) solid solution. Continued milling may then produce the amorphous phase. But, if the intermetallic melts congruently (irreversibly ordered or permanently ordered intermetallic), then milling of the intermetallic will produce an amorphous phase directly. This has been shown to be true in a number of cases [48]. Thus, introduction of mechanical energy into the system is equivalent to heating the alloy to higher temperatures (Fig. 30). That is, an alloy can become disordered either at higher temperatures or on mechanical milling. Depending on the nature of the phase, either melting or formation of an amorphous phase can occur in some cases. It has been noted that among about 700 binary intermetallic compounds only very few compounds such as CuZn and Cu_3Au are reversibly ordered compounds, i.e., they exhibit the order–disorder transformation before melting. Table 16 lists the compounds that have been disordered by MM. In this Table, adapted from Ref. [48], the third column gives the type of disorder: a question mark means that the type of disorder has not been investigated; "anti-site" means anti-site disorder, "triple-defect" means triple-defect disorder, and "red. int." means redistribution of interstitials. The fourth column gives the type of transformation: "Amorphous" means that the compound has become amorphous after milling and "SS" means that the compound has transformed to a solid solution phase; the crystal structure of the solid solution is

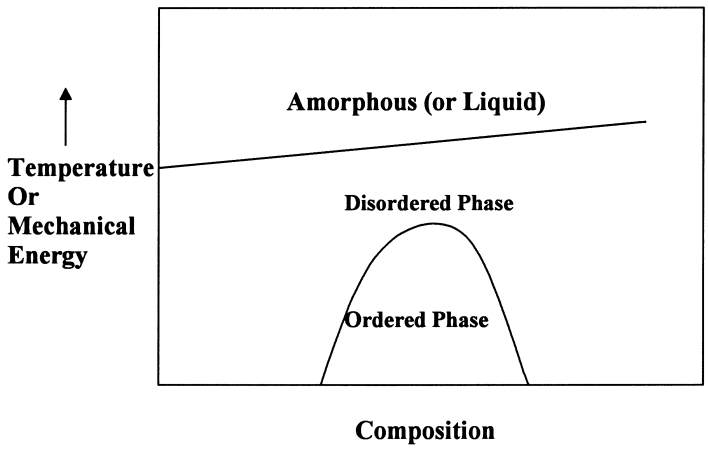

Fig. 30. Equivalence of mechanical energy and temperature in the disordering of intermetallic compounds.

Table 16
Disordering of intermetallics by mechanical milling

Compound	Crystal structure	Type of disorder	End product	Phase diagram	Reference
Nb_3Al	A15	?	SS (bcc)	?	[621,622]
Nb_3Au	A15	Anti-site	SS (bcc)	SS > T_c	[255,623]
Nb_3Sn	A15	Anti-site	Amorphous	Liq.	[624,625]
NiV_3	A15	?	SS (bcc)	?	[358]
V_3Ga	A15	?	SS (bcc)	SS > T_c	[84]
CoAl	B2	Triple defect	None	Irrelevant	[626]
CoGa	B2	Triple defect	None	Irrelevant	[627]
CoZr	B2	Anti-site	Amorphous	Liq.	[354,620]
NiAl	B2	Triple-defect	None	Irrelevant	[628]
RuAl	B2	Triple-defect?	None	Irrelevant?	[617]
Fe_3Ge_2	$B8_2$	Red. int.	None	Irrelevant	[629]
Mn_3Sn_2	$B8_2$	Red. int.	None	Irrelevant	[629]
LaAu	B27	?	Amorphous	LTP → HTP → liq.	[630]
NiZr	B_r	?	Amorphous	Liq.	[631,632]
Fe_3Ge	$L1_2$	Anti-site	SS (bcc)	?	[48]
Ni_3Al	$L1_2$	Anti-site	SS (fcc) + am	?	[615,619,633]
Ni_3Ge	$L1_2$	?	SS (fcc) + am	?	[631,634]
Ni_3Si	$L1_2$	Anti-site	SS (fcc)	?	[354,635,636]
Zr_3Al	$L1_2$	?	Amorphous	?	[637]
$Co_{41}Cr_{59}$	σ-Phase	?	None	σ → δ→ liq.	[638]
CoV	σ-Phase	Disorder	Amorphous	Liq.	[639]
$Cr_{53}Fe_{47}$	σ-Phase	Disorder	SS (bcc)	SS > T_c	[95]
FeV	σ-Phase	?	SS (bcc)	SS > T_c	[631,638]
NiV_2	σ-Phase	?	Amorphous	σ → σ′ → liq.	[358]
Ni_4V_6	σ-Phase	?	Amorphous	σ → σ′ → liq.	[631]
Co_2Ge	Co_2Si	Anti-site	Amorphous	LTP → HTP → liq.	[640]
Co_2Ge	Ni_2In	Anti-site	Amorphous	HTP → liq.	[640]
Co_3Sn_2	Orthorhombic	Red. int.	LTP → HTP	LTP → HTP	[452]
Cu_2MnAl		Disorder			[641]
Fe_2Sc	C14	?	Amorphous	?	[642]
Fe_2Y	C15	?	Amorphous	?	[642]
$GdAl_2$	Cu_2Mg	?	None	Liq.	[643]
$Nb_{60}Au_{40}$	A15 + tetra.	?	SS (bcc)	SS > T_c	[255]
$Nb_{58}Au_{42}$	AlB_2 + tetra.	?	SS (bcc/fcc)	SS > T_c	[255]
$Nb_{50}Au_{50}$	AlB_2 + tetra.	?	SS (fcc)	SS > T_c	[255]
$NbAu_2$	AlB_2	?	SS (fcc)	SS > T_c	[255]
$Ni_{45}Nb_{55}$	W_6Fe_7	?	Amorphous	?	[211]
Ni_3Sn	DO_{19}	?	Amorphous	LTP → HTP → liq.	[644]
Ni_3Sn_2	Orthorhombic	Red. int.	LTP → HTP	LTP → HTP	[466]
$NiTi_2$	E93	?	Amorphous	?	[645]
Ni_3V	DO_{22}	?	SS (fcc)	SS > T_c	[358]
Ni_2V	$MoPt_2$	?	SS (fcc)	SS > T_c	[358]
$TiAl_3$	DO_{22}	Anti-site	SS (fcc)	?	[246]
Ti_5Si_3	$D8_3$	?	Amorphous	Liq.	[246]
$TiSi_2$	C54	?	C54 → C49	Irrelevant	[246]
YCo_2	Cu_2Mg	?	Amorphous	?	[20]
YCo_3	$CeNi_3$	?	Amorphous	?	[20]
Y_2Co_7	Co_7Er_2	?	Amorphous	?	[20]
YCo_5	Co_5Y	?	Amorphous	?	[20]
Y_2Co_{17}	$Ni_{17}Th_2$	?	Amorphous	?	[20]

mentioned within parentheses. "None" means that no transformation was observed and LTP → HTP means a transformation from the low-temperature phase to a high-temperature phase in the phase diagram. Information on the type of transformation from the phase diagram is given in Column 5. A question mark means that either the information is not available or not clear; "liq" means that the compound melts directly from its crystal structure, suggesting amorphization; $SS > T_c$ means the formation of a solid solution above a critical temperature, which could point in the direction of formation of a solid solution.

It should also be remembered that contamination can play a very significant role in determining the nature of the final phase formed after milling. It was shown that milling of the Nb_3Al intermetallic in a SPEX mill produced the expected bcc solid solution phase after 3 h. But, when milling was conducted in an improperly sealed vial, an amorphous phase was produced after 10 h, which on heat treatment, transformed to the crystalline niobium nitride phase. This suggests that the amorphous phase in this system formed because of nitrogen contamination of the powder during milling [622].

The crystal structure of the phase alone does not appear to decide whether the intermetallic forms a solid solution or an amorphous phase on MM. The three intermetallics — Ni_3Al, Ni_3Ge, and Zr_3Al — have the $L1_2$-type cubic structures. On mechanically milling, both Ni_3Al and Ni_3Ge form a disordered nanocrystalline fcc solid solution and do not show any tendency for amorphization. On the other hand, Zr_3Al amorphizes completely after a short milling time. These differences in the milling behavior have been attributed partly to the differences in the lattice stability terms of their respective disordered fcc phases [646].

It was mentioned earlier that materials in a partially ordered state are stronger than those completely disordered or fully ordered. It was shown that the microhardness of mechanically milled Ni_3Al powders exhibited a pronounced sharp maximum corresponding to $S = 0.5$ [615]. This work suggests that the greater is the ordering energy, the steeper will be this maximum of strength (or hardness). It may also be mentioned in passing that all order states ($S = 0$–1) cannot be accessed by traditional methods of disordering. For example, in equilibrium, the order parameter for Cu_3Au jumps discontinuously from 0.8 to zero at the critical temperature. But, mechanical milling can be used to obtain different degrees of order so that the effect of order parameter on structure and mechanical properties of alloys can be investigated.

There have also been several studies on reordering of disordered phases obtained by MM (see, for example, Refs. [647–650]). It was reported that on heating the milled powder in a differential scanning calorimeter (DSC), two distinct exothermic peaks were observed (Fig. 31). The transformations that occurred were irreversible. The low-temperature low-intensity peak is attributed to the re-establishment of short-range order. This was confirmed by the results obtained from electron energy loss fine structure studies. The absence of such a peak during reheating of mechanically milled elemental powders also indirectly confirms this hypothesis since chemical reordering cannot occur in pure metal powders. The second major peak is associated with the simultaneous evolution of

ordering and grain growth [648]. The apparent activation energy for the transformation is found to be lower than expected during ordering of a conventional alloy. The explanation could be that the high density of point defects such as vacancies and anti-site defects, generated during milling, assist the diffusive processes and help in achieving reordering easily.

Most of the mechanically milled disordered intermetallics exhibit these two peaks in their DSC plots, with the difference that the actual temperatures and peak shapes and heights could be different depending on the nature and composition of the alloy and milling time. In ternary intermetallics, however, a third low intensity peak, often overlapping the second major peak, is observed (Fig. 31b). Although a clear explanation is not available for this it is thought that this could be due to annealing out of dislocations, usually not mobile at temperatures as low as those of the first two peaks.

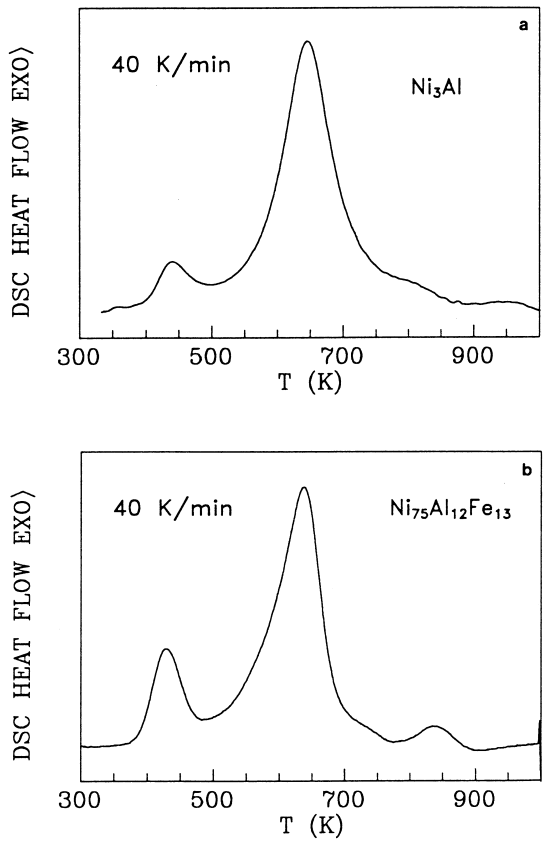

Fig. 31. DSC curves from (a) Ni_3Al milled for 4 h and (b) $Ni_{75}Al_{12}Fe_{13}$ milled for 8 h. Two distinct exothermic peaks can be seen in (a) and an additional low-intensity peak at higher temperatures in (b).

11. Solid-state amorphization

Amorphous alloys were first synthesized by vapor deposition in the form of thin films by Buckel and Hilsch [651]. However, the synthesis of a non-crystalline phase by rapid solidification from the liquid state by Pol Duwez and his associates in 1960 [652] paved the way for an enormous amount of activity during the last four decades. These amorphous alloys (also referred to as metallic glasses) have an unusual combination of properties such as high strength, good bend ductility, high fracture toughness, good corrosion resistance, and desirable soft magnetic properties. Because of this, metallic glasses have found several industrial applications, the most important of which is for core laminations in distribution transformers. Information on the synthesis, properties, and applications of metallic glasses produced by the technique of rapid solidification from the melt may be found in several reviews and books [2–4,653–657].

A solid alloy with a liquid-like (non-crystalline) atomic arrangement is called a metallic glass or an amorphous (metallic) alloy. A glass is obtained when a liquid is cooled into a state of rigidity without crystallizing; such an alloy will exhibit a glass transition temperature. On the other hand, if a material with a similar structure is made by some processes other than cooling then it is called an amorphous alloy. Non-crystalline alloys are now formed in suitable systems by processing techniques such as rapid solidification from the liquid state, vapor deposition, plasma processing, and laser processing [2,656]. In these methods, there is a change in the state of matter, i.e., a solid phase is formed from either the liquid or the vapor phase, and the high effective ''quenching'' rate and associated undercooling have been shown to be responsible for the amorphization process. There are also methods of amorphizing a solid without passing through the liquid state at any stage. Known as solid-state amorphization reactions (SSAR), these include irradiation, hydrogen-assisted amorphization, interdiffusion of elemental metals, pressure-induced vitrification, and mechanical deformation. The present Section will discuss recent results on the formation of amorphous phases by mechanical alloying and/or milling.

The synthesis of an amorphous phase in the Ni–Nb system by MA starting from blended elemental powders of Ni and Nb in 1983 [21] has given rise to increased research activity in this area and there have been a number of reports on the formation of amorphous phases by MA in several binary and ternary (and a few higher order) alloy systems. Amorphization of intermetallic compounds (e.g. YCo_3, Y_2Co_7, YCo_5) by MM was reported earlier by Ermakov et al. [20,658]. Thus, amorphous phases have been synthesized by MA or MM starting from:

1. blended elemental powder mixtures,
2. prealloyed powders and/or intermetallics,
3. mixtures of intermetallics, or
4. mixture of intermetallics and elemental powders.

An exhaustive listing of the alloy systems in which amorphous phases have been found to form by MA or MM is presented in Tables 17 and 18, respectively. Since

Table 17
Amorphous phases formed in blended elemental powder mixtures by MA

System	Mill	Vial material	Grinding medium material	BPR	Speed (rpm)	MA time (h)	Glass-forming range (at%)	Reference
Ag–Pd	SPEX 8000			10.4:1	–	65	50	[196]
Al–18.2Co	Planetary ball mill QM–1F	SS	Hardened steel	20:1	200	80		[401]
Al + $Al_{13}Co_4$ (Al–15Co)	Fritsch P5	SS	SS	10:1	150	100		[659]
Al–15Cr	Ball mill	SS	SS	120:1		1000	Partly Am.	[204]
Al–20Cr	Ball mill	SS	SS	120:1		[a]	Partly Am.	[204]
Al–20Cu–15Fe	Planetary ball mill QM–1SP	Steel	Hardened steel	10:1	200–300	300		[660]
Al–20Cu–15Mn	Fritsch P5			15:1	Int. 5	510		[217]
Al–20Fe	Ball mill					170		[661]
Al–20Fe	Fritsch P7	Hardened steel	Hardened steel	6:1	–	40		[482]
Al–24.4Fe	Ball mill	SS	SS	90:1				[294]
Al– 1 to 25 Fe	SPEX mill	Steel	521000 steel	10:1	–	50	25	[228]
Al–25Fe	Horizontal ball mill	SS	SS		90	600		[662]
Al–33Fe	Ball mill		SS	90:1		454		[221]
Al–40Fe	Horizontal ball mill	SS	SS	50:1	90			[662]
Al–Fe	Conventional ball mill	SS	SS	90:1	–	454	17–33Fe	[133]
Al–Fe	Planetary ball mill	Steel	Steel		230	180	20–50Fe	[663]
Al–25Ge–10Fe	Vibratory ball mill	SS	SS	5:1	–	80		[664]
Al–50Hf								[665]
Al–14Mn	Planetary ball mill			60:1	720	300	[b]	[666]
Al–20Mn–30Si	Fritsch			20:1	450–650	85		[424]
Al–50Nb	Rod mill				400			[667]
Al–50Nb	Rod mill	SS	SS	30:1	–	40		[668]
Al–40Ni	Low energy vibrating mill							[669]
$(Al_{80}Ni_8Co_4)_{100-x}$ Zr_x	Fritsch			10:1	120		$x = 4$	[238]
$Al_{88}Ni_8Fe_4Gd_8$								[670]
Al–33 Ni–33Ti	Ball mill	SS	SS	100:1		1000		[374]
Al–50Ta	Ball mill	SS	SS	30:1		20		[671]
Al–50Ta		SS	SS	36:1, 108:1	–	400		[672]
Al–Ta	Rod mill	SS	SS	30:1		400	33–67Ta	[673,674]
Al–6Ti	Attritor	SS	Hardened steel	220:1		1300		[675]
Al–12.4Ti	Attritor	SS	Hardened steel	220:1	175	400		[675]
Al–25Ti	Fritsch P7	Hardened steel	Hardened steel	10:1	645	28		[242]
Al–33.3Ti	Rod mill	SS	SS		400			[676]
Al–35 to 48Ti	Planetary ball mill	Steel		30:1		90		[677]
Al–45Ti	Planetary ball mill			60:1		40		[252]
Al–23Ti–23C	Planetary ball mill	Steel		30:1		90		[677]
Al–12Ti–7Fe	Planetary ball mill	SS	SS			100		[145]
$Al_{85}Y_8Ni_5Co_2$	Planetary ball mill Retsch PM 4000	Hardened steel	Hardened steel	15:1		100	Only a small amount of Am.	[678]

$Al_{88}Y_2Ni_6Fe_4$	Planetary ball mill Retsch PM 4000	Hardened steel	Hardened steel	15:1		100	Only a small amount of Am.	[678]
Al–50 Zr	Rod mill	SS	SS	30:1		400		[679]
Al_2O_3–38 mol% ZrO_2	Planetary ball mill G7	Steel	Steel	7:1	500/700	72	Am + trace Al_2O_3	[454,680]
Al_2O_3–38 mol% ZrO_2–3 mol% Y_2O_3	Planetary ball mill G7	Steel	Steel	7:1	500/700	72	Am + trace Al_2O_3	[454]
Al_2O_3–40 mol% $ZrSiO_4$	Planetary ball mill G7	Steel	Steel	7:1	500/700	240		[680]
Au–45La	Fritsch P0	WC-lined hardened steel	WC-lined hardened steel			130		[630]
$BiFeO_3$						65		[681]
$BiFeO_3$–25 mol% $ZnFe_2O_4$		SS	SS		80–110	250		[682]
C (graphite)	SPEX 8000	WC	WC	4:1	–	206		[683]
Co–20B	Fritsch P5	Tempered steel		10:1	320	45		[451]
Co–33B	Fritsch P5	Tempered steel		10:1	320	13		[451,684]
Co–33B	Fritsch P5	Tempered steel		5.5:1		70	Partly Am.	[685]
Co–B	Fritsch P5	Tempered steel	SS	10:1	250	18–34	33–50Co	[576]
Co–Nb	Attritor, Kitui Miike MA 1D	SS	SS		300	60	15–20Nb	[686]
Co–25Si	Planetary ball mill	Hardened tool steel	Hardened tool steel	11.3:1		220		[687]
Co–66.7Si	Lab ball mill	SS	SS	64:1	360	25		[688]
Co–Si	Fritsch P5	SS	SS	9.6:1		200	33Si	[541]
Co–Si	Lab ball mill	SS	SS	64:1	360	30	30–70Si	[689]
Co–10 and 20Sn		SS		150:1	110	300	Partly Am.	[690]
Co–25Ti	Fritsch P5	SS	SS	17:1	250	3		[500]
Co–25Ti	Fritsch P5	SS	SS	10:1		48		[500]
Co–50Ti	Fritsch P5	SS	SS	17:1	250	6		[501]
Co–Ti	Attritor, Kitui Miike MA 1D	SS	SS		300	50	15–20Ti	[686]
Co–V						60	33–60V	[259]
Co–15Zr	High energy ball mill				300	8.5		[691]
Co–45Zr	Planetary ball mill			13:1		30		[692]
Co–Zr	Planetary ball mill					60	8–73Zr	[259]
Cr	Vibrational mill		SS	45:1		100	[c]	[208]
Cr–30Cu	Vibrational mill		SS	45:1		100	[d,e]	[208]
Cr–15 to 65Fe	SPEX 8000	Hardened steel	Hardened steel	7:1	–		28Fe	[693]
Cr–33.3Nb	Fritsch P7			4:1		60	Partly Am.	[505]
Cr–Nb	Planetary mill						30–68Nb	[694]
Cr–Nb–Si	Fritsch P7	Hardened steel	Hardened steel			24		[695]
Cr–25Si	Planetary ball mill	Hardened tool steel	Hardened tool steel	11.3:1		220		[687]
Cu–42Nb–14Ge	Lab mill	WC–Co	WC–Co	50:1		24		[696]
Cu–42Nb–14Si	Lab mill	WC–Co	WC–Co	50:1		24		[696]
Cu–35Nb–20Sn	Lab mill	WC–Co	WC–Co	50:1		24		[697]
Cu–42Nb–14Sn	Lab mill	WC–Co	WC–Co	50:1		24		[696,697]
Cu–50Nb–5Sn	Lab mill	WC–Co	WC–Co	50:1		24		[697]
Cu–11Ni–18P	Horizontal ball mill	SS	SS	30:1	80	300		[507]
Cu–20P	Horizontal ball mill	SS	SS	30:1	80	800	Partly Am.	[284]
Cu–50 and 70Sb	Fritsch P0	SS	Hardened steel	220:1			Sb becomes Am.	[120]
Cu–10 and 20Sn		SS		150:1	110	300	Partly Am.	[690]
Cu–40Ti	Planetary ball mill	Steel	Hardened steel	10:1–15:1	–	16		[698]
Cu–42Ti	Fritsch P5	SS	SS	4:1	436	43		[699]

(continued on next page)

Table 17 (*continued*)

System	Mill	Vial material	Grinding medium material	BPR	Speed (rpm)	MA time (h)	Glass-forming range (at%)	Reference
Cu–50Ti	SPEX 8000					16	Am. + TiH_2	[700]
Cu–50Ti	SPEX 8000	Hardened steel	SS	6:1	–	16		[268]
Cu–60Ti	SPEX 8000				–	42		[701]
Cu–Ti	SPEX 8000	Hardened steel		8.3:1	–	16	25–50Ti; 25–70Ti with 4–10 at % H_2	[161]
Cu–Ti		Tool steel or WC	WC	3:1–10:1		6	13–90 Ti	[702]
Cu–55[$(1-x)$Ti + xTiH_2]	SPEX 8000	Hardened steel or Cu–Be		–			x = 0 and 0.02	[703]
Cu–20Ti–20Zr	Planetary ball mill	Steel	Hardened steel	10:1WC–Co15:1		16		[698]
Cu–50V	Fritsch P5	Cu–Be	Cu–Be		573	120		[97]
Cu–W	Fritsch P5	Tempered steel	Steel				30–90W	[291]
Cu–40Zr	Fritsch	Steel		13:1		20		[704]
Cu–40Zr	Planetary ball mill	Steel		13:1		30		[692]
Cu–40 to 60Zr	SPEX 8000	Hardened tool steel	440C steel	10:1	–	13		[705]
Cu–50Zr	SPEX 8000	Hardened steel	SS	6:1	–	24		[706]
Cu–Zr							40–60Zr	[704,705]
Fe + FeB (Fe–20B)	Fritsch P5			5:1		350		[707]
Fe–20 B	Planetary ball mill					100		[516]
Fe–50B	Fritsch		WC	50:1		30		[446]
Fe–50B	Ball mill	SS	Hardened steel	10:1		250		[577]
Fe–60B	Ball mill	SS	Hardened steel	10:1		300		[577]
Fe–B	Planetary ball mill	SS		15:1	200		35–40 B	[708]
Fe–15B–10Si	Fritsch P5			5:1		350		[707]
Fe–25C	Ball mill	SS	Hardened steel			700	Mostly Am. (+ α-Fe)	[709]
Fe–70C	Ball mill	SS	SS	100:1		1000		[584]
Fe–C	Planetary ball mill	SS		15:1	200	72	20–25C	[708]
Fe–C	Ball mill	SS	SS	100:1		200	17–60C	[582]
Fe–32C–14Si	Ball mill	SS	SS	100:1		500		[584]
Fe–16C–16Si	Ball mill	SS	SS	100:1		500		[584]
Fe–30C–25Si	Ball mill	SS	SS	100:1		500		[584]
Fe–15C–29Si	Ball mill	SS	SS	100:1		500		[584]
Fe–50Cr	Fritsch P5	SS	SS		430	200	Milled in N_2 atmosphere	[306]
$Fe_{83-x}Cr_xC_{17}$ (x = 10 to 60)	Planetary ball mill			11.3:1		200		[710]
$Fe_{80-x}Cr_xN_{20}$ (x = 0 to 24)	Planetary ball mill			11.3:1		200		[710]
$Fe_{83-x}Mo_xC_{17}$ (x = 5 to 60)	Planetary ball mill			11.3:1		200		[710]
$Fe_{75-x}V_xC_{25}$ (x =0 −30)	Planetary mill			11.3:1		200		[710]

Fe + Ni + Fe-B ($Fe_{40}Ni_{40}B_{20}$)	Fritsch P5	SS	SS	9.6:1	573	280		[699]
Fe + Ni + Fe-B + Fe-P ($Fe_{40}Ni_{40}P_{14}B_6$)	Fritsch P5	SS	SS	9.6:1	573	24		[699]
Fe–38Ni–12Si–10B	SPEX 8000	Hardened tool steel		8:1	–	30	Partly Am.	[711]
Fe–P	Planetary ball mill	SS		15:1	200		≈ 25P	[712]
Fe–10 and 20Si	Planetary ball mill					300		[516]
Fe–15Si–15B	Planetary ball mill					300		[516]
Fe–Si	Lab ball mill	SS	SS	64:1	360	250	10–40Si	[689]
Fe–67Sn							Partly Am.	[713,714]
Fe–33Ti	SPEX 8000	WC	SS		–	16		[715]
Fe–Ti	SPEX 8000	WC–coated	SS				–	[518]
Fe–V	SPEX 8000	WC	WC	6:1	–	24–48	Partly Am.	[716]
Fe–30W	Fritsch P5	Hardened steel	Hardened steel	10:1	153	1700		[717]
Fe–50W	Fritsch P5	Hardened steel	Hardened steel	10:1	153	1700		[717]
Fe–16 and 20Zr	Fritsch P5	Steel	Steel			60		[327]
Fe–33Zr	Fritsch P5	Tempered steel		30:1–90:1				[520]
Fe–40Zr	Planetary ball mill			13:1		30		[692]
Fe–60Zr	Fritsch	Steel		13:1		20		[704]
Fe–Zr	Fritsch P5	Steel	Steel			60	20Zr	[327]
Fe–Zr							22–70Zr	[333,704]
Fe–Zr–B							21–25Zr and 0–15 B	[328]
Ge–S	Planetary ball mill	Hard bearing steel		40:1		60	61–72S	[718]
Ge–25 to 75 w/o Si	Fritsch P7/P5	Tempered steel						[719]
Hf–Cu		Hardened steel	Hardened steel or WC			17	20–90Cu	[720]
Hf–Cu	SPEX 8000	WC	WC	5:1	–	12	30–70Cu	[523,721]
Hf–Ni	SPEX 8000	WC	WC	5:1	–	12	15–65Ni	[721]
Hf–Ni		Hardened steel	Hardened steel or WC			17	10–85Ni	[720]
La–Al–Ni	Planetary ball mill	WC–Co	WC–Co	20:1	180		30–70 La; 10–50Ni	[722]
Mg–Ni	Planetary ball mill	–	–	10:1	–	–	50–80Ni	[349]
Mg_2Ni + Ni	Planetary ball mill	–	–	10:1	–	–	50Ni	[349]
$MgNi_2$ + Mg	Planetary ball mill	–	–	10:1	–	–	50Ni	[349]
Mg–Ni	Planetary ball mill	–	–	15:1	–	120	40–70Ni	[723]
Mg–57Al–5Ca	SPEX 8000		52100 steel		–			[724]
Mg–15Y–25Cu	Planetary ball mill Retsch PM 4000	Hardened steel	Hardened steel	15:1		170	Partly Am.	[678]
Mg–10Y–30Cu	Planetary ball mill Retsch PM 4000	Hardened steel	Hardened steel	15:1		170	Partly Am.	[678]
Mg–15Y–30Cu	Planetary ball mill Retsch PM 4000	Hardened steel	Hardened steel	15:1		170	Partly Am.	[678]
Mg–10Y–35Cu	Planetary ball mill Retsch PM 4000	Hardened steel	Hardened steel	15:1		170	Partly Am.	[678]
Mn–25Si	Planetary ball mill	Hardened tool steel	Hardened tool steel	11.3:1	–	220		[687]
Mn–66.7Si	Lab ball mill	SS	SS	64:1		25		[688]
Mn–40Zr	Planetary ball mill			13:1		30		[692]
Mo–50Ni	SPEX 8000	Hardened tool steel		10:1	–	28	Partly Am.	[725]
Mo–25Si	Planetary ball mill			20:1	600 m/s^2	10 min		[465]
Mo–25S	Planetary ball mill	Hardened tool steel	Hardened tool steel	11.3:1	–	220		[687]

(continued on next page)

Table 17 (*continued*)

System	Mill	Vial material	Grinding medium material	BPR	Speed (rpm)	MA time (h)	Glass-forming range (at%)	Reference
Nb–25 and 33.3Al	Vibration mill	SS	SS	5:1		40–20		[336]
Nb–Al	SPEX 8000	Steel	52100 steel	10:1	–		25–85Al	[236]
Nb–Fe	Planetary ball mill QM–4H	Tool steel	SS	10:1	–	–	30–70Fe	[726]
Nb–25Ge	SPEX 8000				–	5	12–34Ge	[340]
Nb–Ge	High energy ball mill	WC or Hardened tool steel	WC or Hardened tool steel			10–16	18–27Ge	[727]
Nb–Ge	SPEX 8000	Hardened tool steel	440C steel	10:1	–	10–15	12–30Ge	[728]
Nb–Ge							25–27	[727]
$Nb_{75}Ge_{25-x}Al_x$							$x = 6, 12, 19$	[727]
Nb-(x) Ge-(25 − x) Si	High energy ball mill	WC or hardened tool steel	WC or Hardened tool steel			8	$x = 6 - 19$	[727]
Nb–Mn						35–60 Mn		[694]
Nb–16Si	SPEX 8000		SS	15:1	–	4		[729]
Nb–25Si	High energy ball mill	WC or Hardened tool steel	WC or hardened tool steel			8		[727]
Nb–27Si	SPEX 8000	WC-lined steel	52100 steel	10:1	–	12		[532]
Nb–50Si	Planetary ball mill QF–1	Steel	Steel	34:1		150		[730]
Nb–66.7Si	Fritsch P7			4:1		60	Partly Am.	[505]
Nb–Sn							25	[696,731]
$(Nb_{0.7}Ta_{0.3})_5Si_3$	SPEX 8000	WC– lined steel	52100 steel	10:1	–			[532]
$(Nb_{0.8}Ta_{0.2})_5Si_3$	SPEX 8000	WC– lined steel	52100 steel	10:1	–			[532]
Nd–77Fe–8B	High energy ball mill	WC	WC	40:1	750	100		[729]
Nd–74Fe–15Mo	Lab ball mill	SS	SS	100:1	100	Am. + α-Fe + Mo		[732,733]
Nd–82Fe–7Ti	Lab ball mill	SS	SS	100:1	95	100	Am. + α-Fe	[733]
Nd–74Fe–15Ti	Lab ball mill	SS	SS	100:1	95	100	Am. + α-Fe	[732]
Nd–74Fe–15V	Lab ball mill	SS	SS	100:1	95	100	Am. + α-Fe	[732,733]
Nd–81Fe–4Ti– 4Mo	Lab ball mill	SS	SS	100:1	95	100	Am. + α-Fe + Mo	[732]
Ni–Al	Lab ball mill	Hardened steel	Hardened steel	10:1			27–35Al	[345]
Ni–25Al–25Ti	SPEX 8000	Hardened steel		10:1	–	30	Partly Am.	[538]
Ni–Mg	Planetary ball mill			10:1		180	20–50Mg	[349]
Ni–50Mo	SPEX 8000	Hardened tool steel		10:1	–	10–32	Partly Am.	[734,735]
Ni–20Nb	Fritsch P6			10:1		80		[146]
Ni–40Nb	Fritsch P6			10:1		85		[146]
Ni–40Nb	SPEX 8000	Hardened tool steel	52100 steel	3:1	-	9–11		[21,736]
Ni–40Nb	Lab ball mill	SS	Hardened steel			200		[737]
Ni–55Nb	Ball mill	SS	SS			11		[211]
Ni–60Nb	Fritsch P6			10:1		95		[146]
Ni–Nb	Planetary ball mill		Cr–steel	4:1			20–80Nb	[738]
Ni–Nb	SPEX 8000	Hardened tool steel	440 C steel	10:1	–		21–80Nb	[739]
Ni–18P	Horizontal rotating ball mill	SS	SS	30:1	80	800	Partly Am.	[284]
Ni–30Si	Planetary ball mill	Hardened tool steel	Hardened tool steel	11.3:1		167		[687]
Ni–33Si	Planetary ball mill	Hardened tool steel	Hardened tool steel	11.3:1		220		[687]
Ni–33.3Si	Fritsch P5	SS	SS	9.6:1		200		[541]

Ni–Sn							20–40Sn	[739]
Ni–25Ta	Planetary ball mill	WC–Co	WC–Co			20	Partly Am.	[740]
Ni–50Ta	Planetary ball mill	WC–Co	WC–Co			20	Partly Am.	[740]
Ni–Ta	Fritsch P7			5:1			40–80Ta	[741]
Ni–40Ti	Planetary ball mill					200		[742]
Ni–40Ti	Planetary ball mill	Hardened steel	Hardened steel	30:1	720	14 in N_2, 20 in Ar, 32 in O_2		[542,543]
Ni–50Ti	Ball mill	SS	WC				20	[743]
Ni–50Ti	SPEX 8000	Hardened steel	SS	6:1	–	24		[706]
Ni–50Ti	SPEX 8000	Tool steel				25–35		[744]
Ni–66.7Ti	Ball mill	SS	SS			17		[211]
Ni–Ti	Hardened steel	440C steel					30–67Ti	[357]
Ni–V	Conventional ball mill	SS	Steel		110	400	40–65V	[745]
Ni–31Zr	Attritor, Mitui Miike MA 1D	SS	SS		300	16		[746]
Ni–32Zr	Fritsch P5	Steel	Steel	13:1		20		[692]
Am Ni–32Zr + Zr	Fritsch P7	Steel	Steel			20	35–72Zr	[747]
Ni–35Zr	Fritsch P5	Steel	Steel					[748]
Ni–38Zr	Uni ball mill					60 HE mode 240 LE mode	Partly Am.	[105]
Ni–50Zr	SPEX 8000	Hardened tool steel	440C steel	10:1	–	18		[749]
Ni–50Zr	SPEX 8000	Hardened steel	SS	6:1	–	24		[706]
Ni–50Zr	Super Misuni NEV-MA8	SS	SS	7:1	–	15	−180°C, no Am. 25°C, partly Am. 200°C, Am.	[177]
Ni–60Zr	SPEX 8000	Hardened tool steel	440 C steel	10:1	–	12		[749]
Ni + $NiZr_2$	SPEX 8000	Hardened tool steel	440C steel	10:1	–	15	20–60Zr	[186]
$Ni_{11}Zr_9 + NiZr_2$	SPEX 8000	Hardened tool steel	440C steel	10:1	–		15–76Zr	[186,749]
$Ni_{10}Zr_7$ + $Ni_{21}Zr_8$			Hardened steel			21		[52]
Am–Ni–32Zr + Zr						20	35–72Zr	[747]
Ni–Zr [333,393,632,704,747,750]							15–73Zr	
Ni–Zr	Fritsch P5	SS	SS		710	15–20	20–80Zr	[751]
Ni–Zr	Planetary ball mill	Steel	Hardened steel				35–45Zr	[752]
Ni–Zr	Vibratory ball mill		WC or 440 C steel	54:1		32	30–80Zr	[753]
Ni–Zr	High energy ball mill	Steel		4:1		120	30–80Zr	[750]
Pd–17Si	Lab ball mill	SS	Hardened steel			200		[754]
Pd–20Si	Fritsch P5	Tempered steel		5:1		10–15		[755]
Pd–20Si		WC–Co	WC–Co			13	Am. + Pd_3Si	[756]
Pd–Si	SPEX 8000	Hardened steel	SS	5:1	–	8	19Si	[547]
Pd–Si	Fritsch P5						13.5–25Si	[757]
Pd–Ti	WC–Co	WC–Co					42–85Ti	[756]
PTFE–Cu	Vibration high energy mill	SS	SS	47:1				[757]
PTFE–Ni	Vibration high energy mill	SS	SS	47:1				[757]
Si–30Fe								[513]
Si–10 to 20Sn	Fritsch P7/P5	Tempered steel		1.4:1				[758]

(continued on next page)

Table 17 (*continued*)

System	Mill	Vial material	Grinding medium material	BPR	Speed (rpm)	MA time (h)	Glass-forming range (at%)	Reference
Sm–87.5Fe	Planetary ball mill Retsch PM 4000						Am. (Sm–Fe) + α-Fe	[759]
Sm–Fe	SPEX 8000	Hardened steel	Hardened steel	10:1	–	48	Am. (Sm–Fe) + α-Fe	[549]
Ta–30Al	Rod mill	SS	SS	36:1	85	400		[51]
Ta–33Al	Rod mill	SS	SS	30:1	85	400		[364]
Ta–Al	Ball mill	SS	SS	108:1	85	300	10–90Al	[760]
Ta–20 to 50Cu	Fritsch P5	SS	SS	4:1	Int. 7 or 5	15	20Cu	[96]
Ta–20 to 50Cu	Fritsch P5	Cu–Be	Cu–Be	4:1	Int. 7 or 5	75	30Cu	[96]
Ta–30Cu	Super Misuni NEV–MA8	Cu–Be	Cu–Be			60 (200 °C)	Partly Am.	[98]
Ta–30Cu	Fritsch P5	Cu–Be	Cu–Be	7:1	Int. 5	120		[99]
Ta–30Cu	Planetary ball mill	Steel	Steel	15:1		100		[761]
Ta–Cu	Planetary ball mill	Steel	Steel	15:1			30–50Cu	[762]
Ta–5Fe	Fritsch P5	SS	SS	4:1		30		[96]
Ta–Ni	Fritsch P7	High speed steel	Cr-steel	5:1		120	20–60Ni	[741]
Ta–Ni	SPEX 8000	High speed steel	Cr-steel	2:1	–	15–20	10–80Ni	[182]
Ta–37.5Si	SPEX 8000	WC–lined SS	52100 steel	5:1	–	12		[532,533]
Ti–25Al	SPEX 8000	Hardened tool steel			–	9–16		[736]
Ti–25Al	SPEX 8000	WC		8:1	–	20–24		[370]
Ti–25Al	Ball mill	SS	SS	100:1		50		[342]
Ti–25Al	Vibration mill	SS	SS	5:1		25	Am. + microc rystalline	[336]
Ti–50Al	Ball mill	SS	SS	100:1		500		[342]
Ti–50Al	Fritsch P5	SS	SS	18:1		20		[763]
Ti–50Al	Szegvari attritor					60		[764]
Ti–50Al	Attritor	SS	SS	15:1	150	15		[765]
Ti–50Al	Planetary ball mill			60:1	720	30 in N_2 100 in Ar		[766]
Ti–50Al	Planetary ball mill			20:1		40		[767]
Ti–50Al		SS	Hardened steel	70:1 to 100:1		75		[768]
Ti–50Al	Horizontal ball mill	SS	440C steel	40:1		500		[769]
Ti–50Al	Horizontal ball mill	SS	SS	30:1 to 60:1	150	80		[770]
Ti–50Al	Vibration mill	SS	SS	5:1				[336]
Ti–50Al	Vibratory ball mill	SS	SS	15:1		80		[765]
Ti–50Al	Planetary ball mill Retsch PM 4000	SS	SS	15:1	150			[765,770]
Ti–60Al	Vibration mill	SS	SS	5:1		25		[336]
Ti–60Al	Fritsch P5	Hardened steel	Hardened steel	10:1		25–30	20–60Al	[111]

Ti–Al							45–65Al	[328]
Ti–Al	Lab mill	SS	SS	100:1	95		50–75Al	[771]
Ti–Al	Fritsch	Hardened steel	Hardened steel	10:1			20–50Al	[367]
Ti–Al	Fritsch P7	Hardened steel	Hardened steel	10:1	490	40	10–60Al	[242]
Ti–Al	Fritsch P5	Hardened steel	Hardened steel	10:1		15–75	20–50Al	[368]
Ti–Al	Fritsch P5	Steel	Steel	10:1			10–75Al	[242]
Ti–Al	Rod mill	SS	SS	30:1	85	200	25–67Al	[772]
Ti–48Al–2Cr	Horizontal ball mill		SS	30:1	100	500	Partly Am.	[551]
Ti–40Al–10Ni	SPEX 8000	Steel	Steel	8:1	–	40		[773]
Ti–25Al–25Ni	SPEX 8000	Steel	Steel	8:1		20		[773]
Ti–25Al–25Ni	Ball mill	SS	SS	100:1		100		[374]
Ti–20Al–20Ni	SPEX 8000	Steel	Steel	8:1	–	40		[773]
Ti–15Al–15Ni	SPEX 8000	Steel	Steel	8:1	–	20		[773]
Ti–10Al–30Ni	Ball mill	SS	SS	100:1		100		[374]
Ti–Al–Ni	Ball mill	SS	SS	100:1		500	0–50Al, 0–50Ni, 30–90Ti	[374]
Ti–50Co	SPEX 8000			15:1				[764]
Ti–50Cu		SS	Hardened steel	70:1 to 100:1		75		[774]
Ti–50Cu		WC–Co	WC–Co					[756]
Ti–Cu		Hardened Tool steel or WC–Co	WC–Co	3:1 to 10:1			10–87Cu	[702]
Ti–Cu		Hardened steel	Hardened steel or WC			17	10–90Cu	[720]
Ti–Cu	Fritsch P7	WC	WC	10:1	490	20	10–50Cu	[775]
Ti–40 to 60Mn	Fritsch P6	Ti	Ti	5:1 to 7:1	460	55–40		[776]
Ti–24.3 Ni	Ball mill				110	400		[777]
Ti–33Ni	Ball mill	SS	SS			17		[211]
Ti–33Ni	SPEX 8000	Hardened steel	Hardened steel					[645]
Ti–35Ni	SPEX 8000	Hardened steel	Hardened steel			11		[736]
Ti–40Ni	Planetary ball mill			30:1	720	15 min		[778]
Ti–50Ni	Ball mill	SS	SS	90:1		300		[534]
Ti–Ni	Fritsch P7	WC	WC	10:1	Int. 6	20 h	10–70 Ni	[775]
Ti–Ni	SPEX 8000	Hardened steel					35–50 Ni	[779]
$Ti_{50}Ni_xAl_{50-x}$							x = 10, 25	[773]
$Ti_{60}Ni_xAl_{40-x}$							x = 15, 20	[773]
$Ti_{60}Ni_{1-x}Cu_x$ (x = 10, 20, and 30)	Fritsch P7	WC	WC	10:1		14–40	x = 30 partly Am.	[780]
Ti–(40 − x)Ni − xCu	Fritsch P7	WC	WC	10:1	490	18	x = 10–20	[775]
Ti–(50 − x)Ni − xCu	Fritsch P7	WC	WC	10:1	490	18	x = 10–30	[775]
Ti–(60 − x)Ni − xCu	Fritsch P7	WC	WC	10:1	490	18	x = 10–40	[775]
Ti–18Ni–15Cu	SPEX 8000	Steel	52100 steel	10:1	–	16		[781]
Ti–Ni–Cu	Fritsch P7	WC	WC	10:1		14–40	10–30Ni, 10–30Cu	[780]
Ti–18Ni–10Fe–16Si	SPEX 8000			6:1	–	30		[433]
Ti–Pd	SPEX 8000	WC–Co or Hardened steel	WC–Co or Hardened steel	5:1		17	15–58Pd	[756,782]
Ti–30Pd–20Cu		WC–Co	WC–Co					[756]
Ti–35Si	Ball mill					180		[59]
Ti–37.5Si	Fritsch P5	Cr steel	Cr steel	10:1	153		Am + Ti_5Si_3	[783]

(continued on next page)

Table 17 (*continued*)

System	Mill	Vial material	Grinding medium material	BPR	Speed (rpm)	MA time (h)	Glass-forming range (at%)	Reference
Ti–37.5Si	Vibration mill	SS	SS	5:1		60		[336]
Ti–37.5Si	Horizontal ball mill	SS	440C steel	40:1		500		[769]
Ti–37.5Si	SPEX 8000	SS	Hardened steel	5:1	–	24		[784]
Ti–66.7Si	Lab ball mill	SS	SS	64:1		25		[785]
Ti–Si	Vibro mill	Hardened steel	WC–Co			37	16–63Si; partly Am. 63–87Si	[786]
Ti–Si	Ball mill	SS	SS	50:1		300	20–50Si	[787]
Ti–50V	Fritsch P5		SS	20:1		7		[557]
Ti–50Zr	Fritsch P5	SS	SS	5:1		24		[607]
Ti–50Zr	Fritsch P5	SS	SS	20:1		285		[785]
$TiH_{1.924}$–25Al	SPEX 8000	Steel	52100 steel	10:1	–	30		[483]
$TiH_{1.924}$ –50Al	SPEX 8000	Steel	52100 steel	10:1		30		[483]
V–40Ni	Bal mill	SS	SS		110	800		[786]
V–25Si	Fritsch P5	SS	SS	10:1	280	30		[114]
V–37.5Si	SPEX 8000	WC–lined SS	52100 steel	10:1	–	12		[533]
W–50Fe	Ball mill	SS	SS	30:1	85	300		[788]
W–50Fe	Ball mill	SS	SS	30:1	250	400		[322]
W–Fe	Fritsch P5	Hardened steel	Hardened steel	20:1			30–70Fe	[789]
Y–Ni–B–C	Super Misuni NEV MA–8	Hardened steel	Hardened steel	10:1, 15:1	–	300, 64		[597]
Y–Ni–B–C + 15 wt% Fe	Super Misuni NEV MA–8	Hardened steel	Hardened steel	10:1	–	64		[597]
Y_2O_3-BaO_2-CuO	SPEX 8000	WC	WC	6:1	–	25		[561]
Zn–Ti	Planetary ball mill	Steel	Hardened steel	6:1 to 10:1	–	26	40Ti	[790]
Zr–30Al	Attritor	ZrO_2 balls		10:1		45		[107]
Zr–50Al	SPEX 8000	Steel	52100 steel	10:1	–	7		[388]
Zr–Al	SPEX 8000	SS	SS	4:1	–	24	17.5–30Al	[791]
Zr–Al	SPEX 8000	SS	SS	4:1	–	24	17.5–40Al	[792]
Zr–Al	SPEX 8000	Hardened steel	WC	4:1	–	12	17.5–40Al	[793]
$Zr_{65}Al_{10}Cu_{25-x}Ni_x$ x = 5 to 20	Planetary ball mill Retsch PM 4000	Hardened steel	Hardened steel	15:1		100		[794]
$Zr_{65}Al_{7.5}Cu_{17.5}Ni_{10}$	Planetary ball mill Retsch PM 4000	Hardened steel	Hardened steel	15:1		60		[678]
$Zr_{50}Al_{13.8}Cu_{26.2}Ni_{10}$	Planetary ball mill Retsch PM 4000	Hardened steel	Hardened steel	15:1		60		[678]
$Zr_{41.2}Al_{13.8}Cu_{26.2}Ni_{18.8}$	Planetary ball mill Retsch PM 4000	Hardened steel	Hardened steel	15:1		60		[678]
$(Zr_{65}Al_{7.5}Cu_{17.5}Ni_{>10})_{100-x}Fe_x$ (x = 0 to 20)	Planetary ball mill Retsch PM 4000	Hardened steel	Hardened steel	15:1		100		[795]
$Zr_{60}Al_{10}Cu_{18}Ni_9Co_3$				6:1		36		[796]
Zr–Co	Fritsch P5	Steel	Steel	15:1		60	27–92Co	[797]
Zr–50Cu		SS	SS	40:1		200		[798,799]
Zr–40Fe	Fritsch			13:1		20		[704]

Zr–Fe	Fritsch P5	Steel	Steel	15:1		60	30–78Fe	[797]
Zr–Fe		Hardened steel	Hardened steel or WC			17	20–50Fe	[720]
Zr–Mn	Fritsch P5	Steel	Steel	15:1		60	20–85Mn	[797]
Zr–Ni	Fritsch P5	Steel	Steel	15:1		60	27–83Ni	[797]
Zr–$NiZr_2$	SPEX 8000	Hardened tool steel	440C steel	10:1	–	15	24–27Ni	[186]
Zr–Pd							45–60Pd	[432]
$Zr_{55}Ti_{2.5}Cu_{27.5}Ni_{15}$	Planetary ball mill Retsch PM 4000	Hardened steel	Hardened steel	15:1		100		[794]
$Zr_{65}Ti_{7.5}Cu_{17.5}Ni_{10}$	Planetary ball mill Retsch PM 4000	Hardened steel	Hardened steel	15:1		60		[678]
$Zr_{50}Ti_{13.8}Cu_{26.2}Ni_{10}$	Planetary ball mill Retsch PM 4000	Hardened steel	Hardened steel	15:1		60		[678]
$Zr_{55}Ti_{13.8}Cu_{26.2}Ni_{5}$	Planetary ball mill Retsch PM 4000	Hardened steel	Hardened steel	15:1		60		[678]
$Zr_{48.9}Ti_{9.5}Cu_{29.6}Ni_{12}$	Planetary ball mill Retsch PM 4000	Hardened steel	Hardened steel	15:1		100		[794]
$Zr_{22.5}Ti_{30}Cu_{30}Ni_{17.5}$	Planetary ball mill Retsch PM 4000	Hardened steel	Hardened steel	15:1		100		[794]
$Zr_{11.9}Ti_{33.4}Cu_{42.7}Ni_{10}$	Planetary ball mill Retsch PM 4000	Hardened steel	Hardened steel	15:1		100		[794]
$Zr_{5}Ti_{45}Cu_{30}Ni_{20}$	Planetary ball mill Retsch PM 4000	Hardened steel	Hardened steel	15:1		100		[794]
Zr–29V	WC-lined	Hardened steel	Hardened steel			140		[798]
ZrO_2-20mol%MgO	Planetary G7	Steel	Steel	7:1	500–700	188	Am. + cubic ZrO_2	[454]

SS: stainless steel; PA: prealloyed.

[a] MA/500 h + anneal at 770 K + quench.

[b] In hydrogen atmosphere.

[c] Argon–nitrogen mixture.

[d] Argon–air mixture.

Table 18
Amorphous phases formed in intermetallics/prealloyed powders by MM[a]

Compound	Mill	Vial material	Grinding medium material	BPR	Speed (rpm)	MA time (h)	Glass-forming range (at%)	Reference
AgPd	SPEX 8000	–	–	10.4:1	–	65		[196]
$Al_{13}Co_4$	Fritsch P5	SS[a]	SS	10:1	150	200		[659]
Al–15Cr (RS)[b]	Ball mill	SS	SS	120:1		1000	Partly Am.	[149]
Al–20Cr (RS)	Ball mill	SS	SS	120:1				[149]
AlTa	Rod mill					40		[800]
C	SPEX 8000	WC	WC	4:1	–	206		[801]
α-Co_2Ge	Fritsch P0	WC bottom-lined steel	Hardened steel			180		[640]
β-Co_2Ge	Fritsch P0	WC bottom-lined steel	Hardened steel			36		[640]
Co_5Y		SS	SS		80–110	300		[682]
CoZr	SPEX 8000	Hardened steel	440 martensitic steel	10:1	–	4–6 h at −85 and −190°C		[180]
CoZr	Vibrating mill	Hardened steel	440C SS	10:1	–	80		[354]
Cr–28Fe		Hardened steel	Hardened steel			200		[742]
CuZr	SPEX 8000	Hardened tool steel	440C steel	10:1	–			[705]
Cu_3Zr_2	SPEX 8000	Hardened tool steel	440C steel	10:1	–	13		[705]
Ge	Fritsch P7/P5	Tempered steel					Partly Am.	[802]
La–25Al–20Ni	Planetary ball mill	WC–Co	WC–Co	20:1	180	12		[803]
$Mg_{70}Zn_{30}$	Planetary ball mill				200	58		[804]
Nb–20Ge	SPEX 8000	Hardened tool steel	440C steel	10:1	–	10–15		[728]
$Nd_2Fe_{14}B$	SPEX 8000	Hardened steel	Hardened steel	10:1	–	24	Am. + α-Fe	[805]

Nd–77Fe–8B	High energy ball mill		SS	18:1		24		[806]
Ni_3Al	Invicta vibrator mill BX920/2	Hardened tool steel	440C SS	10:1		50	Partly Am.	[615]
Ni–55Nb	Ball mill	SS	SS			14		[211]
Ni_5Si_2	Fritsch P5	SS	SS	9.6:1		200		[541]
NiTi	SPEX 8000	Hardened steel	440 C steel	10:1		18 at 220°C, 13 at 60°C, 2 at −190°C		[180]
$NiTi_2$	Ball mill	SS	SS			14		[211]
$Ni_{10}Zr_7$	Fritsch P0	WC	Hardened steel			95		[807]
NiZr	SPEX 8000	Hardened tool steel	440 C steel	10:1	–	18		[749]
NiZr	Fritsch P5	SS	SS	30:1		48		[808]
Ni–60Zr	SPEX 8000	Hardened tool steel	440 C steel	10:1	–	8		[749]
$NiZr_2$	Super Misuni NEV-MA 8	SS	SS	7:1				[177]
Pd–32Ni–20P	Planetary ball mill	WC–Co	WC–Co	20:1	180	24		[803]
Sb–12Ga	Ball mill	Agate				16		[92]
Se	Planetary ball mill						At <50°C	[809]
Si	Fritsch P7/P5	Tempered steel	Steel	1.4:1	Int. 5 or 10	70–95		[758]
Si	SPEX 8000	Hardened tool steel	440C steel	8:1	–	38	Partly Am.	[810]
Talc	Vibration mill	Steel	Steel					[811]
Ti–33Ni	Ball mill	SS	SS			14		[211]
Ti–33Ni	SPEX 8000	Hardened steel	Hardened steel					[645]
TiNi	SPEX 8000	Tool steel	440C steel	10:1	–	13		[77]
Ti–18Ni–15Cu (RS)	SPEX 8000					16		[781]
Ti_5Si_3	Fritsch P5	Cr steel	Cr steel	10:1	228		Partly Am.	[783]
TiV	Fritsch P5		SS	20:1		100[c]		[557]

(continued on next page)

Table 18 (*continued*)

Compound	Mill	Vial material	Grinding medium material	BPR	Speed (rpm)	MA time (h)	Glass-forming range (at%)	Reference
YCo_2	Ball mill	Steel	Steel		110	300		[20,706,812]
YCo_5	Ball mill	Steel	Steel		110	300		[706,812]
Zr_2Co (PA)[d]	Planetary ball mill	Hardened steel			300 m/s^2			[113]
ZrCo (PA)	Planetary ball mill	Hardened steel			600 m/s^2			[113]
Zr_2Ni								[177]
$ZrSiO_4$	Planetary G7	Steel	Steel	7:1	500–700	240		[454]

[a] SS: stainless steel.
[b] RS: rapidly solidified.
[c] Argon–nitrogen mixture.
[d] PA: prealloyed.

the amorphous phase formation is known to be critically dependent on the milling conditions, details about the mill, milling container, grinding medium, BPR, and other parameters are also provided in these tables.

A point to be considered is whether there exists a difference in the way an amorphous phase forms by MA from a mixture of powders (A and B) and by MM from the intermetallic compound (A_mB_n). Two reaction routes are possible:

$$mA + nB \rightarrow (A_mB_n)_{\text{crystalline}} \rightarrow (A_mB_n)_{\text{amorphous}} \tag{13}$$

$$mA + nB \rightarrow (A_mB_n)_{\text{amorphous}} \tag{14}$$

Occurrence of amorphization by both the routes can be found in the literature.

When the starting material is a mixture of elemental powders, i.e., during MA, additional time is required for alloying to occur and then only an amorphous phase can form. On the other hand, when the starting material is an intermetallic, i.e., during MM, no alloying need to occur, but only amorphization. Thus, intuitively one can estimate that the times for amorphization are shorter during MM. It is also of interest to note that formation of a crystalline intermetallic phase has been reported to occur before amorphization. This has been shown to be true in the Cu–Ti [701], Fe–Sn [714], Nb–Ge [728], Nb–Si [730], Nb-Sn [731], Ni-Zr [752], Ti-Ni-Fe-Si [433], and Zr–Al [107], amongst others. In some instances, it has also been reported that a solid solution forms first which on continued milling becomes amorphous. This has been reported to be true in the case of Ta–Al [364], Ti–Al [366], Zr–Al [389], and other systems. In some systems, it was reported that on MA of the blended elemental powder mixture the sequence of phase formation with time was solid solution, intermetallic and finally an amorphous phase [336,369]. Whether an intermetallic or a solid solution phase forms before amorphization depends on the relative free energies of the solid solution and the intermetallic phases; the phase with the lowest free energy forms.

In general, the end product is the same irrespective of whether the starting material is a mixture of the elements, a single intermetallic phase, or a mixture of two or more such phases. This has been shown to be true in the Nb–Al system, where an amorphous phase was obtained whether the starting material was an intermetallic or blended elemental powder mixture. However, in the Mg–Zn system, it has been reported that an amorphous phase can be produced only by starting from the intermetallic $Mg_{70}Zn_{30}$ and not by MA from the blended elemental powder mixture of the Mg–30Zn composition [804]. On the other hand, an Fe–33at%Ti powder mixture could be amorphized by MA while the intermetallic Fe_2Ti could not be amorphized by MM [715].

Amorphization in ordered alloys seems to follow the sequence [615]:

$$\begin{aligned}&\text{Ordered phase} \rightarrow \text{disordered phase (loss of long-range order)}\\ &\rightarrow \text{fine grained (nanocrystalline)phase} \rightarrow \text{amorphous phase}\end{aligned} \tag{15}$$

The formation of an amorphous phase can occur, at least in some cases, without the loss of long-range order (see Section 10 on Disordering of Intermetallics).

Even though it may appear that any alloy can be made amorphous under appropriate conditions of milling, it is not true. This is because a number of variables, the more important of them being milling energy, milling temperature, and impurity contamination, control the constitution of the final product.

The effect of process variables on the amorphization behavior has been studied in several alloy systems. Amongst these, the important variables studied are milling intensity (including higher ball-to-powder weight ratio, BPR) and milling temperature.

Increased milling energy (achieved by a higher ball-to-powder weight ratio, increased speed of rotation, etc.) is normally expected to introduce more strain and increase the defect concentration in the powder and thus lead to easier amorphization. However, higher milling energies also produce more heat (and higher temperatures) and this can result in the crystallization of the amorphous phase. Therefore, a balance between these two effects will determine the nature of the final product phase.

It has been reported in the Ni–Zr system that milling in a planetary ball mill at an intensity of 3 did not produce any amorphous phase [813]; due to the insufficient energy available at low intensities. However, when the intensity was increased to 5, amorphous phase formation was observed in a wide composition range of 30–83 at% Ni. At an intensity of 7, amorphous phase formation was observed, but only between 66 and 75 at% Ni. These observations suggest that with increasing milling energy, the heat generated is also high, which crystallizes the amorphous phase. Similar results were also reported in other systems [745,804,814,815]. Thus, it appears that the maximum amorphization range is observed at intermediate values of milling intensity — too low an intensity does not provide enough energy to amorphize while at very high intensities, the amorphous phase formed would crystallize.

It has also been reported that increasing the BPR has a similar effect. It was shown in the Al–Ta system that a fully amorphous phase was obtained only at a BPR of 36:1 or 108:1. When the BPR used was 12:1 a crystalline phase was obtained, while at a BPR of 324:1, a mixture of an amorphous and crystalline phases was obtained [672]. Paralleling these studies it has been reported that an amorphous was not obtained when large diameter grinding medium was used [111,113,755].

In some cases an amorphous phase may form at both low and high milling intensities, provided that the temperature rise at the high milling intensity is not high enough to cause crystallization of the amorphous phase produced. But, the difference may be in the time for amorphization. It has been reported that amorphization in a Ni–38at% Zr powder mixture requires 60 h in a high-energy mode in a Uni-Ball mill while it takes 240 h at low and intermediate energies; even then it is only partly amorphous.

There have been conflicting results on the effect of milling temperature on the nature of the phase formed. Koch et al. [180] have recently summarized the results

of varying the temperature of the mill on the kinetics of amorphization in intermetallics. They concluded that generally a lower milling temperature accelerated the amorphization process. Since a nanostructured material can be easily produced at lower temperatures of milling, the increased grain boundary area drives the crystal-to-amorphous transformation. For example, the time required for amorphization in NiTi was 2 h at −190°C, 13 h at 60°C, and 18 h at 220°C [180]. Similar results were also reported by others, see, for example, Ref. [807]. Fig. 8(a) shows the grain size obtained at different milling temperatures for the CoZr intermetallic. It can be seen that the grain size is smaller at lower milling temperatures, and therefore it becomes easier to form the amorphous phase at lower temperatures of milling. Note also the band representing the critical grain size for amorphization. The milling time required for obtaining an amorphous phase as a function of the normalized milling temperature (milling temperature/melting temperature) is plotted for NiTi, CoZr, and $NiZr_2$ intermetallics in Fig. 8(b). This figure confirms that the times are shorter at lower homologous temperatures [181]. While majority of the limited number of studies follow the above behavior, there is at least one example, where the reverse behavior is reported. Lee et al. [177] reported that amorphization kinetics were faster at higher temperatures of milling. They indicated that while no amorphization occurred in the NiZr and $NiZr_2$ intermetallics after milling for 15 h at −180°C, full amorphization was observed for the same milling time at 200°C. A partially amorphous phase formed at an intermediate temperature of 25°C. This was explained on the basis of the increased interdiffusion rates at higher temperatures. More recent experiments by Koch [181] confirm that rapid amorphization was achieved in the $NiZr_2$ compound at low temperatures.

Mechanical alloying/mechanical milling introduces contamination into the milled powder and this can substantially alter the constitution and stability of the powder product. Generally, the presence of additional elements favors amorphization (using the confusion principle enunciated for formation of an amorphous phase during RS processing of materials and so frequently obeyed [656]). For example, it has been reported that an amorphous phase was obtained in ball-milled Fe–Cr alloy powders only in the presence of oxygen; an intermetallic formed in the absence of oxygen [306]. A similar situation was obtained in MM of Nb_3Al powders where a disordered solid solution was produced when milled in a clean atmosphere whereas an amorphous phase formed in the presence of nitrogen [622]. Al–Ti [675] and Ni–Nb [127] systems also exhibited a similar behavior. Substantial pick up of nitrogen and oxygen was found to be the reason for amorphization observed in Ti–50 at% Al powders. Improved atmospheric control prevented amorphization even after milling for 100 h [816].

Contamination has also been found to affect the stability of the amorphous phases formed. Formation of a crystalline phase has been reported on continued milling of Ti–Al powders after the formation of the amorphous phase [58]. Chemical analysis of the powder, fine-structure analysis by XPS techniques, and lattice parameter measurements strongly suggested that this fcc crystalline phase is

due to increased nitrogen contamination of the milled powder and the crystalline phase has been identified as TiN [58]. Similar results were reported on milling of Zr–Al powder [389].

11.1. Thermodynamics and kinetics of amorphous phase formation

Metallic glasses have been obtained by rapid solidification techniques in a number of binary and ternary alloy systems [219,653–657]. It has been well established that, amongst other conditions, the likelihood of obtaining a glassy phase is very high near deep eutectics. But, in mechanically alloyed powders an amorphous phase is obtained around the equiatomic composition [817]. This observation can be rationalized with reference to Fig. 32. A hypothetical binary phase diagram featuring some solid solubility on either end and also exhibiting the presence of an intermetallic phase is shown in Fig. 32(a). α and β are the terminal solid solutions, γ is the intermetallic and L represents the liquid phase. The Gibbs free energies of the different phases at a temperature T_r are shown as a function of composition in Fig. 32(b), assuming that the free energy of the undercooled

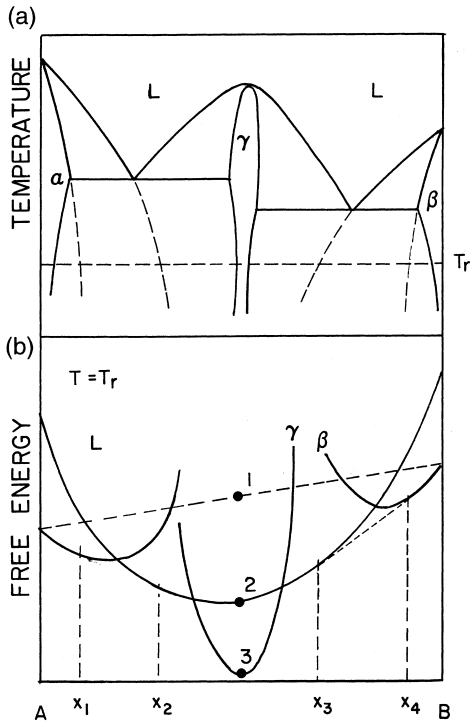

Fig. 32. (a) Hypothetical binary phase diagram featuring some solid solubility on either end and also showing the presence of an intermetallic phase. (b) Gibbs free energy versus composition at a temperature corresponding to T_r in the above diagram.

liquid fairly accurately represents the free energy of the amorphous phase. At this temperature, α, β, γ, and mixtures of these phases are thermodynamically stable, whereas L is metastable.

The equiatomic blended elemental powder mixture has a free energy, G_c corresponding to point 1 in Fig. 32(b), half way along the straight line joining the free energies of pure metals A and B. If the two components are allowed to interdiffuse freely, then the lowest free energy state corresponding to the formation of the γ phase, G_i (point 3) will be obtained. Even though thermodynamically this is the lowest free energy state, this can be kinetically prevented from occurring when the free energy G_a, corresponding to the formation of an amorphous phase (point 2), is reached.

Preventing the reaction c → i from occurring and favoring c → a to occur is possible by a proper choice of metals A and B, the reaction temperature T_r, and the reaction time t_r. Schwarz and Johnson [818] proposed that two conditions need to be satisfied for an amorphous phase to form from a thin film couple (or a blended elemental powder mixture). First, the two metals must have a large negative heat of mixing in the liquid (amorphous) state, and this provides the thermodynamic driving force for the reaction to occur. Hellstern and Schultz [819] confirmed the importance of the large negative heat of mixing by studying the glass-forming ability of several titanium-containing transition metal alloys. Systems such as Cu–Ti, Ni–Ti, and Co–Ti with a large negative heat of mixing could be completely amorphized, while Fe–Ti, Mn–Ti, and Cr–Ti could be only partially amorphized due to their smaller heat of mixing. The isomorphous V–Ti system did not amorphize at all because a solid solution always formed on milling the powder mixture. Alloy systems with a positive heat of mixing have also been amorphized by MA in recent years; but, a large negative heat of mixing is an essential condition for glass formation by RSP. The second criterion is that the two metals must have largely different diffusion rates into each other and in the amorphous alloy phase. This favors the kinetics of reaction path c → a in Fig. 32(b) over that of reaction path c → i. This asymmetry in the diffusivities has been correlated with the difference in atomic sizes for several elements [817].

The reaction temperature is another important parameter. If the temperature at which milling is conducted is high, then formation of the amorphous phase would not be generally expected. This is because the temperature rise during milling and the high temperature of milling together may result in a situation such that the temperature is above the crystallization temperature of the amorphous phase. Consequently, if the amorphous phase were to form it would crystallize. This has been shown to be true when higher milling intensities or higher BPR values were employed during milling. In this respect, it is better that milling is carried out at a relatively low temperature if formation of an amorphous phase is desired. Further, the diffusion of one element into the other is slow at low temperatures and consequently nucleation and growth of the intermetallic would not take place. But, in some cases, it has been reported that an additional heat treatment facilitates complete amorphous phase formation. In the case of an Al–15at%Cr alloy powder mixture, only partial amorphous phase formation was observed after

milling for 1000 h in a low-energy ball mill. But, when this milled powder was annealed at 740 K and quenched, a fully amorphous phase was obtained [204]. A similar observation was made in the Ta–Cu system also [820]. In general, a lower temperature of milling favors amorphization.

The reaction time scales also are important because not only should one allow the formation of the amorphous phase, but also maintain it without transforming to the equilibrium phases. These concepts can be explained with reference to Fig. 33. Like in Fig. 32, if we assume that the free energy of the blended elemental mixture is G_c, that of the amorphous phase as G_a, and that of the intermetallic as G_i, then these are schematically shown in Fig. 33. To prevent the stable intermetallic from forming, the time scale for the formation of the amorphous phase from the blended elemental mixture, i.e., $t_{c\to a}$ should be much shorter than $t_{c\to i}$. Further, since the amorphous phase is metastable, $t_{a\to i}$ should be much longer than $t_{c\to a}$ so that the stability of the amorphous phase can be increased. Thus, the kinetic conditions for the formation of an amorphous phase by solid state reactions can be summarized as:

$$t_{c\to a} \ll t_{c\to i} \quad \text{and} \quad t_{a\to i} \gg t_{c\to a} \tag{16}$$

11.2. Mechanism of amorphization

The mechanism of amorphization by MA and/or MM is not clearly understood. The early investigators [20,658] assumed that the powder particles melted because of the very high rate of plastic deformation, and consequent rise in the powder

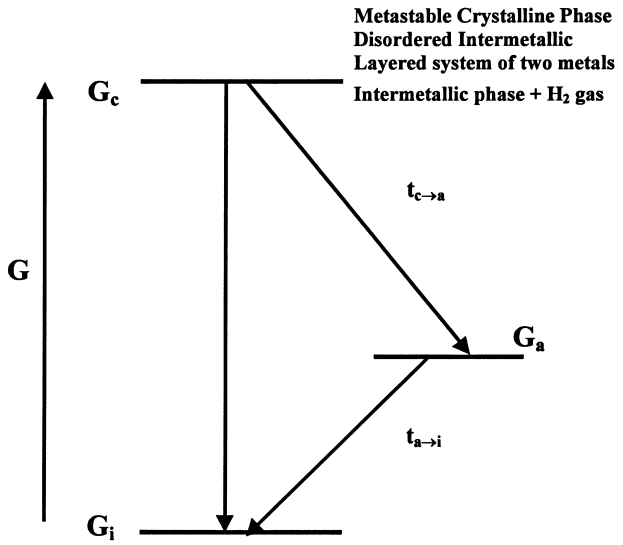

Fig. 33. Schematic free energy diagram indicating the criteria to be met for solid state amorphization.

temperature. Subsequent quenching of the liquid by heat conduction into the less deformed, and hence cooler, interior regions of the particles, resulted in the formation of the amorphous phase (like in RSP). However, energy input calculations and temperature measurements suggest that the temperature rise is not large enough for the powder particles to melt (see also Section 7 on Temperature Rise during Milling). Additionally, if this mechanism were to be true, the glass-forming composition ranges in mechanically alloyed and rapidly solidified alloys should be the same; but this is not true as will be shown later. Researchers now believe that amorphization during MA is not purely a mechanical process and that a solid-state reaction similar to that observed in thin films [818] occurs during MA. During MM, however, destabilization of the crystalline phase is thought to occur by the accumulation of structural defects such as vacancies, dislocations, grain boundaries, and anti-phase boundaries. The continuous decrease in grain size (and consequent increase in grain boundary area) and a lattice expansion would also contribute to the increase in free energy of the system [821]. It has been reported that the stored energy during MA can be about 50% of the enthalpy of fusion, whereas by cold rolling or wire drawing it is only a small fraction of it [167]. These defects raise the free energy of the intermetallic system to a level higher than that of the amorphous phase and consequently, it becomes possible for the amorphous phase to form. It has been reported that amorphization occurs when the strain in the slow diffusing species reaches a maximum [242]. In the case of ordered alloys, amorphization was reported to occur when the long-range order parameter is <0.6 with a corresponding volume of expansion of about 2% [822].

Irradiation of crystalline materials by energetic particles and electrons has been known to cause amorphization when the following criteria are obeyed:

- the intermetallic compound has a narrow or zero homogeneity range,
- the order–disorder transition temperature of the intermetallic, T_c is higher than the melting temperature, T_m,
- the two components (elements) are separated by more than two groups in the periodic table,
- the intermetallic has a complex crystal structure, and
- the fraction of A atoms ($f_A \geq f_B$) is $\geq 1/3$.

Intermetallics have also been amorphized by MM when the above criteria were generally followed. However, there have been several exceptions to the above empirical rules (too many to be ignored). For example, compounds with reasonably wide homogeneity ranges have also been amorphized. Further, a number of compounds with $f_A = 1/4$ have been made amorphous. In view of these observations, it should be realized that the above criteria may only be used as guidelines and not that if they are obeyed, amorphization will be observed.

Beke et al. [823,824] estimated the elastic mismatch energy stored in an ordered solid solution when its long-range chemical order is destroyed. They showed that if $T_c > T_m$ (see the second condition above) and the ratio of the elastic mismatch energy to the ordering energy is high enough, amorphization is expected to occur.

This has been proved to be a valid criterion in many cases of amorphization observed by irradiation.

Recently, attempts have been made to predict the ability of an alloy to become amorphous under MA/MM conditions. Since both atomic sizes and heats of formation are important in the formation of amorphous phases, Zhang [825] plotted $(R_A - R_B)/R_B$ (where R_A and R_B are the atomic radii of the components A and B, respectively) against ΔH, heat of formation of the amorphous phase, and observed that the regions where an amorphous phase forms or does not form can be separated by a straight line given by the equation:

$$(R_A - R_B = \Delta R)/R = 0.068\Delta H + 0.716 \tag{17}$$

The proportion of correct predictions for the glass-forming alloys was 89.2% while that for the non-glass-forming alloys was only 71.4%.

A theoretical model was also proposed in which amorphization was assumed to be realized through interstitial impurity formation during MA [826]. It was assumed that amorphization occurred when impurity atoms penetrated into interstitial sites and distorted the lattice locally. When the local distortions reached some critical value, the long-range order of the lattice was destroyed (destabilization of the crystalline phase) and an amorphous phase formed. It was also shown that the minimum concentration of solute atoms needed to amorphize a binary alloy system by MA was strongly related to the atomic size ratio of the constituents as observed in RSP investigations [827]. For example, in fcc-based metal systems, an amorphous phase was formed by MA when the atomic size ratio was 0.68–1.83 and for bcc-based metal systems it was 0.66–1.31.

It has also been recently shown that large negative values of the interaction parameter ω_{AC} promote amorphization [710]. The interaction parameter ω_{AC} is given by the equation:

$$\omega_{AC} = RT\varepsilon_C^A \tag{18}$$

where R is the gas constant, T is the absolute temperature, and ε_C^A is the interaction coefficient defined as $\varepsilon_C^A = \mathrm{d}\ln\gamma_C/\mathrm{d}X_A$, where γ_C is the activity coefficient and X_A is the atom concentration of component A.

11.3. Theoretical predictions of amorphous-phase-forming range

The formation enthalpies of different competing phases in an alloy system, e.g., solid solution or an amorphous phase, can be calculated using the relations developed by Miedema and co-workers [828] and recently summarized by Bakker [829]. They proposed that for a solid solution the formation enthalpy consists of three terms, viz.,

$$\Delta H\,(\text{solid solution}) = \Delta H_{\text{chem}} + \Delta H_{\text{elast}} + \Delta H_{\text{struct}} \tag{19}$$

where ΔH_{chem} is the chemical contribution due to the mixing of atoms of the two

different metals, ΔH_{elast} is the elastic contribution due to the atomic size mismatch, and ΔH_{struct} represents the variation in the lattice stability as a function of the average number of valence electrons per atom. This term will be present only when alloying occurs between two transition metals.

In an amorphous alloy, the atoms arrange themselves in such a way that elastic mismatch is avoided but, in addition to a chemical term, there is a topological term due to the amorphous character. The total formation enthalpy for an amorphous alloy is estimated as:

$$\Delta H \text{ (amorphous)} = \Delta H_{chem} + 3.5\left(c_A T_{m,\,A} + c_B T_{m,\,B}\right) \tag{20}$$

where $T_{m,\,A}$ and $T_{m,\,B}$ are the melting points, and c_A and c_B are the atomic fractions, of the elements A and B, respectively. Using the above relations one can calculate the enthalpies of formation for the solid solution and amorphous phases. When these enthalpies of formation are plotted against composition, one can obtain the relative stabilities of the competing phases or phase mixtures by using the common tangent construction. Even though this model has been successfully applied with considerable success to predict the formation and stability range of amorphous phases, a few words of caution are in order.

Firstly, we should realize that it is the free energy and not the enthalpy alone, which decides the stability of a phase. In the Miedema calculations, the entropy term is ignored. This is because the Miedema model is strictly valid only at 4.2 K and therefore the enthalpy effects are far more important than the entropy effects. Further, since we are dealing here with situations far from equilibrium, the kinetic path should be taken into account. The thermodynamic parameters (and the common tangent constructions) may then be used only as guidelines. Secondly, significant discrepancies have been observed between the calculated and experimentally observed heats of mixing. Thirdly, the enthalpy calculations do not consider the occurrence of intermetallics in the phase diagram — only the terminal solid solutions and an amorphous phase are expected to be present under metastable conditions. Lastly, the prediction of glass-forming range using this model has been applied mostly to studies on MA and not by other non-equilibrium processing techniques. In spite of these apparent limitations, several researchers have calculated the glass-forming range using the Miedema model and these values are compared with the experimentally observed values in Table 19.

Another common approach of thermodynamic evaluation of binary systems is CALPHAD [833], which uses analytical expressions to describe the free energy of different phases. These expressions are derived from models with parameters obtained from numerical fits to measured equilibrium data. Extrapolations are then used to predict metastable equilibria. The CALPHAD method is usually preferred to the Miedema model since the former is based on more explicit thermodynamic data such as the equilibrium phase diagram. But, these calculations are also sometimes inadequate due to problems associated with insufficient experimental input, fitting errors, and invalid extrapolation to large undercooling.

Generally, the amorphous-phase-forming range is experimentally determined by looking for the presence of broad peaks in the X-ray diffraction patterns of the processed alloy. As mentioned earlier, this may not always prove that the material produced is truly amorphous. It is much more reliable to measure the properties of the samples such as the crystallization temperature, enthalpy of crystallization, saturation magnetization or the superconducting transition temperatures. When these properties are plotted against composition, a sudden change in the slope indicates the solute concentration up to which the amorphous phase is homogeneous [328].

It should be remembered that a good match is not always found between the observed and predicted amorphous-phase-forming composition range. This is essentially because MA is a "complex" process and the mechanically alloyed powder picks up lot of impurities and gets contaminated. The presence of these substitutional and interstitial impurities modifies the stability of the amorphous phase.

Table 19
Comparison of the predicted and observed glass-forming ranges in mechanically alloyed powder mixtures

System	Amorphous-phase-forming range (at% solute)				
	Miedema model	Reference	CALPHAD	Observed	Reference
Al–Fe	25–60Fe	[228]		25Fe	[228]
Co–V				33–60V	[259]
Co–Zr	22–61Zr	[692]		27–92Zr	[797]
Cu–Hf	21–71Hf	[45]		30–70Hf	[523]
Cu–Ti	25–72Ti	[45]		13–90Ti	[702]
Cu–Zr	26–51Zr	[692]			
Fe–B				50–60B	[577]
Fe–Zr	21–73Zr	[45]		22–70Zr	[830]
Fe–Zr	33–54Zr	[692]			
Nb–Fe	30–70Fe			30–70Fe	[726]
Nb–Ge	18–27Ge	[727]		12–30Ge	[728]
Ni–Hf	16–75Hf	[45]		35–85Hf	[523]
Ni–Nb	20–69Nb	[45]		20–79Nb	[127]
Ni–Ti	23–76Ti	[45]		28–72Ti	[357]
Ni–V				45–60V	[831]
Ni–Zr				20–80Zr	[45,751]
Ni–Zr	17–76Zr	[45]		17–73Zr	[830]
Ni–Zr	22–63Zr	[692]	17–67Zr	24–85Zr	[186]
Pd–Ti	46–80Ti	[45]		42–85Ti	[782]
Pd–Zr				40–55Zr	[832]
Ti–Al	15–88Al	[242]	10–96Al	10–75Al	[242]
	35–75Al	[773]			
Ti–Cu	46–65Cu	[775]			
Ti–Ni	25–83Ni	[773,775]			

11.4. Comparison between mechanical alloying and rapid solidification

The radial distribution functions of amorphous alloys synthesized by MA/MM or RSP techniques have been found to be similar. In fact, the structure factors for irradiated, rapidly solidified, and mechanically alloyed amorphous phases of different alloy systems have been found to be very similar [834]. The structural and magnetic properties of mechanically milled and sputtered YCo_2 and YCo_5 intermetallics have also been found to be very similar [706]. The crystallization temperatures of the amorphous alloys produced by MA and RSP techniques have also been found to be similar [328], even though the activation energies for crystallization of RSP alloys are much higher than for MA alloys [189,677]. But, it has been noted that the composition ranges of the amorphous phases are much wider in alloys produced by MA than in those obtained by RSP.

Even though amorphization has been observed by both MA and MM, there is no quantitative data available to define the "critical" energy input (or other parameters) which can be equated to the critical cooling rate which should be exceeded to form the amorphous phase in RSP studies. Modeling of MA/MM (currently in progress in different laboratories) can provide additional information in this direction.

The features of phase diagrams normally provide clues to the possibility of producing amorphous phases. Amorphous alloys are easily produced by RSP techniques in the vicinity of deep eutectics. This is because the reduced glass transition temperature T_r, defined as the ratio of the glass transition temperature T_g to the melting temperature T_m is the highest at the eutectic point. The ease of forming an amorphous phase is higher the higher the T_r value. But, in the case of mechanically alloyed materials the amorphous phase is mostly obtained around the equiatomic composition. Further, the amorphous-phase-forming range is much wider in materials produced by MA than by RSP. Whereas it has been found impossible to amorphize alloys corresponding to melting point maxima by RSP techniques, it has been found that amorphization by MA occurs easily at such compositions [721]. For example, MA was able to amorphize alloys corresponding to the composition $Hf_{50}Ni_{50}$, at which composition an orthorhombic structured line compound exists with a melting point of 1800 K [523]. Similarly, amorphization was reported in Cu–Hf alloys in the composition range of 60–70 at% Hf, close to and on either side of the Hf_2Cu compound having the highest melting point of the compounds in the system [523]. Alloy systems with a positive heat of mixing cannot be amorphized by RSP, but MA can produce them in the amorphous state. In general, it has been noted that it is easier to produce an amorphous phase, and in a wider composition range, in an alloy system by MA than by RSP. There are some systems in which it is possible to produce an amorphous phase by MA but not by RSP techniques. Amongst those the role of contamination on the formation of amorphous phases by MA, at least in some cases, cannot be completely ruled out. Table 20 compares the amorphous-phase-forming range in some alloy systems produced by these two techniques.

Several investigations were conducted on the crystallization behavior of rapidly

Table 20
Comparison of amorphous-phase-forming ranges (at%) by MA and RSP techniques

System	By RSP	By MA	Reference
Ag–Pd	Not reported	50Pd	[196]
Al–Fe	Not reported	20–50Fe	[663]
		17–33Fe	[133]
Al–Ta		33–67Ta	[673,674]
Co–B		33–50B	[576]
Co–Ge	Not reported		[835]
Co–Nb		15–20Nb	[686]
Co–Si		30–70Si	[689]
Co–Ti		15–20Ti	[686]
Co–V		33–60V	[259]
Co–Zr		8–73Zr	[259]
Cr–Fe		28Fe	[693]
Cr–Nb		30–68Nb	[694]
Cu–W		30–90W	[291]
Fe–B		35–40B	[708]
Fe–C		20–25C	[708]
		17–60C	[582]
$Fe_{83-x}Cr_xC_{17}$	24–50Cr	10–60Cr	[710]
$Fe_{83-x}Mo_xC_{17}$	5–26Mo	5–60Mo	[710]
Fe–P		25P	[712]
Fe–Si		10–40Si	[689]
Fe–Zr		22–70Zr	[333,704]
Ge–S		61–72S	[718]
Hf–Cu		20–90Cu	[720]
		30–70Cu	[523,721]
Hf–Ni		15–65Ni	[721]
		10–85Ni	[720]
La–Al–Ni		30–70La	[722]
		10–50Ni	
Mg–Ni		50–80Ni	[349]
		40–70Ni	[723]
Nb–Al		25–85Al	[236]
Nb–Co		35–85Co	[694]
Nb–Cr		32–70Cr	[694]
Nb–Fe		35–75Fe	[694]
Nb–Ge		18–27Ge	[727]
		12–30Ge	[728]
Nb–Mn		35–60Mn	[694]
Nb–Ni	40–60Ni	20–80Ni	[694,738,739]
Ni–Mg		20–50Mg	[349]
Ni–Mo	Not reported	50Mo	[734]
Ni–Sn		20–40Sn	[739]
Ni–Ta	35–65Ta	40–80Ta	[741]
	30–60Ta	20–90Ta	[182]
Ni–V		40–65V	[745]
Ni–Zr	60–80Zr, 30–42Zr	20–80Zr	[751]
		30–80Zr	[753]

Table 20 (*continued*)

System	By RSP	By MA	Reference
Pd–Si	15–23Si	13.5–25Si	[757]
Pd–Ti	Not reported	42–85 Ti	[756,782]
Ta–Al	Not reported	10–90Al	[760]
Ta–Cu		20–50Cu	[762]
Ti–Al	Not reported	10–60Al	[242]
		10–75Al	[242]
		20–50Al	[366,367]
		20–60Al	[111]
		25–67Al	[772]
		45–65Al	[328]
		50–75Al	[771]
Ti–Al–Ni		0–50Al, 0–50Ni, 30–90Ni	[374]
Ti–Cu	30–70Cu	10–87Cu	[702]
		10–90Cu	[720]
Ti–Ni		10–70Ni	[775]
		35–50Ni	[779]
$Ti_{50}Ni_xAl_{50-x}$		x = 10, 25	[773]
$Ti_{60}Ni_xAl_{40-x}$		x = 15, 20	[773]
Ti–$(40-x)$Ni–xCu		x = 10–20	[775]
Ti–$(50-x)$Ni–xCu		x = 10–30	[775]
Ti–$(60-x)$Ni–xCu		x = 10–40	[775]
Ti–Ni–Cu		10–30Ni, 10–30Cu	[780]
Ti–Si		16–63Si	[786]
Zn–Ti		40Ti	[790]
W–Fe		30–70Fe	[789]
Zr–Al		17.5–30Al	[791]
		17.5–40 Al	[792,793]
Zr–Co	20–57Co	27–92Co	[797]
Zr–Cu	25–90Cu	40–60Cu	[704,705]
Zr–Fe	8–17Fe	20–50Fe	[720]
	60–80Fe	30–78Fe	[325,327,797]
Zr–Mn		20–50Mn	[797]
Zr–Ni	20–40Ni and 58–70Ni	27–83Ni	[797]
Zr–Pd	20–35Pd	45–60Pd	[434]

solidified alloys and also their transformation behavior on application of pressure (see the relevant chapters in refs. [3,4,653–657]). But, only a few reports are available on such transformations of amorphous phases produced by MA/MM. An important difference observed between amorphous phases synthesized by MA and RSP techniques is the degree of thermal relaxation. Since MA is conducted at or near room temperature, the amorphous alloy samples are in a very unrelaxed state [748]. This may prove to be very useful in probing the microscopic origin of the relaxation processes. Another important difference is in the nature of the transformation. For example, the amorphous phase at the Zr–24at%Fe composition synthesized by MA directly transforms to the equilibrium Zr_3Fe phase. But, the first crystallization products of rapidly solidified (melt-spun) alloy

are metastable Zr_2Fe, ω-Zr, and α-Zr, which were not observed during the decomposition of the mechanically alloyed powder [836].

Amorphous phases are synthesized by many other methods also such as laser processing, sputtering, ion mixing, etc. Differences have been observed in the amorphous-phase-forming composition range between MA and these methods. Fig. 34 compares the amorphous-phase-forming composition range for the Ni-Nb system.

There has been lot of activity in recent times on the synthesis/processing and characterization of bulk amorphous alloys [837]. These alloys, characterized by a wide supercooled liquid region (large temperature differences between the crystallization and glass transition temperatures), can be synthesized at extremely low cooling rates. Such alloys have also been synthesized by MA in the multicomponent Zr–Ti–Cu–Ni, Zr–Al–Cu–Ni, and Mg–Y–Cu systems [678]. Applications for such bulk amorphous alloys include the 3 mm-thick faceplate inserts for high-end golf club heads [838].

12. Nanostructured materials

Nanocrystalline materials are single-phase or multi-phase materials, the crystal size of which is of the order of a few (typically 1–100) nanometers in at least one dimension. Because of the extremely small size of the grains, a large fraction of

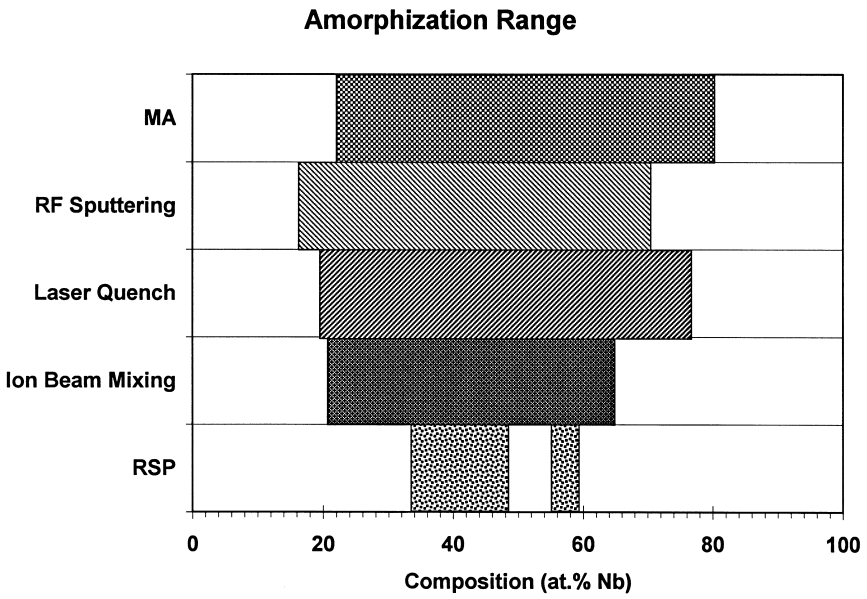

Fig. 34. Comparison of amorphous phase forming range achieved in the Ni–Nb system by different non-equilibrium processing routes.

the atoms in these materials is located in the grain boundaries (Fig. 35) and thus the material exhibits enhanced combinations of physical, mechanical, and magnetic properties (compared to material with a more conventional grain size, i.e., >1 μm). Nanocrystalline materials show increased strength, high hardness, extremely high diffusion rates, and consequently reduced sintering times for powder compaction. Several excellent reviews are available giving details of the processing, properties, and applications of these materials [183,184,839,840].

Nanocrystalline materials have been synthesized by a number of techniques starting from the vapor phase (e.g., inert gas condensation), liquid phase (e.g., electrodeposition, rapid solidification), and solid state (e.g., mechanical attrition). The advantage of using MA for the synthesis of nanocrystalline materials lies in its ability to produce bulk quantities of material in the solid state using simple equipment and at room temperature. The first report of formation of a nanostructured material synthesized by MA is by Thompson and Politis in 1987 [782], even though the specific mention of formation of "nanometer order crystalline structures produced by mechanical alloying" was by Shingu et al. in 1988 [841]. Koch [183] has summarized the results on the synthesis and structure of nanocrystalline structures produced by mechanical attrition and has recently updated the situation [842].

Grain sizes with nanometer dimensions have been observed in almost all mechanically alloyed pure metals, intermetallics, and alloys (if they continue to be crystalline). Thus, it appears to be a ubiquitous phenomenon. In spite of this, there have not been many investigations to explain why and how the nanometer-sized grains are obtained in these materials. Hellstern et al. [843] have described the mechanism of formation of nanostructures by MA/MM. From high-resolution

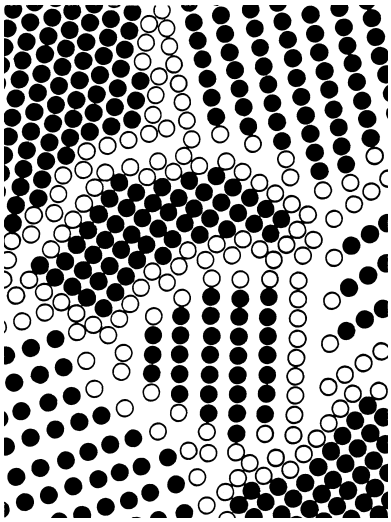

Fig. 35. Schematic arrangement of atoms in an equiaxed nanocrystalline metal.

TEM observations, these authors reported that at the early stages of MA, shear bands were observed due to the high deformation rates experienced during MA. These shear bands, which contain a high dislocation density, have a typical width of approximately 0.5–1.0 μm. With continued milling, the average atomic level strain increases due to the increasing dislocation density, and at a certain dislocation density within these heavily strained regions, the crystal disintegrates into subgrains that are separated by low-angle grain boundaries. This results in a decrease of the lattice strain. On further processing, deformation occurs in shear bands located in previously unstrained parts of the material. The grain size decreases steadily and the shear bands coalesce. The small angle boundaries are replaced by higher angle grain boundaries, implying grain rotation, as reflected by the absence of texture in the electron diffraction patterns and random orientation of the grains observed from the lattice fringes in the high-resolution electron micrographs. Consequently, dislocation-free nanocrystalline grains are formed.

Li et al. [844] have also proposed a model for the refinement of grain size during ball milling and noted that the grain size in the early stages of milling follows the relation:

$$d = Kt^{-2/3} \tag{21}$$

where d is the grain size, t is the time and K is a constant.

The minimum grain size achievable by milling is determined by the competition between the plastic deformation via dislocation motion and the recovery and recrystallization behavior of the material [845,846] This balance gives a lower bound for the grain size of pure metals and alloys. The minimum grain size, $d_{\min}$ obtained by MM was found to vary inversely with the melting point of Al, Ag, Cu, and Ni (all having an fcc structure) [845], and directly with the stacking fault energy. However, when data from the bcc and hcp metals as well as several intermetallics are included, only fcc metals (with a relatively low melting point) showed this clear inverse dependence of minimum grain size on the melting point [183,842]. The minimum grain size was virtually independent of the melting point for the hcp, bcc, and other fcc metals with high melting points. For these elements it appears that $d_{\min}$ is in the order: fcc < bcc < hcp. Since a number of process variables (method to estimate the grain size, milling intensity, milling temperature, alloying effects, contamination, etc.) can influence the minimum grain size achieved, systematic investigations are required to be conducted before serious explanations can be offered for these variations.

Several nanocomposites have also been synthesized by MA. Nanocomposites have also been obtained when the amorphous phases obtained by MA/MM are crystallized at relatively low temperatures [847]. An important attribute of these nanocomposites is in preventing or minimizing grain growth till very high temperatures. Reinforcement of Cu and Mg with Al_2O_3 was reported to prevent grain growth up to the melting point of the metals [848]. Alloys in the nanocrystalline form have also been shown to have much higher hydrogen

sorption properties at low temperature than their polycrystalline coarse-grained counterparts [849]. These materials are not also sensitive to exposure to air.

A number of reviews have been written recently on the synthesis, properties, and applications of nanostructured materials processed by MA/MM (see, for example, Ref. [840,842]) and so this topic will not be discussed further.

13. Mechanochemical synthesis

It was first reported in 1989 that MA could be used to induce a wide variety of solid–solid and even liquid–solid chemical reactions [850,851]. It was demonstrated that CuO could be reduced to pure metal Cu by ball milling CuO at room temperature with a more reactive metal like Ca. Milling together of CuO and ZnO with Ca has resulted in the direct formation of β′-brass [851]. But, it has been reported that such types of chemical reaction were observed as early as 1894 where the conversion of mechanical energy into chemical energy was utilized to bring about chemical reactions [852]. This has been referred to in the literature as mechanosynthesis or mechanochemical synthesis. McCormick [23] has presented a review of the work from his group a few years ago. In fact, most of the work in this subarea of MA is due to McCormick [23], Takacs [118], and Matteazzi [329].

Most of the mechanosynthesis reactions studied have been displacement reactions of the type:

$$MO + R \rightarrow M + RO \tag{22}$$

where a metal oxide (MO) is reduced by a more reactive metal (reductant, R) to the pure metal M. Metal chlorides and sulfides have also been reduced to pure metals this way and the results available to-date are summarized in Table 21.

The reactions listed in Table 21 are characterized by a large negative free energy change and are therefore thermodynamically feasible at room temperature. The occurrence of these reactions at ambient temperatures is thus limited by kinetic considerations alone.

A characteristic feature of all solid-state reactions is that they involve the formation of product phase(s) at the interfaces of the reactants. Further growth of the product phase involves diffusion of atoms of the reactant phases through the product phase, which constitutes a barrier layer preventing further reaction. Thus, these reactions require elevated temperatures to proceed at reasonable rates.

Mechanical alloying can provide the means to substantially increase the reaction kinetics of the reduction reactions. This is because the repeated welding and fracturing of powder particles increases the area of contact between the reactant powder particles due to a reduction in particle size and allows fresh surfaces to come into contact repeatedly; this allows the reaction to proceed without the necessity for diffusion through the product layer. As a consequence, reactions that normally require high temperatures will occur at lower temperatures during MA without any externally applied heat. In addition, the high defect densities induced

Table 21
Mechano-chemical reactions studied

Reaction	Mill	BPR	%Excess reductant	ΔH (kJ)	T_{ad} (K)	t_{ig} (min)	Reference
$3Ag_2O + 2Al \rightarrow 6Ag + Al_2O_3$	–	–	–	−532	4914	86	[853]
$2AlCl_3 + 3CaO \rightarrow \gamma\text{-}Al_2O_3$[a] $+ 3CaCl_2$	SPEX 8000	–	–	–	–	–	[854]
$CdO + Ca \rightarrow Cd + CaO$	SPEX 8000	3:1	10	− 377	3561	37	[851]
$CoCl_2 + 2Na \rightarrow Co + 2NaCl$	SPEX 8000	3:1	25	−495		20	[855]
$3CoS + 2Al \rightarrow 3Co + Al_2S_3$	SPEX 8000	11:1		−405	1710	–	[329]
$Cr_2O_3 + 2Al \rightarrow 2Cr + Al_2O_3$	SPEX 8000	33:1	10	− 273	–	–	[453]
$Cr_2O_3 + 3Zn \rightarrow 2Cr + 3ZnO$	SPEX 8000	33:1	10	+49	–	–	[453]
$CuCl_2 + 2Na \rightarrow Cu + 2NaCl$	SPEX 8000						[856]
$3CuO + 2Al \rightarrow 3Cu + Al_2O_3$	SPEX 8000	33:1	10	− 1197	5151	15	[857]
					5394	37	[851,858]
$2CuO + C \rightarrow 2Cu + CO_2$ (24 h)	SPEX 8000	12:1	40	− 135	–	–	[859]
$CuO + Ca \rightarrow Cu + CaO$ (100 min)	SPEX 8000	3:1	–	−473	4716	6.5	[850,851,860]
						19	[857]
$4CuO + 3Fe \rightarrow 4Cu + Fe_3O_4$ (20 h)	SPEX 8000	3:1	10	−488	1380	170	[851,857]
	Planetary mill	30:1			1668	153	[861–863]
$CuO + 2H \rightarrow Cu + H_2O$ (3 h)	Attritor			−87			[864]
$CuO + Mg \rightarrow Cu + MgO$	SPEX 8000	3:1	10	−445	4531	34	[857]
						90	[851]
$CuO + Mn \rightarrow Cu + MnO$	SPEX 8000	3:1	10	−231	2227	43	[857]
$CuO + Ni \rightarrow Cu + NiO$	SPEX 8000	3:1	10	−382	988	–	[851]
					1288		[857]
$2CuO + Si \rightarrow 2Cu + SiO_2$ (24 h)	Stirring ball mill	30:1 to 80:1	10	−596	–	–	[865]
$2CuO + Ti \rightarrow 2Cu + TiO_2$	SPEX 8000	3:1	10	−633	4175	0.3	[851]
						2.8	[857,858]
$Cu_2O + Mg \rightarrow 2Cu + MgO$	SPEX 8000			−434		20	[866]
$Cu_2O + Zn \rightarrow 2Cu + ZnO$	SPEX 8000			−183		44	[866]
$CuO + ZnO + Ca \rightarrow \beta'$-brass $+ CaO$ (24 h)	SPEX 8000	3:1	10	–			[850]
$3Cu_2S + 2Al \rightarrow 6Cu + Al_2S_3$	SPEX 8000	10:1		−485	1740		[329]
$Cu_2S + Fe \rightarrow 2Cu + FeS$	SPEX 8000	8:1		−71	590		[329]

$2ErCl_3 + 3Ca \rightarrow 2Er + 3CaCl_2$				−407			[867]
$FeCl_3 + 3Na \rightarrow Fe + 3NaCl$ (3 h)	SPEX 8000						[868]
$3Fe_3O_4 + 8Al \rightarrow 9Fe + 4Al_2O_3$	SPEX 8000	8:1	10	−1716	3805		[869]
		12:1	−75 to +100				[870]
$Fe_3O_4 + 2Ti \rightarrow 3Fe + 2TiO_2$	SPEX 8000	8:1	10	−395	2737	20	[453]
$Fe_3O_4 + 4Zn \rightarrow 3Fe + 4ZnO$	SPEX 8000	16:1	10	−143	–	–	[117,453]
$Fe_2O_3 + 3Ca \rightarrow 2Fe + 3CaO$	SPEX 8000	3:1		−1080	3498	24	[851]
$3\alpha\text{-}Fe_2O_3 + C \rightarrow 3FeO + Fe_3O_4 + CO_2$	SPEX 8000	11:1					[460]
$3FeS + 2Al \rightarrow 3Fe(Al) + Al_2S_3$	SPEX 8000	9:1		−271	1146		[329]
$FeS + Mn \rightarrow Fe + MnS$	SPEX 8000	10:1		−117	1300		[329]
$2FeS + Si \rightarrow 2Fe(Si) + SiS_2$	SPEX 8000	12:1		+88	–		[329]
$2GdCl_3 + 3Ca \rightarrow 2Gd + 3CaCl_2$				−378			[867]
$NiCl_2 + Mg \rightarrow Ni + MgCl_2$	SPEX 8000	10:1				42	[871]
$NiCl_2 + 2\ Na \rightarrow Ni + 2NaCl$	SPEX 8000	3:1	50	−507			[855]
$3PbS + 2Al \rightarrow 3Pb + Al_2S_3$	SPEX 8000	13:1		−267	1247		[329]
$SmCl_3 + 3Na \rightarrow Sm + 3NaCl$	SPEX 8000	10:1	15	−202			[872]
$2TaCl_5 + 5Mg \rightarrow 2Ta + 5MgCl_2$	SPEX 8000	7:1	10	−745	1616		[873,874]
$TiCl_4 + 2Mg \rightarrow Ti + 2MgCl_2$	SPEX 8000	3:1 to 12:1	15	−479			[875]
$3V_2O_5 + 10Al \rightarrow 6V + 5Al_2O_3$	SPEX 8000	7:1	10	−3727	3468		[876]
$V_2O_5 + 5Mg \rightarrow 2V + 5MgO$	SPEX 8000	7:1	10	−1457	3354	–	[876]
$2V_2O_5 + 5Ti \rightarrow 4V + 5TiO_2$	SPEX 8000	7:1	10	−1623	2658	–	[876]
$WO_3 + 3Mg \rightarrow W + 3MgO$	SPEX 8000	10:1	10				[877]
$ZnO + Ca \rightarrow Zn + CaO$ (24 h)	SPEX 8000	3:1	10	−285	2242	87	[850,851]
$ZnO + Mg \rightarrow Zn + MgO$	SPEX 8000	7:1	10	−253	2006	45	[878]
$2ZnO + Ti \rightarrow 2Zn + TiO_2$	SPEX 8000	3:1	10	−249	1982		[853]
$3ZnS + 2Al \rightarrow 3Zn + Al_2S_3$	SPEX 8000	13:1		−107	493		[329]
$ZrCl_4 + 2CaO \rightarrow ZrO_2$[b] $+ 2CaCl_2$ (20 h)	SPEX 8000	5:1	–	−440	–	–	[879]
$ZrCl_4 + 2Mg \rightarrow Zr + 2MgCl_2$	SPEX 8000	10:1	10	−303			[874]

[a] $\gamma\text{-}Al_2O_3$ formed only after heating the milled powder to $>300°C$.
[b] ZrO_2 formed only after heating the milled powder to $>400°C$.

by MA accelerate the diffusion process. Alternatively, the particle refinement and consequent reduction in diffusion distances (due to microstructural refinement) can at least reduce the reaction temperatures significantly, even if they do not occur at room temperature.

Depending on the milling conditions, two entirely different reaction kinetics are possible [857,870,880]:

1. the reaction may extend to a very small volume during each collision, resulting in a *gradual* transformation, or
2. if the reaction enthalpy is sufficiently high, a *self-propagating combustion reaction* can be initiated.

The latter type of reactions require a critical milling time for the combustion reaction to be initiated. If the temperature of the vial is recorded during the milling process, the temperature initially increases slowly with time. After some time, the temperature increases abruptly, suggesting that ignition has occurred, and this is followed by a relatively slow decrease. This time at which the sudden increase in temperature occurs is referred to as the ignition time, t_{ig} and these values also are listed in Table 21. Fig. 36 shows schematically the variation of temperature with time during the milling operation. Measurements of the ignition time provide a useful means of characterizing the structural and chemical evolution during MA [881]. It has been noted that there is only particle refinement during milling until the combustion reaction occurs. The reduction reaction occurs only after the combustion reaction. Accordingly, it was observed that no reaction occurs between PbO_2 and TiO until 28 min 21 s at which time combustion takes place. The reaction resulting in the formation of $PbTiO_3$ is complete at 28 min 23 s [882].

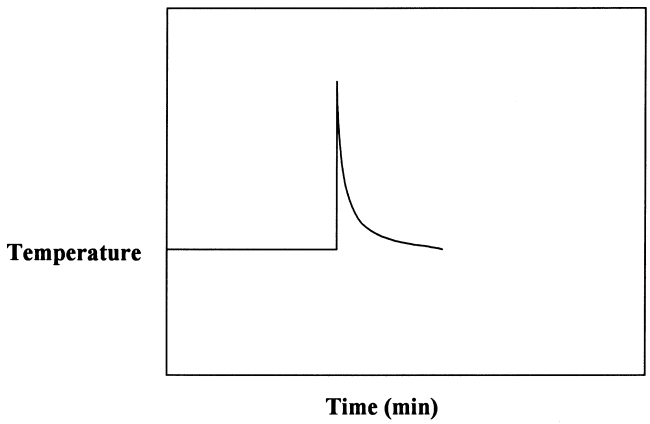

Fig. 36. Variation of milling vial temperature during mechanical alloying when a combustion reaction takes place.

Intimate contact between the reactant powder particles is an essential requirement for combustion to occur. This condition is easily met during milling of ductile–brittle systems. In these mixtures the microstructure consists of brittle oxide particles dispersed in the ductile matrix (Fig. 15) and therefore intimate contact exists between the two types of particles. On the other hand, if both the oxide (which is brittle) and the reductant are hard and brittle, agglomerates of reactant particles cannot develop and combustion is not initiated. This may be the reason why combustion was not achieved in the CuO/Cr couple and even the gradual reaction is extremely slow between CuO and Si. This point highlights the necessity of an intimate contact for achieving faster kinetics during the reduction process.

The product of the displacement reactions normally consists of two phases — the metal (or a solid solution or a compound) and the oxide or chloride associated with the reductant. The removal of the unwanted reaction by-product can be difficult due to the high reactivity of the metal phase associated with the nanocrystalline grain sizes and intermixing of the phases induced by the MA process. The by-product phase can be removed by leaching in a dilute acid or hot water, or by vacuum distillation. It was reported that the salt (by-product $MgCl_2$) formed during the reduction of $TiCl_4$ with Mg was removed either by vacuum distillation at 900°C for 24 h, or by washing the powder in 10% nitric acid [875]. An important requirement for easy removal of the salt from the mixture is that it should be contiguous so that the leachant can easily reach it. The use of carbon or hydrogen as a reductant produces either gaseous CO_2 or water vapor as the by-product and obviates the need for leaching/distillation.

13.1. Process parameters

Process parameters such as milling temperature, grinding ball diameter, ball-to-powder weight (charge) ratio, use of a process control agent, and relative proportion of the reactants seem to play an important role on the nature and kinetics of the product phase obtained by the displacement reactions. For example, a combustion reaction could be initiated during the reduction of copper oxide by iron; but the same reaction progresses gradually under slightly different milling conditions. Consequently, results from different laboratories can be effectively compared only if the exact conditions under which the reaction takes place are reported. These conditions need to be optimized for the best yield.

13.1.1. Milling temperature

McCormick et al. [875] investigated the reduction of $TiCl_4$ with Mg both at room temperature (20°C) when $TiCl_4$ is in the liquid state and at −55°C when it is in the solid state. They observed that the milling time required to synthesize Ti was reduced by a factor of 6 when milling was conducted at −55°C. This was explained on the basis of the greater efficiency of solid–solid collision events occurring during MA. However, if both the reactants were to be in the solid state at both the temperatures, the enhanced diffusivity at the higher temperatures will

increase the reaction kinetics and consequently the times required for reduction will be shorter. No such measurements have been made to date.

13.1.2. Ball-to-powder weight ratio

The time required for the reduction reaction to be completed decreased with an increase in the ball-to-powder weight ratio (BPR). For example, the time required to form Ti during the reduction of $TiCl_4$ with Mg at 20°C was 48 h at a BPR of 2:1, while it was only 18 h at a BPR of 12:1. A similar 3-fold reduction in time with increasing BPR was also noted at −55°C; the minimum milling time required being 3 h at a BPR of 12:1 at this temperature.

Xi et al. [865] studied the effect of BPR on the reduction of CuO by Si during MA in a stirring ball mill. They noted that CuO was completely reduced to the pure metal Cu only at a BPR of 80:1. At lower BPR values, CuO was reduced only partially to Cu and Cu_2O (BPR 60:1), and at a BPR of 30:1, CuO was reduced only to Cu_2O; no Cu was obtained. This result has been explained on the basis that at a high BPR, the collision energy is high and therefore complete reduction to the pure metal could be obtained.

Schaffer and McCormick [881] conducted a systematic investigation on the effect of BPR on the ignition temperature and time. They observed that the ignition temperature T_{ig} decreased with increasing milling time, suggesting that the reaction kinetics increase during milling; during conventional solid-state reactions the reaction rates decrease with time. Further, the rate of decrease of T_{ig} increased with increasing BPR and this is related to the decrease in particle size. The values of t_{ig} also decreased with increasing BPR. Both these effects are related to the average frequency of collisions that increases with increasing BPR. They also noted that the combustion reaction did not occur when small grinding medium (1 and 3 g balls) was used, but it occurred only when large (8 g) balls were used [868].

13.1.3. Process control agent

In many of the investigations on reduction reactions, the components involved are generally brittle and therefore a process control agent (PCA) was not used. However, it was used in a few specific instances with interesting results. When CuO was ball milled with reactive metals in the absence of any PCA, a self-propagating combustion reaction occurred after an incubation period [857,858]. On the other hand, when toluene was used as a PCA, the reduction of CuO proceeded in a controlled manner and reached completion in about 24 h [857]. The use of a PCA acts likes an additive (diluent) and either delays or completely suppresses the combustion event. The PCA also inhibits inter-particle welding during collisions, slowing down the reaction rate as well as decreasing the particle size. It may be noted in passing that a combustion reaction should be avoided if one is interested in producing the metal in a nanocrystalline state. This is because combustion may result in partial melting and subsequent solidification will lead to the formation of a coarse-grained structure. Another requirement for formation of

nanometer-sized particles is that the volume fraction of the by-product phase must be sufficient to prevent particle agglomeration.

13.1.4. Relative proportion of the reactants

Normally about 10–15% stoichiometric excess of the reductant has been used in most of the investigations conducted so far. This excess reductant is used partly to compensate for the surface oxidation of the reactive reductant powder particles, e.g., Al [869]. There have been very few investigations that discussed the effect of the ratio of the constituent reactants (off-stoichiometry).

Takacs [870] investigated the displacement reaction

$$3Fe_3O_4 + 8Al \rightarrow 9Fe + 4Al_2O_3 \tag{23}$$

without the use of a PCA and studied the effect of off-stoichiometry by milling mixtures corresponding to $3Fe_3O_4 + xAl$, where $2 \leq x \leq 16$. A combustion reaction occurred in all the cases except when $x = 2$. However, the nature of the product phases was quite different depending upon the value of x, and the results are summarized in Table 22. It has been noted that a slight decrease in the amount of Al results in the formation of $FeAl_2O_4$ instead of Al_2O_3; excess Al suppresses the formation of metastable γ-Al_2O_3 and $FeAl_2O_4$ and results in the formation of random bcc α-Fe(Al) solid solution and α-Al_2O_3.

13.1.5. Grinding ball diameter

Yang and McCormick [873] investigated the effect of grinding ball diameter on the combustion reaction during milling of a mixture of $TaCl_5$ and Mg. They observed that the ignition time, t_{ig}, for the combustion reaction decreased with an increase in ball diameter.

Combustion requires that the powder mixture reaches the ignition temperature T_{ig}. Since T_{ig} is dependent on the microstructural features, it has been found that T_{ig} decreases with a refinement in the microstructure. During MA the collision

Table 22
Incubation time and phase constitution after milling a mixture of $3Fe_3O_4 + xAl$ for 2 h. Milling of samples 8b, 8c, and 8d was interrupted immediately after, somewhat before, and 5 min after combustion

Sample, x	Incubation time (min)	Major (minor) phases present
2	No combustion	Fe_3O_4, (Al)
6	53	α-Fe, $FeAl_2O_4$
8a	10	α-Fe, α-Al_2O_3, (γ-Al_2O_3, $FeAl_2O_4$)
11	14	α-$FeAl_{0.333}$, α-Al_2O_3
16	56	α-$FeAl_{0.890}$, α-Al_2O_3
8b	8	α-Fe, α-Al_2O_3, γ-Al_2O_3, $FeAl_2O_4$, (Fe_3O_4, Al)
8c	–	Fe_3O_4, Al
8d	23	α-Fe, α-Al_2O_3, γ-Al_2O_3, $FeAl_2O_4$

between the powder particles and the balls raises the powder temperature, T_c. It has been postulated [853] that the ignition time, t_{ig} is equal to the milling time required for T_{ig} to decrease to T_c. Since increasing ball size increases the collision energy and therefore T_c, it is expected that t_{ig} decreases with an increase in the ball diameter.

13.2. Phase formation

It is normally expected that the reactions follow the route indicated in Table 21. Further, the heats of formation are also calculated assuming that these reactions take place according to that sequence. However, it has been noted that many of these reactions do not go to completion directly; instead, intermediate phases are formed. There are also instances when the phases formed are quite different from the expected ones. For example, it was noted that one of the phases becomes amorphous and so could not be detected after milling. This was reported to be true for $AlCl_3$ during milling with CaO when diffraction peaks due to CaO only were observed in the X-ray diffraction patterns [854]. It was inferred that $AlCl_3$ became amorphous during milling. Similar results were reported for $ZrCl_4$ [879], $TaCl_5$ [873], and SiO_2 [874].

Formation of an intermediate product phase has been observed during the reduction reactions of Cr_2O_3 with Al and Zn [453], Fe_3O_4 with Al [869], Ti and Zn [453], and CuO with Fe [861–863] or graphite [859]. For example, during reduction of CuO with Fe, it was observed that the reaction proceeds in various stages that can be represented as:

$$8CuO + 3Fe \rightarrow 4Cu_2O + Fe_3O_4, \tag{24}$$

or

$$5CuO + 3Fe \rightarrow Cu_2O + 3Cu + Fe_3O_4 \tag{25}$$

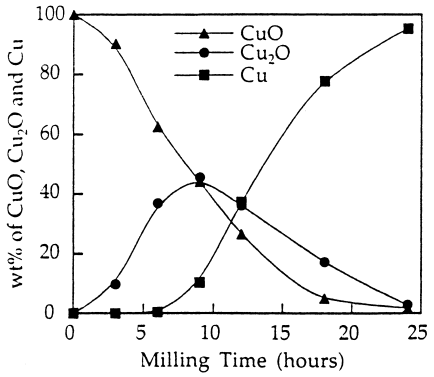

Fig. 37. Effect of milling time on reaction kinetics during reduction of CuO with graphite.

$$4Cu_2O + 3Fe \rightarrow 8Cu + Fe_3O_4 \quad (26)$$

Formation of Cu_2O as an intermediate product was also reported during the reduction of CuO with graphite [859]. Similarly, it was reported that Ti_2O_3 formed as an intermediate product (instead of TiO_2) during the reduction of V_2O_5 with titanium [876]. The amount of CuO was reported to decrease monotonically during milling and the proportion of Cu_2O increased reaching a maximum of 45 wt% after milling for 9 h. Subsequently, it decreased to zero after milling the powder mixture for 24 h (Fig. 37).

The investigation of the nature and the role of such intermediate phases is important in order to understand the reaction mechanism. It should also be mentioned that the reactions stop with the formation of an intermediate phase when the reactions are endothermic. Accordingly, the metal Cr does not form when Cr_2O_3 is reduced with Zn [453].

In a few instances it has also been noted that instead of a pure metal, a solid solution is formed. For example, an Fe(Zn) solid solution is formed during the reduction of Fe_3O_4 with Zn [453] and an Fe(Al) solid solution containing 1.7 at% Al is formed when Fe_2O_3 is reduced with Al [883] or 7 at% Al when FeS is reduced with Al [329].

It has also been observed that in some cases the final phase formed is quite different from the expected phase. During the displacement reactions of FeS, WS_2, and MoS_2 with CaO, it was noted that the corresponding simple oxides did not form; instead, complex oxides, e.g., $CaFeO_3$, $CaWO_4$, and $CaMoO_4$ formed [329]. The product phase in some cases has also been found to be amorphous in nature [865,873].

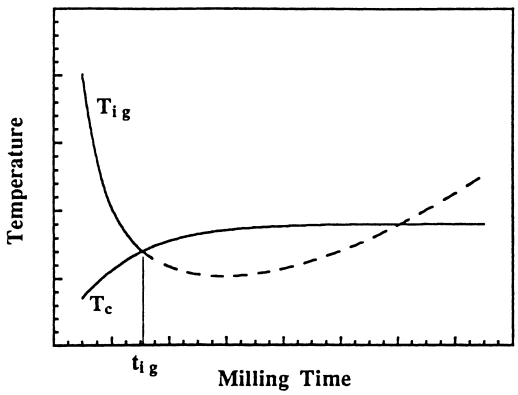

Fig. 38. Schematic representation of the variation of T_{ig} and T_c with milling time. The point of intersection at t_{ig} represents the minimum ignition time.

13.3. Combustion reaction

Milling-induced combustion was first observed by Tschakarov et al. [884] during the mechanochemical synthesis of metal chalcogenides from a mixture of elemental powders. Subsequently, a number of similar reactions were reported to occur during chemical reduction of oxides with reactive metals under mechanical alloying conditions.

The large enthalpy changes associated with the chemical reactions have been identified to be responsible for the occurrence of the combustion reaction. If the temperature generated during the milling process (due to ball-to-ball and ball-to-powder collisions), T_c is higher than the ignition temperature, T_{ig}, then the combustion reaction can occur. The ignition temperature is a function of the enthalpy change and microstructural parameters such as particle size and crystal size. Since the MA process refines the particle size and crystal size, T_{ig} decreases with milling time. But, with increasing milling time T_c increases and reaches a steady state. The time at which the T_{ig} and T_c intersect is the critical milling time, t_{ig} at which combustion would occur (Fig. 38).

It may also be interpreted that during t_{ig}, intermixing of the particles, particle refinement, and accumulation of lattice defects occurs and these appear to favor the combustion reaction. Further, room temperature aging was found to significantly accelerate the onset of combustion thereby substantially reducing the overall milling time [853].

13.4. Mechanosynthesis of compounds and composites

Apart from the displacement reactions described above to reduce oxides, chlorides and sulfides to pure metals, the MA technique was also used to synthesize compounds and nanocomposites using the mechanochemical reactions. In this category, a variety of borides, carbides [580,885], fluorides, nitrides, oxides, silicides [580], stannides, and composites [880,883,886,887] have been synthesized by ball milling the respective powders for a few hours at room temperature. An important characteristic of such phases produced is that they are nanocrystalline in nature and consequently they exhibit properties and performance much improved over their conventional coarse-grained counterparts. These nanocrystalline oxides can be used for dispersion strengthening the metals to improve the high-temperature mechanical properties. Table 23 summarizes the results available so far.

Composites consisting of a metal oxide as a major phase (ranging from 48 to 73 vol%) and a metal have been synthesized according to the reaction:

$$3/y\ \mathrm{M}_x\mathrm{O}_y + 2\mathrm{Al} \rightarrow \mathrm{Al}_2\mathrm{O}_3 + 3x/y\ \mathrm{M} \tag{27}$$

In some cases, instead of the pure metal, alloys have also been synthesized as in the case of Fe–50at%Cr or Fe–18at%Cr–8at%Ni. The crystallite size of the α-Al_2O_3 phase in all the cases is in the range of 10–20 nm. The great advantage of

Table 23
Synthesis of nanocomposites by mechanochemical synthesis reactions

Reaction	Mill	BPR	Time for reaction (h)	Reference
$2BN + 3Al \rightarrow 2AlN + AlB_2$	Planetary ball mill	4:1	20	[888]
$3CoO + 2Al \rightarrow 3Co + Al_2O_3$	Fritsch P7	42:1	1.5	[883]
$Cr_2O_3 + 2Al \rightarrow 2Cr + Al_2O_3$	Fritsch P7	42:1	1.5	[883]
$CuO + Al \rightarrow Cu + Al_2O_3$	Fritsch P7	40:1	1.5	[883]
$Dy_2O_3 + 4Fe + 3Ca \rightarrow 2DyFe_2$[a] $+ 3CaO$	SPEX 8000		24	[889]
$Fe_3C + Cr \rightarrow Cr_{23}C_6 + (Cr,Fe)_7C_3$	SPEX 8000	8:1	24	[886]
$FeF_3 + C \rightarrow FeF_2 + FeF_3 + (CF)_n$	SPEX 8000	14:1	24	[886]
$2Fe_{2.5}N + 2Al \rightarrow 2AlN + 5Fe(Al)$	SPEX 8000	10:1	24	[886]
$Fe_{2.5}N + Si \rightarrow Si_3N_4 + Fe(Si) + FeSi_2$	SPEX 8000	10:1	24	[886]
$Fe_2O_3 + 2Al \rightarrow Fe(Al) + Al_2O_3$	Fritsch P7	40:1	3	[883]
	SPEX 8000	11:1	24	
$Fe_2O_3 + Cr_2O_3 + 2Al \rightarrow Fe–Cr + 2Al_2O_3$	Fritsch P7	31:1	3	[883]
$Fe_2O_3 + Cr_2O_3 + 3NiO + 3Al \rightarrow Fe–Cr–Ni + 3Al_2O_3$	Fritsch P7	32:1	3	[883]
$3MnO_2 + 2Al \rightarrow 3Mn + 2Al_2O_3$	Fritsch P7	31:1	3	[883]
$MoO_3 + 2Al \rightarrow Mo + Al_2O_3$	SPEX 8000	10:1	24	[883]
$6Nb_2O_5 + 10Al \rightarrow 12Nb + 5Al_2O_3$	Fritsch P7	42:1	1.5	[883]
$3NiO + 2Al \rightarrow 3Ni + Al_2O_3$	Fritsch P7	42:1	1.5	[883]
$2NiO + Si \rightarrow 2Ni + SiO_2$	Planetary ball mill	10:1	43	[890]
$3SiO_2 + 2Al \rightarrow 3Si + 2Al_2O_3$	SPEX 8000	23:1	24	[883]
$3SiO_2 + 4N_2 \rightarrow 2\alpha\text{-}Si_3N_4$[b] $+ 3O_2\uparrow$	Planetary ball mill		623	[891]
$6V_2O_5 + 10Al \rightarrow 12V + 5Al_2O_3$	Fritsch P7	31:1	3	[883]
$WO_3 + 2Al \rightarrow W + Al_2O_3$	SPEX 8000	7:1	24	[883]
$WO_3 + 3Mg + C \rightarrow WC + 3MgO$	Fritsch P6	10:1	48	[596]
$2WO_3 + 3Ti \rightarrow 2W + 3TiO_2$	SPEX 8000	9:1	24	[883]
$3ZnO + 2Al \rightarrow 3Zn + Al_2O_3$	Fritsch P7	42:1	1.5	[883]

[a] Formed after annealing the milled powder for 2 h at 500°C.
[b] Formed after annealing the milled powder for 4 h at 900°C.

producing composites this way is that pure metal oxides or aluminum are not required; one could use recycled aluminum for large-scale production. Metal ores can also be used instead of pure aluminum. This is because, as described above the oxide ores can be reduced to pure metals, as has been shown in the case of Al_2O_3–Fe composite.

The mechanically-driven chemical reduction process (mechanosynthesis) has a number of advantages over the conventional metal processing techniques. It enables the reduction of metal oxides and halides directly to pure metals or alloys without first having to convert the oxides to pure metals and then to the desired alloy. For powder metallurgy applications it allows the direct formation of a powder product without first having to manufacture the bulk alloy and then convert it to powder form. In addition to potential cost savings that may arise from the reduced number of processing steps required, additional benefits accrue because the reactions occur at room temperature. In fact, the trend in recent times has been to use the mechanosynthesis route to produce commercially useful materials at reduced costs. For example, rutile and metallic iron have been produced by ball milling an ilmenite and carbon mixture at room temperature [131,892]. Further, production of nanocomposites consisting of finely dispersed ferromagnetic Fe particles in a non-magnetic matrix such as Al_2O_3 can provide interesting combination of magnetic properties, including the giant magnetoresistance effect.

14. Powder contamination

A major concern in the processing of metal powders by MA is the nature and amount of impurities that get into the powder and contaminate it. The small size of the powder particles, availability of large surface area, and formation of new fresh surfaces during milling all contribute to the contamination of the powder. Thus, it appears as though powder contamination is an inherent drawback of the technique, unless very special precautions are taken to avoid/minimize it.

As mentioned earlier, in the early stages of MA, the metal powder coats the surface of the grinding medium and the inner walls of the container. This was expected to prevent contamination of the powder and so no attention was paid, especially in the early years of MA, to the problem of powder contamination. However, when different results were reported by different groups of researchers on the same alloy system, it was recognized that different levels of contamination could be the reason for the differences. This problem appears to be ubiquitous and is now encountered in many investigations, especially when reactive metals such as titanium and zirconium are milled. The magnitude of contamination appears to depend on the time of milling, the intensity of milling, the atmosphere in which the powder is milled, and difference in the strength/hardness of the powder and the milling medium. Whereas 1–4 wt% Fe has been found to be normally present in most of the powders milled with the steel grinding medium, amounts as large as 20 at% Fe in a W–C mixture milled for 310 h and 33 at% Fe

Table 24
Powder contamination during MA[a]

System	Mill	Milling medium	BPR	Milling time (h)	Contamination (at%)			Reference
					Oxygen	Nitrogen	Iron	
Al	SPEX 8000	Hardened steel	4:1	32	–	–	5	[167]
Al–20Cu–15Fe	Planetary ball mill QM-1SP	Hardened steel	10:1	300	–	–	1.2	[434]
Al–6Ti	Attritor	Steel	–	1300	44.8	8.25	–	[675]
Al–12Ti	Attritor	Steel	–	1300	36.5	–	–	[675]
Al–12Ti	Attritor	Steel	–	400	–	22.6	–	[675]
Al–Ti	Planetary ball mill	Hardened steel	60:1	120	–	–	1.5 and 0.3 Cr	[140]
B	Fritsch P5	SS	10:1	15	–	–	6	[451]
Co–B	Fritsch P5	SS	10:1	–	–	–	2	[451]
Cu	SPEX 8000				–	–	≤ 1	[894]
Cu	Planetary ball mill G5	Tempered steel	–	240	–	–	12.7 w/o, 0.8 w/o Cr	[163]
Cu–40 w/o Fe	Planetary ball mill G5	Tempered steel	–	240	–	–	20.7 w/o, $\leq$2.5 w/o Cr	[163]
$Cu_{44}Nb_{42}Sn_{14}$	Lab ball mill	WC–Co	50:1	24	2.96 w/o	0.47 w/o		[697]
Cu–Ta	Fritsch P5	SS	4:1	30	–	–	4–5 and 1–2 Cr	[96]
Cu–50Zr	SPEX 8000	440C SS	10:1	13	3.3	–	0.25	[705]
CuZr	SPEX 8000	WC 440C SS	10:1	13 (WC vial) (steel vial)	2.3	–	– 4.6	[705]
Ir	SPEX 8000	Hardened steel	4:1	8	–	–	5	[167]
Mo–66.7Si	Planetary ball mill G5	Tempered steel	–	48	–	–	10.5	[64]
Nb–Al	Planetary ball mill	–	–	60	–	–	3	[333]
Nb–92Be	SPEX 8004	WC	7:1	6	5–6			[338]
Nb–25Ge	SPEX 8000	–	–	13	10	–	1.5	[340]
Ni	SPEX 8000				–	–	13	[894]
Ni–25Al	SPEX 8000	–	–	40	–	–	4	[649]
Ni–40Nb	SPEX 8000	52100 steel	3:1	14 (air)	3.4 w/o	0.47 w/o	2.0 w/o	[21]
Ni–40Nb	SPEX 8000	52100 steel	3:1	11 (helium)	0.46 w/o	0.38 w/o	4.11 w/o	[21]
Ni–80.5W				24	–	–	6.4	[359]

(continued on next page)

Table 24 (*continued*)

System	Mill	Milling medium	BPR	Milling time (h)	Contamination (at%)			Reference
					Oxygen	Nitrogen	Iron	
Ni–30Zr	Vibratory ball mill	440C SS	7–81:1	32	–	–	3.7	[753]
Ni–Zr	Fritsch P7	Hardened steel	–	20	–	–	2	[747]
Am–$Ni_{68}Zr_{32}$ + Zr	Fritsch P7	Hardened steel	–	20	–	—	5	[747]
NiZr	Fritsch P5	SS	30:1	10 (nitrogen)	–	–	12	[808]
				100 (argon)			6	
Ru	SPEX 8000	Hardened steel	–	8 (argon)	–	–	3	[617]
				16 (argon)			5	
				32 (argon)			10	
Ru	SPEX 8000	Hardened steel	4:1	8 (methane)	–	–	3	[895]
				16 (methane)			8	
				32 (methane)			22	
Ru–20C	SPEX 8000	Hardened steel	–	8 (argon)	–	–	0.3	[895]
				16 (argon)			1.5	
				32 (argon)			18	
Si	Uni-Ball mill	–	–	300 (nitrogen)	16.63[a]	–	0.95[a]	[896]
Si_3N_4	Planetary ball mill Retsch PM4	WC–Co	–	150	–	–	16.25 w/o of W + Co	[195]
Ta–30Al	Rod mill	SS	36:1	400	–	–	5	[51]
	Ball mill			400			16	
Ti	Vibrational ball mill	SS	45–90:1	(nitrogen)	–	–	8.8 and 3.0 Cr	[604]
Ti–5Al	SPEX 8000	Hardened steel	10:1	30	21	33	–	[606]
Ti–50Al	SPEX 8000	Hardened steel	10:1	70	10	26	–	[606]
Ti–60Al	Fritsch P5	–	10:1	70	3.3 w/o	3.2 w/o	–	[111]
Ti–37.5Si	SPEX 8000	Hardened steel	5:1	24	1.82 w/o	0.66 w/o	–	[784]
V–C	Planetary ball mill	Hardened steel	–	70	–	–	8.6 (high energy) 0.6 (LE mode)	[591]
W	SPEX mill	440C SS	4:1	50	–	–	33	[897]
W–C	Ball mill	Hardened SS	30:1	310	–	–	20	[593]
W–10w/o Cu	Fritsch P5	Steel	–	140–180	–	–	24.9 w/o	[291]
W–25w/o Cu	Fritsch P5	Steel	–	140–180	–	–	24.5 w/o	[291]

W–5Ni	SPEX 8000	Hardened steel	11:1	60	–	–	60	[893]
W–30Ni	SPEX 8000	Hardened steel	11:1	60	–	–	50	[893]
W–40Ni	SPEX 8000	Hardened steel	11:1	60	–	–	40	[893]
Zr	Uni-Ball mill	–	–	50 (ammonia)	–	–	10	[104]
				250 (nitrogen)			1.5	
Zr–30Ni	Fritsch P5	SS	–	35	–	–	9.9	[751]
Zr–70Ni	Fritsch P5	SS	–	120	–	–	13.8	[751]

[a] After MA in nitrogen atmosphere plus annealing for 10 h at 800°C.

in pure W milled for 50 h in a SPEX mill were also reported [593]. In fact, amounts as large as 60 at% Fe were reported during milling of W–5Ni alloy for 60 h in a SPEX mill [893]. These are very high levels of contamination. Similarly, large amounts of oxygen (up to 44.8 at%) [675] and nitrogen (up to 33 at%) have also been reported to be present in Al–6Ti powders milled for 1300 h in a low energy ball mill, and in a Ti–5Al powder milled in SPEX mill for 30 h, respectively [606]. The extent of powder contamination during milling of different types of powder is summarized in Table 24. The type of mill, the BPR, and the milling time employed are also listed. The major impurities listed are oxygen and nitrogen, mainly from the atmosphere and/or PCAs used, and iron from the steel grinding medium and the steel container. The levels of chromium and other impurities are also listed in some cases.

Contamination of metal powders can be traced to (i) chemical purity of the starting powders, (ii) milling atmosphere, (iii) milling equipment (vial and grinding medium), and (iv) the process control agents added to the powders. Contamination from source (i) can be either substitutional or interstitial in nature, while contamination from source (ii) is essentially interstitial in nature and that from (iii) is mainly substitutional, even though carbon from the steel milling equipment can be an interstitial impurity. Contamination from the PCA leads to interstitial contamination. The presence of interstitial impurities such as oxygen and nitrogen is deleterious to reactive metals like titanium and zirconium and therefore maximum impurity levels are generally specified for acceptable microstructural and mechanical properties. Substantial amounts of nitrogen and oxygen (the amount of nitrogen is much more than oxygen) are picked up during the milling of titanium and zirconium alloys and the presence of these impurities led to a change in the constitution of the alloys [444,898,899]. For example, the formation of an amorphous phase in Ti–Al alloys and a crystalline phase with a face-centered cubic (fcc) structure in powders milled beyond the formation of an amorphous phase have been attributed to the presence of large quantities of nitrogen in these alloys [58].

During MA the powder particles get trapped between the grinding medium and undergo severe plastic deformation; fresh surfaces are created due to the fracture of the powder particles. Additionally, collisions occur between the grinding medium and the vial, and also amongst the grinding balls. All these effects cause wear and tear of the grinding medium and the vial resulting in the incorporation of these impurities into the powder. The extent of contamination increases with increasing milling energy and also use of higher BPR, higher speed of milling, etc.

Several attempts have been made in recent years to minimize the powder contamination during MA. One way of minimizing the contamination from the grinding medium and the container is to use the same material for the container and grinding medium as the powder being milled. Thus, one could use copper balls and copper container for milling copper and copper alloy powders. In this case also there will be wear and tear of the grinding medium and this gets incorporated into the powder. Thus, even though there is no contamination, the

chemistry of the final powder will be different from the starting powder; the metallic content in the final powder (from the container and balls) would be higher than in the initial powder. This can be compensated for if one has a knowledge of the extent of increase of the metallic content in the final powder.

The above solution may be possible in some cases; but it is difficult in many cases due to the non-availability of the special grinding medium and containers. The problem is becoming more and more complex since the technique of MA is now being applied to a variety of materials such as metals, alloys, ceramics, polymers, and composites and it is almost impossible to get containers and grinding media of all these different types of materials. If a container of the same material to be milled is not available, then a thin adherent coating on the internal surface of the container (and also on the surface of the grinding medium) with the material to be milled will minimize the contamination. Thus, it has been shown that the extent of iron contamination during milling of Ta–Al alloy powders is less in the second run and much less in the third run [51]. The idea here is to mill the powder once allowing the powder to be coated onto the grinding medium and the inner walls of the container. This powder is then discarded and a fresh batch of powder is milled. If this operation is continued for a few times, then contamination due to the grinding medium and the vessel is likely to be minimum, provided that the powder does not cake up at the bottom of the vial and get peeled off.

In general, a simple rule that should be followed to minimize contamination from the container and grinding medium is that the container and grinding medium should be harder/stronger than the powder being milled. Thus, the reason for a high amount of iron contamination during milling of tungsten and tungsten alloy powders is that a steel container and steel milling medium, which are much softer than tungsten, were used [893]. But, a disadvantage of using very hard grinding medium such as tungsten carbide during milling of very soft powders is that the tungsten carbide (or other hard grinding media such as Al_2O_3) can get incorporated into the powder and thus contaminate it. In fact, the amount incorporated into the powder can be so much that clear diffraction peaks from the contaminant could be observed in the X-ray diffraction patterns of the milled powder [753].

The problem of milling atmosphere is serious and has been found to be the major cause of contamination in many cases. (This contamination, which is unwanted, should be distinguished from intentional milling of powder in reactive atmospheres to synthesize nitrides, carbides, oxides, etc.) In fact, it has been observed that if the container is not properly sealed, the atmosphere surrounding the container, usually air (containing essentially nitrogen and oxygen), leaks into the container and contaminates the powder. Thus, when reactive metals like titanium and zirconium are milled in improperly sealed containers, the powders are contaminated with nitrogen and oxygen. In most cases, the nitrogen pick up has been found to be much more than that of oxygen. The formation of a cubic phase at long times of milling titanium alloys has been attributed to the formation of titanium nitride having a cubic structure [58]. It has been reported that flushing

Table 25
Oxygen and nitrogen contents of Ti–24Al–11Nb powders milled for 24 h in a SPEX mill with a BPR of 4:1 and using two different types of atmosphere. No PCA was used during milling

Powder	Oxygen content (wt%)		Nitrogen content (wt%)	
	AT1	AT2	AT1	AT2
Prealloyed Ti–24Al–11Nb (at%)	3.6	0.10	6.8	0.015
Blended elemental Ti–24Al–11Nb (at%)	4.8	0.48	7.6	0.035

with argon gas will not remove oxygen and nitrogen absorbed on the internal surfaces. Pick-up of impurities during milling would reduce the pressure within the container allowing the outside atmosphere to continuously leak into the container through an ineffective seal. In practice, it has been noted that if it is difficult to open the container lid, due to the vacuum present inside, it is an indication that contamination of the powder is minimum. Use of vacuum or an inert gas is desirable to prevent or minimize the powder contamination. It has been reported that a teflon seal could be used to prevent air from leaking from outside into the container [900].

Attempts have been made to improve the container seal integrity to prevent the outside atmosphere from leaking inside. Goodwin and Ward-Close [901] used two different types of milling atmosphere and compared the powder contamination levels during milling of both prealloyed and blended elemental powders. In the first atmosphere, referred to as AT1, the steel vial was loaded in a glove box containing research grade argon (99.995% pure) and the vial was sealed using an "O" ring of circular cross section. In the second atmosphere, AT2, higher purity argon (guaranteed 99.998%), which is subsequently passed through moisture and oxygen filter towers to further purify it, was used and the gasket used to obtain a more leak-tight seal was a flat neoprene gasket. The contamination levels obtained using these two types of atmosphere are listed in Table 25. It has been shown that by careful control of the purity of the atmosphere and improvements of the seal quality, the interstitial contaminants in the titanium alloy could be reduced to as

Table 26
Chemical analysis of the γ-Ti–48Al–2W (at%) prealloyed powder milled in different atmospheres for a total of 20 h in a SPEX mill with a BPR of 10:1

Atmosphere	Maximum expected value (wt%)		Measured values (wt%)	
	Oxygen	Nitrogen	Oxygen	Nitrogen
Starting powder	–	–	0.093	< 0.001
Air	0.69	1.97	2.08	4.66
Oxygen	2.99	–	1.49	0.63
Nitrogen	–	2.61	4.72	9.87
Argon	–	–	0.80	1.52

low as 100 ppm of oxygen and 15 ppm of nitrogen [899]. With additional control of the atmosphere this could be reduced even further. This process, however, may not be economically viable and hence may not be feasible on an industrial scale.

The contamination levels obtained by milling the γ-Ti–48Al–2W (at%) prealloyed powder in different atmospheres were evaluated [902]. This was done by loading the powder in the particular atmosphere, milling it for 4 h, opening the lid and resealing the container lid in the appropriate atmosphere. This was done repeatedly to achieve a total milling time of 20 h. From a knowledge of the vial volume, the maximum expected amount of pick up of nitrogen and oxygen from pure oxygen, nitrogen, or air atmospheres were calculated to be 2.99 wt% oxygen, 2.69 wt% nitrogen, and 0.69 wt% oxygen and 1.97 wt% nitrogen, respectively. These values should be compared with the actual values observed, which are listed in Table 26. It is to be noted that the amount of nitrogen is very high when the powder is milled either in a pure nitrogen or air atmosphere. As expected, the nitrogen content in the powder is very low when it is milled in an oxygen atmosphere. But, it is most surprising that the oxygen content in the powder is higher when milled both in air or nitrogen atmosphere than when milled in a ''pure'' oxygen atmosphere. This result can only be rationalized by assuming that air was continuously entering the vial during milling due to an improper seal. During milling the powder reacts with nitrogen and oxygen inside the vial and creates a vacuum. The more oxygen and nitrogen in the initial atmosphere, the greater the vacuum in the vial. Air is then drawn from outside at a rate dictated by the magnitude of the pressure difference across the seal and also the integrity of the vial seal.

The contamination from the process control agents (PCAs) is perhaps the most ubiquitous. Since most of the PCAs used are organic compounds, which have low melting and boiling points, they decompose during milling due to the heat

Table 27
Chemical analysis (wt%) of prealloyed Ti–48Al–2W (at%) powder milled for 24 h in a SPEX mill using different PCAs

Condition	PCA	Chemical composition (wt%)			
		Iron	Carbon	Oxygen	Nitrogen
Gas atomized	–	0.08	0.02	0.084	0.006
Milled	None	1.04	0.08	1.81	5.09
	Seasoned[a]	0.46	0.03	1.60	4.82
Milled	Stearic acid	0.78	0.78	1.79	4.82
	Seasoned	0.43	0.85	1.74	4.06
Milled	Boric acid	0.44	0.08	1.28	0.41
	Seasoned	0.06	0.03	1.32	0.71
Milled	Borax	0.26	0.02	1.35	1.20
	Seasoned	0.09	0.03	1.46	1.47

[a] ''Seasoned'' means that the powder coated the grinding medium during the first run.

generated. The decomposition products consisting of carbon, oxygen, and hydrogen react with the metal atoms and form undesirable carbides, oxides, nitrides, etc. For example, use of Nopcowax 22-DS during milling of aluminum powder in a SPEX mill has resulted in the formation of oxide and carbide dispersoids [903]. Formation of carbide and hydride phases was reported during the milling of Ti–Al powders using hexane as a PCA [141]. Formation of Fe_3O_4 and Fe_3C contaminants was reported during milling of Cu–Fe powders with ethanol as a PCA [163]. Similarly other PCAs can introduce different types and amounts of impurities into the milled material. Mishurda et al. [904] studied the effect of several PCAs on Fe and interstitial contamination during milling of prealloyed T–48Al–2W (at%) powder in a SPEX mill. The results of the contamination, summarized in Table 27, show that boric acid and borax were quite effective in reducing the iron contamination from 1.04 wt% (when no PCA was used) to 0.44 wt% and 0.26 wt%, respectively. Using a vial that was "seasoned" twice ("seasoning" here means that the powder was milled in the container using a particular grinding medium, during which time the powder coats the grinding medium. This powder is subsequently discarded and the same set of vial and grinding medium is again used) resulted in even lower values of iron contamination — 0.06 wt% with boric acid and 0.09 wt% with borax. Similarly, it was shown [163] that milling of Fe–Cu alloy powders without any PCA introduced considerable contamination from the steel milling tools. This reached as much as 20.7 wt% Fe and 2.5 wt% Cr for a Cu–40 wt% Fe composition. But, when powder of the same composition was milled under identical conditions, but with ethanol as a PCA, the contamination was found to be much less — 2.9 wt% Fe and <0.1 wt% Cr. This has been explained on the basis of the decreased cold welding between the milled powder and the balls and walls. Thus, a proper choice of PCA can substantially reduce the powder contamination. Of course, the best situation would be not to use PCA at all, if it could be avoided.

It is also important to remember that cross contamination could occur if a container that was used earlier to mill some powder is used again to mill another powder without properly cleaning it.

The level of contamination may be different under different processing conditions and is dependent on the type of mill, intensity of milling, nature of the powder, nature of the grinding medium and container, ambient atmosphere, ball-to-powder weight ratio, seal integrity, and others. Claims have been made in the literature about the superiority of certain mills and practices over others. But, systematic investigations on milling the same powder and under identical conditions in different mills and evaluating the contamination levels have not been undertaken; and this appears to be an important aspect to produce clean powders.

15. Modeling studies and milling maps

From the description of the process it is easy to realize that MA is a process involving a number of both independent and interdependent variables. Like in any

other process, modeling of MA is also carried out to identify the salient factors affecting the process and establish process control instrumentation. By modeling the process effectively, it is possible to bring down the number of actual experiments to be conducted to optimize the process and achieve a particular application. A highly successful model would also be able to predict the outcome of the process. In MA, for example, if one can predict the nature of the phase produced under a given set of conditions, it would be considered a very successful model.

15.1. Modeling studies

Mechanical alloying is a stochastic process and the number of variables involved in the process is very large. For a particular alloy system the variables include the type of mill, intensity of milling (velocity of the grinding medium, frequency of impacts, energy transfer efficiency, etc.), type of milling media, ball-to-powder weight ratio, the atmosphere under which the powder is milled, purity of the powders, milling time, milling temperature, and nature and amount of the PCA used. All these have a significant effect on the constitution of the powder. Even on a local scale, the nature of impacts between two balls, the frequency of impacts, and the amount of powder trapped between two balls during a collision could vary from point to point. Thus, modeling the MA process is a difficult task. In spite of this some attempts have been made in recent times and moderate success has been achieved in modeling the physics and mechanics of the process. From the actual experiments conducted, attempts have also been made to correlate the phases formed with the process parameters during milling and milling maps have been constructed. But, we are far from a situation where we can predict the final chemical constitution of the powder (type and description of phases formed).

Modeling of the MA process has been conducted by several groups in recent years. The very first attempt at estimating the time required for alloying to occur was modeled by Benjamin and Volin [185]. They suggested that the rate of structural refinement was dependent upon the rate of mechanical energy input to the process and the work hardening rate of the material being processed. They also concluded that the specific times to develop a given structure in any system would be a function of the initial particle size and characteristics of the ingredients as well as the particular apparatus and operating parameters. Subsequently, more rigorous modeling was done. The most important groups who conducted very detailed modeling studies are those led by Courtney [24,905,906], Gaffet [907], Magini [908], Koch [181], and Watanabe [909]. A few others have also attempted the modeling [910–913].

Modeling of the MA process has been broadly classified into two categories: local and global modeling. A typical collision involving powder trapped between two grinding media is considered in the "local" modeling. The type of machine, the impact velocity and frequency are considered constant and the ball-to-powder weight ratio (BPR) and the mechanical characteristics of the powder are also

specified before hand. With these constraints, one calculates (a) the deformation the particle experiences, (b) the change in powder particle shape, (c) the probability of a particle coalescing, and (d) the probability of a particle fracturing. In "global" modeling, one seeks to specify the frequency of *effective* media impacts by considering the collision velocities, frequencies, and powder coating thickness. Aikin and Courtney [914,915] subsequently developed a phenomenological description of the process based on the kinetic principles. Using these models, the authors were able to estimate the plastic strain and strain rate, local temperature rise due to a collision, particle hardness due to work hardening, the lamellar thickness, and the impact frequency and velocity. In fact, in a recent publication Maurice and Courtney [916] compared the alloying behavior in the SPEX mill and the attritor and identified some of the commonalities and differences between the two devices. While the lamellar thickness of the component metals and the hardness are almost the same in both the milling devices, the time required for completion of the process was estimated as 15 minutes in the SPEX mill and 11,000 minutes in the attritor. The composite particle diameter was also calculated to be 52 μm in the SPEX mill while it was 910 μm in the attritor. They showed that these differences arise because of the differences in the average impact velocity (0.5 m/s in the attritor and 4 m/s in the SPEX mill) and the average impact frequency (0.88/s in the attritor and 7/s in the SPEX mill). Although it has been long known that the SPEX mill is much more energetic than the attritor, this provides a more quantitative comparison. Similarly Abdellaoui and Gaffet [917] calculated the velocity of the ball, kinetic energy per impact, shock frequency and power for different types of mills and these results are presented in Table 28. The topic of modeling has been well discussed in two recent reviews [8,9] and so this will not be further discussed here.

It is important to realize that these models cannot provide information on all the aspects of the process. As Courtney and Maurice [918] succinctly put it "It is important to appreciate what can be expected of even the most successful efforts of this kind. 'Absolute' predictions are unlikely; this is exacerbated in the case of MA by its inherently stochastic nature. In addition, models require input 'data'; material properties (often not known to precision, particularly at the high strain levels to which powder is often subjected during MA) and process characteristics (collision frequency and velocity, also seldom known a priori). Thus, realistic goals of process modeling are to correctly predict general trends, and perhaps even to predict resulting properties/dimensions within an order of magnitude. The benefits of successful models lie not in their abilities to predict outcomes, but in that they help identify critical process and material variables, and reduce the amount of testing needed for process optimization".

15.2. Milling maps

The above modeling studies have not been able to take into account the type of phase formed under different milling conditions. The ability to be able to predict the nature of the phase formed is a great advantage in designing the

Table 28
Kinetic energy, shock frequency, and shock power for different types of mills

Parameter	Attritor	Vibratory mills		Planetary ball mills			Horizontal rod mill
		Pulverisette "O"	SPEX mill	Pulverisette P5	Pulverisette G7	Pulverisette G5	
Velocity of the ball (m/s)	0-0.8	0.14–0.24	< 3.9	2.5–4.0	0.24–6.58	0.28–11.24	0–1.25
Kinetic energy (10^{-3} J/hit)	< 10	3–30	< 120	10–400	0.4–303.2	0.53–884	0–190
Shock frequency (Hz)	> 1000	15–50	200	~100	5.0-92.4 (5 balls)	4.5–90.7 (5 balls)	0–2.4 (1 rod)
Power (W/g/ball or rod)	< 0.001	0.005–0.14	< 0.24	0.01–0.8	0–0.56	0–1.604	0–0.1

microstructure and constitution of the alloy. Some investigations have been carried out with this objective in view. In all these investigations, the energy (or other parameter) calculations are always compared with the experimentally obtained phase constitution and conclusions are arrived at.

Abdellaoui and Gaffet [917,919] studied the amorphization behavior of $Ni_{10}Zr_7$ in different types of mills and also evaluated the shock power that is transmitted to the powder. Based on a mathematical treatment of the process taking place, they calculated the shock frequency and the shock power. Irrespective of the device used to accomplish the milling process, it was shown that the injected shock power is the unique physical parameter governing the phase transformation. For the prealloyed $Ni_{10}Zr_7$ intermetallic compound, a homogeneous amorphous phase was obtained only when the injected shockpower was in the range of 0.4–0.8 W/g. At power values <0.4 or >0.8 W/g, a mixture of amorphous and crystalline phases was obtained (Fig. 39).

Since the phase transformations in mechanically alloyed powders occur due to the energy transferred from the milling media to the powder, it would be useful to calculate the energy transferred. This, of course, will depend on the type of mill and the operating parameters. It was shown that the energy dissipated per hit during milling increases with increasing rotation speed and also with increasing size of the grinding ball [908]. These calculations assumed that the collisions are perfectly inelastic. But, it was shown through video recordings that the movements of the balls are rather different from the expected ones and that one should

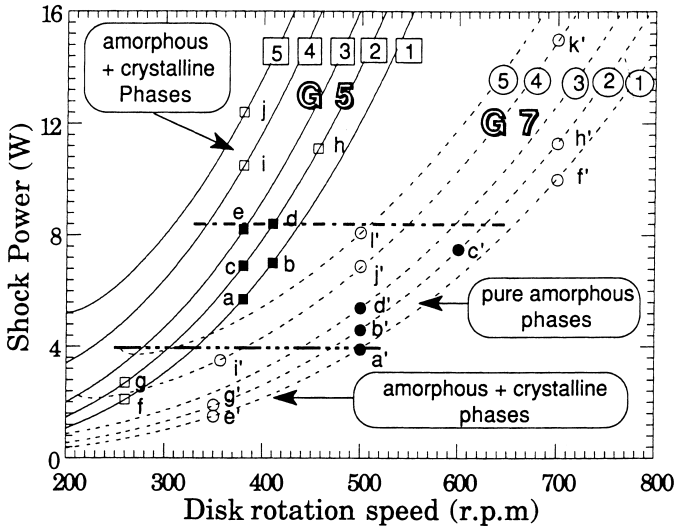

Fig. 39. Injected shock power as a function of the disk and vial rotation speeds for the G5 (———) and G7 (- - - -) planetary ball mills. The vial rotation speed values (in rpm) are referred by the numbers 1–5 written near each corresponding curve: 1 = 150, 2 = 250, 3 = 350, 4 = 500, and 5 = 600 rpm.

consider a "slip factor" that takes into account the sliding phenomena between balls and the container wall [920]. The energy released by one ball as a function of the specific power (power per unit weight of the powder) was calculated. By comparing these calculations with the experimentally determined phase constitution, a critical energy was identified below which the phase formed is amorphous and above that it is an intermetallic. This has been shown to be true in the case of the Fe–Zr system [520] and also in the Pd–Si system [908]. A similar calculation for the case of a SPEX mill is difficult because the mill is subjected to impulses in three directions. Since the vibration frequency is fixed for the SPEX mill, the situation can be compared to that in a planetary ball mill at fixed rotation speed. A diagram featuring the phase constitution in the Pd–Si system is shown in Fig. 40. It may be noted that the amorphous phase forms below a critical energy and above this value the intermetallic forms.

A milling map describing the phases present in a Ti–33 at% Al powder mix at different milling times and for different BPR values is shown in Fig. 41 [121]. It was shown that the time required for the formation of a particular phase was

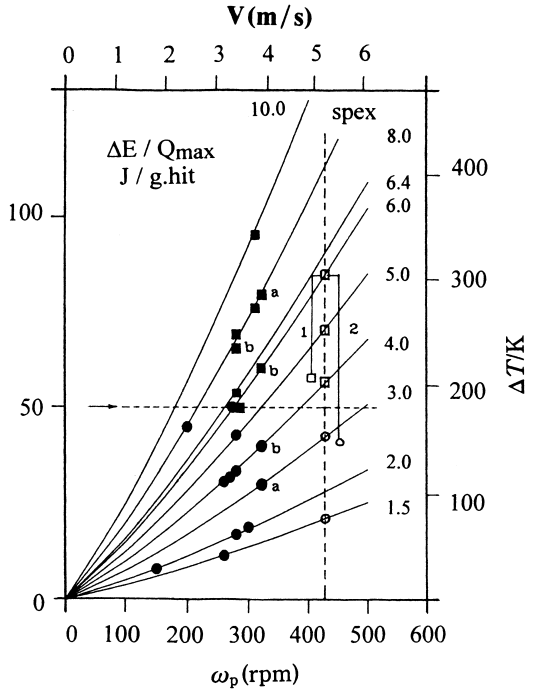

Fig. 40. Energy transferred per hit and per unit mass for the Pd–Si system as a function of the rotation speed of the planetary ball mill for different ball diameters (given in mm near each curve). The filled symbols represent experiments carried out in the planetary ball mill and the open symbols for the SPEX mill. The horizontal broken line refers to the critical energy above which an intermetallic forms and below which an amorphous phase forms. The experiments have been carried out with a Pd–20at%Si composition except in (a) Pd–13.5at%Si and (b) Pd–17at%Si.

shorter at higher BPR since the higher BPR value translates to higher mechanical energy input per unit mass of the powder. At a constant BPR, the sequence of phase formation can be determined as a function of milling time. Similarly, at a constant milling time, the phases occurring with increasing BPR can be identified. Thus, this map is somewhat similar to a phase diagram, except that the milling map is for a particular alloy composition while the phase diagram is for the whole alloy system. It has been reported earlier that increased speed of milling [217,520] or very high BPR [672] generate more heat and lead to the formation of crystalline phases either by crystallization of the amorphous phase or by other mechanisms. Thus, the *Y*-axis on the milling map may be equated to "temperature" and so the milling map can be considered as a constant composition section of a ternary phase diagram where the three axes are milling time, composition, and BPR (temperature). These milling maps should be very useful in quickly identifying the phases present at any milling time for a specific BPR and in defining the final phases produced by the MA process.

16. Applications of mechanical alloying

The technique of MA has been shown to produce a variety of materials. The most important reason for the invention and development of the MA process was the production of oxide dispersion strengthened (ODS) materials in which fine particles of Y_2O_3 or ThO_2 were uniformly dispersed in a nickel- or iron-based

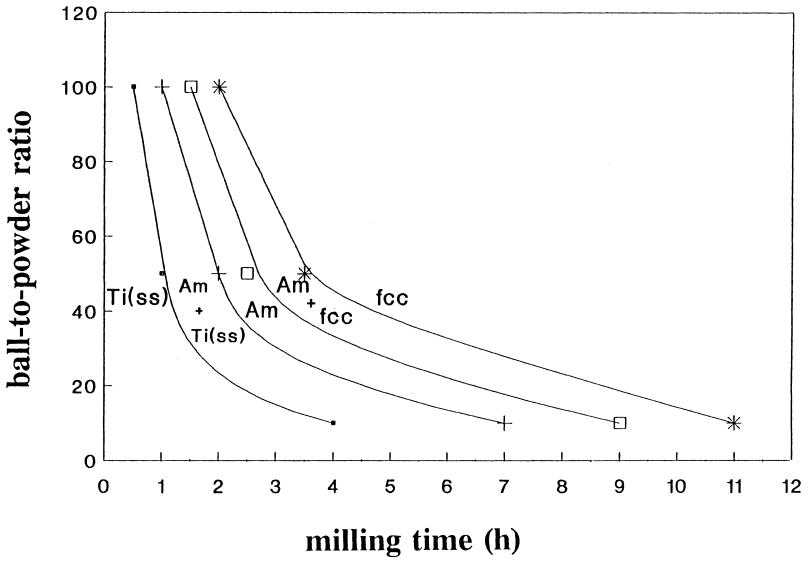

Fig. 41. Milling map for a Ti–33at%Al powder relating the ball-to-powder ratio (BPR) and milling time to the phases present.

superalloy. In the mid-1980s, it was realized that MA was also capable of producing true alloys from elements that are not either easy to form by conventional means or sometimes even impossible to prepare, e.g., elements which are immiscible under equilibrium conditions. Investigations have revealed that metastable phases such as supersaturated solid solutions, non-equilibrium crystalline or quasicrystalline intermediate phases and amorphous alloys can be synthesized by MA [5–9]. In addition, nanostructures with a grain size of a few nanometers, typically <100 nm, are produced. These metastable phases have interesting combinations of physical, chemical, mechanical, and magnetic properties and are being widely explored for potential applications. It will be impossible to go into details of each and every one of these developments and so only a very brief survey of the ODS alloys will be presented here. The two production facilities of Inco Alloys International have a combined capacity approaching 300,000 kg. The yield of the final product varies greatly with the product form and size, but the final wrought capacity is over 200,000 kg.

Mechanically alloyed materials (including those synthesized by mechanochemistry and mechanical activation of solids) find applications in a variety of industries. The applications include synthesis and processing of advanced materials (magnetic materials, superconductors, functional ceramics), intermetallics, nanocomposites, catalysts, hydrogen storage materials, food heaters, gas absorbers, and also in the modification of solubility of organic compounds, waste management, and production of fertilizers. But, the major industrial applications of mechanically alloyed materials have been in the areas of thermal processing, glass processing, energy production, aerospace, and other industries. These applications are based on the oxide-dispersion strengthening effect achieved in mechanically alloyed nickel-, iron-, or aluminum-based alloys. These will be briefly described now.

Mechanically alloyed ODS materials are strong both at room and elevated temperatures (Table 29). The elevated temperature strength of these materials is derived from more than one mechanism. First, the uniform dispersion (with a

Table 29
Room temperature and elevated temperature mechanical properties of commercial ODS nickel- and iron-base superalloys (see Tables 30 and 31 for the chemical compositions of the alloys)

Alloy	Test temperature (°C (°F))	0.2% YS (MPa)	UTS (MPa)	%El.	%R.A.
MA 6000	Room temperature	1220	1253	7.2	6.5
	871 (1600)	675	701	2.2	4.6
	982 (1800)	445	460	2.8	1.9
MA 754	Room temperature	586	965	21	33
	871 (1600)	214	248	31	58
	982 (1800)	169	190	18	34
MA 956	Room temperature	517	655	20	35
	1000 (1832)	97	100	–	–
	1100 (2192)	69	72	12	30

spacing of the order of 100 nm) of very fine (5–50 nm) oxide particles (commonly used are Y_2O_3 (yttria), ThO_2 (thoria), and La_2O_3 (lanthana)), which are stable at high temperatures, inhibit dislocation motion in the metal matrix and increase the resistance of the alloy to creep deformation. Another function of the dispersoid particles is to inhibit the recovery and recrystallization processes, because of which a very stable large grain size is obtained; these large grains resist grain rotation during high temperature deformation. A stable large grain size can also be obtained by secondary recrystallization mechanisms. Secondly, the very homogeneous distribution of alloying elements during MA gives both the solid-solution strengthened and precipitation-hardened alloys more stability at elevated temperatures and overall improvement in properties. Mechanically alloyed materials also have excellent oxidation and hot corrosion resistance. The increased resistance to oxidation–sulfidation attack is due to the homogeneous distribution of the alloying elements and the improved scale adherence due to the dispersoid itself [921,922]. Elliott and Hack [923] have presented an overview of the use of mechanically alloyed products for aerospace applications and deBarbadillo and Smith [924] have described the unique challenges to manufacture and use posed by ODS alloys. A very recent survey of the applications of mechanically alloyed products can be found in Refs. [76,925]. The different brochures produced by INCO should also be consulted for recent developments and applications of mechanically alloyed products.

16.1. Nickel-base alloys

Typical compositions of the commercially available mechanically alloyed nickel-base superalloys are presented in Table 30. The most significant advantage of oxide-dispersion strengthened superalloys is the increased stress rupture properties. Fig. 42 compares the specific rupture strength (strength/density) for a 1000-h life as a function of temperature for several nickel-base superalloys used for turbine blade applications. Mar-M200 is a nickel-base alloy containing by weight percent 9.0Cr, 5.0Al, 2.0Ti, 12.0W, 10.0Co, 1.0Nb, and 1.8Hf, while PWA454 is a nickel-base alloy containing 10.0Cr, 5.0Al, 1.5Ti, 12.0Ta, 4.0W, and 5.0Co, and TD Ni

Table 30
Nominal compositions (wt%) of mechanically alloyed nickel-base superalloys

Alloy	Ni	Cr	Al	Ti	Mo	W	Y_2O_3	Ta
INCONEL alloy MA 754	Bal.	20	0.3	0.5	–	–	0.6	–
INCONEL alloy MA 757	Bal.	16	4.0	0.5	–	–	0.6	–
INCONEL alloy MA 758	Bal.	30	0.3	0.5	–	–	0.6	–
INCONEL alloy MA 760	Bal.	20	6.0	–	2.0	3.5	0.95	–
INCONEL alloy MA 6000	Bal.	15	4.5	0.5	2.0	4.0	1.1	2.0
TMO-2[a]	Bal.	6	4.2	0.8	2.0	12.4	1.1	4.7

[a] This alloy additionally contains 9.7 wt% cobalt.

is nickel containing 2.0 wt% ThO_2. It is clear from this figure that the MA 6000 alloy can maintain a given stress for a much longer time than a conventional alloy for similar vane applications. This is mainly due to the benefits of the combined strengthening modes in the mechanically alloyed material.

The mechanically alloyed nickel-base superalloys are considered mainly for three groups of applications — gas turbine vanes, turbine blades, and sheets for use in oxidizing/corrosive atmospheres. The largest use of MA 754 is as vanes and bands for aircraft gas turbine engines (Fig. 43). For applications requiring good resistance to thermal fatigue, such as gas turbine vanes, Inconel MA 754 is given a strong texture. The majority of the grains are aligned so that their ⟨100⟩ axes are parallel to the principal working direction and along the length of the bar. Such texture results in low modulus of elasticity (149 GPa) in the longitudinal direction. The low modulus improves resistance to thermal fatigue by lowering stresses for given thermal strains. Components are fabricated from bar stock using state-of-the-art machining and brazing processes typical for conventional wrought superlloys. Alloy MA 758 is used in a number of industrial applications where its high chromium content makes it resistant to extremes of temperature and

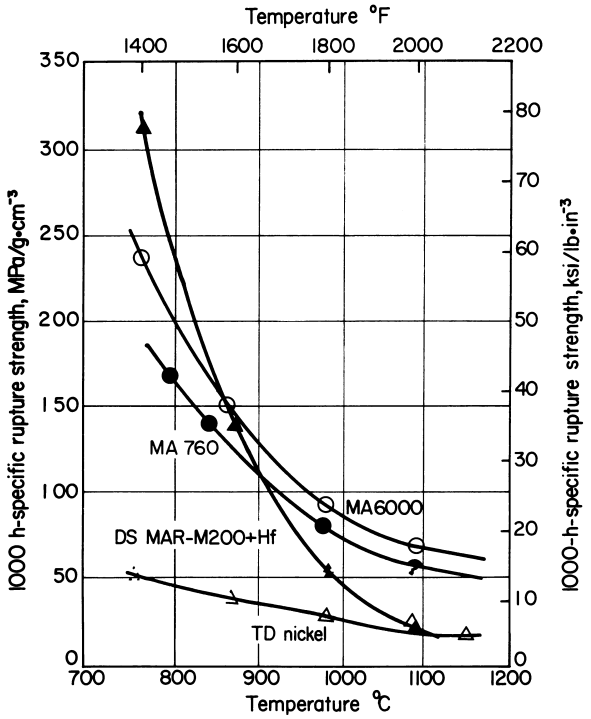

Fig. 42. Comparison of 1000-h specific rupture strength of INCONEL MA6000 with dispersion strengthened Mar-M200 + Hf, TD Ni, and single crystal PWA 454. Courtesy of Inco Alloys International.

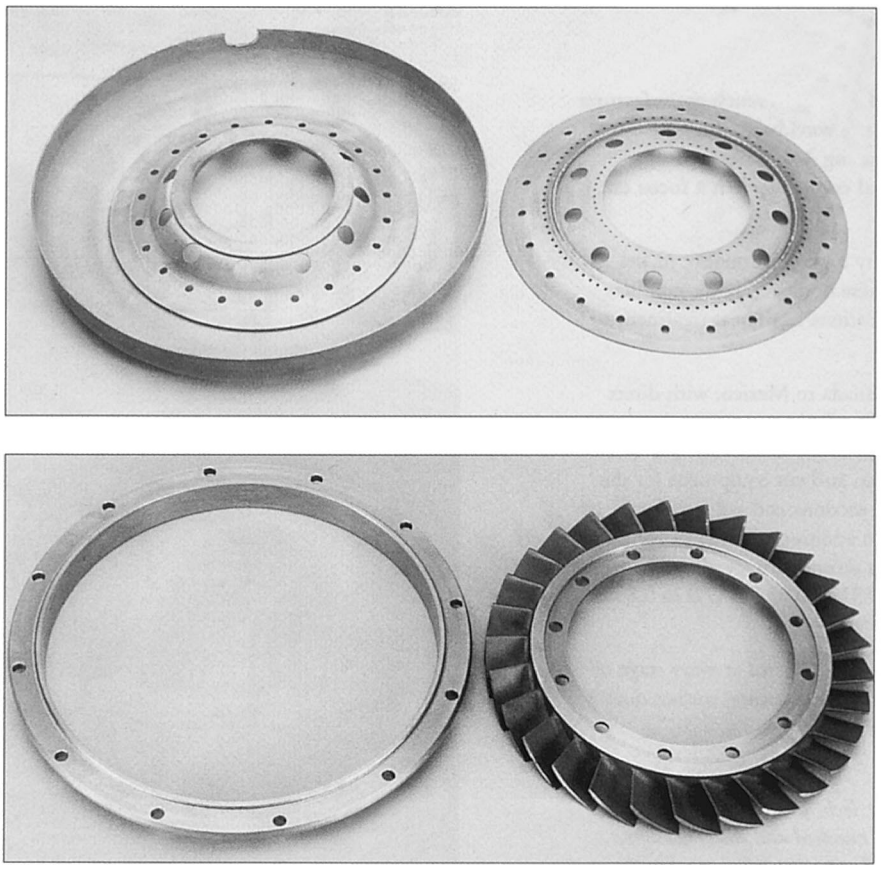

Fig. 43. Some typical gas turbine engine components made of INCONEL alloy MA 754. Courtesy of Inco Alloys International.

environment. The alloy is used in glass industry for high temperature components requiring both elevated temperature strength and resistance to extremely corrosive molten glass. Alloy MA 758 is also used for internal combustion engine components, mainly in critical fuel injection parts. One novel industrial application of alloy MA 754 is a high-temperature atmosphere-circulation fan in a "floating" furnace design being commercialized in Japan. Large rounds are used

Table 31
Nominal compositions (wt%) of mechanically alloyed iron-base superalloys

Alloy	Fe	Cr	Al	Ti	Mo	Y_2O_3
INCOLOY alloy MA 956	Bal.	20	4.5	0.5	–	0.5
INCOLOY alloy MA 957	Bal.	14	–	1.0	0.3	0.25

for the hub and plate material is used for blades of the fan, which operates at temperatures over 1100°C.

New product forms of the commercial alloys continue to be developed. Large diameter, thin wall tubing of alloy MA 754 has been produced and evaluated for radiant tube applications, and alloy MA 758 has been used as tubing in heat exchangers and process equipment operating at very high temperatures.

The alloy MA 754 is used for brazed nozzle guide vane and band assemblies in US military aero engines. The principal advantages of the alloy for these applications are thermal fatigue resistance, long-term creep strength and high melting point.

The MA 6000 alloy is a more complex alloy developed as a blade material for advanced gas turbines. It is used for first and second stage turbine vanes and blades machined form solid bar. Unlike cast alloys, MA 6000 exhibits nearly flat rupture-life curves at high temperatures due to the combination of oxide dispersion strengthening and high grain-to-width ratios (typically >10 to 1). Because of its composition, MA 6000 has excellent resistance to oxidation and sulfidation. The characteristics of this alloy allow blade cooling to be reduced or eliminated as the metal temperature can be increased by 100°C or more in engines where the stresses are medium or low.

16.2. Iron-base alloys

Table 31 lists the chemical compositions of mechanically alloyed iron-base superalloys. These alloys combine the high-temperature strength and stability of oxide dispersion strengthening with excellent resistance to oxidation, carburization, and hot corrosion. These alloys are suitable for use in gas turbine combustion chambers. Incoloy alloy MA 956 is particularly well suited for use in heat processing applications. For example, vacuum furnace fixtures made of MA 956 have shown excellent durability and are able to compete with wrought molybdenum, which is also used in these applications. In comparison to molybdenum, MA 956 is about 30% lower in density, providing weight savings and cost advantages. Further, since MA 956 has a lower vapor pressure than molybdenum, it will not coat the inside of the vacuum chamber or the parts being heat treated. Thus, MA 956 rods, flats, and sheets are used in numerous atmosphere and vacuum furnace applications including muffles, baskets, trays, and thermowells. Alloy MA 956 in tubing form has also been used for high

Table 32
Nominal compositions (wt%) of mechanically alloyed dispersion-strengthened aluminum-base alloys

Alloy	Al	Mg	Li	C	O
IncoMAP alloy AL-9021	Bal.	1.5	–	1.1	0.8
IncoMAP alloy AL-9052	Bal.	4.0	–	1.1	0.6
IncoMAP alloy AL-905XL	Bal.	4.0	1.3	1.1	0.6

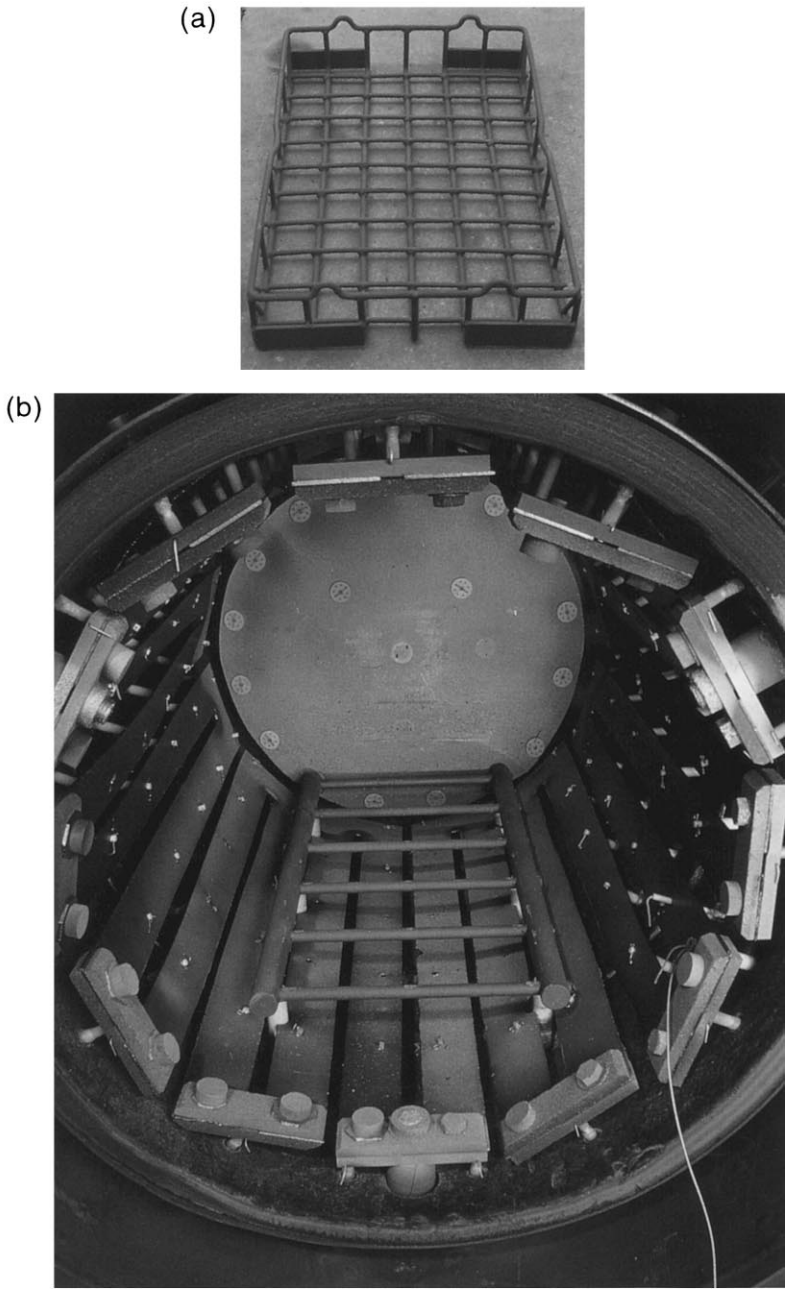

Fig. 44. (a) Furnace baskets made of INCOLOY alloy MA 956 operating in air at temperatures above 1200°C. (b) Removable hearth of vacuum heat treating furnace fabricated from 1.0 and 0.5″ dia rods of INCOLOY alloy MA 956. The hearth legs are encased in alumina sleeves to prevent direct contact with the graphite heating elements. Courtesy of Inco Alloys International.

temperature, severe service applications such as coke injection lance pipes in steel making. The alloy MA 956 is also being used in glass processing industry because of its resistance to attack by molten glass. Because of this corrosion resistance, the alloy is being evaluated for applications such as firing-kiln rollers, muffle tubes, and furnace racks. Other applications include molten-glass resistance heaters, thermocouple protection tubes, glass-processing components used in nuclear waste disposal and the bushings used to make single and multi-strand fibers.

More recently, MA 957 has been evaluated for use as the fuel cladding in fast neutron, breeder reactors. Conventional austenitic alloys are unsuitable for this application due to the dimensional swelling phenomenon caused by the high neutron fluxes. The mechanically alloyed materials are also being evaluated for heat exchanger components in high-temperature gas-cooled reactors. Fig. 44 shows some typical high-temperature applications of the alloy MA 956.

16.3. Aluminum-base alloys

The success of mechanically alloyed superalloys led to the development of dispersion-strengthened aluminum alloys. Table 32 lists the compositions of the mechanically alloyed dispersion-strengthened aluminum alloys. Since an aluminum oxide layer is always present either on the surface of the powder particles at the start of processing or during milling, its incorporation into the alloy contributes to significant improvements in the properties of the alloy. Further, since aluminum is a ductile metal, PCAs are added to assist in minimizing cold welding during processing. Aluminum carbides are formed during MA by the decomposition of the PCA. Both the oxide or carbide type dispersions are about 30–50 nm in size and stabilize the ultrafine grain size. This results in 50% increase in strength, higher fracture toughness and improved resistance to stress corrosion cracking and fatigue crack growth of the mechanically alloyed materials. IncoMAP alloy AL-9052 has a density 5% less than that of conventional age-hardenable aluminum alloy of comparable strengths such as 2024. With its combination of lightweight, high strength, and corrosion resistance, IncoMAP alloy AL-9052 is evaluated for aerospace applications where marine corrosion is also a factor.

Addition of lithium to mechanically alloyed aluminum alloys has produced an ultra lightweight alloy IncoMAP alloy AL-905XL. Its density is 8% lower and stiffness 10% greater than the age-hardenable conventional alloy 7075-T73 of comparable strength. The excellent combination of the properties makes this alloy very attractive for airframe applications. In particular, the freedom from age-hardening treatments makes it possible to produce forgings and heavy sections with homogeneous metallurgical structures.

Recently, high strength Al–Ti alloys have been developed using MA by dispersing nanometer or submicron-sized Al_3Ti intermetallic particles (in addition to the Al_2O_3 and Al_4C_3 dispersoids from addition of PCAs) in an Al matrix. Similar approaches could be used to develop high strength alloys in other systems.

16.4. Magnesium-base alloys

A useful application of the MA technique was in the production of supercorroding magnesium alloys that operate as short-circuited galvanic cells to corrode (react) rapidly and predictably with an electrolyte such as seawater to produce heat and hydrogen gas [926,927]. Such an alloy system is suitable as a heat source for warming deep-sea divers, as a gas generator to provide gas for buoyancy, or as a fuel in hydrogen engines or fuel cells. The corrosion rate of alloys can be maximized by providing (a) a short electrolyte path, (b) a large amount of exposed surface area, and (c) a strong bond (weld) between the cathode and the anode. It is also useful to provide a very low resistance path for external currents to flow through the corroding pairs. All these requirements can be met with MA processing. Consequently, magnesium-base alloys containing Fe, Cu, C, Cr, or Ti have been evaluated for such applications. The Mg–5 to 20 at% Fe alloy is ideal because of its extremely fast reaction rate, high power output, and the high percentage of theoretical completion of the actual reaction. For corrodable release links an alloy with a slower reaction rate, such as Mg–5at%Ti is useful.

There have also been a number of investigations in recent years to use the MA processing technique to produce metal hydrides. This is because metal hydrides are materials for safe storage of hydrogen and they can store hydrogen with a higher volume density than liquid hydrogen. However, these are sensitive to surface oxidation and hence can be a limiting factor in their commercial utilization. Nanocrystalline hydrides have a high density of defects and interfaces that could enhance diffusion, and therefore nanocrystalline intermetallics would not require activation treatments at high temperatures and pressures after exposure to air [928]. In comparison to coarse-grained materials, mechanically alloyed nanocrystalline intermetallics exhibit a narrower absorption plateau and a lower plateau pressure. Their hydrogen storage behavior is typical of amorphous systems. Several magnesium-base and iron-base intermetallics are being evaluated for this application.

16.5. Other applications

Mechanically alloyed Fe-, Co-, and Ni-base alloy powders can be used to produce corrosion- and wear-resistant coatings by plasma spraying or other processes. These coatings are generally of the type MCrAl where M is Fe, Co, Ni or a combination of these elements. The oxide and carbide dispersions formed in-situ during MA can be beneficial for environmental protection [929]. Additions of yttrium can form Y_2O_3 dispersoids and such composites can be used as diffusion barrier coatings [930]. This type of barrier reduces the adverse effects of concentration gradients between the substrate and an overlay coating.

Mechanical alloying can also be used to produce feed stock for powder injection. This is because MA can easily achieve a very intimate mixture of the constituents. It has been recently reported that mechanically alloyed Fe–SiC

composite powders can be coated with a detonation gun to improve the wear resistance of medium carbon steel [931]. There was very little SiC phase in the coating layer when the powder was not mechanically alloyed. Mechanical alloying helped in uniformly distributing up to about 60 vol% of SiC powder in the iron matrix.

17. Safety hazards

The processing of powders in mechanical alloying equipment has special safety hazards due to the fine size of the powders and additional factors. Although handling of powders is well regulated, the safety hazards are accentuated during MA wherein conversion processes occur in temperature–time–stress regimes beyond those of conventional powder metallurgy. These concerns have been addressed by Weber et al. [932].

The safety hazards related to the MA process include heat evolution, reaction rates, gas evolution causing pressure build-up in the milling chamber or ancillary equipment, and finally explosions. As mentioned earlier, the temperature increases during milling operations due to energy added via the mechanical system used to drive the mill, and heat generated by exothermic processes occurring during the milling process. If this temperature exceeds some critical "reaction temperature" for one or more of the components being milled, uncontrolled reactions can occur and can lead to explosions. This heat generated can also increase the reaction rates of the system. Gases may also be produced during milling due to the decomposition of PCAs or due to the reactions between the components. Some of the gases produced may be flammable and so the potential for fire or explosion exists.

Some safety hazards exist which are related to handling of MA powders. The mechanically alloyed powders are very fine in size and consequently have a large surface area. Such powders have an increased tendency toward pyrophoricity. The cleaner and fresh powder surfaces produced during MA accentuate their sensitivity to pyrophoricity.

Special precautions should also be taken during unloading of the powders after MA. Immediately after MA, the powders are hot (or at least warm) and therefore the lid should not be immediately opened and the powder exposed to atmosphere. In such an event, the powder may catch fire because of interaction with the oxygen. This is much more important when dealing with powders like magnesium.

18. Concluding remarks

Mechanical alloying is a simple, elegant, and useful processing technique that continues to attract the serious attention of researchers. Even though the technique was originally developed to produce ODS superalloys, the synthesis of a variety of alloy phases including solid solutions, quasicrystalline and crystalline

intermetallic phases, and amorphous phases has spurred lots of research investigations in recent years. It is estimated that so far about 4000 research/review papers have been published in this area, with nearly 500 per year during the last 2–3 years (Fig. 45). This plot shows the same trend of increased research activity as was shown by the RSP technique in the early 1960s and 70s. Both equilibrium and non-equilibrium phases and commercially useful materials could be synthesized starting from elemental powders. This also appears to be an economical process with vast potential. One of the greatest advantages of MA is in the synthesis of novel alloys that are not possible by any other technique, such as alloying of normally immiscible elements. This is because MA is a completely solid-state processing technique and therefore limitations imposed by phase diagrams do not apply here. But, the number of investigations that deal with the decomposition behavior of metastable phases obtained by MA is very few.

On an industrial scale, this is an accepted process. The ODS alloys have a higher temperature operating capability at the same stress or increased load-bearing capability at the same temperature than alloys without an oxide dispersion. The ODS alloys continue to find applications in a wide variety of industries.

In spite of a lot of research effort, the mechanism of phase formation during MA is not well understood. It is most often proposed that the process of MA introduces a variety of defects (vacancies, dislocations, grain boundaries, stacking faults, etc.) which raise the free energy of the system making it possible to

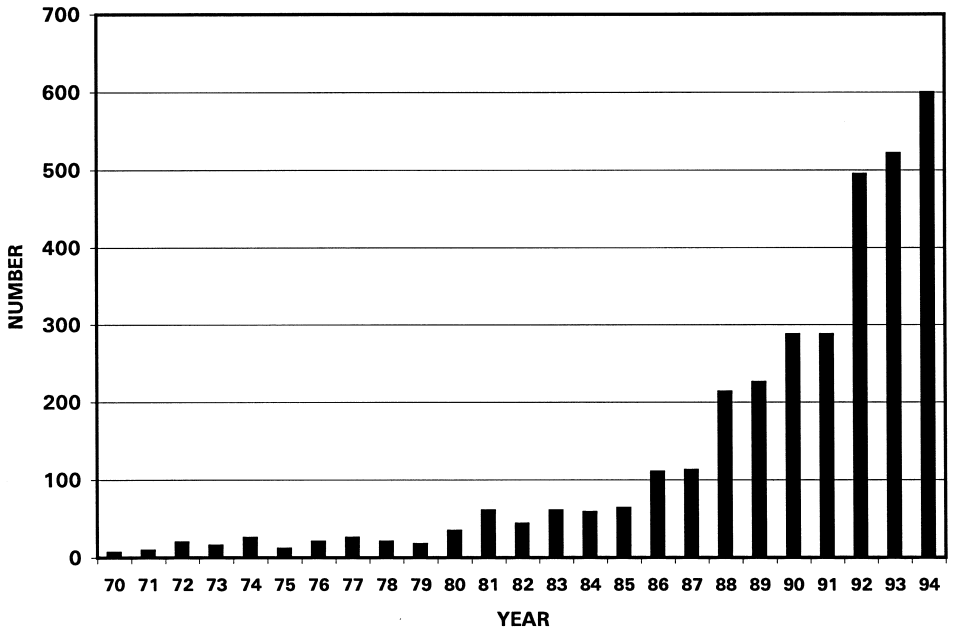

Fig. 45. Growth rate of publications in the area of mechanical alloying during 1970–1994.

produce metastable phases. But, there are very few investigations that deal with the characterization and quantification of the defects produced in mechanically alloyed powders. Further, properties of the mechanically alloyed products (after consolidation of the powders) are not reported except for the ODS alloys. This is understandable because researchers are still struggling to find out the mechanism of formation of the different phases — another area that is not well understood.

Mechanical alloying is a complex process that involves many variables, and many of them interdependent. Therefore, modeling of the MA process is very difficult. In spite of some success, one has to go much farther in developing models that can reach the final goal of predicting the nature of phases produced under a given set of milling conditions. Enough investigations have not been carried out to predict the formation of different types of phases based on thermodynamic or other models.

As mentioned in the text in different places, mechanically alloyed powders produce a variety of metastable phases. Since there are many other non-

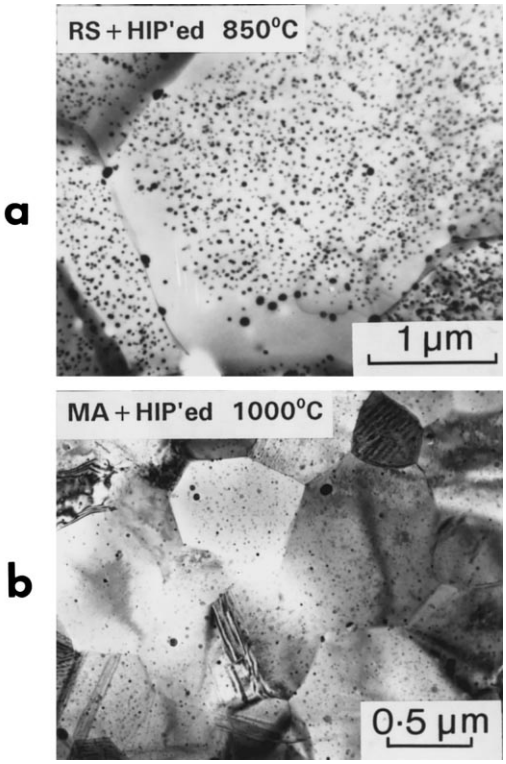

Fig. 46. Transmission electron micrographs showing the difference in the matrix grain size, and size and distribution of dispersoids in rapidly solidified (RS) and mechanically alloyed (MA) materials.

equilibrium-processing techniques that produce similar phases, comparisons are frequently made. The major comparison has been between MA and RSP techniques. Each has its own advantages and limitations. An important difference between mechanically alloyed and rapidly solidified alloys containing dispersoids appears to be in the size and distribution of dispersoids. Fig. 46 shows a pair of transmission electron micrographs comparing the matrix grain sizes, and size and distribution of dispersoids in HIP compacts of Ti_3Al-based alloys containing Er_2O_3 dispersoids. The rapidly solidified alloy was Ti_3Al to which 2 wt% Er was added and this was HIPed at 850°C after rapid solidification. The mechanically alloyed material was Ti–25Al–10Nb–3V–1Mo (at%) to which 2 wt% Er was added and the alloy powder was HIPed at 1000°C after MA. Even after HIPing at a higher temperature, in comparison to the RSP alloy, the mechanically alloyed material showed a finer matrix grain size, more uniform distribution of the dispersoids, absence of large dispersoids at the grain boundaries, and absence of dispersoid-free zones near the grain boundaries.

From the foregoing it is clear that research in the area of MA is continuing to flourish. There is so much more to learn on the "science" of MA, that the future of MA is assured for several years into the next millennium.

Acknowledgements

The author is grateful to Professor Brian Cantor of Oxford University, UK for the invitation to write this review and to Professor John Moore of the Colorado School of Mines for his generous support and constant encouragement. He also would like to thank the researchers who have provided the figures used in this review.

References

[1] Bloor D, Brook RJ, Flemings MC, Mahajan S, editors. The encyclopedia of advanced materials. Oxford: Pergamon Press, 1994.
[2] Suryanarayana C, editor. Non-equilibrium processing of materials. Oxford: Pergamon Press, 1999.
[3] Liebermann HH, editor. Rapidly solidified alloys: Processes, structures, properties, applications. New York, NY: Marcel Dekker, 1993.
[4] Anantharaman TR, Suryanarayana C. Rapidly solidified metals — a technological overview. Aedermannsdorf, Switzerland: Trans Tech Publications, 1987.
[5] Koch CC. In: Cahn RW, editor. Processing of metals and alloys, vol. 15 of materials science and technology — a comprehensive treatment. Weinheim, Germany: VCH Verlagsgesellschaft GmbH, 1991. p. 193–245.
[6] Suryanarayana C. Bibliography on mechanical alloying and milling. Cambridge, UK: Cambridge International Science Publishing, 1995.
[7] Suryanarayana C. Metals and Materials 1996;2:195–209.
[8] Lai MO, Lu L. Mechanical alloying. Boston, MA: Kluwer Academic Publishers, 1998.
[9] Murty BS, Ranganathan S. Internat Mater Rev 1998;43:101–41.

[10] Upadhya K, editor. Plasma synthesis and processing of materials. Warrendale, PA: TMS, 1993.
[11] Bickerdike RL, Clark D, Easterbrook JN, Hughes G, Mair WN, Partridge PG, Ranson HC. Internat J Rapid Solidification 1984;1:305–25.
[12] Turnbull D. Metall Trans 1981;12A:695–708.
[13] Martin G, Bellon P. Solid State Phys 1997;50:189–331.
[14] Shingu PH. In: Henein H, Oki T, editors. Processing materials for properties. Warrendale, PA: TMS, 1993. p. 1275–80.
[15] Froes FH, Suryanarayana C, Russell K, Ward-Close CM. In: Singh J, Copley SM, editors. Novel techniques in synthesis and processing of advanced materials. Warrendale, PA: TMS, 1994. p. 1–21.
[16] Froes FH, Suryanarayana C, Russell K, Li C-G. Mater Sci and Engng 1995;A192/193:612–23.
[17] Benjamin JS. Sci Amer 1976;234(5):40–8.
[18] Benjamin JS. In: Arzt E, Schultz L, editors. New materials by mechanical alloying techniques. Oberursel, Germany: DGM Informationgesellschaft, 1989. p. 3–18.
[19] Benjamin JS. Metal Powder Rep 1990;45:122–7.
[20] Ermakov AE, Yurchikov EE, Barinov VA. Phys Met Metallogr 1981;52(6):50–8.
[21] Koch CC, Cavin OB, McKamey CG, Scarbrough JO. Appl Phys Lett 1983;43:1017–9.
[22] Heinicke G. Tribochemistry. Berlin, Germany: Akademie Verlag, 1984.
[23] McCormick PG. Mater Trans Japan Inst Metals 1995;36:161–9.
[24] Maurice DR, Courtney TH. Metall Trans 1990;A21:289–303.
[25] Benjamin JS, editor. Frontiers of high-temperature materials. New York, NY: INCO Alloys International, 1981.
[26] Benjamin JS, Benn RC, editors. Frontiers of high-temperature materials II. New York, NY: INCO Alloys International, 1983.
[27] Arzt E, Schultz L, editors. New materials by mechanical alloying techniques. Oberursel, Germany: DGM Informationgesellschaft, 1989.
[28] Clauer AH, deBarbadillo JJ, editors. Solid state powder processing. Warrendale, PA: TMS, 1990.
[29] Froes FH, deBarbadillo JJ, editors. Structural applications of mechanical alloying. Materials Park, OH: ASM International, 1990.
[30] Yavari AR, Desré PJ, editors. Proceedings of the Conference on Multilayer Amorphization by Solid-State Reaction and Mechanical Alloying, J. Physique Colloq. 1990;C4(Suppl.14):51.
[31] Shingu PH, editor. Mechanical Alloying. In: Mater Sci Forum, 88–90. Aedermannsdorf, Switzerland: Trans Tech Publications, 1992.
[32] deBarbadillo JJ, Froes FH, Schwarz R, editors. Mechanical alloying for structural applications. Materials Park, OH: ASM International, 1993.
[33] Baláž P, Plesingerova B, Šepelk V, Stevulova N, editors. Proceedings of the First International Conference on Mechanochemistry. Cambridge, UK: Cambridge Interscience Publishing, 1994.
[34] Cochrane RW, Srom-Olsen JO, editors. Proceedings of the Sixth International Conference on Rapidly Quenched Metals; Mater Sci and Engng 1988;97–9.
[35] Frederiksson H, Savage SJ, editors. Proceedings of the Seventh International Conference on Rapidly Quenched Metals; Mater Sci and Engng 1991;A133–134.
[36] Masumoto T, Hashimoto K, editors. Proceedings of the Eighth International Conference on Rapidly Quenched Metals; Mater Sci and Engng 1994;A179–182.
[37] Duhaj P, Mrafko P, Švec P, editors. Proceedings of the Ninth International Conference on Rapidly Quenched Metals; Mater Sci and Engng 1997;A226–228.
[38] Yavari AR, editor. Proceedings of the International Symposium on Metastable, Mechanically Alloyed and Nanocrystalline Materials (ISMANAM- 94). In: Mater Sci Forum. Switzerland: Trans Tech Publications: Zürich, 1995. p. 179–81.
[39] Schulz R, editor. Proceedings of the International Symposium on Metastable, Mechanically Alloyed and Nanocrystalline Materials (ISMANAM-95). In: Mater Sci Forum, 225–7. Zürich, Switzerland: Trans Tech Publications, 1996.
[40] Fiorani D, Magini M, editors. Proceedings of the International Symposium on Metastable, Mechanically Alloyed and Nanocrystalline Materials (ISMANAM-96). In: Mater Sci Forum, 235–8. Zòrich, Switzerland: Trans Tech Publications, 1997.

[41] Baró MD, Suriñach S, editors. Proceedings of the International Symposium on Metastable, Mechanically Alloyed and Nanocrystalline Materials (ISMANAM-97). In: Mater Sci Forum, 269–72. Zürich, Switzerland: Trans Tech Publications, 1998.
[42] Gilman PS, Benjamin JS. Annu Rev Mater Sci 1983;13:279–300.
[43] Singer RF, Gessinger GH. In: Gessinger GH, editor. Powder Metallurgy of Superalloys. London, UK: Butterworths, 1984. p. 213–92.
[44] Sundaresan R, Froes FH. J Metals 1987;39(8):22–7.
[45] Weeber AW, Bakker H. Physica 1988;B153:93–135.
[46] Koch CC. Annu Rev Mater Sci 1989;19:121–43.
[47] Schaffer GB, McCormick PG. Mater Forum 1992;16:91–7.
[48] Bakker H, Zhou GF, Yang H. Prog Mater Sci 1995;39:159–241.
[49] Shingu PH, editor. Special Issue on Mechanical Alloying; Mater Trans Japan Inst Metals 1995;36:83–388.
[50] Schwarz RB, editor. Viewpoint set on mechanical alloying. Scripta Mater. 1996;34:1–73.
[51] El-Eskandarany MS, Aoki K, Suzuki K. J Less-Common Metals 1990;167:113–8.
[52] Weeber AW, Bakker H, deBoer FR. Europhys Lett 1986;2:445–8.
[53] Jangg G, Kuttner F, Korb G. Aluminium 1975;51:641–5.
[54] Jangg G. In: Arzt E, Schultz L, editors. New materials by mechanical alloying techniques. Oberursel, Germany: DGM Informationgesellschaft, 1989. p. 39–52.
[55] Avvakumov EG. Mechanical methods of activation of chemical processes. Novosibirsk, Russia: Nauka, 1986.
[56] Calka A, Nikolov JJ, Williams JS. Mater Sci Forum 1996;225-227:527–32.
[57] Calka A. Appl Phys Lett 1991;59:1568–9.
[58] Suryanarayana C. Intermetallics 1995;3:153–60.
[59] Radlinski AP, Calka A. Mater Sci and Engng 1991;A134:1376–9.
[60] Calka A, Radlinski AP. J Less-Common Metals 1990;161:L23–L26.
[61] Luton MJ, Jayanth CS, Disko MM, Matras MM, Vallone J. In: McCandlsih LE, Polk DE, Siegel RW, Kear BH, editors. Multicomponent ultrafine microstructures, vol. 132. Pittsburgh, PA: Mater Res Soc, 1989. p. 79–86.
[62] Aikin BJM, Juhas JJ. In: Froes FH, Hebeisen JC, editors. Advanced particulate materials and processes — 1997. Princeton, NJ: Metal Powder Industries Federation, 1997. p. 287–94.
[63] Gaffet E, Malhouroux N, Abdellaoui M. J Alloys and Compounds 1993;194:339–60.
[64] Gaffet E, Malhouroux-Gaffet N. J Alloys and Compounds 1994;205:27–34.
[65] Froyen L, Delaey L, Niu X-P, LeBrun P, Peytour C. JOM 1995;47(3):16–9.
[66] LeBrun P, Froyen L, Delaey L. Mater Sci and Engng 1992;A157:79–88.
[67] Charlot F, Gaffet E, Zeghmati B, Bernanrd F, Niepce JC. Mater Sci and Engng 1999;A262:279–88.
[68] Gauthier V, Josse C, Bernard F, Gaffet E, Larpin JP. Mater Sci and Engng 1999;A265:117–28.
[69] Ivanov E. Mater Sci Forum 1992;88–90:475–80.
[70] Yamazaki T, Terayama K, Shimazaki T, Sugimoto K. J Mater Sci Lett 1997;16:1357–9.
[71] Okada K, Kikuchi S, Ban T, Otsuka N. J Mater Sci Lett 1992;11:862–4.
[72] Nicoara G, Fratiloiu D, Nogues M, Dormann JL, Vasiliu F. Mater Sci Forum 1997;235-238:145–50.
[73] Bellosi A, Montverde F, Botti S, Martelli S. Mater Sci Forum 1997;235-238:255–60.
[74] Dolgin BP, Vanek MA, McGory T, Ham DJ. J Non-Cryst Solids 1986;87:281–9.
[75] Blaskov V, Radev DD, Klissurski D, Yordanov ND. J Alloys and Compounds 1994;206:267–70.
[76] Suryanarayana C. In: Powder metal technologies and applications. ASM Handbook, vol. 7. Materials Park, OH: ASM International, 1998. p. 80–90.
[77] Yamada K, Koch CC. J Mater Res 1993;8:1317–26.
[78] Thümmler F, Oberacker R. In: Introduction to powder metallurgy. London, UK: The Institute of Materials, 1993. p. 12.
[79] Szymanski K, Zaleski P, Rećko K, Waliszewski J. Mater Sci Forum 1997;235–238:223–8.
[80] Basset D, Matteazzi P, Miani F. Mater Sci and Engng 1993;A168:149–52.
[81] Kimura H, Kimura M, Takada F. J Less-Common Metals 1988;140:113–8.

[82] Kobayashi O, Aizawa T, Kihara J. Mater Trans Japan Inst Metals 1996;37:1497–504.
[83] Kerr I. Metal Powder Rep 1993;48:36–8.
[84] Di LM, Bakker H. J Phys C: Condens Matter 1991;3:3427–32.
[85] Suryanarayana C, Ivanov E, Noufi R, Contreras MA, Moore JJ. J Mater Res 1999;14:377–83.
[86] Chu B-L, Chen C-C, Perng T-P. Metall Trans 1992;A23:2105–10.
[87] Tokumitsu K. Mater Sci Forum 1997;235-238:127–32.
[88] Yen BK, Aizawa T, Kihara J. Mater Sci and Engng 1996;A 220:8–14.
[89] Yen BK, Aizawa T, Kihara J. Mater Sci Forum 1997;235-238:157–62.
[90] El-Eskandarany MS. J Alloys and Compounds 1994;203:117–26.
[91] El-Eskandarany MS, Sumiyama K, Aoki K, Masumoto T, Suzuki K. J Mater Res 1994;9:2891–8.
[92] Tonejc A, Dužević D, Tonejc AM. Mater Sci and Engng 1991;A134:1372–5.
[93] Ohtani T, Maruyama K, Ohshima K. Mater Res Bull 1997;32:343–50.
[94] El-Eskandarany MS. Metall Mater Trans 1996;A27:2374–82.
[95] Abe O, Suzuki Y. Mater Sci Forum 1996;225-227:563–8.
[96] Fukunaga T, Nakamura K, Suzuki K, Mizutani U. J Non-Cryst Solids 1990;117–118:700–3.
[97] Fukunaga T, Mori M, Inou K, Mizutani U. Mater Sci and Engng 1991;A134:863–6.
[98] Lee CH, Fukunaga T, Mizutani U. Mater Sci and Engng 1991;A134:1334–7.
[99] Lee CH, Mori M, Fukunaga T, Sakurai K, Mizutani U. Mater Sci Forum 1992;88-90:399–406.
[100] Sakurai K, Lee CH, Kuroda N, Fukunaga T, Mizutani U. J Appl Phys 1994;75:7752–5.
[101] Harringa JL, Cook BA, Beaudry BJ. J Mater Sci 1992;27:801–4.
[102] Kaloshkin SD, Tomlin IA, Andrianov GA, Baldokhin UV, Shelekhov EV. Mater Sci Forum 1997;235–238:565–70.
[103] Kuhrt C, Schropf H, Schultz L, Arzt E. In: deBarbadillo JJ, et al., editors. Mechanical alloying for structural applications. Materials Park, OH: ASM International, 1993. p. 269–73.
[104] Calka A, Nikolov JI, Ninham BW. In: deBarbadillo JJ, et al., editors. Mechanical alloying for structural applications. Materials Park, OH: ASM International, 1993. p. 189–95.
[105] Calka A, Radlinski AP. Mater Sci and Engng 1991;A134:1350–3.
[106] Larson JM, Luhman TS, Merrick HF. In: Meyerhoff RW, editor. Manufacture of superconducting materials. Materials Park, OH: ASM International, 1977. p. 155–63.
[107] Biswas A, Dey GK, Haq AJ, Bose DK, Banerjee S. J Mater Res 1996;11:599–607.
[108] Katamura J, Yamamoto T, Qi X, Sakuma T. J Mater Sci Lett 1996;15:36–7.
[109] Watanabe R, Hashimoto H, Park Y-H. In: Pease III LF, Sansoucy RJ, editors. Advances in powder metallurgy 1991, vol. 6. Princeton, NJ: Metal Powder Industries Federation, 1991. p. 119–30.
[110] Park Y-H, Hashimoto H, Watanabe R. Mater Sci Forum 1992;88–90:59–66.
[111] Guo W, Iasonna A, Magini M, Martelli S, Padella F. J Mater Sci 1994;29:2436–44.
[112] Padella F, Paradiso E, Burgio N, Magini M, Martelli S, Guo W, Iasonna A. J Less-Common Metals 1991;175:79–90.
[113] Gerasimov KB, Gusev AA, Ivanov EY, Boldyrev VV. J Mater Sci 1991;26:2495–500.
[114] Liu L, Casadio S, Magini M, Nannetti CA, Qin Y, Zheng K. Mater Sci Forum 1997;235-238:163–8.
[115] Atzmon M. Phys Rev Lett 1990;64:487–90.
[116] Gavrilov D, Vinogradov O, Shaw WJD. In: Poursartip A, Street K, editors. Proc. Inter. Conf. on Composite Materials, ICCM-10, vol. III. Woodhead Publishing, 1995, p. 11.
[117] Takacs L, Pardavi-Horvath M. J Appl Phys 1994;75:5864–6.
[118] Takacs L. In: Suryanarayana C, et al., editors. Processing and properties of nanocrystalline materials. Warrendale, PA: TMS, 1996. p. 453–64.
[119] Chin Z-H, Perng T-P. Mater Sci Forum 1997;235-238:121–6.
[120] Kis-Varga, Beke DL. Mater Sci Forum 1996;225-227:465–70.
[121] Suryanarayana C, Chen GH, Froes FH. Scripta Metall Mater 1992;26:1727–32.
[122] Goodwin PS, Mukhopadhyay DK, Suryanarayana C, Froes FH, Ward-Close CM. In: Blenkinsop P, et al., editors. Titanium '95, vol. 3. London: Institute of Materials, 1996. p. 2626–33.

[123] Miki M, Yamasaki T, Ogino Y. Mater Trans Japan Inst Metals 1992;33:839–44.
[124] Calka A, Williams JS. Mater Sci Forum 1992;88–90:787–94.
[125] Chen Y, Williams JS. Mater Sci Forum 1996;225–227:881–8.
[126] Ogino Y, Yamasaki T, Maruyama S, Sakai R. J Non-Cryst Solids 1990;117/118:737–40.
[127] Lee PY, Koch CC. J Non-Cryst Solids 1987;94:88–100.
[128] Imamura H, Sakasai N, Kajii Y. J Alloys and Compounds 1996;232:218–23.
[129] Lee W, Kwun SI. J Alloys and Compounds 1996;240:193–9.
[130] Rodriguez JA, Gallardo JM, Herrera EJ. J Mater Sci 1997;32:3535–9.
[131] Millet P, Calka A, Ninham BW. J Mater Sci Lett 1994;13:1428–9.
[132] Harris AM, Schaffer GB, Page NW. In: deBarbadillo JJ, et al., editors. Mechanical alloying for structural applications. Materials Park, OH: ASM International, 1993. p. 15–9.
[133] Huang B, Ishihara KN, Shingu PH. Mater Sci and Engng 1997;A231:72–9.
[134] Öveçoğlu ML, Nix WD. Internat J Powder Metall 1986;22:17–30.
[135] Morris DG, Morris MA. Mater Sci and Engng 1990;A125:97–106.
[136] Ameyama K, Okada O, Hirai K, Nakabo N. Mater Trans Japan Inst Metals 1995;36:269–75.
[137] Suzuki TS, Nagumo M. Mater Sci Forum 1995;179–181:189–94.
[138] Srinivasan S, Desch PB, Schwarz RB. Scripta Metall Mater 1991;25:2513–6.
[139] Tracy MJ, Groza JR. Nanostructured Mater 1992;1:369–78.
[140] Fan GJ, Gao WN, Quan MX, Hu ZQ. Mater Lett 1995;23:33–7.
[141] Keskinen J, Pogany A, Rubin J, Ruuskanen P. Mater Sci and Engng 1995;A196:205–11.
[142] Zdujic M, Kobayashi KF, Shingu PH. Z Metallkde 1990;81:380–5.
[143] Cabañas-Moreno JG, Dorantes H, López-Hirata VM, Calderón HA, Hallen-López JM. Mater Sci Forum 1995;179–181:243–8.
[144] López Hirata VM, Juárez Martinez U, Cabañas-Moreno JG. Mater Sci Forum 1995;179–181:261–6.
[145] Saji S, Neishi Y, Araki H, Minamino Y, Yamane T. Metall Mater Trans 1995;A26:1305–7.
[146] Enayati MH, Chang ITH, Schumacher P, Cantor B. Mater Sci Forum 1997;235–238:85–90.
[147] Arce Estrada EM, Díaz De la Torre S, López Hirata VM, Cabañas-Moreno JG. Mater Sci Forum 1996;225–227:807–12.
[148] Li F, Ishihara KN, Shingu PH. Metall Trans 1991;A22:2849–54.
[149] Kobayashi KF, Tachibana N, Shingu PH. J Mater Sci 1990;25:801–4.
[150] Fair GH, Wood JV. Powder Metall 1993;36:123–8.
[151] Lu L, Lai MO, Zhang S. Key Engng Mater 1995;104–107:111.
[152] Hida M, Asai K, Takemoto Y, Sakakibara A. Mater Sci Forum 1997;235–238:187–92.
[153] Wang JSC, Donnelly SG, Godavarti P, Koch CC. Internat J Powder Metall 1988;24:315–25.
[154] Suryanarayana C, Froes FH. J Mater Res 1990;5:1880–6.
[155] Wolski K, Le Caër G, Delcroix P, Fillit R, Thévenot F, Le Coze J. Mater Sci and Engng 1996;A207:97–104.
[156] Liang G, Li Z, Wang E. J Mater Sci 1996;31:901–4.
[157] Pabi SK, Murty BS. Mater Sci and Engng 1996;A214:146–52.
[158] Chitralekha J, Raviprasad K, Gopal ESR, Chattopadhyay K. J Mater Res 1995;10:1897–904.
[159] Frazier WE, Koczak MJ. Scripta Metall 1987;21:129–34.
[160] Chen G, Wang K, Wang J, Jiang H, Quan M. In: deBarbadillo JJ, et al., editors. Mechanical alloying for structural applications. Materials Park, OH: ASM International, 1993. p. 183–7.
[161] Ivison PK, Cowlam N, Soletta I, Cocco G, Enzo S, Battezzati L. Mater Sci and Engng 1991;A134:859–62.
[162] Ivison PK, Soletta I, Cowlam N, Cocco G, Enzo S, Battezzati L. J Phys C: Condens Matter 1992;4:1635–45.
[163] Gaffet E, Harmelin M, Faudot F. J Alloys and Compounds 1993;194:23–30.
[164] Ivison PK, Soletta I, Cowlam N, Cocco G, Enzo S, Battezzati L. J Phys C: Condens Matter 1992;4:5239–48.
[165] Hwang SJ, Nash P, Dollar M, Dymek S. Mater Sci Forum 1992;88–90:611–8.
[166] Huang B-L, Perez RJ, Crawford PJ, Nutt SR, Lavernia EJ. Nanostructured Mater 1996;7:57–65.
[167] Eckert J, Holzer JC, Krill III CE, Johnson WL. Mater Sci Forum 1992;88–90:505–12.

[168] LeBrun P, Froyen L, Munar B, Delaey L. Scand J Metall 1990;19:19–22.
[169] Niu XP, PhD Thesis, Katholieke University, Leuven, Belgium, 1991.
[170] Weber JH. In: Clauer AH, deBarbadillo JJ, editors. Solid state powder processing. Warrendale, PA: TMS, 1990. p. 227–39.
[171] Hong LB, Bansal C, Fultz B. Nanostructured Mater 1994;4:949–56.
[172] Qin Y, Chen L, Shen H. J Alloys and Compounds 1997;256:230–3.
[173] Klassen T, Herr U, Averback RS. Acta Mater 1997;45:2921–30.
[174] Fu Z, Johnson WL. Nanostructured Mater 1993;3:175–80.
[175] Mishurda JC, University of Idaho, Moscow, ID, unpublished results, 1993.
[176] Kimura H, Kimura M. In: Clauer AH, deBarbadillo JJ, editors. Solid state powder processing. Warrendale, PA: TMS, 1990. p. 365–77.
[177] Lee CH, Mori M, Fukunaga T, Mizutani U. Japan J Appl Phys 1990;29:540–4.
[178] Chen Y, Le Hazif R, Martin G. Mater Sci Forum 1992;88–90:35–41.
[179] Gaffet E, Yousfi L. Mater Sci Forum 1992;88–90:51–8.
[180] Koch CC, Pathak D, Yamada K. In: deBarbadillo JJ, et al., editors. Mechanical alloying for structural applications. Materials Park, OH: ASM International, 1993. p. 205–12.
[181] Koch CC. Mater Trans Japan Inst Metals 1995;36:85–95.
[182] Lee PY, Yang JL, Lin HM. J Mater Sci 1998;33:235–9.
[183] Koch CC. Nanostructured Mater 1993;2:109–29.
[184] Suryanarayana C. Internat Mater Rev 1995;40:41–64.
[185] Benjamin JS, Volin TE. Metall Trans 1974;5:1929–34.
[186] Lee PY, Koch CC. J Mater Sci 1988;23:2837–45.
[187] Davis RM, Koch CC. Scripta Metall 1987;21:305–10.
[188] Davis RM, McDermott B, Koch CC. Metall Trans 1988;A19:2867–74.
[189] Lee PY, Koch CC. Appl Phys Lett 1987;50:1578–80.
[190] Harris CC. Trans Soc Min Engrs 1967;238:17.
[191] German RM. In: Powder metallurgy science, 2nd ed. Princeton, NJ: Metal Powder Industries Federation, 1994. p. 28–78.
[192] Harris AM, Schaffer GB, Page NW. J Mater Sci Lett 1993;12:160–1.
[193] Suryanarayana C, Norton MG. X-ray diffraction: a practical approach. New York, NY: Plenum, 1998.
[194] McCandlish LE, Seegopaul P, Wu L. In: Kneringer G, Rödhammer P, Wilhartitz P, editors. Proc. 14th International Plansee Seminar, vol. 4. Reutte, Tyrol, Austria: Plansee AG, 1997. p. 363–75.
[195] Lonnberg B. J Mater Sci 1994;29:3224–30.
[196] Aymard L, Dehahaye-Vidal A, Portemer F, Disma F. J Alloys and Compounds 1996;238:116–27.
[197] Cargill III GS. Solid State Phys 1975;30:227.
[198] Cocco G. Mater Sci Forum 1992;88-90:703–10.
[199] Hunt J, Soletta I, Battezzati L, Cowlam N, Cocco G. J Alloys and Compounds 1993;194:311–7.
[200] Hunt JA, Rose P, Li M, Soletta I, Cowlam N, Cocco G, Enzo S, Battezzati L. Key Engng Mater 1993;81–83:115–20.
[201] Chen LC, Spaepen F. Nature 1988;336:366–7.
[202] Chen LC, Spaepen F. Mater Sci and Engng 1991;A133:342–5.
[203] Koch CC. Internat J Mechanochem and Mech Alloying 1994;1:56–67.
[204] Kobayashi KF, Tachibana N, Shingu PH. J Mater Sci 1990;25:3149–54.
[205] Zhang DL, Massalski TB, Paruchuri MR. Metall Mater Trans 1994;A25:73–9.
[206] Cho JS, Kwun SI. In: Kim NJ, editor. Light metals for transportation systems, Center for Advanced Aerospace Materials. Pohang, South Korea: Pohang Univ. of Sci. and Tech, 1993. p. 423–33.
[207] Matyja H, Oleszak D, Latuch J. Mater Sci Forum 1992;90:297–303.
[208] Ogino Y, Maruyama S, Yamasaki T. J Less-Common Metals 1991;168:221–35.
[209] Borzov AB, Kaputkin EYa. In: deBarbadillo JJ, et al., editors. Mechanical alloying for structural applications. Materials Park, OH: ASM International, 1993. p. S1–S4.
[210] Schulz R, Trudeau M, Huot JY, Van Neste A. Phys Rev Lett 1989;62:2849–52.

[211] Schwarz RB, Koch CC. Appl Phys Lett 1986;49:146–8.
[212] Bhattacharya AK, Arzt E. Scripta Metall Mater 1992;27:749–54.
[213] Magini M, Colella C, Guo W, Iasonna A, Martelli S, Padella F. Internat J Mechanochem and Mech Alloying 1994;1:14–25.
[214] Tonejc A, Tonejc AM, Dužević D. Scripta Metall Mater 1991;25:1111–3.
[215] Tonejc A, Stubicar M, Tonejc AM, Kosanović K, Subotić B, Smit I. J Mater Sci Lett 1994;13:519–20.
[216] Tonejc A, Tonejc AM, Bagović D, Kosanović C. Mater Sci and Engng 1994;A181/182:1227–31.
[217] Eckert J, Schultz L, Urban K. Z Metallkde 1990;81:862–8.
[218] Mikhailenko SD, Kalinina OT, Dyunusov AK, Fasman AB, Ivanov E, Golubkova GB. Siberian J Chem 1991;5:93–104.
[219] Anantharaman TR, Suryanarayana C. J Mater Sci 1971;6:1111–35.
[220] Paruchuri MR, Zhang DL, Massalski TB. Mater Sci and Engng 1994;A174:119–25.
[221] Shingu PH, Ishihara KN, Uenishi K, Kuyama J, Huang B, Nasu S. In: Clauer AH, deBarbadillo JJ, editors. Solid state powder processing. Warrendale, PA: TMS, 1990. p. 21–34.
[222] Uenishi K, Kobayashi KF, Ishihara KN, Shingu PH. Mater Sci and Engng 1991;A134:1342–5.
[223] Najafabadi R, Srolovitz DJ, Ma E, Atzmon M. J Appl Phys 1993;74:3144–9.
[224] Tang J. Mater Sci Forum 1996;225-227:477–82.
[225] Clark CR, Suryanarayana C, Froes FH. In: Phillips M, Porter J, editors. Advances in powder metallurgy and particulate materials — 1995: Part I. Princeton, NJ: Metal Powder Industries Federation, 1995. p. 135–43.
[226] Clark CR, Suryanarayana C, Froes FH. In: Froes FH, Suryanarayana C, Ward-Close CM, editors. Synthesis and processing of lightweight metallic materials. Warrendale, PA: TMS, 1995. p. 175–82.
[227] Fadeeva VI, Leonov AV. Mater Sci Forum 1992;88-90:481–8.
[228] Mukhopadhyay DK, Suryanarayana C, Froes FH. Metall Mater Trans 1995;A26:1939–46.
[229] Polkin IS, Kaputkin Eya, Borzov AB. In: Froes FH, deBarbadillo JJ, editors. Structural applications of mechanical alloying. Materials Park, OH: ASM International, 1990. p. 251–6.
[230] Radlinski AP, Calka A, Ninham BW, Kaczmarek WA. Mater Sci and Engng 1991;A134:1346–9.
[231] Calka A, Kaczmarek W, Williams JS. J Mater Sci 1993;28:15–8.
[232] Suryanarayana C, Sundaresan R. Mater Sci and Engng 1991;A131:237–42.
[233] Zdujic MV, Kobayashi KF, Shingu PH. J Mater Sci 1991;26:5502–8.
[234] Peng Z, Suryanarayana C, Froes FH. Scripta Metall Mater 1992;27:475–80.
[235] Peng Z, Suryanarayana C, Froes FH. Metall Mater Trans 1996;A27:41–8.
[236] Peng Z, Suryanarayana C, Froes FH. In: deBarbadillo JJ, et al., editors. Mechanical alloying for structural applications. Materials Park, OH: ASM International, 1993. p. 335–41.
[237] Shingu PH. In: Hirano K, et al., editors. Science and engineering of light metals. Tokyo: Japan Inst. Light Metals, 1991. p. 677–84.
[238] Benameur T, Inoue A, Masumoto T. Nanostructured Mater 1994;4:303–22.
[239] Xu Y, Makhlouf SA, Ivanov E, Wakoh K, Sumiyama K, Suzuki K. Nanostructured Mater 1994;4:437–44.
[240] Uenishi K, Kobayashi KF, Ishihara KN, Shingu PH. Mater Sci Forum 1992;88-90:453–8.
[241] Cocco G, Soletta I, Battezzati L, Baricco M, Enzo S. Phil Mag 1990;B61:473–86.
[242] Murty BS, Naik MD, Mohan Rao M, Ranganathan S. Mater Forum 1992;16:19–26.
[243] Abe S, Saji S, Hori S. J Japan Inst Metals 1990;54:895–902.
[244] Saji S, Neishi Y, Araki H, Minamino Y, Yamane T. Metall Mater Trans 1995;A26:1305–7.
[245] Miki M, Yamasaki T, Ogino Y. Mater Trans Japan Inst Metals 1993;34:952–9.
[246] Oehring M, Yan ZH, Klassen T, Bormann R. Phys Stat Sol (a) 1992;131:671–89.
[247] Oehring M, Klassen T, Bormann R. J Mater Res 1993;8:2819–29.
[248] Fan GJ, Quan MX, Hu ZQ. Scripta Metall Mater 1995;33:377–81.
[249] Leonov AV, Szewczak E, Gladilina OE, Matyja H, Fadeeva VI. Mater Sci Forum 1997;235–238:67–72.
[250] Fan GJ, Quan MX, Hu ZQ. Scripta Metall Mater 1995;32:247–52.
[251] Saji S, Araki H, Hashimoto K, Murata E. Mater Trans Japan Inst Metals 1996;37:1061–6.

[252] Fan GJ, Quan MX, Hu ZQ. J Mater Sci 1995;30:4847–51.
[253] Che X, Wang Q, Hu G. Scripta Metall Mater 1995;33:2019–23.
[254] Jiang JZ, Mørup S, Linderoth S. Mater Sci Forum 1996;225–227:489–96.
[255] Di LM, Bakker H, Bárczy P, Gácsi Z. Acta Metall Mater 1993;41:2923–32.
[256] Martin-Lopez R, Zandona M, Scherrer H. J Mater Sci Lett 1996;15:16–8.
[257] Mukhopadhyay DK, Suryanarayana C, Froes FH. Scripta Metall Mater 1994;30:133–7.
[258] Tanaka T, Ishihara KN, Shingu PH. Metall Trans 1992;A23:2431–5.
[259] Eckert J, Schultz L, Urban K. J Less-Common Metals 1990;166:293–302.
[260] Gente C, Oehring M, Bormann R. Phys Rev 1993;B48:13244–52.
[261] Huang JY, Wu YK, He AQ, Ye HQ. Nanostructured Mater 1994;4:293–302.
[262] Cabañas-Moreno JG, Dorantes H, López-Hirata VM, Calderon HA, Hallen-Lopez JM. Mater Sci Forum 1995;179–181:243–8.
[263] Arce Estrada EM, Díaz De la Torre S, López Hirata VM, Cabañas Moreno JG. Mater Sci Forum 1996;225–227:807–12.
[264] Kuhrt Ch, Schultz L. J Appl Phys 1992;71:1896–900.
[265] Antolini E, Daturi M, Ferretti M. J Mater Sci Lett 1996;15:416–8.
[266] Aymard L, Dumont B, Viau G. J Alloys and Compounds 1996;242:108–13.
[267] Uenishi K, Kobayashi KF, Ishihara KN, Shingu PH. Mater Sci Forum 1992;88–90:459–66.
[268] Baricco M, Battezzati L, Enzo S, Soletta I, Cocco G. Spectrochim Acta 1993;A49:1331–44.
[269] Huang JY, Yu YD, Wu YK, Li DX, Ye HQ. J Mater Res 1997;12:936–46.
[270] Ogino Y, Murayama S, Yamasaki T. J Less-Common Metals 1991;168:221–35.
[271] Barro MJ, Navarro E, Agudo P, Hernando A, Crespo P, Garcia Escorial A. Mater Sci Forum 1997;235–238:553–8.
[272] Enzo S, Mulas G, Frattini R, Principi G, Gupta R, Cooper R, Cowlam N. Mater Sci Forum 1997;235–238:529–34.
[273] Ueda Y, Ikeda S, Mori Y, Zaman H. Mater Sci and Engng 1996;A217/218:371–5.
[274] Eckert J, Holzer JC, Krill III CE, Johnson WL. J Mater Res 1992;7:1980–3.
[275] Macri PP, Rose P, Frattini R, Enzo S, Principi G, Hu WX, Cowlam N. J Appl Phys 1994;76:4061–7.
[276] Eckert J, Holzer JC, Johnson WL. J Appl Phys 1993;73:131–41.
[277] Eckert J, Holzer JC, Krill III CE, Johnson WL. J Appl Phys 1993;73:2794–802.
[278] Uenishi K, Kobayashi KF, Nasu S, Hatano H, Ishihara KN, Shingu PH. Z Metallkde 1992;83:132–5.
[279] Ma E, Atzmon M, Pinkerton FE. J Appl Phys 1993;74:955–62.
[280] Qi M, Zhu M, Yang DZ. J Mater Sci Lett 1994;13:966–8.
[281] Huang JY, Wu YK, Hu KY, Meng XM. Acta Metall Sinica 1993;B29:60–3.
[282] Huang JY, He AQ, Wu YK. Nanostructured Mater 1994;4:1–10.
[283] Benghalem A, Morris DG. Scripta Metall Mater 1992;27:739–44.
[284] Kim KJ, Sumiyama K, Suzuki K. J Non-Cryst Solids 1994;168:232–40.
[285] Shen TD, Koch CC. Mater Sci Forum 1995;179–181:17–24.
[286] Ivanov E. In: deBarbadillo JJ, et al., editors. Mechanical alloying for structural applications. Materials Park, OH: ASM International, 1993. p. 171–6.
[287] Yazenko SP, Hayak VG, Filipov VA, Ivanov E, Grigorieva TF, USSR Patent # 472 5973.
[288] Ivanov E, Patton V, Grigorieva TF. Mater Sci Forum 1996;225–227:575–80.
[289] Ivanov EY, Grigorieva TF. Solid State Ionics 1997;101–103:235–41.
[290] Murty BS, Mohan Rao M, Ranganathan S. Nanostructured Mater 1993;3:459–67.
[291] Gaffet E, Louison C, Harmelin M, Faudot F. Mater Sci and Engng 1991;A134:1380–4.
[292] Kuyama J, Ishihara KN, Shingu PH. Mater Sci Forum 1992;90:521–8.
[293] Jiang HG, Perez RJ, Lau ML, Lavernia EJ. J Mater Res 1997;12:1429–32.
[294] Nasu S, Imaoka S, Morimoto S, Tanimoto H, Huang B, Tanaka T, Kuyama J, Ishihara KN, Shingu PH. Mater Sci Forum 1992;88–90:569–76.
[295] Bonetti E, Scipione G, Valdre G, Cocco G, Frattini R, Macri PP. J Appl Phys 1993;74:2053–7.
[296] Bonetti E, Valdre G, Enzo S, Cocco G, Soletta I. Nanostructured Mater 1993;2:369–75.
[297] Bansal C, Gao ZQ, Hong LB, Fultz B. J Appl Phys 1994;76:5961–6.

[298] Gialanella S. Intermetallics 1995;3:73–6.
[299] Liu ZG, Guo JT, He LL, Hu ZQ. Nanostructured Mater 1994;4:787–94.
[300] Schropf H, Kuhrt C, Arzt E, Schultz L. Scripta Metall Mater 1994;30:1569–74.
[301] Perez RJ, Huang BL, Crawford PJ, Sharif AA, Lavernia EJ. Nanostructured Mater 1996;7:47–56.
[302] Stiller C, Eckert J, Roth S, Schäfer R, Klement U, Schultz L. Mater Sci Forum 1996;225–227:695–700.
[303] Huang BL, Perez RJ, Lavernia EJ, Luton MJ. Nanostructured Mater 1996;7:67–79.
[304] Yang H, Di LM, Bakker H. Intermetallics 1993;1:29–33.
[305] Koyano T, Mizutani U, Okamoto H. J Mater Sci Lett 1995;14:1237–40.
[306] Koyano T, Takizawa T, Fukunaga T, Mizutani U, Kamizuru S, Kita E, Tasaki A. J Appl Phys 1993;73:429–33.
[307] Wang X-M, Aoki K, Masumoto T. Mater Sci Forum 1996;225–227:423–8.
[308] Fultz B, Gao Z-Q, Hamdeh HH, Oliver SA. Phys Rev 1994;B49:6312–5.
[309] Kataoka N, Suzuki K, Inoue A, Masumoto T. J Mater Sci 1991;26:4621–5.
[310] Hightower A, Fultz B, Bowman Jr RC. J Alloys and Compounds 1997;252:238–44.
[311] Hays V, Marchand R, Saindrenan G, Gaffet E. Nanostructured Mater 1996;7:411–20.
[312] Xia SK, Scorzelli RB, Souza Azevedo I, Baggio-Saitovich E, Takeuchi Y. Mater Sci Forum 1996;225–227:453–8.
[313] Garcia-Escoral A, Adeva P, Cristina MC, Martin A, Carmona F, Cebollada F, Martin VE, Leonato M, Gonzalez JM. Mater Sci and Engng 1991;A134:1394–7.
[314] Kohmoto O, Yamaguchi N, Mori T. J Mater Sci 1994;29:3221–3.
[315] Abdellaoui M, Barradi T, Gaffet E. J de Phys IV 1992;2:73–8.
[316] Gao Z, Fultz B. Nanostructured Mater 1993;2:231–40.
[317] Zhou T, Zhong J, Xu J, Yu Z, Gu G, Wang D, Huang H, Du Y, Wang J, Jiang Y. J Mag Mag Mater 1996;164:219–24.
[318] Nasu S, Shingu PH, Ishihara KN, Fujita FE. Hyperfine Interactions 1990;55:1043–50.
[319] Cabrera AF, Sánchez FH, Mendoza-Zélis L. Mater Sci Forum 1995;179–181:231–6.
[320] Schlump W, Grewe H. In: Arzt E, Schultz L, editors. New materials by mechanical alloying techniques. Oberursel, Germany: Deutsche Gesellschaft für Metallkunde, 1989. p. 307–18.
[321] Oleszak D, Jachimowicz M, Matyja H. Mater Sci Forum 1995;179–181:215–8.
[322] El-Eskandarany MS, Sumiyama K, Suzuki K. Acta Mater 1997;45:1175–87.
[323] Bai HY, Michaelsen C, Sinkler W, Bormann R. Mater Sci Forum 1997;235–238:361–6.
[324] Herr U, Samwer K. Nanostructured Mater 1992;1:515–21.
[325] Hellstern E, Schultz L. Appl Phys Lett 1986;49:1163–5.
[326] Michaelsen C, Hellstern E. J Appl Phys 1987;62:117–9.
[327] Hellstern E, Schultz L. Mater Sci and Engng 1988;97:39–42.
[328] Schultz L. Mater Sci and Engng 1988;97:15–23.
[329] Matteazzi P, Le Caër G. Mater Sci and Engng 1992;A156:229–37.
[330] Gaffet E, Faudot F, Harmelin M. Mater Sci and Engng 1991;A149:85–94.
[331] Boolchand P, Koch CC. J Mater Res 1992;7:2876–83.
[332] Hida M, Asai K, Takemoto Y, Sakakibara A. Mater Trans Japan Inst Metals 1996;37:1679–83.
[333] Hellstern E, Schultz L, Bormann R, Lee D. Appl Phys Lett 1988;53:1399–401.
[334] Groza JR, Tracy MJH. In: deBarbadillo JJ, et al., editors. Mechanical alloying for structural applications. Materials Park, OH: ASM International, 1993. p. 327–34.
[335] Goodwin PS, Ward-Close CM. In: Froes FH, editor. P/M in aerospace, defense, and demanding applications. Princeton, NJ: Metal Powder Industries Federation, 1995. p. 89–95.
[336] Oleszak D, Burzynska-Szyszko M, Matyja H. J Mater Sci Lett 1993;12:3–5.
[337] Oehring M, Bormann R. J de Physique 1990;51:169–74.
[338] Di LM, Bakker H. J Phys C: Condens Matter 1991;3:9319–26.
[339] Chou TC, Nieh TG, Wadsworth J. Scripta Metall Mater 1992;27:881–6.
[340] Kenik EA, Bayuzick RJ, Kim MS, Koch CC. Scripta Metall 1987;21:1137–42.
[341] Lou T, Fan G, Ding B, Hu Z. J Mater Res 1997;12:1172–5.
[342] Itsukaichi T, Shiga S, Masuyama K, Umemoto M, Okane I. Mater Sci Forum 1992;88–90:631–8.

[343] Cardellini F, Cleri F, Mazzone G, Montone A, Rosato V. J Mater Res 1993;8:2504–9.
[344] Lu L, Lai MO, Zhang S. Mater and Design 1994;15:79–86.
[345] Ivanov E, Grigorieva TF, Golubkova GV, Boldyrev VV, Fasman AB, Mikhailenko SD, Kalinina OT. Mater Lett 1988;7:51–4.
[346] Gialanella S, Delorenzo R, Marino F, Guella M. Intermetallics 1995;3:1–8.
[347] Boldyrev VV, Golubkova GV, Grigorieva TF, Ivanov E, Kalinina OT, Mihailenko SD, Fasman AB. Doklady Akad Nauk SSSR 1987;297:1181.
[348] Grigorieva TF, Barinova AP, Boldyrev VV, Ivanov EY. Mater Sci Forum 1996;225–227:417–22.
[349] Yang QM, Lei YQ, Wu J, Qang QD, Lu GL, Chen LS. Key Engng Mater 1993;81–83:169–73.
[350] Huot JY, Trudeau ML, Schulz R. J Electrochem Soc 1991;138:1316–21.
[351] Portnoy VK, Fadeeva VI, Zaviyalova IN. J Alloys and Compounds 1995;224:159–61.
[352] Van Neste A, Lamarre A, Trudeau ML, Schulz R. J Mater Res 1992;7:2412–7.
[353] Jang JSC, Tsau CH, Chen WD, Lee PY. J Mater Sci 1998;33:265–70.
[354] Cho YS, Koch CC. J Alloys and Compounds 1993;194:287–94.
[355] Lee PY, Chen TR. J Mater Sci Lett 1994;13:888–90.
[356] Battezzati L, Cocco G, Schiffini L, Enzo S. Mater Sci and Engng 1988;97:121–4.
[357] Schwarz RB, Petrich RR, Saw CK. J Non-Cryst Solids 1985;76:281–302.
[358] Yang H, Bakker H. In: deBarbadillo JJ, et al., editors. Mechanical alloying for structural applications. Materials Park, OH: ASM International, 1993. p. 401–8.
[359] Mi S, Courtney TH. Scripta Mater 1998;38:637–44.
[360] Zbiral J, Jangg G, Korb G. Mater Sci Forum 1992;88–90:19–26.
[361] Bryden KJ, Ying JY. Mater Sci Forum 1996;225–227:895–900.
[362] Ishida T. J Mater Sci Lett 1994;13:623–8.
[363] Gaffet E, Harmelin M. In: Froes FH, deBarbadillo JJ, editors. Structural applications of mechanical alloying. Materials Park, OH: ASM International, 1990. p. 257–64.
[364] El-Eskandarany MS. Metall Mater Trans 1996;A27:3267–78.
[365] Liu L, Chu ZQ, Dong YD. J Alloys and Compounds 1992;186:217–21.
[366] Suryanarayana C, Chen GH, Frefer A, Froes FH. Mater Sci and Engng 1992;A158:93–101.
[367] Burgio N, Guo W, Martelli S, Magini M, Padella F, Soletta I. In: Froes FH, deBarbadillo JJ, editors. Structural applications of mechanical alloying. Materials Park, OH: ASM International, 1990. p. 175–83.
[368] Guo W, Martelli S, Burgio N, Magini M, Padella F, Paradiso E, Soletta I. J Mater Sci 1991;26:6190–6.
[369] Bonetti E, Cocco G, Enzo S, Valdre G. Mater Sci and Tech 1990;6:1258–62.
[370] Bonetti E, Valdre G, Enzo S, Cocco G. J Alloys and Compounds 1993;194:331–8.
[371] Fadeeva VI, Leonov AV, Szewczak E, Matyja H. Mater Sci and Engng 1998;A242:230–4.
[372] Chen GH, Suryanarayana C, Froes FH. Scripta Metall Mater 1991;25:2537–40.
[373] Suryanarayana C, Chen GH, Froes FH. In: Froes FH, et al., editors. Advancements in synthesis and processing. Covina, CA: SAMPE, 1992. p. M671–M683.
[374] Itsukaichi T, Norimatsu T, Umemoto M, Okane I, Wu B-Y. In: Tamura I, editor. Heat and Surface '92. Tokyo, Japan: Japan Tech. Info. Center, 1992. p. 305–8.
[375] Abe YR, Johnson WL. Mater Sci Forum 1992;88–90:513–20.
[376] Zhou E, Suryanarayana C, Froes FH. Mater Lett 1995;23:27–31.
[377] Sundaresan R, Froes FH. Key Engng Mater 1989;29-31:199–206.
[378] Sundaresan R, Froes FH. In: Arzt E, Schultz L, editors. New materials by mechanical alloying techniques. Oberursel, Germany: Deutsche Gesellschaft für Metallkunde, 1989. p. 243–62.
[379] Wilkes DMJ, Goodwin PS, Ward-Close CM, Bagnall K, Steeds J. In: Bormann R, et al., editors. Metastable phases and microstructures, vol. 400. Pittsburgh, PA: Mater. Res. Soc, 1996. p. 267–74.
[380] Wilkes DMJ, Goodwin PS, Ward-Close CM, Bagnall K, Steeds JW. Mater Lett 1996;27:47–52.
[381] Skakov YuA, Edneral NV, Frolov EV, Povolovzki JA. Mater Sci Forum 1995;179–181:33–8.
[382] Yan ZH, Oehring M, Bormann R. J Appl Phys 1992;72:2478–87.
[383] Shen TD, Wang KY, Quan MX, Wang JT. Mater Sci Forum 1992;88–90:391–7.
[384] Herr U, Samwer K. Nanostructured Mater 1992;1:515–21.

[385] Öveçoğlu ML, Özkal B, Suryanarayana C. J Mater Res 1996;11:673–82.
[386] Ivanov E, Suryanarayana C, Bryskin BD. Mater Sci and Engng 1998;A251:255–61.
[387] Ivanov E, Sumiyama K, Yamauchi H, Suzuki K. In: deBarbadillo JJ, et al., editors. Mechanical alloying for structural applications. OH: ASM International: Materials Park, 1993. p. 409–13.
[388] Chen GH, Suryanarayana C, Froes FH. In: deBarbadillo JJ, et al., editors. Mechanical alloying for structural applications. OH: ASM International: Materials Park, 1993. p. 367–75.
[389] Fecht HJ, Han G, Fu Z, Johnson WL. J Appl Phys 1990;67:1744–8.
[390] Ma E, Atzmon M. Phys Rev Lett 1991;67:1126–9.
[391] Ma E, Atzmon M. J Alloys and Compounds 1993;194:235–44.
[392] Ma E, Atzmon M. Mater Sci Forum 1992;88–90:467–74.
[393] Schultz L, Hellstern E, Thoma A. Europhys Lett 1987;3:921–6.
[394] Katamura J, Yamamoto T, Qin X, Sakuma T. J Mater Sci Lett 1996;15:36–7.
[395] Tonejc AM, Tonejc A. Mater Sci Forum 1996;225–227:497–502.
[396] Kim H-S, Suhr D-S, Kim G-H, Kum D-W. Metals and Materials 1996;2:15–21.
[397] Gayle FW, Biancaniello FS. Nanostructured Mater 1995;6:429–32.
[398] Klassen T, Herr U, Averback RS. In: Bormann R, et al., editors. Metastable phases and microstructures, vol. 400. Pittsburgh, PA: Mater. Res. Soc, 1996. p. 25–30.
[399] Ma E, He J-H, Schilling PJ. Phys Rev 1997;B55:5542–5.
[400] Yavari AR, Desré P. Mater Sci Forum 1992;88–90:43–50.
[401] Sui HX, Zhu M, Qi M, Li GB, Yang DZ. J Appl Phys 1992;71:2945–9.
[402] Veltl G, Scholz B, Kunze H-D. Mater Sci and Engng 1991;A134:1410–3.
[403] Fecht HJ, Hellstern E, Fu Z, Johnson WL. Metall Trans 1990;A21:2333–7.
[404] Desré PJ. Nanostructured Mater 1994;4:957–63.
[405] Yavari AR, Desré PJ, Benamuer T. Phys Rev Lett 1992;68:2235–8.
[406] Yavari AR. Mater Sci and Engng 1994;A179/180:20–6.
[407] Drbohlav O, Yavari AR. Acta Mater 1995;43:1799–809.
[408] Jiang JZ, Gente C, Bormann R. Mater Sci and Engng 1998;A242:268–77.
[409] Hume-Rothery W, Raynor GV. The structure of metals and alloys. London: Institute of Metals, 1962.
[410] Darken LS, Gurry RW. Physical chemistry of metals. New York, NY: McGraw-Hill, 1962.
[411] Boettinger W, Perepezko JH. In: Liebermann HH, editor. Rapidly solidified alloys: processes, structures, properties, applications. New York, NY: Marcel-Dekker, 1993. p. 17–78.
[412] Morris DG. Mechanical behaviour of nanostructured materials. Zuerich, Switzerland: Trans Tech Publications, 1998.
[413] Koch CC, Morris DG, Lu K, Inoue A. MRS Bulletin 1999;24(2):54–8.
[414] Suryanarayana C, Jones H. Internat J Rapid Solidification 1988;3:253–93.
[415] Kelton KF. Internat Mater Rev 1993;38:105–37.
[416] Eckert J, Schultz L, Urban K. Appl Phys Lett 1989;55:117–9.
[417] Ivanov E, Konstanchuk IG, Bokhonov BD, Boldyrev VV. Reactivity of Solids 1989;7:167–72.
[418] Eckert J. Mater Sci Forum 1992;88–90:679–86.
[419] Nasu S, Miglierini M, Ishihara KN, Shingu PH. J Phys Soc Japan 1992;61:3766–72.
[420] Asahi N, Maki T, Matsumoto S, Sawai T. Mater Sci and Engng 1994;A181/182:841–4.
[421] Bahadur D, Singh K, Roy M. Mater Sci and Engng 1992;A154:79–84.
[422] Politis C, Krauss W, Leitz H, Schommers W. Mod Phys Lett 1989;3:615–8.
[423] Asahi N, Noguchi S, Matsumura K. Mater Sci and Engng 1994;A181/182:819–22.
[424] Roy M, Singh K, Bahadur D. J Mater Sci Lett 1992;11:858–61.
[425] Meyer M, Mendoza-Zélis L, Sánchez FH. Mater Sci Forum 1995;179–181:177–82.
[426] Asahi N. Mater Sci and Engng 1997;A226:67–9.
[427] Ivanov Eyu, Konstanchuk IG, Bokhonov BD, Boldyrev VV. Doklady Phys Chem 1989;304(1–3):82–5.
[428] Ivanov E, Bokhonov B, Konstanchuk I. J Japan Soc Powder Powder Metall 1991;38:903–5.
[429] Takeuchi T, Yamada Y, Fukunaga T, Mizutani U. Mater Sci and Engng 1994;A181/182:828–32.
[430] Ivanov E, Bokhonov B, Konstanchuk I. J Mater Sci 1991;26:1409–11.
[431] Ivanov E, Bokhonov B, Konstanchuk I, Boldyrev VV. In: deBarbadillo JJ, et al., editors.

Mechanical alloying for structural applications. Materials Park, OH: ASM International, 1993. p. 421–4.
[432] Bokhonov B, Konstanchuk I, Ivanov E, Boldyrev VV. J Alloys and Compounds 1992;187:207–14.
[433] Bahadur D, Dunlap RA, Foldeaki M. J Alloys and Compounds 1996;240:278–84.
[434] Zhang FX, Wang WK. J Alloys and Compounds 1996;240:256–60.
[435] McDermott BT, Koch CC. Scripta Metall 1986;20:669–72.
[436] Martelli S, Mazzone G, Scaglione S, Vittori M. J Less-Common Metals 1988;145:261–70.
[437] Moore JJ, Feng HJ. Prog Mater Sci 1995;39:243–316.
[438] Rawers J, Govier D, Cook D. Scripta Metall Mater 1995;32:1319–24.
[439] Yvon PJ, Schwarz RB. In: deBarbadillo JJ, et al., editors. Mechanical alloying for structural applications. Materials Park, OH: ASM International, 1993. p. 393–400.
[440] Chattopadhyay K, Wang X-M, Aoki K, Masumoto T. J Alloys and Compounds 1996;232:224–31.
[441] Martelli S, Mazzone G, Vittori-Antisari M. J Mater Res 1991;6:499–504.
[442] Schwarz RB, Desch PB, Srinivasan S. In: deBarbadillo JJ, et al., editors. Mechanical alloying for structural applications. Materials Park, OH: ASM International, 1993. p. 227–35.
[443] Li W, Suryanarayana C, Froes FH. In: Phillips MA, Porter J, editors. Advances in powder metallurgy and particulate materials: Part I. Princeton, NJ: Metal Powder Industries Federation, 1995. p. 145–57.
[444] Klassen T, Oehring M, Bormann R. J Mater Res 1994;9:47–52.
[445] Suryanarayana C, Li W, Froes FH. Scripta Metall Mater 1994;31:1465–70.
[446] Barinov VA, Tsurin VA, Elsukov EP, Ovechkin LV, Dorofeev GA, Ermakov AE. Phys Metals and Metallogr 1992;74(4):412–5.
[447] Clark CR, Wright C, Suryanarayana C, Baburaj EG, Froes FH. Mater Lett 1997;33:71–5.
[448] El-Eskandarany MS, Sumiyama K, Aoki K, Suzuki K. J Mater Res 1992;7:888–93.
[449] Kostić E, Kiss Š, Bošković S, Zec S. Powder Tech 1997;91:49–54.
[450] Huang JY, Wu YK, Ye HQ. Acta Mater 1996;44:1201–9.
[451] Corrias A, Ennas G, Marongiu G, Musinu A, Paschina G. J Mater Res 1993;8:1327–33.
[452] Di LM, Zhou GF, Bakker H. Phys Rev 1993;B47:4890–5.
[453] Takacs L. Nanostructured Mater 1993;2:241–9.
[454] Gaffet E, Michel D, Mazerolles L, Berthet P. Mater Sci Forum 1997;235–238:103–8.
[455] Han SH, Gshneidner KA, Beaudry BJ. Scripta Metall Mater 1991;25:295–8.
[456] Barinov VA, Dorofeev GA, Ovechkin LV, Elsukov EP, Ermakov AE. Phys Stat Sol (a) 1991;123:527–34.
[457] Balogh J, Bujdoso L, Faigel Gy, Granasy L, Kemeny T, Vincze I, Szabo S, Bakker H. Nanostructured Mater, 1993;2:11–8.
[458] Barinov VA, Dorofeev GA, Ovechkin LV, Elsukov EP, Ermakov AE. Phys Metals and Metallogr 1992;73(1):93–6.
[459] Foct J, de Figueiredo RS. Nanostructured Mater 1994;4:685–97.
[460] Matteazzi P, Le Caër G. Mater Sci and Engng 1991;A149:135–42.
[461] Torres Sanchez RM. J Mater Sci Lett 1996;15:461–2.
[462] Sorescu M. J Mater Sci Lett 1998;17:1059–61.
[463] Chen Y, Williams JS, Wang GM. J Appl Phys 1996;79:3956–62.
[464] Bart JCJ. J Mater Sci 1993;28:278–84.
[465] Bokhonov BB, Konstanchuk IG, Boldyrev VV. J Alloys and Compounds 1995;218:190–6.
[466] Zhou GF, Di LM, Bakker H. J Appl Phys 1993;73:1521–7.
[467] Kosmac T, Courtney TH. J Mater Res 1992;7:1519–25.
[468] Mashimo T, Tashiro S. J Mater Sci Lett 1994;13:174–6.
[469] Chaudhuri J, Ram ML, Sarkar BK. J Mater Sci 1994;29:3484–8.
[470] Millet P, Hwang T. J Mater Sci 1996;31:351–5.
[471] Sen S, Ram ML, Roy S, Sarkar BK. J Mater Res 1999;14:841–8.
[472] Ivanov E, Sumiyama K, Yamauchi H, Suzuki K. Solid State Ionics 1993;59:175–7.
[473] Ivanov E, Sumiyama K, Yamauchi H, Suzuki K. J Alloys and Compounds 1993;192:251–2.

[474] Liu ZT, Uwakweh ONC. J Mater Res 1996;11:1665–72.
[475] Michel D, Faudot F, Gaffet E, Mazerolles L, Rev. Metall.-CIT 1993:219–25.
[476] Bailey JE. J British Ceram Soc 1972;71:25.
[477] Ohtani T, Motoki M, Koh K, Ohshima K. Mater Res Bull 1995;30:1495–504.
[478] Alonso T, Liu Y, Parks TC, McCormick PG. Scripta Metall Mater 1991;25:1607–10.
[479] Alonso T, Liu Y, Parks TC, McCormick PG. Scripta Metall Mater 1992;26:1931–2.
[480] Makhlouf SA, Ivanov E, Sumiyama K, Suzuki K. J Alloys and Compounds 1992;189:117–21.
[481] Morris MA, Morris DG. Mater Sci and Engng 1991;A136:59–70.
[482] Morris MA, Morris DG. Mater Sci Forum 1992;88–90:529–35.
[483] Cardellini F, Contini V, Mazzone G, Montone A. Phil Mag 1997;B76:629–38.
[484] Mukhopadhyay DK, Suryanarayana C, Froes FH. Scripta Metall Mater 1994;31:333–8.
[485] Burzynska-Szyszko M, Fadeeva VI, Matyja H. Mater Sci Forum 1997;235–238:97–102.
[486] LeBrun P, Froyen L, Delaey L. In: Froes FH, deBarbadillo JJ, editors. Structural applications of mechanical alloying. Materials Park, OH: ASM International, 1990. p. 155–61.
[487] Zdujić M, Poleti D, Karanović Lj, Kobayashi KF, Shingu PH. Mater Sci and Engng 1994;A185:77–86.
[488] Kaneyoshi T, Takahashi T, Hayashi Y, Motoyama M. In: Capus JM, German RM, editors. Advances in powder metallurgy and particulate materials, vol. 7. Princeton, NJ: Metal Powder Industries Federation, 1992. p. 421–9.
[489] Kim DK, Okazaki K. Mater Sci Forum 1992;88–90:553–60.
[490] Kawanishi S, Ionishi K, Okazaki K. Mater Trans Japan Inst Metals 1993;34:43–8.
[491] Ivanov E, Golubkova GV, Grigorieva TF. Reactivity of Solids 1990;8:73–6.
[492] Ivanov E, Makhlouf SA, Sumiyama K, Yamauchi H, Suzuki K, Golubkova G. J Alloys and Compounds 1992;185:25–34.
[493] Schultz L, Hellstern E, Zorn Z. Z Phys Chem 1988;157:203–10.
[494] Liu ZG, Guo JT, Hu ZQ. Mater Sci and Engng 1995;A192/193:577–82.
[495] Lerf R, Morris DG. Mater Sci and Engng 1990;A128:119–27.
[496] Zhang LP, Shi J, Zin JZ. Mater Lett 1994;21:303–6.
[497] Mukhopadhyay DK, Suryanarayana C, Froes FH, Yolton CF. In: deBarbadillo JJ, et al., editors. Mechanical alloying for structural applications. Materials Park, OH: ASM International, 1993. p. 131–8.
[498] Ahn HJ, Lee KY. Mater Trans Japan Inst Metals 1995;36:297–304.
[499] López Hirata VM, Juárez Martinez U, Cabañas-Moreno JG. Mater Sci Forum 1995;179–181:261–6.
[500] El-Eskandarany MS, Aoki K, Sumiyama K, Suzuki K. Appl Phys Lett 1997;70:1679–81.
[501] El-Eskandarany MS, Aoki K, Sumiyama K, Suzuki K. Scripta Mater 1997;36:1001–9.
[502] Ivanov E, Golubkova GV. J Alloys and Compounds 1992;190:L25–L26.
[503] Morris MA, Morris DG. In: Yavari AR, Desré P, editors. Multilayer amorphization by solid-state reaction and mechanical alloying, vol. 51, Colloq. C4., Suppl. 14, Les Ulis Cedex, France: Les editions de Physique, 1990, p. 211–7.
[504] Bampton CC, Rhodes CG, Mitchell MR, Vassiliou MS, Graves JA. In: Yavari AR, Desré P, editors. Multilayer amorphization by solid-state reaction and mechanical alloying, vol. 51, Colloq. C4., Suppl. 14. Les Ulis Cedex, France: Les editions de Physique, 1990, p. 275–82.
[505] Morris MA, Morris DG. J Mater Sci 1991;26:4687–96.
[506] Xi S, Zhou J, Zhang D, Wang X. Mater Lett 1996;26:245–8.
[507] Kim KJ, El-Eskandarany MS, Sumiyama K, Suzuki K. J Non-Cryst Solids 1993;155:165–70.
[508] Mizutani U, Imaeda C, Murasaki S, Fukunaga T. Mater Sci Forum 1992;88–90:415–22.
[509] Koyano T, Lee CH, Fukunaga T, Mizutani U. Mater Sci Forum 1992;88–90:809–16.
[510] Fair GH, Wood JV. J Mater Sci 1994;29:1935–9.
[511] Elkalkouli R, Grosbras M, Dinhut JF. Nanostructured Mater 1995;5:733–43.
[512] Baláž P, Bastl Z, HavlÍk T, Lipka J, Toth I. Mater Sci Forum 1997;235–238:217–22.
[513] Malhouroux-Gaffet N, Gaffet E. J Alloys and Compounds 1993;198:143–54.
[514] Umemoto M, Shiga S, Okane I. In: Henein H, Oki T, editors. Processing materials for properties. Warrendale, PA: TMS, 1993. p. 679–82.

[515] Umemoto M, Shiga S, Raviprasad K, Okane I. Mater Sci Forum 1995;179–181:165–70.
[516] Ruuskanen P, Heczko O. Key Engng Mater 1993;81–83:159–68.
[517] Pan CW, Hung MP, Chang YH. Mater Sci and Engng 1994;A185:147–52.
[518] Trudeau ML, Schulz R, Zaluski L, Hosatte S, Ryan DH, Doner CB, Tessier P, Strom-Olsen JO, Van Neste A. Mater Sci Forum 1992;88–90:537–44.
[519] Oleszak D, Jachimowicz M, Matyja H. Mater Sci Forum 1995;179–181:215–8.
[520] Burgio N, Iasonna A, Magini M, Martelli S, Padella F. Il Nuovo Cimento 1991;13D:459–76.
[521] Alonso T, Liu Y, McCormick PG. J Mater Sci Lett 1992;11:164–6.
[522] Šepelák V, Rogachev Ayu, Steinike U, Uecker D-Chr, Krumeich F, Wiβmann S, Becker KD. Mater Sci Forum 1997;235–238:139–44.
[523] Thompson JR, Politis C, Kim YC. Mater Sci and Engng 1988;97:31–4.
[524] Chen J, Dou SX, Liu HK. J Alloys and Compounds 1996;244:184–9.
[525] Munoz-Palos JM, Cristina MC, Adeva P. Mater Trans Japan Inst Metals 1996;37:1602–6.
[526] Crew DC, McCormick PG, Street R. Scripta Metall Mater 1995;32:315–8.
[527] Iwamoto N, Uesaka S. Mater Sci Forum 1992;88–90:763–70.
[528] Fei GT, Liu L, Ding XZ, Zhang LD, Zheng QQ. J Alloys and Compounds 1995;229:280–2.
[529] Ma E, Pagan J, Cranford G, Atzmon M. J Mater Res 1993;8:1836–44.
[530] Lee PY, Chen TR, Yang JL, Chin TS. Mater Sci and Engng 1995;A192/193:556–62.
[531] Perdigão MNRV, Jordão JAR, Kiminami CS, Botta Filho WJ. Mater Sci Forum 1997;235–238:151–6.
[532] Kumar KS, Mannan SK. In: Liu CT, Taub AI, Stoloff NS, Koch CC, editors. High temperature ordered intermetallic alloys III, vol. 133. Pittsburgh, PA: Mater. Res. Soc, 1989. p. 415–20.
[533] Viswanadham RK, Mannan SK, Kumar KS. Scripta Metall 1988;22:1011–4.
[534] Esaki H, Tokizane M. Mater Sci Forum 1992;88–90:625–30.
[535] Ochiai S, Shirokura T, Doi Y, Kojima Y. ISIJ Internat 1991;31:1106–12.
[536] Lu L, Lai MO, Zhang S. J Mater Proc Technol 1995;48:683–90.
[537] Schaffer GB, Heron AJ. In: deBarbadillo JJ, et al., editors. Mechanical alloying for structural applications. Materials Park, OH: ASM International, 1993. p. 197–203.
[538] Liu ZG, Guo JT, Hu ZQ. J Alloys and Compounds 1996;234:106–10.
[539] Liu ZG, Guo JT, Hu ZQ. Mater Sci and Engng 1995;A192/193:577–82.
[540] Baláz P, Havlík T, Brianćin J, Kammel R. Scripta Metall Mater 1995;32:1357–62.
[541] Omuro K, Miura H. Japan J Appl Phys 1991;30(5A):L851–853.
[542] Wang KY, Shen TD, Wang JT, Quan MX. Scripta Metall Mater 1991;25:2227–31.
[543] Wang KY, Shen TD, Wang JT, Quan MX. J Mater Sci 1993;28:6474–8.
[544] Oh TS, Choi JS, Hyun DB. Scripta Metall Mater 1995;32:595–600.
[545] Aning AO, Hong C, Desu SB. Mater Sci Forum 1995;179–181:207–13.
[546] Calka A, Radlinski AP. Scripta Metall 1989;23:1497–550.
[547] Zhang DL, Massalski TB. J Mater Res 1994;9:53–60.
[548] Tan M. J Mater Sci 1994;29:1306–9.
[549] Ding J, McCormick PG, Street R. J Alloys and Compounds 1992;189:83–6.
[550] Ameyama K, Okada O, Hirai K, Nakabo N. Mater Trans Japan Inst Metals 1995;36:269–75.
[551] Ahn JH, Chung H. In: Ravi VA, Srivatsan TS, Moore JJ, editors. Processing and fabrication of advanced materials III. Warrendale, PA: TMS, 1994. p. 227–37.
[552] Ahn JH, Lee KR, Cho HK. Mater Sci Forum 1995;179–181:153–8.
[553] Skakov YuA, Edneral NV, Frolov EV, Povolozki JA. Mater Sci Forum 1995;179–181:33–8.
[554] Blouin M, Guay D, Huot J, Schulz R. J Mater Res 1997;12:1492–500.
[555] Oehring M, Bormann R. Mater Sci and Engng 1991;A134:1330–3.
[556] Zotov N, Parlapanski D. J Mater Sci 1994;29:2813–20.
[557] Aoki K, Memezawa A, Masumoto T. J Mater Res 1994;9:39–46.
[558] Abe O, Suzuki Y. Mater Sci Forum 1996;225–227:563–8.
[559] Ivanov E. In: deBarbadillo JJ, et al., editors. Mechanical alloying for structural applications. Materials Park, OH: ASM International, 1993. p. 415–9.
[560] Bokhonov B, Ivanov E, Boldyrev VV. J Alloys and Compounds 1993;199:125–8.

[561] Schiffini L, Mulas G, Daturi M, Ferretti M. In: deBarbadillo JJ, et al., editors. Mechanical alloying for structural applications. Materials Park, OH: ASM International, 1993. p. 457–61.
[562] Cardellini F, Contini V, Mazzone G, Vittori M. Scripta Metall Mater 1993;28:1035–8.
[563] Froes FH, Suryanarayana C. In: Stoloff NS, Sikka VK, editors. Physical metallurgy and processing of intermetallic compounds. New York, NY: Chapman and Hall, 1996. p. 297–350.
[564] Frefer A, Suryanarayana C, Froes FH. In: Moore JJ, Lavernia EJ, Froes FH, editors. Advanced synthesis of engineered materials. Materials Park, OH: ASM International, 1993. p. 213–9.
[565] Qi M, Zhu M, Li GB, Sui H-X, Yang DZ. J Mater Sci Lett 1993;12:66–9.
[566] Gauvin R, Bernier MA, Joy DC, Schmidt M. In: deBarbadillo JJ, et al., editors. Mechanical alloying for structural applications. Materials Park, OH: ASM International, 1993. p. 93–100.
[567] Suryanarayana C, Sundaresan R, Froes FH. Mater Sci and Engng 1992;A150:117–21.
[568] Mukhopadhyay DK, Suryanarayana C, Froes FH. In: Froes FH, Caplan I, editors. Titanium '92: Science and technology. Warrendale, PA: TMS, 1993. p. 829–35.
[569] Radev DD, Klissurski D. J Alloys and Compounds 1994;206:39–41.
[570] Maric R, Ishihara KN, Shingu PH. J Mater Sci Lett 1996;15:1180–3.
[571] Schaffer GB. Scripta Metall Mater 1992;27:1–5.
[572] Stoloff NS, Davies RG. Prog Mater Sci 1966;13:77.
[573] Suryanarayana C, Zhou E, Peng Z, Froes FH. Scripta Metall Mater 1994;30:781–5.
[574] Li W, Suryanarayana C, Froes FH. In: Froes FH, Suryanarayana C, Ward-Close CM, editors. Synthesis/processing of lightweight metallic materials. Warrendale, PA: TMS, 1995. p. 203–13.
[575] Corrias A, Ennas G, Licheri G, Marongiu, Paschina G. Mater Sci and Engng 1991;A145:123–5.
[576] Corrias A, Ennas G, Licheri G, Marongiu, Musinu A, Paschina G. In: deBarbadillo JJ, et al., editors. Mechanical alloying for structural applications. Materials Park, OH: ASM International, 1993. p. 451–6.
[577] Calka A, Radlinski AP. Appl Phys Lett 1991;58:119–21.
[578] Corrias A, Ennas G, Morangiu G, Musinu A, Paschina G, Zedda D. Mater Sci and Engng 1995;A204:211–6.
[579] Millet P, Hwang T. J Mater Sci 1996;31:351–5.
[580] Matteazzi P, Basset D, Miani F, LeCaër G. Nanostructured Mater 1993;2:217–29.
[581] Huang H, McCormick PG. J Alloys and Compounds 1997;256:258–62.
[582] Tanaka T, Nasu S, Ishihara KN, Shingu PH. J Less-Common Metals 1991;171:237–47.
[583] Wang GM, Calka A, Campbell SJ, Kaczmarek WA. Mater Sci Forum 1995;179–181:201–5.
[584] Tanaka T, Nasu S, Nakagawa K, Ishihara KN, Shingu PH. Mater Sci Forum 1992;88–90:269–74.
[585] Murphy BR, Courtney TH. Nanostructured Mater 1994;4:365–9.
[586] Gaffet E, Marco P, Fedoroff M, Rouchaud JC. Mater Sci Forum 1992;88–90:383–90.
[587] El-Eskandarany MS, Sumiyama K, Suzuki K. J Mater Res 1995;10:659–67.
[588] Malchere A, Gaffet E. In: deBarbadillo JJ, et al., editors. Mechanical alloying for structural applications. Materials Park, OH: ASM International, 1993. p. 297–305.
[589] Ye LL, Quan MX. Nanostructured Mater 1995;5:25–31.
[590] El-Eskandarany MS, Konno TJ, Sumiyama K, Suzuki K. Mater Sci and Engng 1996;A217/218:265–8.
[591] Calka A, Kaczmarek WA. Scripta Metall Mater 1992;26:249–53.
[592] Calka A, Williams JS. Scripta Metall Mater 1992;27:999–1004.
[593] Wang GM, Campbell SJ, Calka A, Kaczmarek WA. J Mater Sci 1997;32:1461–7.
[594] Xueming MA, Gang JI. J Alloys and Compounds 1996;245:L30–L32.
[595] Wang GM, Millet P, Calka A, Campbell SJ. Mater Sci Forum 1995;179–181:183–8.
[596] El-Eskandarany MS, Omori M, Ishikuro M, Konno TJ, Takada K, Sumiyama K, Suzuki K. Metall Mater Trans 1996;27A:4210–3.
[597] Eckert J, Jost K, De Haas O, Schultz L. Mater Sci Forum 1997;235–238:133–8.
[598] El-Eskandarany MS, Sumiyama K, Aoki K, Suzuki K. Mater Sci Forum 1992;88–90:801–8.
[599] Millet P, Calka A, Williams JS, Vantenaar GJH. Appl Phys Lett 1993;63:2505–7.
[600] Bodart M, Moret F, Baccino R. In: Capus JM, German RM, editors. Advances in powder

metallurgy and particulate materials, vol. 7. Princeton, NJ: Metal Powder Industries Federation, 1992. p. 207–19.
[601] Chin ZH, Perng TP. Mater Sci Forum 1997;235–238:73–8.
[602] Chin ZH, Perng TP. Appl Phys Lett 1997;70:2380–2.
[603] Shen TD, Koch CC. Nanostructured Mater 1995;5:615–29.
[604] Ogino Y, Miki M, Yamasaki T, Inuma T. Mater Sci Forum 1992;88–90:795–800.
[605] Ogino Y, Yamasaki T, Miki M, Atsumi N, Yoshioka K. Scripta Metall Mater 1993;28:967–71.
[606] Guo W, Martelli S, Padella F, Magini M, Burgio N, Paradiso E, Franzoni U. Mater Sci Forum 1992;88–90:139–46.
[607] Aoki K, Memezawa A, Masumoto T. Appl Phys Lett 1992;61:1037–9.
[608] Brand K, Suryanarayana C, Kieback BF, Froes FH. In: Cadle TM, Narasimhan KS, editors. Advances in powder metallurgy and particulate materials — 1996, vol. 2. Princeton, NJ: Metal Powder Industries Federation, 1996. p. 49–58.
[609] Russel KC. Prog Mater Sci 1985;28:229.
[610] Liu BX. In: Suryanarayana C, editor. Non-equilibrium processing of materials. Oxford: Pergamon, 1999. p. 197–224.
[611] Koch CC. Internat Mater Rev 1988;33:201–19.
[612] Ermakov AE, Yurchikov EE. Elsukov EP Fiz Tverd Tela 1982;4:1947–52.
[613] Elsukov EP, Barinov VA, Galakhov VR, Yurchikov EE, Ermakov AE. Phys Metals and Metallogr 1983;55(2):119–23.
[614] Bakker H, Zhou GF, Yang H. Mater Sci Forum 1995;179–181:47–52.
[615] Jang JSC, Koch CC. J Mater Res 1990;5:498–510.
[616] Seki Y, Johnson WL. In: Clauer AH, deBarbadillo JJ, editors. Solid state powder processing. Warrendale, PA: TMS, 1990. p. 287–97.
[617] Hellstern E, Fecht HJ, Fu Z, Johnson WL. J Appl Phys 1989;65:305–10.
[618] Bakker H, Modder IW, Zhou GF, Yang H. Mater Sci Forum 1997;235–238:477–86.
[619] Gialanella S, Newcomb SB, Cahn RW. In: Yavari AR, editor. Ordering and disordering in alloys. London: Elsevier Applied Science Publishers, 1992. p. 67–78.
[620] Zhou GF, Bakker H. Scripta Mater 1996;34:29–35.
[621] Oehring M, Bormann R. J Phys Colloq 1990;51:169–74.
[622] Mukhopadhyay DK, Suryanarayana C, Froes FH. In: Phillips M, Porter J, editors. Advances in powder metallurgy and particulate materials — 1995, vol. 1. Princeton, NJ:: Metal Powder Industries Federation, 1995. p. 123–33.
[623] Di LM, Bakker H. J Appl Phys 1992;71:5650–3.
[624] Di LM, Loeff PI, Bakker H. J Less-Common Metals 1991;168:183–93.
[625] Koch CC, Cho YS. Nanostructured Mater 1992;1:207–12.
[626] Di LM, Bakker H, de Boer FR. Physica 1992;B182:91–8.
[627] Di LM, Bakker H, Tamminga Y, de Boer FR. Phys Rev 1991;B44:2444–51.
[628] Gialanella S, Guella M, Baró MD, Malagelada JM, Suriñach S. In: deBarbadillo JJ, et al., editors. Mechanical alloying for structural applications. Materials Park, OH: ASM International, 1993. p. 321–5.
[629] Zhou GF, Bakker H. Phys Rev 1994;B49:12507–18.
[630] Loeff PI, Bakker H. Scripta Metall 1988;22:401–4.
[631] Suzuki K, Fukunaga T. J Alloys and Compounds 1993;194:303–9.
[632] Weeber AW, Bakker H. J Less-Common Metals 1988;141:93–102.
[633] Koch CC, Jang JSC, Lee PY. In: Arzt E, Schultz L, editors. New materials by mechanical alloying techniques. Oberursel, Germany: DGM Informationgesellschaft, 1989. p. 101–10.
[634] Wernick JH. In: Westbrook JH, editor. Intermetallic compounds. New York, NY: Wiley, 1967. p. 197.
[635] Zhou GF, Bakker H. Acta Metall Mater 1994;42:3009–17.
[636] Jang JSC, Tsau CH. J Mater Sci 1993;28:982–8.
[637] Gialanella S, Yavari AR, Cahn RW. Scripta Metall Mater 1992;26:1233–8.
[638] Yang H, Bakker H. Mater Sci Forum 1994;150–151:109.
[639] Zhou GF, Bakker H. Intermetallics 1994;2:103–10.

[640] Zhou GF, Bakker H. Phys Rev 1993;B48:13383–98.
[641] Robinson JS, McCormick PG, Street R. J Phys C: Condens Matter 1995;7:4259.
[642] Xia SK, Larica C, Rodriguez VA, Rizzo Assunção FC, Baggio-Saitovitch. Mater Sci Forum 1996;225:389–94.
[643] Zhou GF, Bakker H. Phys Rev Lett 1994;73:344–7.
[644] Di LM, Loeff PI, Bakker H. Phys Stat Sol (a) 1989;117:K99–K101.
[645] Schwarz RB, Petrich RR. J Less-Common Metals 1988;140:171–84.
[646] Benameur T, Yavari AR. J Mater Res 1992;7:2971–7.
[647] Yavari AR. Acta Metall 1993;41:1391–6.
[648] Baró MD, Suriñach S, Malagelada J. In: deBarbadillo JJ, et al., editors. Mechanical alloying for structural applications. Materials Park, OH: ASM International, 1993. p. 343–8.
[649] Cardellini F, Contini V, Mazzone G. Scripta Metall Mater 1995;32:641–6.
[650] Gialanella S, Delorenzo R, Marino F, Guella M. Intermetallics 1995;3:1–8.
[651] Buckel W, Hilsch R. Z Phys 1952;131:420.
[652] Klement W, Willens RH, Duwez P. Nature 1960;187:869–71.
[653] Luborsky FE, editor. Amorphous metallic alloys. London: Butterworths, 1983.
[654] Anantharaman TR, editor. Metallic glasses — production, properties, and applications. Aedermannsdorf, Switzerland: Trans Tech, 1984.
[655] Güntherodt HJ, Beck H, editors. Glassy metals, vol. 1 and 2. Berlin, Germany: Springer-Verlag, 1981, 1983.
[656] Cahn RW. In: Zarzycki J, editor. Glasses and amorphous materials, vol. 9 of Materials Science and Technology — a comprehensive treatment. Weinheim, Germany: VCH Verlagsgesellschaft, 1991. p. 493–548.
[657] Cahn RW, Greer AL. In: Cahn RW, Haasen P, editors. Physical metallurgy, 4th ed, vol. II. Amsterdam, The Netherlands: Elsevier Science BV, 1996. p. 1723–830.
[658] Ermakov AE, Barinov VA, Yurchikov EE. Phys Met Metallogr 1982;54(5):90–6.
[659] Tsurui T, Tsai AP, Inoue A, Masumoto T. J Alloys and Compounds 1995;218:L7–L10.
[660] Zhang FX, Wang WK. J Alloys and Compounds 1996;240:256–60.
[661] Wang G, Zhang D, Chen H, Lin B, Wang W, Dong Y. Phys Lett 1991;A155:57–61.
[662] Oleszak D, Shingu PH. Mater Sci Forum 1997;235–238:91–6.
[663] Dong YD, Wang WH, Liu L, Xiao KQ, Tong SH, He YZ. Mater Sci and Engng 1991;A134:867–71.
[664] Burzynska-Szyske M, Fadeeva VI, Matyja H. Mater Sci Forum 1997;235–238:97–102.
[665] Schwarz RB, Hannigan JW, Sheinberg H, Tiainen T. In: Gummeson PU, Gustafson DA, editors. Modern developments in powder metallurgy, vol. 21. Princeton, NJ: Metal Powder Industries Federation, 1988. p. 415–27.
[666] Chen G, Wang K, Wang J, Jiang H, Quan M. In: deBarbadillo JJ, et al., editors. Mechanical alloying for structural applications. Materials Park, OH: ASM International, 1993. p. 183–7.
[667] El-Eskandarany MS, Aoki K, Suzuki K. Scripta Metall Mater 1991;25:1695–700.
[668] El-Eskandarany MS, Aoki K, Suzuki K. J Appl Phys 1992;71:2924–30.
[669] Makhlouf SA, Sumiyama K, Suzuki K. J Alloys and Compounds 1993;199:119–24.
[670] Dougherty GM, Shiflet GJ, Poon SJ. Acta Metall Mater 1994;42:2275–83.
[671] El-Eskandarany MS, Aoki K, Suzuki K. Appl Phys Lett 1992;60:1562–3.
[672] El-Eskandarany MS, Aoki K, Itoh H, Suzuki K. J Less-Common Metals 1991;169:235–44.
[673] El-Eskandarany MS, Aoki K, Suzuki K. J Alloys and Compounds 1992;186:15–31.
[674] El-Eskandarany MS, Aoki K, Suzuki K. J Non-Cryst Solids 1992;150:472–7.
[675] Saji S, Abe S, Matsumoto K. Mater Sci Forum 1992;88–90:367–74.
[676] Kojima Y, Senna M, Shinohara T, Ono S, Sumiyama K, Suzuki K. J Alloys and Compounds 1995;227:97–101.
[677] Wu NQ, Wu JM, Li ZZ, Wang GX. Mater Trans Japan Inst Metals 1997;38:255–9.
[678] Eckert J, Seidel M, Schultz L. Mater Sci Forum 1996;225–227:113–8.
[679] El-Eskandarany MS, Aoki K, Suzuki K. Metall Trans 1992;23A:2131–40.
[680] Michel D, Mazerolles L, Berthet P, Gaffet E. Eur J Solid State Inorg Chem 1995;32:673–82.

[681] Sakurai M, Fukunaga T, Sumiyama K, Suzuki K. J Japan Soc Powder Powder Metall 1991;38:63–6.
[682] Suzuki K. J Non-Cryst Solids 1989;112:23–32.
[683] Tang J. Mater Sci Forum 1996;225–227:477–82.
[684] Atzeni C, Pes M, Sanna U, Corrias A, Paschina G, Zedda D. Adv Perform Mater 1994;1:243–53.
[685] Corrias A, Ennas G, Marongiu G, Paschina G. J Mater Sci 1991;26:5081–4.
[686] Kimura H, Takada F, Myung WN. Mater Sci and Engng 1988;97:125–8.
[687] Omuro K, Miura H. Appl Phys Lett 1992;60:1433–5.
[688] Okadome K, Unno K, Arakawa T. J Mater Sci 1995;30:1807–10.
[689] Sadano H, Arakawa T. Mater Trans Japan Inst Metals 1996;37:1099–102.
[690] López-Hirata VM, Juárez Martínez U, Cabañas-Moreno JG. Mater Sci Forum 1995;189–191:261–6.
[691] Kimura H, Kimura M, Ban T. In: Lee PW, Moll JH, editors. Rapidly solidified materials: properties and processing. Materials Park, OH: ASM International, 1988. p. 171–6.
[692] Hellstern E, Schultz L. Phil Mag 1987;B56:443–8.
[693] Xia SK, Rizzo Assunção FC, Baggio-Saitovich E. Mater Sci Forum 1996;225–227:459–64.
[694] Schanzer M, Mehrer H. J de Physique 1990;51(Colloq. 4, Suppl. 14):87–93.
[695] Morris MA. Mater Sci Forum 1992;88–90:671–8.
[696] Matsuki K, Inoue A, Kimura HM, Masumoto T. Mater Sci and Engng 1988;97:47–51.
[697] Inoue A, Kimura HM, Matsuki K, Masumoto T. J Mater Sci Lett 1987;6:979–81.
[698] Zhang H, Naugle DG. Appl Phys Lett 1992;60:2738–40.
[699] Miura H, Isa S, Omuro K. Japan J Appl Phys 1990;29:L339–L342.
[700] Battezzati L, Baricco M, Enzo S, Schiffini L, Soletta I, Cocco G. Mater Sci Forum 1992;88–90:771–8.
[701] Hunt JA, Soletta I, Enzo S, Meiya L, Havill RL, Battezzati L, Cocco G, Cowlam N. Mater Sci Forum 1995;179–181:255–60.
[702] Politis C, Johnson WL. J Appl Phys 1986;60:1147–51.
[703] Baricco M, Battezzati L, Cocco G, Soletta I, Enzo S. J Non-Cryst Solids 1993;156–158:527–31.
[704] Hellstern E, Schultz L. Appl Phys Lett 1986;48:124–6.
[705] Jang JSC, Koch CC. Scripta Metall 1989;23:1805–10.
[706] Boldrick MS, Wagner CNJ. Mater Sci and Engng 1991;A134:872–5.
[707] Suriñach S, Baro MD, Segura J, Clavaguera-Mora MT, Clavaguera N. Mater Sci and Engng 1991;A134:1368–71.
[708] Osagawara T, Inoue A, Masumoto T. Mater Sci Forum 1992;88–90:423–30.
[709] Nasu T, Koch CC, Nagaoka K, Itoh N, Sakurai M, Suzuki K. Mater Sci and Engng 1991;A134:1385–8.
[710] Omuro K, Miura H. Mater Sci Forum 1995;179–181:273–8.
[711] Miao WF, Li GS, Li SL, Wang JT. Acta Phys (Sinica) 1992;41:924–8.
[712] Osagawara T, Inoue A, Masumoto T. Mater Sci and Engng 1991;A134:1338–71.
[713] Le Caër G, Matteazzi P, Fultz B. J Mater Res 1992;7:1387–95.
[714] Pan CW, Hung MP, Chang YH. Mater Sci and Engng 1994;A185:147–52.
[715] Enzo S, Macri P, Rose P, Cowlam N. In: deBarbadillo JJ, et al., editors. Mechanical alloying for structural applications. Materials Park, OH: ASM International, 1993. p. 101–8.
[716] Fultz B, Le Caër G, Matteazzi P. J Mater Res 1989;4:1450–5.
[717] Bai H, Michaelsen C, Sinkler W, Bormann R. Mater Sci Forum 1997;235–238:361–6.
[718] Shen TD, Wang KY, Quan MX, Hu ZQ. Appl Phys Lett 1993;63:1637–9.
[719] Gaffet E. Mater Sci and Engng 1991;A149:85–94.
[720] Krauss W, Politis C, Weimar P. Metal Powder Rep 1988;43:231–8.
[721] Thompson JR, Politis C, Kim YC. Mater Sci Forum 1992;88–90:545–52.
[722] Matsuki K, Abe F, Inoue A, Masumoto T. Mater Sci Forum 1992;88–90:313–20.
[723] Liu W, Wu H, Lei Y, Wang Q, Wu J. J Alloys and Compounds 1997;252:234–7.
[724] Hazelton LE, Nielsen CA, Deshmukh UV, Pierini PE. In: Froes FH, deBarbadillo JJ, editors.

Structural applications of mechanical alloying. Materials Park, OH: ASM International, 1990. p. 243–50.
[725] Cocco G, Enzo S, Barrett N, Roberts KJ. J Less-Common Metals 1989;154:177–86.
[726] Yang JY, Zhang TJ, Cui K, Li XG, Zhang J. J Alloys and Compounds 1996;242:153–6.
[727] Politis C. Physica 1985;B135:286–9.
[728] Cho YS, Koch CC. Mater Sci and Engng 1993;A161:65–73.
[729] Harada T, Kuji T. J Alloys and Compounds 1996;232:238–43.
[730] Li B, Liu L, Ma XM, Dong YD. J Alloys and Compounds 1993;202:161–3.
[731] Kim MS, Koch CC. J Appl Phys 1987;62:3450–3.
[732] Hirosawa S, Makita K, Ikegami T, Umemoto M. In: Proc. Sixth International Conf. on Ferrite, Japan Soc. Powder Powder Metall: Tokyo, Japan. 1992. p. 1100–3.
[733] Itsukaichi T, Umemoto M, Okane I, Horosawa S. J Alloys and Compounds 1993;193:262–5.
[734] Cocco G, Enzo S, Barrett NT, Roberts KJ. Phys Rev 1992;B45:7066–76.
[735] Li M, Enzo S, Soletta I, Cowlam N, Cocco G. J Phys C: Condens Matter 1993;5:5235–44.
[736] Enzo S, Bonetti E, Soletta I, Cocco G. J Phys D: Appl Phys 1991;24:209–16.
[737] Nasu T, Nagaoka K, Takahashi S, Suganuma E, Sekiuchi T, Fukunaga T, Suzuki K. Mater Trans Japan Inst Metals 1989;30:620–3.
[738] Petzoldt F. J Less-Common Metals 1988;140:85–92.
[739] Tiainen TJ, Schwarz RB. J Less-Common Metals 1988;140:99–112.
[740] Merk N, Tanner LE. Scripta Metall Mater 1991;25:309–13.
[741] Lee PY, Chen TR. J Mater Sci Lett 1994;13:888–90.
[742] Xia SK, Baggio-Saitovich E, Rizzo Assunçao FC, Peña Rodriguez VA. J Phys C: Condens Matter 1993;5:2729–38.
[743] Sun DZ, Cheng LZ, Zhang YM, Ho KY. J Alloys and Compounds 1992;186:33–5.
[744] Cocco G, Enzo S, Schiffini L, Battezzati L. Mater Sci and Engng 1988;97:43–6.
[745] Fukunaga T, Homma Y, Suzuki K, Misawa M. Mater Sci and Engng 1991;A134:987–91.
[746] Kimura H, Takada F. Mater Sci and Engng 1988;97:53–7.
[747] Weeber AW, Bakker H. J Phys F: Metal Phys 1988;18:1359–69.
[748] Brüning R, Altounian Z, Srom-Olsen JO, Shultz L. Mater Sci and Engng 1988;97:317–20.
[749] Lee PY, Koch CC. Appl Phys Lett 1987;50:1578–80.
[750] Petzoldt F, Scholz B, Kunze HD. Mater Sci and Engng 1988;97:25–9.
[751] Mizutani U, Lee CH. J Mater Sci 1990;25:399–406.
[752] Weeber AW, Wester AJH, Haag WJ, Bakker H. Physica 1987;B145:349–52.
[753] Haruyama O, Asahi N. Mater Sci Forum 1992;88–90:333–8.
[754] Nasu T, Nagaoka K, Takahashi S, Fukunaga T, Suzuki K. Mater Trans Japan Inst Metals 1989;30:146–9.
[755] Padella F, Paradiso E, Burgio N, Magini M, Martelli S, Guo W, Iasonna A. J Less-Common Metals 1991;175:79–90.
[756] Politis C, Thompson JR. In: Tenhover M, Johnson WL, Tannner LE, editors. Science and technology of rapidly quenched alloys, vol. 80. Pittsburgh, PA: Mater. Res. Soc, 1987. p. 91–6.
[757] Ishida T, Tamaru S. J Mater Sci Lett 1993;12:1851–3.
[758] Gaffet E, Harmelin M. In: Froes FH, deBarbadillo JJ, editors. Structural applications of mechanical alloying. Materials Park, OH: ASM International, 1990. p. 257–64.
[759] Schnitzke K, Schultz L, Wecker J, Katter M. Appl Phys Lett 1990;57:2853–5.
[760] El-Eskandarany MS, Itoh F, Aoki K, Suzuki K. J Non-Cryst Solids 1990;117–118:729–32.
[761] Liu L, Chu ZQ, Dong YD. J Alloys and Compounds 1992;186:217–21.
[762] Veltl G, Scholz B, Kunze HD. Mater Sci and Engng 1991;A134:1410–3.
[763] Suzuki T, Ino T, Nagumo M. Mater Sci Forum 1992;88–90:639–46.
[764] Nash P, Kim H, Choo H, Ardy H, Hwang SJ, Nash AS. Mater Sci Forum 1992;88–90:603–10.
[765] Ahn JH, Choi CJ, Chung HS. In: Ravi VA, Srivatsan TS, editors. Processing and fabrication of advanced materials for high temperature applications II. Warrendale, PA: TMS, 1993. p. 33–44.
[766] Chen G, Wang K. In: deBarbadillo JJ, et al., editors. Mechanical alloying for structural applications. Materials Park, OH: ASM International, 1993. p. 149–55.
[767] Qi M, Zhu M, Li GB, Sui HX, Yang DZ. J Mater Sci Lett 1993;12:66–9.

[768] Park YH, Hashimoto H, Watanabe R. Mater Sci Forum 1992;88–90:59–66.
[769] Ahn JH, Chung HS, Watanabe R, Park YH. Mater Sci Forum 1992;88–90:347–54.
[770] Ahn JH, Lee KR, Cho HK. Mater Sci Forum 1995;179–180:153–8.
[771] Itsukaichi T, Masuyama K, Umemoto M, Okane I, Cabanas-Moreno JG. J Mater Res 1993;8:1817–28.
[772] El-Eskandarany MS. J Alloys and Compounds 1996;234:67–82.
[773] Nagarajan R, Ranganathan S. Mater Sci and Engng 1994;A179/180:168–72.
[774] Park YH, Hashimoto H, Watanabe R. Mater Sci Forum 1992;88–90:59–66.
[775] Murty BS, Ranganathan S, Mohan Rao M. Mater Sci and Engng 1992;A149:231–40.
[776] Chu BL, Chen CC, Perng TP. Metall Trans 1992;A23:2105–10.
[777] Fukunaga T, Misawa M, Suzuki K, Mizutani U. Mater Sci Forum 1992;88–90:325–32.
[778] Wang KY, He A, Quan M, Chen G. In: deBarbadillo JJ, et al., editors. Mechanical alloying for structural applications. Materials Park, OH: ASM International, 1993. p. 21–5.
[779] Battezzati L, Enzo S, Schiffini L, Cocco G. J Less-Common Metals 1988;145:301–8.
[780] Murty BS, Mohan Rao M, Ranganathan S. Scripta Metall Mater 1990;24:1819–24.
[781] Sundaresan R, Jackson AG, Krishnamurthy S, Froes FH. Mater Sci and Engng 1988;97:115–9.
[782] Thompson JR, Politis C. Europhys Lett 1987;3:199–205.
[783] Oehring M, Yan ZH, Klassen T, Bormann R. Phys Stat Sol (a) 1992;131:671–89.
[784] Counihan PJ, Crawford A, Thadhani NN. Mater Sci and Engng 1999;A267:26–35.
[785] Parlapanski D, Denev S, Ruseva R, Gatev E. J Less-Common Metals 1991;171:231–6.
[786] Fukunaga T, Homma Y, Misawa M, Suzuki K. J Non-Cryst Solids 1990;117–118:721–4.
[787] Yamasaki T, Ogino Y, Morishita K, Fukuoka K, Atou F, Syono Y. Mater Sci and Engng 1994;A179/180:220–3.
[788] El-Eskandarany MS, Sumiyama K, Suzuki K. Sci Rep RITU 1996;A42:31–8.
[789] Herr U, Samwer K. Nanostructured Mater 1992;1:515–21.
[790] Zhang H, Su Y, Wang L, Wu L, Tan Z, Zhang B. J Alloys and Compounds 1994;204:27–31.
[791] Ma E, Atzmon M. Phys Rev Lett 1991;67:1126–9.
[792] Ma E, Atzmon M. J Alloys and Compounds 1993;194:235–44.
[793] Fecht HJ, Han G, Fu Z, Johnson WL. J Appl Phys 1990;67:1744–8.
[794] Eckert J, Seidel M, Schlorke N, Kübler A, Schultz L. Mater Sci Forum 1997;235–238:23–8.
[795] Seidel M, Eckert J, Schultz L. Mater Sci Forum 1997;235–238:29–34.
[796] Sagel A, Wunderlich RK, Fecht H. J Mater Sci Forum 1997;235–238:389–94.
[797] Eckert J, Schultz L, Urban K. J Less-Common Metals 1988;145:283–91.
[798] Weeber AW, Bakker H. Mater Sci and Engng 1988;97:133–5.
[799] Ahn JH, Park YK. J Mater Sci Lett 1999;18:17–9.
[800] El-Eskandarany MS, Aoki K, Suzuki K. J Alloys and Compounds 1991;177:229–44.
[801] Tang J, Zhao W, Li L, Falster AU, Simmons Jr WB, Zhou WL, Ikuhara Y, Zhang JH. J Mater Res 1996;11:733–8.
[802] Gaffet E. Mater Sci and Engng 1991;A136:161–9.
[803] Inoue A, Matsuki K, Masumoto T. Mater Sci Forum 1992;88:305–12.
[804] Calka A, Radlinski AP. Mater Sci and Engng 1989;A118:131–5.
[805] Alonso T, Yang H, Liu Y, McCormick PG. Appl Phys Lett 1992;60:833–4.
[806] Nakamura T, Inoue A, Matsuki K, Masumoto T. J Mater Sci Lett 1989;8:13–6.
[807] Chen Y, Le Hazif R, Martin G. Mater Sci Forum 1992;88–90:35–41.
[808] Aoki K, Memezawa A, Masumoto T. J Mater Res 1993;8:307–13.
[809] Takeuchi T, Koyano T, Utsumi M, Fukunaga T, Kaneko K, Mizutani U. Mater Sci and Engng 1994;A179/180:224–8.
[810] Shen TD, Koch CC, McCormick TL, Nemanich RJ, Huang JY, Huang JG. J Mater Res 1995;10:139–48.
[811] Liao J, Senna M. Mater Sci Forum 1992;88–90:753–8.
[812] Fukamichi K, Goto T, Fukunaga T, Suzuki K. Mater Sci and Engng 1991;A133:245–7.
[813] Eckert J, Schultz L, Hellstern E, Urban K. J Appl Phys 1988;64:3224–8.
[814] Trudeau ML, Schulz R, Dussault D, Van Neste A. Phys Rev Lett 1990;64:99–102.
[815] Trudeau ML. Appl Phys Lett 1994;64:3661–3.

[816] Nash P, Higgins GT, Dillinger N, Hwang SJ, Kim H. In: Gasbarre TG, Jandeska WF, editors. Advances in powder metallurgy — 1989, vol. 2. Princeton, NJ: Metal Powder Industries Federation, 1989. p. 473–9.
[817] Schwarz RB, Rubin JB. J Alloys and Compounds 1993;194:189–97.
[818] Schwarz RB, Johnson WL. Phys Rev Lett 1983;51:415–8.
[819] Hellstern E, Schultz L. Mater Sci and Engng 1987;93:213–6.
[820] Lee CH, Fukunaga T, Yamada Y, Mizutani U, Okamoto H. J Phase Equilibria 1993;14:167–71.
[821] Gaffet E, Faudot F, Harmelin M. Mater Sci Forum 1992;88–90:375–82.
[822] Massobrio C. J de Physique 1990;51(Colloq. 4, Suppl. 14):55–61.
[823] Beke DL, Loeff PI, Bakker H. Acta Metall Mater 1991;39:1259–66.
[824] Beke DL, Bakker H, Loeff PI. Acta Metall Mater 1991;39:1267–73.
[825] Zhang H. J Phys C: Condens Matter 1993;5:L337–L342.
[826] Chakk Y, Berger S, Weiss BZ, Brook-Levinson E. Acta Metall Mater 1994;42:3679–85.
[827] Egami T, Waseda Y. J Non-Cryst Solids 1984;64:113–34.
[828] Miedema AR, Philips Tech. Rev. 1976;36:217. Also, deBoer FR, Boom R, Mattens WCM, Miedema AR, Niessen AK. In: deBoer FR, Pettifor DG, editors. Cohesion in metals. Elsevier, North-Holland: Amsterdam, The Netherlands, 1988.
[829] Bakker H. In: Enthalpies in alloys — Miedema's semi-empirical model. Zuerich, Switzerland: Trans Tech Publications, 1998 (vol. 1 of Materials Science Foundations).
[830] Weeber AW, Loeff PI, Bakker H. J Less-Common Metals 1988;145:293–9.
[831] Eckert J, Schultz L, Urban K. In: Arzt E, Schultz L, editors. New materials by mechanical alloying techniques. Oberursel, Germany: DGM Informationgesellschaft, 1989. p. 85–90.
[832] Loeff PI, Spit FHM, Bakker H. J Less-Common Metals 1988;145:271–5.
[833] Saunders N, Miodownik AP. CALPHAD. Oxford: Pergamon, 1998.
[834] Wagner CNJ, Boldrick MS. J Alloys and Compounds 1993;194:295–302.
[835] Zhou GF, Bakker H. Phys Rev Lett 1994;72:2290–3.
[836] Biegel W, Krebs HU, Michaelsen C, Freyhardt HC, Hellstern E. Mater Sci and Engng 1988;97:59–62.
[837] Inoue A. In: Suryanarayana C, editor. Non-equilibrium processing of materials. Oxford, UK: Pergamon, 1999. p. 375–415.
[838] Ashley S. Mech Engng 1998;120(6):72–4.
[839] Gleiter H. Prog Mater Sci 1989;33:223–315.
[840] Suryanarayana C, Koch CC. In: Suryanarayana C, editor. Non-equilibrium processing of materials. Oxford: Pergamon, 1999. p. 313–46.
[841] Shingu PH, Huang B, Nishitani SR, Nasu S. Suppl Trans Japan Inst Metals 1988;29:3–10.
[842] Koch CC. Nanostructured Mater 1997;9:13–22.
[843] Hellstern E, Fecht HJ, Garland C, Johnson WL. In: McCandlish LE, Polk DE, Siegel RW, Kear BH, editors. Multicomponent ultrafine microstructures, vol. 132. Pittsburgh, PA: Mater. Res. Soc, 1989. p. 137–42.
[844] Li S, Wang K, Sun L, Wang Z. Scripta Metall Mater 1992;27:437–42.
[845] Eckert J, Holzer JC, Krill III CE, Johnson WL. J Mater Res 1992;7:1751–61.
[846] Börner I, Eckert J. Mater Sci Forum 1996;225–227:377–82.
[847] Suryanarayana C, Froes FH. Nanostructured Mater 1993;3:147–53.
[848] Naser J, Reinhemann W, Ferkel H. Mater Sci and Engng 1997;A234:467–9.
[849] Zaluski L, Zaluska A, Tessier P, Ström-Olsen JO, Schulz R. Mater Sci Forum 1996;225–227:853–8.
[850] Schaffer GB, McCormick PG. Appl Phys Lett 1989;55:45–6.
[851] McCormick PG, Wharton VN, Schaffer GB. In: Small WM, editor. Physical chemistry of powder metals production and processing. Warrendale, PA: TMS, 1989. p. 19–34.
[852] Carry M. Phil Mag 1894;34:470–5.
[853] Schaffer GB, McCormick PG. Metall Trans 1991;A22:3019–24.
[854] Ding J, Tsuzuki T, McCormick PG. J Amer Ceram Soc 1996;79:2956–8.
[855] Ding J, Tsuzuki T, McCormick PG, Street R. J Phys D: Appl Phys 1996;29:2365–9.
[856] Ding J, Tsuzuki T, McCormick PG, Street R. J Alloys and Compounds 1996;234:L1–L3.

[857] Schaffer GB, McCormick PG. Metall Trans 1990;A21:2789–94.
[858] Schaffer GB, McCormick PG. J Mater Sci Lett 1990;9:1014–6.
[859] Yang H, Nguyen G, McCormick PG. Scripta Metall Mater 1995;32:681–4.
[860] Schaffer GB, McCormick PG. Scripta Metall 1989;23:835–8.
[861] Takacs L, Pardavi-Horvath M. In: Shull RD, Sanchez JM, editors. Nanophases and nanocrystalline structures. Warrendale, PA: TMS, 1994. p. 135–44.
[862] Shen TD, Wang KY, Quan MX, Wang JT. Scripta Metall Mater 1991;25:2143–6.
[863] Shen TD, Wang KY, Wang JT, Quan MX. Mater Sci and Engng 1992;A151:189–95.
[864] Durisin J, Orolínová M, Durisinová K, Katana V. J Mater Sci Lett 1994;13:688–9.
[865] Xi S, Zhou J, Wang X, Zhang D. J Mater Sci Lett 1996;15:634–5.
[866] Takacs L. Mater Sci Forum 1996;225–227:553–8.
[867] McCormick PG, Alonso T, Liu Y, Lincoln FJ, Parker TC, Schaffer GB. In: Bautista RG, Jackson N, editors. Rare earths — resources, science, technology, and applications. Warrendale, PA: TMS, 1992. p. 247.
[868] Ding J, Miao WF, McCormick PG, Street R. Appl Phys Lett 1995;67:3804–6.
[869] Pardavi-Horvath M, Takacs L. IEEE Trans Mag 1992;28:3186–8.
[870] Takacs L. Mater Lett 1992;13:119–24.
[871] Baburaj EG, Hubert KT, Froes FH. J Alloys and Compounds 1997;257:146–9.
[872] Alonso T, Liu Y, Dallimore MP, McCormick PG. Scripta Metall Mater 1993;29:55–8.
[873] Yang H, McCormick PG. J Mater Sci Lett 1993;12:1088–91.
[874] McCormick PG, Liu Y, Yang H, Nguyen G, Alonso T. In: deBarbadillo JJ, et al., editors. Mechanical alloying for structural applications. Materials Park, OH: ASM International, 1993. p. 165–9.
[875] McCormick PG, Wharton VN, Reyhani MM, Schaffer GB. In: Van Aken DC, Was GS, Ghosh AK, editors. Microcomposites and nanophase materials. Warrendale, PA: TMS, 1991. p. 65–79.
[876] Yang H, McCormick PG. J Solid State Chem 1994;110:136–41.
[877] Mukhopadhyay DK, Prisbrey KA, Suryanarayana C, Froes FH. In: Bose A, Dowding RJ, editors. Tungsten and refractory metals 3. Princeton, NJ: Metal Powder Industries Federation, 1996. p. 239–46.
[878] Yang H, McCormick PG. J Solid State Chem 1993;107:258–63.
[879] Ding J, Tsuzuki T, McCormick PG. Nanostructured Mater 1997;8:75–81.
[880] Takacs L. Mater Res Soc Symp Proc 1993;286:413–8.
[881] Schaffer GB, McCormick PG. Metall Trans 1992;A23:1285–90.
[882] Aning AO, Hong C, Desu SB. Mater Sci Forum 1995;179–181:207–14.
[883] Matteazzi P, Le Caër G. J Amer Ceram Soc 1992;75:2749–55.
[884] Tschakarov ChrG, Gospodinov GG, Bontschev A. J Solid State Chem 1982;41:244.
[885] Matteazzi P, Le Caër G. J Amer Ceram Soc 1991;74:1382–90.
[886] Matteazzi P, Le Caër G. J Alloys and Compounds 1992;187:305–15.
[887] Pardavi-Horvath M, Takacs L. Scripta Metall Mater 1995;33:1731–40.
[888] Du Y, Li S, Zhang K, Lu K. Scripta Mater 1997;36:7–14.
[889] Milham CD. In: Henein H, Oki T, editors. Processing materials for properties. Warrendale, PA: TMS, 1993. p. 449–52.
[890] Corrias A, Paschina G, Sirigu P, Zedda D. Mater Sci Forum 1997;235–238:199–204.
[891] Chen Y, Ninham BW, Ogarev V. Scripta Metall Mater 1995;32:19–22.
[892] Chen Y, Hwang T, Marsh M, Williams JS. Metall Mater Trans 1997;A28:1115–21.
[893] Courtney TH, Wang Z. Scripta Metall Mater 1992;27:777–82.
[894] Shen TD, Koch CC. Acta Mater 1996;44:753–61.
[895] Eckert J, Holzer JC, Li M, Johnson WL. Nanostructured Mater 1993;2:433–9.
[896] Calka A, Williams JS, Millet P. Scripta Metall Mater 1992;27:1853–7.
[897] Yang E, Wagner CNJ, Boldrick MS. Key Engng Mater 1993;81–83:663–8.
[898] Chen GH, Suryanarayana C, Froes FH. Metall Mater Trans 1995;A26:1379–87.
[899] Goodwin PS, Ward-Close CM. Mater Sci Forum 1995;179–181:411–8.
[900] Chen Y, Hwang T, Marsh M, Williams JS. Metall Mater Trans 1997;A28:1115–21.

[901] Goodwin PS, Ward-Close C. In: deBarbadillo JJ, et al., editors. Mechanical alloying for structural applications. Materials Park, OH: ASM International, 1993. p. 149–55.
[902] Goodwin PS, Mukhopadhyay DK, Suryanarayana C, Froes FH, Ward-Close CM. In: Blenkinsop P, et al., editors. Titanium '95, vol. 3. London, UK: Institute of Materials, 1996. p. 149–55.
[903] Singer RF, Oliver WC, Nix WD. Metall Trans 1980;A11:1895–901.
[904] Mishurda JC, Suryanarayana C, Froes FH, University of Idaho, Moscow, ID, 1994, unpublished research.
[905] Courtney TH. Reviews in Particulate Materials 1994;2:63–116.
[906] Courtney TH. Mater Trans Japan Inst Metals 1995;36:110–22.
[907] Gaffet E, Abdellaoui M, Gaffet NM. Mater Trans Japan Inst Metals 1995;36:198–209.
[908] Magini M, Iasonna A. Mater Trans Japan Inst Metals 1995;36:123–33.
[909] Watanabe R, Hashimoto H, Lee GG. Mater Trans Japan Inst Metals 1995;36:102–9.
[910] Le Brun P, Froyen L, Delaey L. Mater Sci and Engng 1993;A161:75–82.
[911] Bassett D, Matteazzi P, Miani F. Mater Sci and Engng 1994;A174:71–4.
[912] Dallimore MP, McCormick PG. Mater Trans Japan Inst Metals 1996;37:1091–8.
[913] Bhattacharya AK, Arzt E, Scripta Metall. Mater. 1992;27:635–9; 1993;28:395–400.
[914] Aikin BJM, Courtney TH. Metall Trans 1993;A24:645–57.
[915] Aikin BJM, Courtney TH. Metall Trans 1993;A24:2465–71.
[916] Maurice D, Courtney TH. Metall Mater Trans 1996;A27:1981–6.
[917] Abdellaoui M, Gaffet E. Acta Mater 1996;44:725–34.
[918] Courtney TH, Maurice DR. Scripta Mater 1996;34:5–11.
[919] Abdellaoui M, Gaffet E. J Alloys and Compounds 1994;209:351–61.
[920] McCormick PG, Huang H, Dallimore MP, Ding J, Pan J. In: deBarbadillo JJ, et al., editors. Mechanical alloying for structural applications. Materials Park, OH: ASM International, 1993. p. 45–50.
[921] Hack GAJ. Metals and Mater 1987;3:457–62.
[922] Fischer JJ, deBarbadillo JJ, Shaw MJ. Heat Treating 1991;23(5):15–6.
[923] Elliott IC, Hack GAJ. In: Froes FH, deBarbadillo JJ, editors. Structural applications of mechanical alloying. Materials Park, OH: ASM International, 1990. p. 15–24.
[924] deBarbadillo JJ, Smith GD. Mater Sci Forum 1992;88–90:167–74.
[925] Suryanarayana C, Ivanov E, Boldyrev VV, Mater Sci and Engng 2000, in press.
[926] Black SA. Development of supercorroding alloys for use as timed releases for ocean engineering applications. Port Hueneme, CA: Civil Engng. Lab. (Navy), 1979 Report 40.
[927] Sergev SS, Black SA, Jenkins JF. US Patent No. 4,264,362, 13 August 1979.
[928] Tessier P, Zaluski L, Zaluska A, Ström-Olsen JO, Schulz R. Mater Sci Forum 1996;225–227:869–74.
[929] Rairden JR, Habesch EM. Thin Solid Films 1981;83:353–60.
[930] Gedwill MA, Glasgow TK, Levine SR. In: Metallurgical coatings, vol. 1. New York: Elsevier Sequoia, 1982.
[931] Jia C, Li Z, Xie Z. Mater Sci and Engng 1999;A263:96–100.
[932] Weber JH, deBarbadillo JJ, Mehltretter JC. In: Paper presented at the 2nd International Conference on Structural Applications of Mechanical Alloying, Vancouver, British Columbia, Canada, September 20–22. 1993. (not included in the Proceedings).